UNIVERSITY OF CALGARY

Multipath Mitigation in TOA Estimation Based on AOA

by

Dingchen Lu

A THESIS

SUBMITTED TO THE FACULTY OF GRADUATE STUDIES

IN PARTIAL FULFILMENT OF THE REQUIREMENTS FOR THE

DEGREE OF DOCTOR OF PHILOSOPHY

DEPARTMENT OF ELECTRICAL AND COMPUTER ENGINEERING

CALGARY, ALBERTA

AUGUST, 2007

Abstract

A wireless location system including hardware and software for multipath is developed and evaluated using measured data from CDMA base stations. An AOA (angle-of-arrival)-assisted and correlation slope-based TOA/TDOA method is proposed, which is a sub-optimal estimation for TOA/TDOA.

The AOA estimation is based on a Forward/Backward Smooth Multiple Signals Classification algorithm through the use of an antenna array. A beamforming technique is applied to partially mitigate multipath and the initial correlation function rising part is used to further mitigate multipath based on the estimation of its slope and starting point. So the correlation peak can be located to obtain TOA / TDOA.

The Cramer-Rao Lower Bounds of both the joint AOA / TOA method and the proposed method are also investigated. The experimental results agree with the theoretical analysis. The standard deviation of TDOA is 8 m in a real environment, where the signal to noise ratio at the correlation peak after 3 PN epochs integration is 30 dB (multipath strength may be also very strong at the correlation peak). It meets the FCC requirements of 50 to 150 metres. The data was collected outdoor under various conditions with little or strong multipath effect. It shows that the proposed method works efficiently when Line-of-Sight (LOS) signals exist in the multipath environments and deteriorates when LOS signals do not exist.

Acknowledgements

I would like to express my sincere thanks to my supervisors, Dr. John Nielsen and Dr. Gérard Lachapelle, for giving me an opportunity to conduct my Ph.D. studies in Electrical and Computer Engineering with the PLAN group of Geomatics Engineering. Thanks for their great guidance and support during my years of study, which was a precious period of time in my life.

Many thanks go to my team members' help, namely Alfredo Lopez, Surendram K. Shanmugam, Hendry Agus, Nazila Slami, Ahmad Reza Moghaddam, Ali Broumandan, Upal Mahfuz, Tao Lin. I gained much from our interaction.

Also special thanks to Chanling Ma, Ning Luo, Rob Watson from the PLAN group for their time to help me figure out some problems during the project and thesis completion.

Finally but not least, I thank my husband Ming for his continuous support and our daughter Sherry for bringing happy time to our family. I also thank my parents for raising me and teaching me the importance of love.

Table of Contents

List of Tables

List of Figures

List of Symbols

[ ]*: conjugate of a complex signal

$[\ ]^H$: Hermitian Transpose

$[\ ]^T$: Transpose

$a_i = e^{-j2\pi q \cos\beta_i}$ $(i = 1, 2, \cdots, K)$: phase factor on different antenna elements

a(β): direction vector ($M \times 1$ dimension for MUSIC, $m \times 1$ for subspace MUSIC)

$\mathbf{A} = [\mathbf{a}(\beta_1), \ldots, a(\beta_K)]$: direction matrix ($M \times K$ for MUSIC, $m \times k$ for subspace MUSIC)

b: linear combination of all correlated signal direction vectors $\mathbf{a}(\beta_i)$

$\mathbf{B} = diag\ [a_1, a_2, \ldots, a_K]$

c: light speed

$\mathbf{C} = \mathbf{D\Lambda}$: $K \times L$ matrix

d: distance between two antenna elements

$d^2(\ )$: Euclidean distance

$$\mathbf{D} = \begin{bmatrix} w_1 & & & \mathbf{0} \\ & w_2 & & \\ & & \ddots & \\ \mathbf{0} & & & w_K \end{bmatrix}$$: diagonal matrix

$\mathbf{E} = \mathbf{F\Lambda}$: $K \times L$ matrix

f_c : carrier frequency of the received CDMA signal

f_l : local carrier frequency

$f_e = f_c - f_l$: carrier frequency difference between the transmitter and the receiver

$\hat{f}_e$: estimate of f_e

$\Delta f_e = f_e - \hat{f}_e$: difference between f_e and $\hat{f}_e$

$$\mathbf{F} = \begin{bmatrix} \delta_1 & & & \mathbf{0} \\ & \delta_2 & & \\ & & \ddots & \\ \mathbf{0} & & & \delta_K \end{bmatrix}$$: diagonal matrix

G_P: processing gain

$\mathbf{G} = \mathbf{D}\mathbf{G}_0$, $\mathbf{G}_0 = [\mathbf{\Lambda} \vdots \mathbf{H}\mathbf{\Lambda}]$

$\mathbf{H}$: matrix of observation equation coefficients

I: identity matrix

$\mathbf{J} = \mathbf{D}^{-1}\mathbf{F} = diag[\varepsilon_1, \varepsilon_2, \cdots, \varepsilon_K]$ $(k = 1, 2, \cdots, K)$

L: number of subarrays

K: number of the incident rays on the antenna elements; length of PN sequences

m: size of each subarray

M: size of the antenna array (element)

$\mathbf{n}(t) = [n_1(t), n_2(t), \ldots, n_M(t)]^{\mathrm{T}}$: $M \times 1$ noise vector

$\mathbf{n}_l^b(t)$: noise vector of the l^{th} backward subarray

$\mathbf{n}_l^f(t)$: noise vector of the l^{th} forward subarray

$P(\beta)$: spatial spectrum for MUSIC algorithm

q: ratio of d/λ

$r_\Sigma(\tau_1)$: sampled value of the summation of five correlator output at time point τ_1

$r_{\Sigma n}(\tau_1)$: noise component of $r_\Sigma(\tau_1)$

$\mathbf{R}$: $M \times M$ array auto-correlation matrix

$\mathbf{R}_S$: $K \times K$ signal auto-correlation matrix

$\mathbf{R}_l^b$: auto-correlation matrix of the l^{th} backward subarray

$\mathbf{R}^b$: smoothed auto-correlation matrix for all backward subarrays

$\mathbf{R}_S^b$: backward smoothed source signal auto-correlation matrix

$\mathbf{R}_l^f$: auto-correlation matrix of the l^{th} forward subarray

$\mathbf{R}^f$: smoothed auto-correlation matrix for all forward subarrays

$\mathbf{R}_S^f$: forward smoothed source signal auto-correlation matrix

$\mathbf{R}^{f/b}$: smoothed auto-correlation matrix for all forward/backward subarrays

$\mathbf{R}_S^{f/b}$: forward/backward smoothed source signal auto-correlation matrix

$\mathbf{s}(t) = [s_1(t),\ldots,s_K(t)]^T$: K source signals vector

$s_1(t) = A\left[PN_I(t-t_d)\cos(2\pi f_e t+\varphi) + PN_Q(t-t_d)\sin(2\pi f_e t+\varphi)\right]$: received I signal

$s_2(t) = A\left[-PN_I(t-t_d)\sin(2\pi f_e t+\varphi) + PN_Q(t-t_d)\cos(2\pi f_e t+\varphi)\right]$: received Q signal

$s_3(t) = s_1(t) + j\,s_2(t)$: complex expression of the received signal

$\tilde{s}_3(t) = s_3(t)\exp[j2\pi \hat{f}_e t]$: modified $s_3(t)$

$\tilde{s}_3(n)$: discrete signal of $\tilde{s}_3(t)$

$s_l(t) = \left[PN_I(t) + j\,PN_Q(t)\right]\exp[-j2\pi \hat{f}_e t]$: local signal

$\tilde{s}_l(t) = [PN_I(t) + j\,PN_Q(t)]$: modified $s_l(t)$

$\tilde{s}_l(n)$: discrete signal of $\tilde{s}_l(t)$

t_0 : initial LOS delay estimation after coarse acquisition

T : integration time of correlation processing; one period of PN sequence

T_c : chip period

T_S : sampling interval of the data

$\mathbf{V}_N$: noise subspace matrix whose columns are the noise eigenvectors

$\mathbf{w} = [w_1, w_2, \ldots, w_K]^T$: complex weight coefficients vector for correlated signals $\mathbf{s}(t)$

$\mathbf{x}(t) = \left[x_1(t), x_2(t), \cdots, x_M(t)\right]$: measured data vector

$\mathbf{x}_l^b(t) = [x_{M-l+1}^*(t), x_{M-l}^*(t), \ldots, x_{L-l+1}^*(t)]^T$: measured l^{th} backward subarray data

$\mathbf{x}_l^f(t) = [x_l(t), x_{l+1}(t), \ldots, x_{l+m-1}(t)]^T$: measured l^{th} forward subarray data vector

β : signal's angle of arrival with respect to the array line

$\hat{\beta}$: estimate of β

φ : phase difference between antenna elements

$\delta_k = w_k^* a_k^{-(M-1)}; \quad a_k^{-(M-1)} = e^{j2\pi(M-1)\ q\cos\beta_k} \qquad k = 1, 2, \cdots, K$

$\varepsilon_k = \dfrac{\delta_k}{w_k}$

γ : Amplitude of the measured carrier signal

ϕ : Initial phase of the measured carrier signal

γ_i : eigenvector of auto-correlation matrix $\mathbf{R}$

λ: wavelength of the received RF signal

λ_i : eigenvalue of auto-correlation matrix $\mathbf{R}$

$$\mathbf{\Lambda} = \begin{bmatrix} 1 & a_1 & a_1^2 & \cdots & a_1^{L-1} \\ 1 & a_2 & a_2^2 & \cdots & a_2^{L-1} \\ \vdots & \vdots & \vdots & \ddots & \vdots \\ 1 & a_K & a_K^2 & \cdots & a_K^{L-1} \end{bmatrix}$$: Vandermonde structure

θ : unknown parameter to be estimated

$\hat{\theta}$: estimate of unknown parameter θ

σ^2 : variance of the additive Gaussian noise at each antenna element

σ_r^2 : noise variance at each correlator output

$\sigma_{\Sigma\, n}^2$: noise variance summation of five correlators outputs

σ_p : standard deviation of the final position estimate

σ_r : standard deviation of the ranging estimate

σ_β : standard deviation of the angle estimate

ρ_{xy} : correlation coefficient of two signals x and y

$\boldsymbol{\rho}$: vector of the real range measurements

$\hat{\boldsymbol{\rho}}$: vector of the expected ranges at the guess position

$\Delta\boldsymbol{\rho} = \hat{\boldsymbol{\rho}} - \boldsymbol{\rho}$: vector of difference between $\hat{\boldsymbol{\rho}}$ and $\boldsymbol{\rho}$

$\Delta\mathbf{x}$: vector of position and receiver clock corrections

τ : multipath delay resolution

List of Abbreviations

ADC: Analog to Digital Converter

ADEV: Allan Deviation

AMPS: Advanced Mobile Phone Service

AOA: Angle-of-Arrival

BS: Base Station

CDMA: Code Division Multiple Access

CRLB: Cramer-Rao Lower Bound

CW: Continuous Wave

DAQ: Data Acquisition

DFT: Discrete Fourier Transform

DLL: Delay Lock Loop

DOP: Dilution of Precision

ESPRIT: Estimation of Signal Parameters via Rotational Invariance Techniques

GDOP: Geomatic Dilution of Precision

FBSMUSIC: Forward / Backward Smooth MUltiple SIgnal Classification

FCC: Federal Communications Commissions

FFT: Fast Fourier Transform

FM: Frequency Modulation

FPGA: Field Programmable Gate Array

GPS: Global Positioning System

GSM: Global System for Mobile Communications

iid: independently and identically distributed

LO: Local Oscillator

LOS: Line-of-Sight

ML: Maximum Likelihood

MS: Mobile Station

MUSIC: MUltiple SIgnal Classification

NLOS: Non-Line-of-Sight

PDF: Probability Density Function

PDP: Power Delay Profile

PN: Pseudo Noise

RF: Radio Frequency

SIR: Signal to Interference Ratio

SNR: signal to noise ratio at the sampled point or before despreading

TCXO: Temperature Compensated Crystal Oscillator

TDOA: Time-Difference-of-Arrival

TOA: Time-of-Arrival

ULA: Uniform Linear Array

VGA: Variable Gain Amplifier

VHF: Very High Frequency

XOR: Exclusive OR

Chapter One: Introduction

1.1 Introduction

Terrestrial-based location systems have been researched and successfully deployed for a few decades but with limitations in accuracy due to multipath and geometry, and complexity in infrastructure development. Code-division multiple access (CDMA) systems have partially overcome this deficiency, as its wide bandwidth is inherently able to resolve some of the multipath. CDMA systems assign each user a unique pseudonoise (PN) spreading code, which makes the identification of multipath with delay over one PN code chip epoch efficient by signal correlation processing because the correlation peak of multipath over one chip does not affect the correlation peak position of direct signal. In CDMA systems, one chip epoch is about 800 ns that equal to 240 metres in distance. However the intra-chip multipath, that is the reflected rays arriving within a chip period of the first ray, cannot be resolved by a correlation technique and is still a significant factor limiting location accuracy. The accuracy requirements of the enhanced 911(E-911) mandate proposed by the Federal Communications Commissions (FCC) were set to within 50 m for 67% of calls and within 150 m for 95% of calls for handset-based solutions (FCC 2001). In order to meet the accuracy requirements in handset-based solutions, the mitigation of the effects of intra-chip multipath must be considered.

Many existing wireless location systems, such as the Global Positioning System (GPS) and Loran C, utilize radiolocation techniques. In these systems, the mobile station (MS)

estimates its own position. As an alternative, cellular networks can be used to provide the location service when GPS signals are very weak. An advantage of this approach is that the signals from the cellular base stations travel shorter distances than the GPS signals and the signal to noise ratio received by CDMA receivers is comparatively strong compared to GPS signals. Also the pseudo-code used in cellular networks is longer than that of the GPS, so it has better cross correlation characteristics. However the cellular networks are initially designed for communication and not for location application. For example, the time synchronization quality and the signal bandwidth requirement are different from GPS. So the terrestrial-based location systems have lower location accuracy than GPS, which can be at the centimetre level when used outdoor (e.g. Lachapelle & Cannon 2004). Even so, ground-based systems remain an alternative to provide location in the situations where the GPS signal availability and accuracy are still limited as indoors and in other signal shaded areas (*ibid*).

There are two major methods to implement a cellular network-based location system. In the first approach, the mobile station (MS) receives signals from the base stations (BS) to calculate its own position, as in GPS. In the second approach, the BSs process the signals from the MS to locate the user. The second approach has the advantage of no modification requirement on users. There are several systems using cellular network-based or GPS-assisted cellular network-based solution for location, such as gpsOne® by Qualcomm, in which a cell phone user receives GPS signals and is connected to a network-based location server which calculates the user location, and Matrix technology by Cambridge Positioning Systems, which is based on GSM (Global System for Mobile

Communications) system, and Cellocate^{TM} by Cell-Loc Inc., which is based on AMPS (Advanced Mobile Phone Service). For research purpose, the user-based approach is more flexible. The approach investigated herein is based on the present CDMA IS-95 system and uses a prototype CDMA receiver with an antenna array mounted on a vehicle partly developed by Shanmugam et al (2005) to receive IS-95 pilot signals from several base stations to calculate the position of the MS.

1.2 Motivations and Limitations of Previous Research

There are several methods for implementing radiolocation, such as signal strength (Figel et al. 1969), angle of arrival (AOA) (Sakagami et al. 1992), time of arrival (TOA) (Messier & Nielsen 1999) / time difference of arrival (TDOA) (Goud et al. 1991), or their combinations, such as AOA/TOA (Ma 2003). These methods work well under certain conditions of noise, interference, and multipath. Among those error sources, multipath is the most difficult problem to deal with and significantly affects the location accuracy in both GPS and cellular network-based location systems. Especially in urban areas, the location accuracy decreases because more multipath is present. The following characterizes the above location techniques and their drawbacks.

Signal strength based location systems are adversely affected by the changes in the environment. The primary source of error is multipath fading. So this method is usually used to determine the cell by making use of pre-measured signal strength contours mapped out for each BS (Smith 1991).

The accuracy of the AOA method is limited by the physical size of the array, SNR and carrier frequency. And most of the algorithms are based on the assumption that the signal essentially emanates from a single point. This assumption is reasonable for radar and macro-cell (10 km of radius) applications, where the receiver is located relatively far from the source. However for the micro-cell (2 km radius) application, the source cannot be treated as a single source. It should be modeled as a spread source (Svantesson 2001). So the AOA method is impractical for micro-cell. A 1° error can result in 17.5 m of positioning error when the distance between the BS and the MS is 1 km, i.e. $r\sin(\theta_{error})$. So the AOA only method is usually used for lower-accuracy applications or in conjunction with other measurements.

AOA systems are susceptible to angular multipath (Gans 1972). Thus, the TOA method outperforms the AOA method in urban areas where multipath exists significantly, and vice-versa in open areas. Even so, multipath is still a major error in TOA systems. The conventional correlation peak techniques used in the TOA method cannot detect intra-chip multipath components. If the direct ray arrives with less power than the delayed rays, the correlation peak will be shifted due to the stronger multipath signal, which results in a bias in the tracking loop. Several methods have been developed to mitigate multipath, such as the Root-MUSIC algorithm (Klukas 1997, Dumont 1994), the least mean squares (LMS) technique (So & Ching 1993) and the recent multiple DLL architecture (Dovis et al 2004). However the mitigation of multipath is still an on-going area of research.

The TDOA method is a more practical way for location measurements than TOA because it does not require that the entire system be equipped with precisely synchronized clocks and it also does not require the timestamp labelled in the transmitting signal for the receiver to estimate the distance the signal has traveled. It only requires that the synchronized network and the unknown MS clock offset cancels out when differencing any two TOA measurements. However it still needs LOS (Line-Of-Sight) signals as in the techniques above to obtain a good performance. So the TDOA method is still affected by multipath.

A joint AOA and TOA technique had been proposed, such as the Joint Angle and Delay Estimation (JADE) (Van der Veen et al 1997) and the TST-MUSIC (Wang et al 2001). Even though performance improvement is achieved by sacrificing simplicity, the inaccuracy of the estimated AOA and TOA and multipath still affects the results.

Even though numerous methods have been proposed to deal with multipath (Tarighat et al 2003, Kim 2004, Falletti et al 2006), there is still not an efficient way to mitigate multipath due to its complicated characteristics. Multipath is a signal which reflects from various objects. If the signal is reflected from a smooth surface, the reflected signal is specular. If the signal is reflected by sharp edges, the reflected signal is scattered in all direction and called diffuse multipath. Multipath models can be found in (Ertel 1998, Jakes 1993, Rappaport 1991).

There is the case when no LOS signal exists. In this case, an option in principle is to use inertial navigation techniques to bridge gaps in location continuity. Inertial navigation systems (INS) use gyros and accelerometers to update the location by integrating rotation rates to obtain orientation changes and doubly integrating the accelerations to obtain velocity and position increments (Jekeli 2000) from the last previously known position. This technique can be used in cases when buildings obscure line of sight propagation until a new position can be calculated (Petovello 2003). However the cost of sufficiently accurate INS for such purpose is prohibitive. Another option is to extract the LOS from the NLOS with prior PDF by subtracting the known amount of NLOS delay from the total time delay (Qi 2003).

1.3 Objectives and Novel Contributions

The primary objective of the present research is to develop a practical signal processing method in user-based location systems to estimate the angle of arrival (AOA) and then the time of arrival (TOA) for the LOS signal under multipath environments. This is achieved through the use of multi-element receiver antennas which are implemented in hardware suitable for hand set or mounting on a small vehicle.

The major original work is summarized as follows:

1. Propose a practical scheme for AOA-assisted TOA estimation under multipath environment as shown in Figure 1.1

2. Apply Forward/Backward Smooth MUltiple SIgnal Classification (MUSIC) algorithm to a CDMA receiver with a limited capacity of resolvable angles of the incident rays for AOAs estimation in multiple multipath signal environments
3. Derive mathematically the Cramer-Rao Lower Bounds (CRLB) for separate AOA and TOA estimators and joint AOA / TOA estimator in single source signal environments
4. Propose an initial correlation function rising slope-based method to determine the correlation peak of the LOS based on the conclusion through the investigation of AOA CRLB: decreasing the number of source signals is more efficient than increasing the signal to noise ratio
5. Derive the estimated variance for the AOA-assisted TOA estimator
6. Contribute a hardware platform in FPGA design and implementation, real data collection and verification
7. Develop software to implement the proposed algorithm and verify it with actual measured field data.

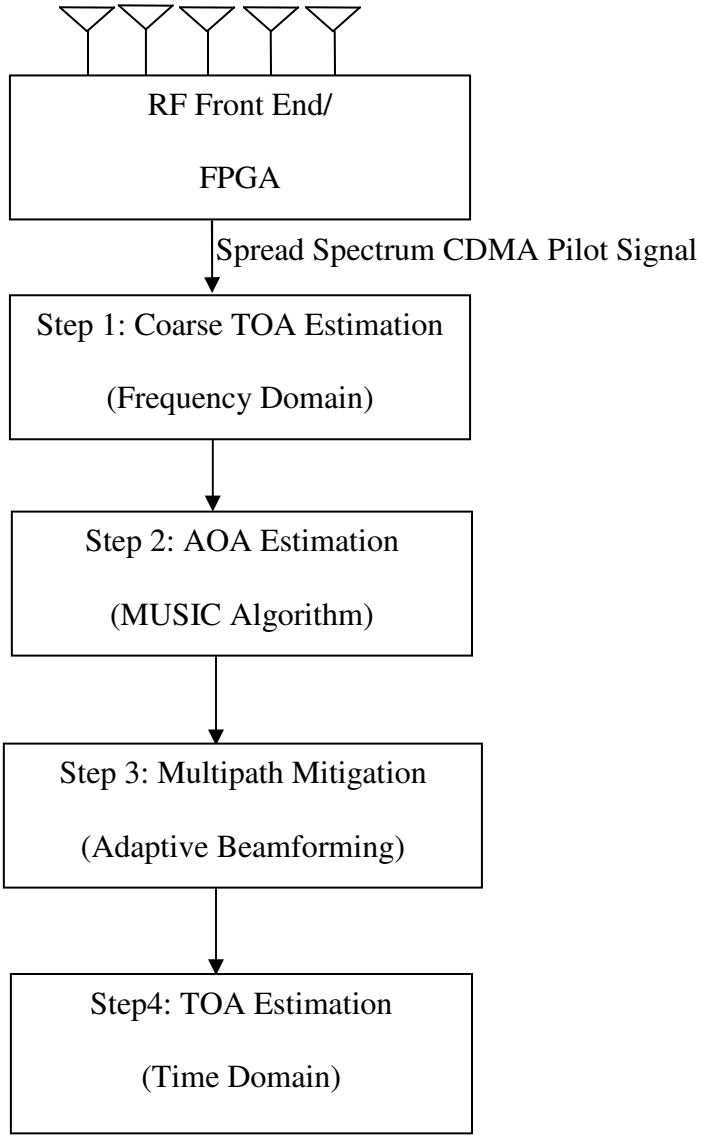

Figure 1.1: Flow Chart of AOA-Assisted TOA Estimation for Multipath Mitigation

The proposed AOA-assisted TOA method consists of five main steps.

The first step is to find the coarse correlation peak position based on the traditional sliding correlation technique using FFT processing. The derived correlation peak is distorted by multipath. We cannot rely on that correlation peak to estimate the TOA.

However the sampled data from five correlation functions can be used for processing by MUSIC to estimate AOAs of the received signals as an initial estimated values to be applied to the TOA technique.

The second step is to use a forward/backward smooth MUSIC algorithm to estimate AOAs of the signals contained in the sampled data. The data to be processed by MUSIC is sampled at the correlation functions in such a way that few multipath signals are contained and only in the initial leading edge of the correlation function, the sampled data contain fewer numbers of signals. Because the forward/backward smooth MUSIC algorithm can resolve three AOAs with five antenna elements (Pillai 1989), so the first and second step are an iterative process until the F/B smooth MUSIC works efficiently on the sampled data.

The third step is to extract the LOS signal from the AOAs estimation derived in step 2 through the adaptive beamforming technique based on the antenna array of five elements and augment the SNR of the LOS signal at the same time, which is described in Chapter 5. The purpose of using AOA estimation is to help identifying LOS and NLOS (Non-Line-Of-Sight) signals and then mitigating NLOS signals through array signal processing technique in order to reconstruct an initial correlation function rising slope with little distortion from multipath. The accuracy of AOA estimation and the number of detected signals obtained by the MUSIC algorithm will affect the improvement of LOS SNR, because the pattern construction of the beamformer is affected by the number of source signals and if the estimated AOA is out of the main lobe range of the beamformer, the desired signal cannot be enhanced.

The fourth step is to apply a correlation technique in the time domain to determine the correlation function rising slope and intercept based on the result from the third step. A linear model needs to be established for the unknown parameters estimation. And that estimator reaches the CRLB.

The fifth step is to derive the starting point of the correlation function based on the estimated correlation function rising slope and intercept from the fourth step. By adding a modified offset of one chip period with $T_C^{'}$ to the starting point, the LOS TOA can be estimated. Because the bottom width of the correlation function of the real data is different from the theoretical value of one chip T_C due to the bandwidth of the base band filter applied, it needs to modify that offset based on the real bandwidth of the received signal. At this time, only the noise will affect the TOA estimation accuracy which has however been improved by the summation of the signals from the five antennas. The assumption of the proposed method is that LOS exists. If the LOS does not exist, the earliest NLOS is assumed to be the LOS, which will result in error. In that case, one needs to consider NLOS with a prior probability density function (Qi 2003).

The proposed method improves the TOA system under multipath environment through the AOA measurements. The AOA estimation is based on the forward/backward smooth MUSIC algorithm because it has a light computation burden compared with the Maximum Likelihood method, which searches the angles in multi-dimensions. The MUSIC algorithm can attain the CRLB for large numbers of samples, large numbers of array elements, and high SNRs. A detailed analysis of the MUSIC estimation errors is

given in Chapter 4. TOA estimation is based on the rising slope of correlation function, whose minimum estimation variance is two times of TOA CRLB. However the practical standard deviation of TDOA is 8 m in a real environment, where the SNR after despreading is 30 dB, which meets the FCC requirements.

To implement the above objective, the following issues are addressed.

- Investigation of the Forward and Backward Smoothing MUltiple SIgnal Classification (MUSIC) algorithm (Pillai 1989) for AOA estimation
- Array signal processing to filter out the NLOS based on the estimated AOA bearing
- Correlation technique for TOA estimation under multipath environments
- CRLB analysis for AOA and TOA/TDOA estimation
- Development and verification of practical algorithms
- Practical implementation onto an FPGA, which is based on real time data collected by a CDMA receiver with five antenna elements. This will provide a means of conveniently obtaining ample experimental data for algorithm development and statistical validation as well as demonstrating the feasibility of the proposed algorithms.
- Hardware assembly and testing for antenna array with five elements to collect real data
- Analysis of the data for AOA and TOA/TDOA estimation

Subsequently, the following tasks are required:

- Design and test a CDMA receiver hardware platform, including antenna array placement, to collect the propagated measurement data
- Develop the software for the forward/backward smooth MUSIC algorithm to derive the AOAs of the received signals
- Design an adaptive beamforming algorithm to filter out the NLOS signals based on the derived AOAs and analyze the effect of the antenna spacing on AOA estimation
- Propose a correlation function slope detection algorithm for TOA estimation
- Analyze the effect of multipath on TOA
- Test the above under field conditions to verify the proposed approach
- Comparison of CRLB based on the estimation theory, simulation and real data

1.4 Thesis Outline

There are seven chapters and six appendices in this dissertation. The subsequent chapters are as follow.

Chapter 2 provides the background knowledge about CDMA-based location systems, including an introduction of the CDMA communication system and IS-95 standards, and several location techniques, such as the TOA, TDOA and AOA method, the effect of geometric dilution of precision (GDOP) and a brief literature review of the present wireless location techniques.

Chapter 3 explains the minimum variance unbiased estimator from the estimation point of view. It discusses the CRLB of AOA estimation and derives the CRLB of TOA estimation in CDMA IS-95 systems. The theoretical variance error analysis for AOA estimation is given based on the direction vector sensitivity and GDOP. The estimation error comparison between AOA CRLB and the MUSIC estimator is given in Chapter 4, and the comparison between TOA CRLB and the proposed TOA estimator is given in Chapter 5. The error analysis with the measurement data is given in Chapter 6.

Chapter 4 describes the AOA estimation algorithm. The signal model for the algorithm is examined. The conventional MUSIC and F/B (forward/backward) Smoothing MUSIC algorithm is fully discussed from the vector space theory point of view, also including the limitations and the AOA estimation error evaluation for the F/B Smooth MUSIC estimator. The F/B Smoothing MUSIC AOA estimator is asymptotically optimal.

In Chapter 5, the AOA-assisted multipath mitigation approach for TOA estimation is described. The array signal processing for the antenna array with five elements is discussed. The SNR improvement of the LOS after the array signal processing is shown. TOA estimation variance is derived based on the linearized vector parameter transformation of the correlation function initial rising slope and its intercept though a coordinate transform.

Chapter 6 describes the hardware system used herein, its design and implementation, including the RF circuit and FPGA circuits. Related firmware development is

demonstrated and its specifications are also provided. The experiment results are also presented in this chapter, including the experiment setup, the calibration of the antenna channel phase. The receiver antenna array is put on the roof of Calgary Centre for Innovative Technology (CCIT) building at the University of Calgary, so the AOAs of the received signals with respect to the surrounding CDMA base stations are determined when the receiver antenna array is rotated in different directions. The experiment result based on the raw data is given for comparison with the simulation results. The effect of the estimated AOA on the TOA is also investigated. The TDOA measurement is given and its standard deviation is compared with the theoretical value.

Chapter 7 concludes the thesis with a research summary including the advantages and the limitations of the proposed algorithm, and recommendations for further investigations.

Finally, the appendices include background information of selected relevant topics, such as CDMA IS-95 signal processing, derivation of CRLB for AOA estimation, Allan variance measurements and the design of the second CDMA receiver.

Chapter Two: CDMA-based Location Systems

2.1 CDMA Communication Systems

In this chapter, some location techniques such as AOA, TOA and TDOA are described. Specifically CDMA IS-95 system is discussed because signals analysis and data measurement are all based on it. CDMA (Code Division Multiple Access), originally commercialized by Qualcomm (Qualcomm 2006), is characterized by its high spectral efficiency and good anti-jam performance. IS-95 CDMA is the second generation of cellular network technology with a typical data rate of 9.6 kbps per channel, which appeared in the 1990's in North America. The following is a general description of the IS-95 CDMA system, which is fundamental to the geolocation system being developed and investigated in this thesis.

In single carrier CDMA systems all users transmit in the same bandwidth simultaneously. To implement this approach, the concept of "spread spectrum systems" was introduced. In this technique, the frequency spectrum of a data-signal is spread using a code uncorrelated with the data-signal. As a result the bandwidth is much higher than required for the data. The codes used for spreading have low cross-correlation values and are unique to every user. So a receiver that has knowledge about the code of the intended transmitter is capable of selecting the desired signal.

Major advantages are:

- **Low power spectral density.** As the signal is spread over a large frequency-band, the Power Spectral Density becomes very small, causing minimal interference with other users using the same band.
- **Privacy due to unknown codes.** The applied codes are usually unknown to a hostile user. This means that it is hardly possible to decode the message of another user.
- **Applying spread spectrum implies the reduction of multipath effects.**
- **Good anti-jam performance.**
- **Frequency diversity.**
- **High spectral efficiency.**

2.1.1 Spread Spectrum

Originally for military used to avoid jamming, spread spectrum modulation is now used in personal communication systems for its superior performance in interference environments and better capacity in wireless fading channels. Spread spectrum means that the data transmitted occupies a larger bandwidth than necessary to avoid interception. The frequency of a conventional wireless signal is kept constant, for example FM 103.1 MHz, so the bandwidth can be kept within certain limits, and the signal can be easily intercepted by someone who wants to retrieve the information. Bandwidth spreading is accomplished before the transmission through the use of a code

with high bit rate, which is independent of the transmitted data. The same code is used to demodulate the data at the receiving end. Figure 2.1 illustrates the spreading done on the data signal x(t) by the spreading signal c(t) resulting in the message signal to be transmitted, m(t).

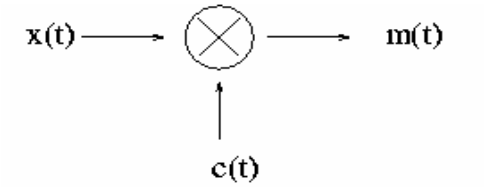

(a) Direct-Sequence Spreading Diagram

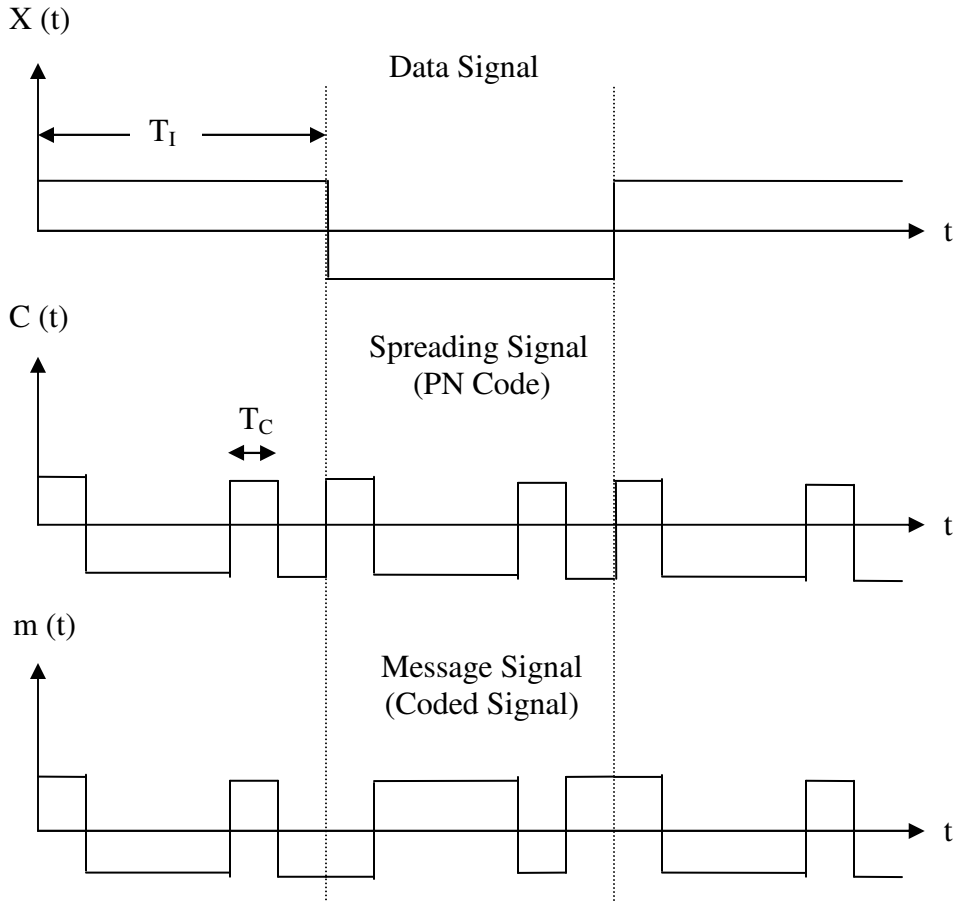

(b) Time Sequence

Figure 2.1: (a) Direct-Sequence Spreading Diagram; (b) Time Sequence

2.1.2 Pseudo-Noise Sequences

In order to overcome narrow band interference, the spreading signal needs to behave like noise (Proakis 2001). Random binary sequences are such functions. They have the following important properties:

- *Balanced*: they have almost equal number of 1's and 0's to avoid mean values (having an extra ’0’)
- Periodic narrow peaks of auto-correlation function as shown in Figure 2.2 (a)

Theoretically, the auto-correlation function of a random binary sequence is a triangular waveform as shown in Figure 2.2 (a), where T_C is the duration of one chip and N is the period of the PN sequence. Practically due to finite bandwidth of the filter in the transmitter and receiver, the auto-correlation function becomes curvy.

PN sequences are periodic sequences that have a noise like behaviour. They are generated using shift registers, modulo-2 adders (XOR gates) and feedback loops, as shown in Figure 2.3.

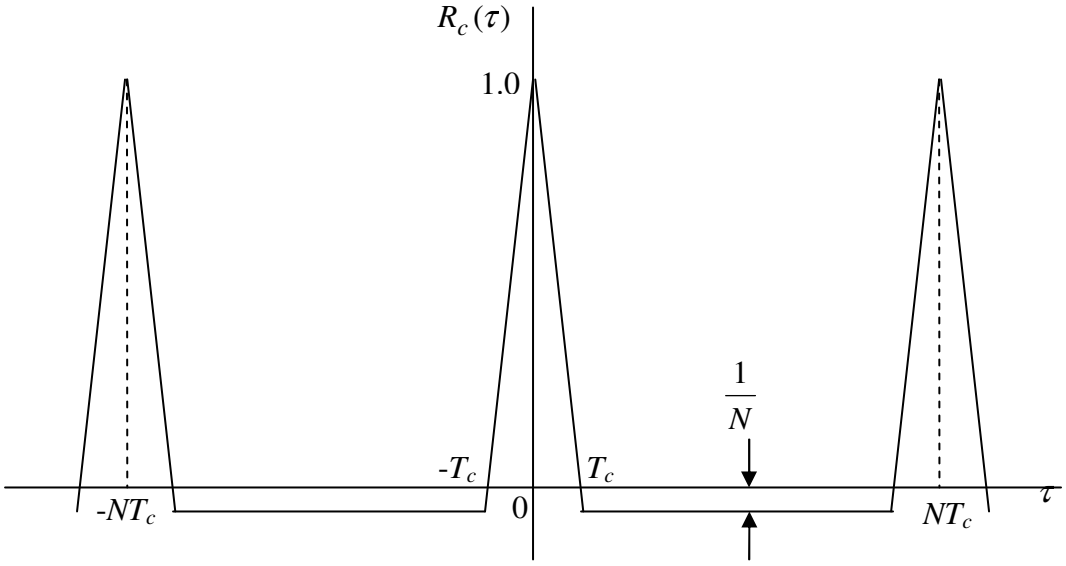

(a) Autocorrelation Function of *m*-Sequence

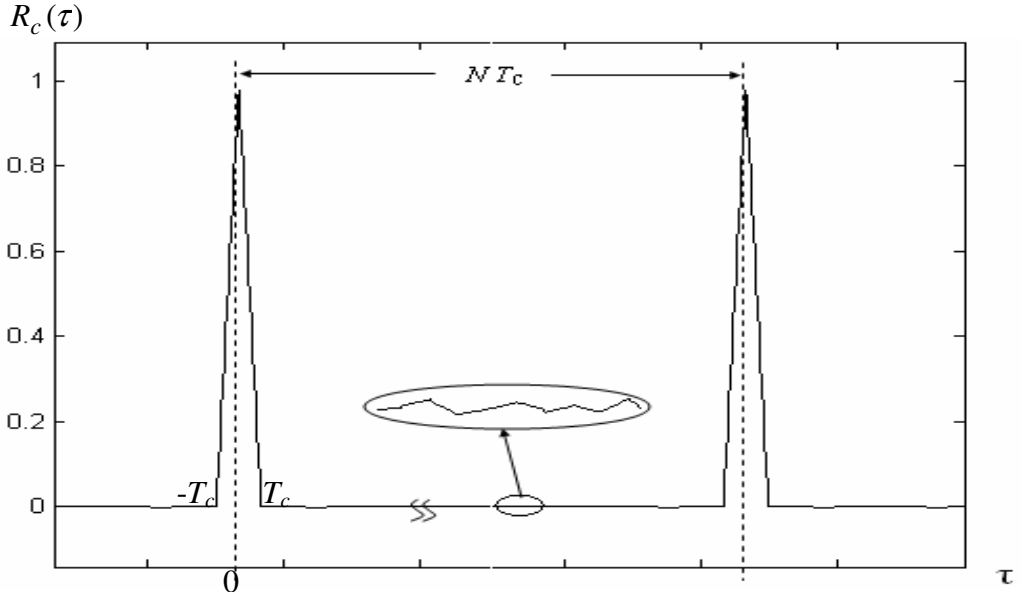

(b) **Autocorrelation Function of Pilot PN Sequence**

Figure 2.2: (a) Autocorrelation Function of *m*-Sequence; (b) Autocorrelation Function of Pilot PN Sequence

The maximum length of a PN sequence is determined by the length of the register and the configuration of the feedback network. With N bits register, since the feedback network performs linear operations, if all the inputs (i.e. the content of the flip-flops) are zero, the output of the feedback network will also be zero. Therefore, the all zero combination will always give a zero output for all subsequent clock cycles, so it is not included in the sequences. Thus, the maximum length of any PN sequence is 2^N-1 instead of 2^N and sequences of that length are called *Maximum-Length Sequences* or *m-sequences*. In IS-95 systems, a zero is inserted in each sequence after the contiguous succession of fourteen zeros to generate the pilot PN sequence of length 2^{15} chips. It is based on the following characteristic polynomials as expressed in equation (2.1) for '*I*' and '*Q*' pilot PN sequences respectively and its autocorrelation function is shown in Figure 2.2 (b). The difference between *m*-sequence correlation function and pilot PN sequence correlation function is that the side lobe of the latter one is not constant.

$$\begin{aligned} P_I(x) &= x^{15} + x^{13} + x^9 + x^8 + x^7 + x^5 + 1 \\ P_Q(x) &= x^{15} + x^{12} + x^{11} + x^{10} + x^6 + x^5 + x^4 + x^3 + 1 \end{aligned} \tag{2.1}$$

Based on the above characteristic polynomials, the pilot PN sequences $I(n)$, for example, can be generated by a 15-stage shift register as shown in Figure 2.3. The last register is numbered zero and the first one is numbered 14. Equation (2.1) tells us that, for '*I*' sequences, registers 0, 5, 7, 8, 9, and 13 should be tapped and summed in a module 2 adder. The output of the adder is then input to register 14.

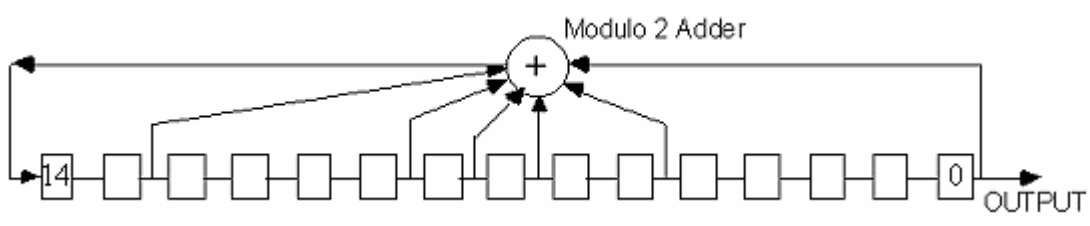

Figure 2.3: IS-95 In-Phase Pilot PN Code Generator

The pilot PN sequences $I(n)$ and $Q(n)$ are generated by the following recursive formulas:

$$\begin{aligned} I(n) &= i(n-15) \oplus i(n-10) \oplus i(n-8) \oplus i(n-7) \oplus i(n-6) \oplus i(n-2) \\ Q(n) &= q(n-15) \oplus q(n-13) \oplus q(n-11) \oplus q(n-10) \oplus q(n-9) \oplus q(n-5) \\ &\quad \oplus q(n-4) \oplus q(n-3) \end{aligned} \tag{2.2}$$

where n equals the number of shift register 15. The initial state of the 'I' and 'Q' pilot PN sequence is defined as the state in which the output of the pilot PN sequence generator is the first '1' output following fourteen consecutive '0' outputs. The rate of this PN sequence (called the chip rate) is 1.2288 Mcps. This results in the bandwidth of the spread signals to be about 1.25 MHz, which is about one-tenth of the total bandwidth allocated to one cellular service carrier. The sequences repeat themselves exactly 75 times every 2 seconds.

2.2 Wireless Location Techniques

Basically there are three types of wireless location techniques:

- Signal power strength method
- Angle of Arrival method
- Time of Arrival / Time Difference of Arrival method

In this thesis, the TOA method is assisted by the AOA method. The investigation of the signal processing is therefore focused on AOA and TOA methods based on the CDMA pilot signal.

2.2.1 AOA Technique and Algorithm

In the AOA method, the location of the desired target in two dimensions can be found by the intersection of two LOS bearings, each formed by a radial from a base station to the mobile target, as shown in Figure 2.4. It does not require the synchronized system time. Only two AOA measurements are needed. For 3D location, the desired target can be calculated from the intersection of a minimum of three surfaces of position if the base station geometry is sufficiently good. The accuracy of the AOA method is dependent on the distances between and relative geometry of the MS to be located and the antenna arrays at BSs. The further the MS is from the antenna arrays, the larger is the positioning uncertainty because $P_{error} \propto r\sigma_\beta$, where r is the distance and σ_β is the estimated AOA error.

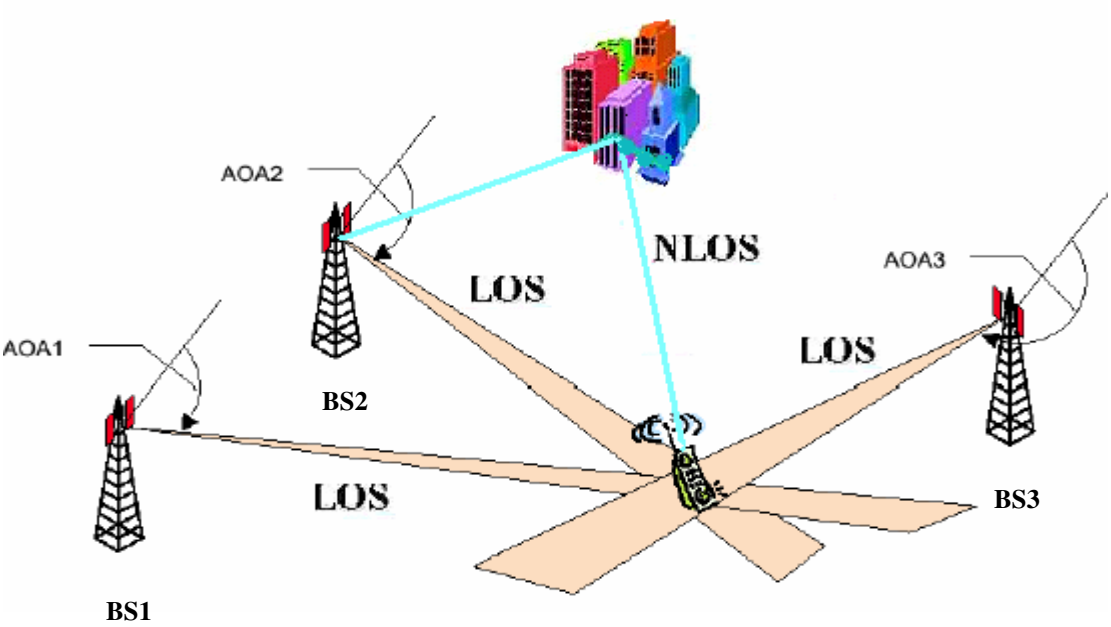

Figure 2.4: AOA Technique

Conventional direction finding technique using *beamformer* dates back to the Second World War for source location in radar and sonar. It is an application of Fourier-based spectral analysis to spatiotemporally sampled data. The advantage of using Discrete Fourier Transform (DFT) is that it can be implemented through Fast Fourier Transform (FFT) to speed up the computation. The drawback of the DFT is its low resolution. To provide high resolution, super-resolution methods, such as the MUltiple SIgnal Classification (MUSIC) (Schmidt 1979), the Estimation of Signal Parameters via Rotational Invariance Techniques (ESPRIT) (Roy & Kailath 1989) and the Maximum Likelihood (ML) (EI-Behery & MacPhie 1977) methods were developed. In this research, a modified MUSIC algorithm called the forward/backward smoothing MUSIC technique is applied because it can estimate AOA under multipath environments and can be implemented in actual hardware (Kim et al 2003). The ESPRIT method cannot give as

narrow peaks as MUSIC does to easily determine AOAs although it is less computationally intensive than MUSIC (Roy & Kailath 1989). The ML solution is computationally prohibitive, especially when multiple sources exist, although it is more robust and has a smaller estimation error as compared with MUSIC (Schmidt 1979). The following is a high level description of the MUSIC algorithm to estimate AOAs. A detailed explanation is given in Chapter 4.

Conventional MUSIC Algorithm

The eigen structure-based super-resolution technique MUSIC was proposed by Schmidt (1979). It is based on a Uniform Linear Array (ULA) to formulate the second order moment of the received signal, i.e. the spatial covariance matrix defined by $\mathbf{R} = E\{\mathbf{x}(t)\mathbf{x}^H(t)\}$, where symbol ($H$) denotes the Hermitian transpose and $\mathbf{x}(t)$ is the array output vector (see equations 4.1 to 4.4). Thus the first step of MUSIC is to decompose the covariance matrix into two parts of eigen signal subspace and eigen noise subspace.

The fundamental properties are:

(1) The noise eigenvectors construct the noise subspace matrix.

(2) The eigenvectors corresponding to the minimal eigenvalue are the noise vectors and orthogonal to the columns of the direction matrix, namely and to the K signal direction vectors.

Based on the above properties, the AOAs can be determined by searching through all possible steering vectors $\mathbf{a}(\beta)$. When $\mathbf{a}^T(\beta)\mathbf{V}_N = 0$, where $\mathbf{V}_N$ is noise subspace matrix defined in equation (4.15), the corresponding β is the AOA of an incident ray, because only the source signal is orthogonal to the noise (property (2)).

For multiple incident signals, the AOAs can be estimated by locating the peaks of a "MUSIC **spatial spectrum**" as expressed in the following equation (Schmidt 1979):

$$P(\beta) = \frac{1}{\mathbf{a}^H(\beta)\mathbf{V}_N\mathbf{V}_N{}^H\mathbf{a}(\beta)}. \tag{2.3}$$

This conventional MUSIC algorithm can resolve the incident rays angles when the signals are uncorrelated. For uncorrelated signals, the source signal covariance matrix is nonsingular. By solving the array output matrix, the eigen vectors corresponding to the source signals can be obtained. So the AOAs of the source signals can be scanned out by the orthogonal noise vector. However when the source signals are correlated which is common in multipath environments, the source signal covariance matrix becomes singular and the noise vectors are no longer orthogonal to the source signal vectors. What really happens is that the signal vectors superimpose to one composite signal eigen vector and the resolved direction is for that composite signal. Therefore, with the conventional MUSIC algorithm, the AOAs of correlated source signals cannot be estimated by scanning the Vandermonde format steering vector $\mathbf{a}(\beta)$ in equation (2.3), because the direction matrix of correlated signals is no longer in the form of a Vandermonde matrix as in the uncorrelated signals case. An example is given in Section 4.4.2. The $M \times K$

direction matrix with the Vandermonde format has the following expression, as explained in detail in Section 4.2:

$$\begin{bmatrix} 1 & 1 & \cdots & 1 \\ x_1 & x_2 & \cdots & x_K \\ x_1^{\,2} & x_2^{\,2} & \cdots & x_K^{\,2} \\ \vdots & \vdots & \ddots & \vdots \\ x_1^{\,M-1} & x_2^{\,M-1} & \cdots & x_K^{\,M-1} \end{bmatrix}.$$

Spatial Smoothing Technique

Several alternatives have been proposed to deal with the singular covariance matrix of the correlated signals, including the *spatial smoothing* technique first studied by Evan et al (1981) and subsequently by Pillai & Kwon (1989) and Shan et al (1985). After the *spatial smoothing* technique is applied, the source signal covariance matrix becomes non-singular. The details are given in Section 4.5.1. Then the conventional MUSIC algorithm can still be used to estimate AOAs of correlated signals.

However it comes with the sacrifice of reducing the number of resolvable source signals. Given M array elements, the conventional MUSIC can resolve M-1 signals. For the *forward-only* smoothing scheme, it can resolve only $M/2$ signals. Because the size of each subarray m in the *forward-only* smoothing scheme must be at least $m = K + 1$ and the number of subarrays $L = M - m + 1$ must be greater than or equal to the number of signals K, i.e. $M - m + 1 >= K$ (Shan 1985), the resolvable number of signals is $K = M/2$. The forward-only spatial smoothing scheme trades off half the effective aperture. For a linear array, the aperture is equal to the distance between the elements on either side of

the array. In order to improve the resolving performance, the Forward/Backward Smoothing Technique was proposed.

Forward/Backward Smoothing Technique

Pillai & Kwon (1989) proved that the *forward/backward smoothing* scheme can resolve (2*M*/3) signals. In this forward/backward smoothing scheme, the number of subarrays is 2*L*. Similar to the forward-only spatial smoothing scheme, it requires $m = K + 1$ and $2*(M - m + 1) >= K$. Therefore, the resolvable number of signals is $K = (2M/3)$. The derivation of this requirement in terms of matrix algebra theory is given in Section 4.5.3. This improvement is not enough for multiple multipath signals environments. For example, in this research, the array elements $M = 5$ and only $K = 3$ signals can be resolved using the Forward/Backward Smoothing MUSIC. In order to overcome this limitation, the data to process is sampled at the initial rising part of the correlation function to make fewer number of signals included. This approach is applicable because multipath signals happen always later than LOS signals.

The performance of the super-resolution method is related with signal to noise ratio (SNR), the number of antenna elements, the number of samples (Friedlander & Porat 1989). The simulation and real data based experiment results are given in Chapter 7.

2.2.2 TOA/TDOA Technique and Algorithm

The measurements required in a TOA system are the absolute signal transmission times between MS and BSs that are equivalent to the MS-BS distances. The MS is located at

the intersection of several circles, of which the centres are the BSs, and the radii are the measured MS-BS distances. At least three TOA measurements are required to uniquely determine the 2-D position of an MS if the entire system is time for synchronized, as shown in Figure 2.5. The observation equations have the form

$$TOA_i = \sqrt{(X_{MS} - X_{BSi})^2 + (Y_{MS} - Y_{BSi})^2}$$

where i = 1, 2, 3.

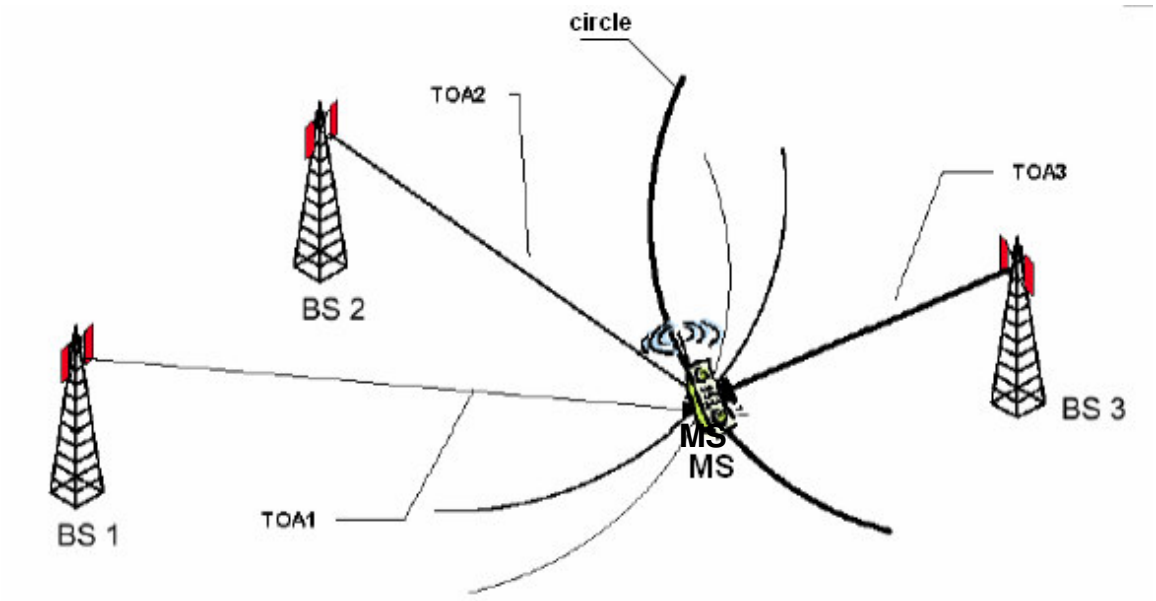

Figure 2.5: TOA Technique

The measurements in a TDOA system are the relative signal transmission times which are equivalent to the distance differences. A TDOA measurement defines a hyperbola with two BSs as the foci. At least three hyperbolae are needed for the unique MS position calculation if the network is synchronized, as shown in Figure 2.6. The observation equations have the following form

$$TDOA_{ij} = \sqrt{(X_{MS} - X_{BSi})^2 + (Y_{MS} - Y_{BSi})^2} - \sqrt{(X_{MS} - X_{BSj})^2 + (Y_{MS} - Y_{BSj})^2}$$

where $i \neq j$, and $i, j = 1, 2, 3$ respectively.

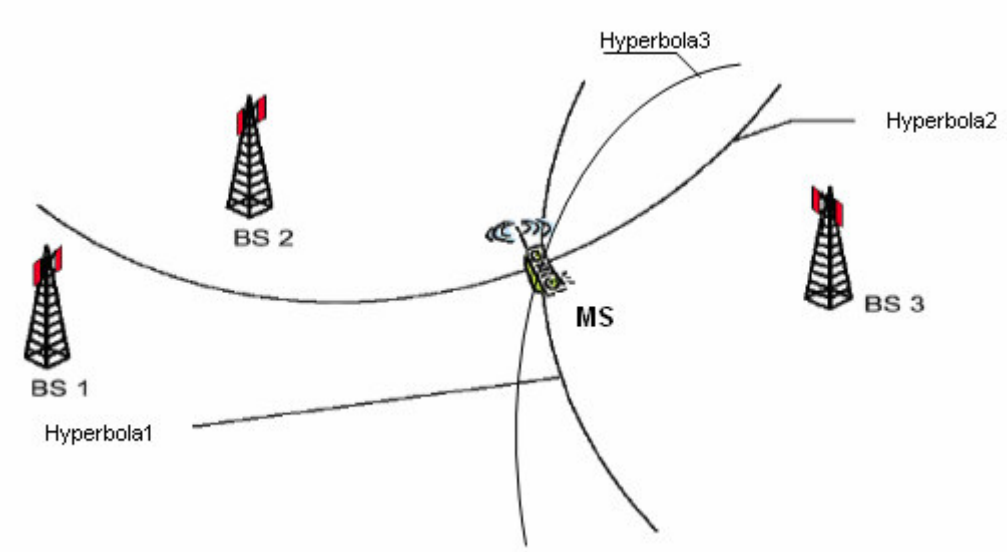

Figure 2.6: TDOA Technique

The conventional correlation-based TOA/TDOA estimation is degraded by multipath due to its limited resolution. The resolution is the chip duration T_c. In an IS-95 CDMA system, the chip duration is about 800 ns, which equals 240 m. So the correlation-based TOA/TDOA only method is not suitable for location in multipath environments. However if multipath can be mitigated from the received signal, the correlation-based method can still be used for TOA/TDOA estimation. Based on this point, the proposed method, as described in Chapter 1, is to estimate AOAs of multipath and mitigate them, and apply the correlation technique to estimate the TOA/TDOA. So it is necessary to investigate the IS-95 CDMA PN pilot signal correlation process.

IS-95 Pilot Signal from the Transmitter

The transmitted IS-95 pilot signal is formulated by the following expression:

$$s_T(t) = 2A\left[PN_I(t)\cos(2\pi f_c t) + PN_Q(t)\sin(2\pi f_c t)\right] \tag{2.4}$$

where $2A$ is the amplitude of the received signal, $PN_I(t)$ and $PN_Q(t)$ are the "*I*" and "*Q*" pilot sequences respectively, and f_c is the carrier frequency. The PN sequences are generated based on the characteristic polynomials as expressed by equation (2.1).

IS-95 Pilot Signal Impinging on the Receiver Antenna

Due to K multipath and transmission propagations at the receiver with M antenna elements mounted on a vehicle, the signal impinging on the jth sensor can be expressed as

$$s_j(t) = 2\sum_{i=1}^{K} A_i\left[PN_I(t-t_{d\,i})\cos(2\pi f_c t + \phi_j(i)) + PN_Q(t-t_{d\,i})\sin(2\pi f_c t + \phi_j(i))\right] \tag{2.5}$$

where $\phi_j(i)$ is the phase shift and $t_{d\,i}$ is the time delay of the ith multipath at sensor j.

The Demodulation of the Input Signal

For simplicity of signal analysis, only one source signal received by one antenna element is considered, as shown in Figure 2.7.

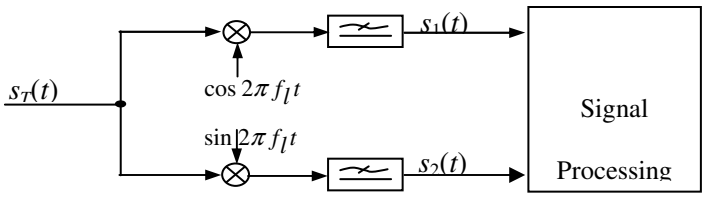

Figure 2.7: Demodulation of the IS-95 CDMA Signal

When the input signal goes through the down-mixers and low pass filters, the baseband signals for *I* and *Q* channels are obtained as follows:

$$\begin{aligned} s_1(t) &= A\left[PN_I(t-t_d)\cos(2\pi f_e t+\phi)+PN_Q(t-t_d)\sin(2\pi f_e t+\phi)\right] \\ s_2(t) &= A\left[-PN_I(t-t_d)\sin(2\pi f_e t+\phi)+PN_Q(t-t_d)\cos(2\pi f_e t+\phi)\right] \end{aligned} \tag{2.6}$$

where $f_e = f_c - f_l$ is the carrier frequency difference between the incoming signal and the local signal, t_d is the time delay and ϕ is the initial phase of the signal. Based on $s_1(t)$ and $s_2(t)$, the complex baseband signal $s_3(t)$ is as follows:

$$\begin{aligned} s_3(t) &= s_1(t) + j\, s_2(t) \\ &= A\left[PN_I(t-t_d) + j\, PN_Q(t-t_d)\right]\exp[-j(2\pi f_e t+\phi)] \end{aligned} \tag{2.7}$$

For multipath cases, the complex expression of $s_3(t)$ at the *j*th antenna element can be expressed as

$$s_{3,j}(t) = \sum_{i=1}^{K} A_i\left[PN_I(t-t_{di}) + j\, PN_Q(t-t_{di})\right]\exp[-j(2\pi f_e t+\phi_j(i))] \tag{2.8}$$

The Local Signal Generation for the Correlation Process

The local signal has the same form as that of the incoming signal, namely:

$$\begin{aligned} s_l(t) &= s_3(t)\big|_{A=1,t_d=0,f_e=\hat{f}_e,\phi=0} \\ &= \left[PN_I(t) + j\, PN_Q(t)\right]\exp[-j\,2\pi \hat{f}_e t] \\ &= \tilde{s}_l(t)\exp[-j\,2\pi \hat{f}_e t] \end{aligned} \tag{2.9}$$

Here f_e is replaced by the estimated carrier frequency difference $\hat{f}_e$, and

$\tilde{s}_l(t) = [PN_I(t) + j\,PN_Q(t)]$.

Time Domain Correlation Processing

In the time domain, the correlation between the received signal $s_3(t)$ and the local signal $s_l(t)$ is written as follows:

$$
\begin{aligned}
&r(\tau, \hat{f}_e) = \int_0^T s_3(t)\, s_l^*(t-\tau)dt = \int_0^T s_3(t)\, \tilde{s}_l^*(t-\tau)\exp[j2\pi \hat{f}_e(t-\tau)]dt \\
&= \int_0^T \Big[PN_I(t-t_d)PN_I(t-\tau) + PN_Q(t-t_d)PN_Q(t-\tau)\Big]\exp[-j(2\pi\Delta f_e t + \phi + 2\pi \hat{f}_e \tau)]dt \\
&\quad - j\int_0^T \Big[PN_I(t-t_d)PN_Q(t-\tau) - PN_I(t-\tau)PN_Q(t-t_d)\Big]\exp[-j(2\pi\Delta f_e t + \phi + 2\pi \hat{f}_e \tau)]dt \\
&\approx \exp[-j(2\pi \hat{f}_e \tau + \phi)] \int_0^T [PN_I(t-t_d)PN_I(t-\tau) + PN_Q(t-t_d)PN_Q(t-\tau)]\exp[-j2\pi\Delta f_e t]dt \\
&(\textit{cross correlation}: \int_0^T PN_I(t-t_d)PN_Q(t-\tau)dt \approx \int_0^T PN_I(t-\tau)PN_Q(t-t_d)dt \approx 0)
\end{aligned}
\tag{2.10}
$$

where T is the integration time and $\Delta f_e = f_e - \hat{f}_e$. Because the factor $\exp[-j2\pi \hat{f}_e \tau]$ does not affect the absolute value of $r(\tau, \hat{f}_e)$, the received signal can be modified by multiplying $s_3(t)$ with $\exp[j2\pi \hat{f}_e t]$ to yield:

$$
\begin{aligned}
\tilde{s}_3(t) &= s_3(t)\exp[j2\pi \hat{f}_e t] \\
&= A\Big[PN_I(t-t_d) + j\,PN_Q(t-t_d)\Big]\exp[-j(2\pi f_e t + \phi)]\exp[j2\pi \hat{f}_e t] \\
&= A\Big[PN_I(t-t_d) + j\,PN_Q(t-t_d)\Big]\exp[-j(2\pi \Delta f_e t + \phi)]
\end{aligned}
\tag{2.11}
$$

Then the correlation function $r(\tau, \hat{f}_e)$ in equation (2.10) can be simplified as follows:

$$
\begin{aligned}
r(\tau, \hat{f}_e) &= \int_0^T \tilde{s}_3(t)\, \tilde{s}_l^{*}(t-\tau)dt \\
&= \int_0^T A\left[PN_I(t-t_d) + j\, PN_Q(t-t_d)\right]\exp[-j(2\pi\Delta f_e\, t + \phi)]\, [PN_I(t-\tau) - j\, PN_Q(t-\tau)]dt \\
&= A\exp[-j\phi]\int_0^T [PN_I(t-t_d)PN_I(t-\tau) + PN_Q(t-t_d)PN_Q(t-\tau)]\exp[-j\,2\pi\Delta f_e t]dt
\end{aligned}
\tag{2.12}
$$

When $\tau = t_d$, it becomes the expression of the correlation peak value. The effect of Δf_e can be seen as follows:

$$
\begin{aligned}
& r(t_d, \hat{f}_e) \\
&= \exp[-j\phi]\int_0^T [PN_I(t-t_d)PN_I(t-t_d) + PN_Q(t-t_d)PN_Q(t-t_d)\exp[-j\,2\pi\Delta f_e t]dt\Big|_{\tau=0} \\
&= 2\exp[-j\phi]\frac{\exp[-j\,2\pi\Delta f_e T]-1}{-j\,2\pi\Delta f_e} = 2\exp[-j(\pi\Delta f_e T + \phi)]\frac{\sin(\pi\Delta f_e T)}{\pi\Delta f_e} \\
&= 2T\,\mathrm{sinc}(\pi\Delta f_e T)\exp[-j(\pi\Delta f_e T + \phi)]
\end{aligned}
\tag{2.13}
$$

Frequency Domain Correlation Processing

When the modified complex incoming signal $\tilde{s}_3(t) = s_3(t)\exp[j2\pi\hat{f}_e t]$ and the simplified local complex signal $\tilde{s}_l(t) = [PN_I(t) + j\, PN_Q(t)]$ are sampled, the discrete signals $\tilde{s}_3(n)$ and $\tilde{s}_l(n)$ can be obtained (n = 0, 1, …, N -1). If the length of the local signal snapshot $\tilde{s}_l(n)$ is a multiple number of IS-95 pilot PN sequence period, for example three periods of IS-95 pilot PN sequences, the correlation function between the received signal $\tilde{s}_3(n)$ and the local signal $\tilde{s}_l(n)$ can be calculated by circular convolution correctly, which can also be implemented by FFT in the frequency domain as expressed below (Philips 2003):

$$r(m,\hat{f}_e)=\sum_{n=0}^{N-1}\tilde{s}_3(n)\tilde{s}_l(n-m)=\mathrm{DF}^{-1}\left[\tilde{S}_3(k)\tilde{S}_l^{*}(k)\right] \tag{2.14}$$

where the symbols DF^{-1} and $()^{*}$ represent the inverse discrete Fourier transform (DFT) and the complex conjugate respectively, m is the time delay, $\tilde{S}_3(k)$ and $\tilde{S}_l(k)$ are the DFT of $\tilde{s}_3(n)$ and $\tilde{s}_l(n)$ respectively. The proof of equation (2.14) is given in Appendix A.

It should be noted that this DFT method cannot give a good resolution. However, the correlation terms are sufficient statistics, i.e. no loss of mutual information. So it is effective for rapid coarse acquisition. In this research, the DFT method is used in the first step to roughly locate the correlation peak, followed by the AOA estimation to mitigate multipath and finally by the correlation peaks detection for TOA/TDOA estimation with multipath mitigated.

2.3 Dilution of Precision

In terrestrial TOA systems, if three base stations are observed, then we can obtain three pseudorange measurements as follow.

$$\begin{aligned}\rho_1&=\sqrt{(x_1-x_u)^2+(y_1-y_u)^2}+ct_u\\ \rho_2&=\sqrt{(x_2-x_u)^2+(y_2-y_u)^2}+ct_u\\ \rho_3&=\sqrt{(x_3-x_u)^2+(y_3-y_u)^2}+ct_u\end{aligned} \tag{2.15}$$

where $\rho_j (j = 1, 2, 3)$ is the pseudorange, and (x_u, y_u) and t_u are unknown 2D user positions and the local clock offset, respectively. $(x_j, y_j)(j = 1, 2, 3)$ are the known *j*th base station's position coordinates in two dimensions and c is the speed of light. For 3D user positioning, one more pseudorange measurement is required and the coordinate of the unknown user positions becomes (x_u, y_u, z_u).

After the linearization of equation (2.15) by using a truncated Taylor series around an approximate position location $(\hat{x}_u, \hat{y}_u)$ and time bias estimate $\hat{t}_u$, the correction to that approximate value is solved as (Kaplan 2005):

$$\hat{\rho}_j - \rho_j = \frac{x_j - \hat{x}_u}{\hat{r}_j}\Delta x_u + \frac{y_j - \hat{y}_u}{\hat{r}_j}\Delta y_u - c t_u \tag{2.16}$$

where $\hat{\rho}_j = \sqrt{(x_j - \hat{x}_u)^2 + (y_j - \hat{y}_u)^2} + c\hat{t}_u \quad (j = 1, 2, 3)$,

$$\hat{r}_j = \sqrt{(x_j - \hat{x}_u)^2 + (y_j - \hat{y}_u)^2} \quad (j = 1, 2, 3),$$

$$\begin{aligned} \Delta x_u &= x_u - \hat{x}_u \\ \Delta y_u &= y_u - \hat{y}_u \end{aligned}.$$

Equation (2.16) can be simplified as follow.

$$\Delta\boldsymbol{\rho} = \mathbf{H}\Delta\mathbf{x} \tag{2.17}$$

or

$$\Delta\mathbf{x} = \mathbf{H}^{-1}\Delta\boldsymbol{\rho} \tag{2.18}$$

where $\Delta\boldsymbol{\rho} = \begin{bmatrix} \Delta\rho_1 \\ \Delta\rho_2 \\ \Delta\rho_3 \end{bmatrix}$ is a vector of differences between the real range measurements and

the expected ranges at the guess position, $\Delta\mathbf{x} = \begin{bmatrix} \Delta x_u \\ \Delta y_u \\ -c\Delta t_u \end{bmatrix}$ a position vector and receiver clock corrections, $\mathbf{H} = \begin{bmatrix} \frac{x_1 - \hat{x}_u}{\hat{r}_1} & \frac{y_1 - \hat{y}_u}{\hat{r}_1} & 1 \\ \frac{x_2 - \hat{x}_u}{\hat{r}_2} & \frac{y_2 - \hat{y}_u}{\hat{r}_2} & 1 \\ \frac{x_3 - \hat{x}_u}{\hat{r}_3} & \frac{y_3 - \hat{y}_u}{\hat{r}_3} & 1 \end{bmatrix}$ is a 3×3 matrix of coefficients.

When more than three base stations are used, $\mathbf{H}$ is non-square and the least-squares of residuals principle is applied as:

$$\Delta\mathbf{x} = (\mathbf{H}^T\mathbf{H})^{-1}\mathbf{H}^T\Delta\boldsymbol{\rho} \tag{2.19}$$

The covariance matrix $C_{\Delta\mathbf{x}}$ of $\Delta\mathbf{x}$ is given by the following equation:

$$C_{\Delta\mathbf{x}} = \begin{bmatrix} \sigma_x{}^2 & 0 \\ 0 & \sigma_y{}^2 \end{bmatrix} = E[(\mathbf{H}^T\mathbf{H})^{-1}\mathbf{H}^T\Delta\boldsymbol{\rho}\ \ \Delta\boldsymbol{\rho}^T\mathbf{H}(\mathbf{H}^T\mathbf{H})^{-1}] = (\mathbf{H}^T\mathbf{H})^{-1}\ \sigma_r{}^2 \tag{2.20}$$

The assumption of the above formula is that the measurements x_u and y_u are uncorrelated, the measurements of $\Delta\boldsymbol{\rho}$ are also uncorrelated and have a diagonal $E[\Delta\boldsymbol{\rho}\ \ \Delta\boldsymbol{\rho}^T]$ with identical elements $\sigma_r{}^2$.

The standard deviation of the final position estimate, σ_p, and the standard deviation of the ranging estimate, σ_r, have the following relationship:

$$\sigma_p = \sqrt{\sigma_x{}^2 + \sigma_y{}^2} = \sqrt{trace((\mathbf{H}^T\mathbf{H})^{-1})}\sigma_r \tag{2.21}$$

By definition the Dilution of Precision (DOP) is as follow (Lachapelle 1998):

$$DOP = \sqrt{trace((\mathbf{H}^T\mathbf{H})^{-1})}\ . \tag{2.22}$$

One also has

$$\sigma_p = DOP\sigma_r . \tag{2.23}$$

It can be seen from the above formula that DOP affects the position accuracy.

For a TDOA system, the DOP calculation is similar except for that the receiver time offset term included in the matrix $\mathbf{H}$ disappears because the differencing of two measurements deletes that common term.

For an AOA system, the DOP can still be calculated by using equation (2.22). However the matrix $\mathbf{H}$ needs to be reconstructed in terms of angles and the standard deviation of the ranging estimate, σ_r, is replaced by the standard deviation of the angle estimate, σ_β (Dempster 2006), that is

$$\sigma_p = DOP\ \sigma_\beta . \tag{2.24}$$

2.4 Literature Review of the Previous Research in CDMA-based Location Systems

The research and development on mobile-communication networks-based location system has been active for the past few decades. Compared with GPS, cellular network-based wireless location is deteriorated in accuracy because of detectability (Reed et al 1998, Ma 2003), which is the ability of a sufficient number of different base stations to detect the user's signal at an acceptable power level, and multipath, which can highly degrade both TOA and AOA estimations (Krizman et al 1997). Therefore, recent research has focused on solving theses problems.

Yousef et al (1999) introduced a power delay profile (PDP) to estimate time-delays and amplitudes for an IS-95 CDMA system. The PDP was built by generating a group of correlation functions with each separated by a fraction of a chip period. Then the earliest arriving ray is selected from the PDP by the earliest correlation peak. The corresponding time offset of the local PN code is the TOA estimate.

Kalman filter-based methods were described by Thomas et al (2001). The proposed method was based on three stages: prefiltering of measurement data to remove NLOS data as much as possible and smooth sampling measurement noise; TDOA-based location estimation using standard weighted least-squares (WLS) solution or Chan's method (Chan 1994); KF tracking to provide a continuous location estimation.

In the paper by Tarighat et al (2003), a parametric method based on Maximum Likelihood for TOA estimates and a Least-Squares method for AOA estimates were discussed for a CDMA2000 system. This method has a heavy computational load due to a multi-dimensional search for the parameters.

Klukas (1997) proposed a Root-MUSIC-based algorithm to estimate the TOA for locating 911 caller in AMPS network which is an analog system deployed in 1984.

Kim (2004) proposed a MUSIC-based algorithm for multipath timing estimation in CDMA system. It investigates how the number of antenna elements affects the

performance. It mainly benefits the capacity improvement under multipath fading channel.

The recent published research by Falletti et al (2006) applied an array of sensors placed on a mobile vehicle to perform self-localization based on AOA-only method with beam-space root MUSIC algorithm (Zoltowski et al 1993). This system focused on practical design and did not much explored multipath mitigation and it was still based on simulation results.

Most of the proposed methods above were network-based schemes and verified from the simulation results. One paper from Wang et al (1994) proposed a method to improve the AOA estimation based on real data from a VHF system. Numerous papers were based on the AOA-only or the TOA-only method. There were also numerous papers estimating both AOA and TOA values from modified MUSIC algorithms since array signal contains both spatial and temporal information (Wang et al 2001, Van der Veen et al 1997, Zoltowski et al 1996).

In this research, a practical method to estimate TOA assisted by AOA information under multipath environment is proposed. AOA values are estimated using an F/B smooth MUSIC algorithm and TOAs are estimated based on the correlation function's rising part. The data for the algorithm verification is collected using an IS-95 CDMA receiver prototype developed by the PLAN Group (Shanmugam et al 2005).

2.5 Conclusions

The characteristics of CDMA system and IS-95 CDMA were introduced in this chapter. The signal to be processed is the forward link pilot PN sequences from IS-95 CDMA base stations. The location techniques of AOA and TOA / TDOA method were discussed. For AOA estimation, the forward/backward smoothing MUSIC algorithm is used because it can resolve fully correlated signals, such as multipath signals and because it is computationally efficient compared with a multiple dimensional search Maximum Likelihood method. The array data processed in an AOA algorithm is sampled from the auto-correlation functions of PN sequences in an antenna array with five elements. That is how the forward/backward smoothing MUSIC algorithm is applied using the limited number of antenna elements. The detailed discussion of the forward/backward smoothing MUSIC algorithm is given in Chapter 4. For TOA / TDOA estimation, the limitations of TOA / TDOA-only method under multipath environments were described. An AOA-assisted TOA / TDOA method was proposed, which is discussed in detail in Chapter 5. The correlation process of the IS-95 CDMA pilot signal is investigated because the data to be processed either by the AOA or TOA / TDOA algorithm are basically from correlation functions of IS-95 PN sequences. The location accuracy is affected by both the AOA/TOA / TDOA measurement accuracy and the DOP. So DOP calculations under different location techniques were derived. Finally a literature review was provided and the AOA-assisted TOA method proposed in this thesis was introduced.

Chapter Three: Theoretical Analysis of Signal Parameter Estimator

3.1 Introduction

Based on the discussion of location errors in Chapter 2, it is clear that the measurement accuracies of AOA and TOA are very important for position estimation. Therefore it is necessary to analyze the AOA and TOA estimation accuracy. Actually, AOA and TOA are the unknown parameters of the received signals and they can be estimated with some algorithms or estimators, for example, ML (Maximum Likelihood) estimator and MUSIC (MUltiple SIgnal Classification) estimator. The studies of estimator performance are within the scope of estimation theory. In this chapter, the analysis of the AOA and TOA estimation performance is based on the unbiased estimator and the Cramer-Rao Lower Bound (CRLB). The CRLB of the AOA estimation and the TOA estimation for a single IS-95 pilot signal are derived separately. The CRLB of the AOA estimation for multiple IS-95 pilot signals is based on Stoica & Nehorai (1989).However, the investigation is carried out further to find out that the AOA CRLB is affected by the angle of the incident rays and that different initial phase of the incident rays results in minimum and maximum CRLBs and that decreasing the number of source signals is more efficient than increasing the SNR which also becomes the impetus of the proposed correlation function rising slope-based method. Finally, the joint AOA and TOA estimation is investigated for comparison. The performances of specific MUSIC approaches for the AOA and AOA-assisted TOA estimators are analyzed in Chapter 4 and Chapter 5, respectively.

3.2 The Parameterized PDF and Unbiased Estimators

3.2.1 The Parameterized PDF

Because the noise $\mathbf{n}(t)$ at different antenna elements is random, so the received signals at different antenna elements $\mathbf{u}(t) = \mathbf{s}(t) + \mathbf{n}(t)$, where $\mathbf{s}(t)$ is source signal, are also random. The random data is described by its probability density function (PDF) with the unknown parameter θ. The PDF with the unknown parameter θ is called the parameterized PDF, denoted by $p(\mathbf{x};\theta)$. If there are *N*-point data set $\{x[0], x[1], \cdots, x[N-1]\}$ at one antenna, which results in a data column vector $\mathbf{x} = [x[0], x[1], \cdots, x[N-1]]^T$, its parameterized PDF can be expressed as:

$$p(\mathbf{x};\theta) = p(x[0], x[1], \cdots, x[N-1]; \theta) \tag{3.1}$$

where a semicolon is used to denote the dependence on the unknown parameter θ.

For White Gaussian Noise (WGN) $w[n]$, its dependence on the parameterized PDF on the unknown noise variance σ^2 is that the smaller noise variance σ^2 results in the narrower PDF $p(w[n];\sigma^2)$.

3.2.2 Unbiased Estimators

Because of noise, the estimator can not always yield the true value of the unknown parameters. If the estimator can yield the true value θ *on the statistic average*

(expectation), it means that the estimated parameter $\hat{\theta}$ is expected to be around θ as formula:

$$E(\hat{\theta}) = \theta \qquad a < \theta < b\,, \tag{3.2}$$

where (a, b) denotes the range of possible values of θ. This kind of estimators is called *unbiased estimators*.

If the estimated parameter $\hat{\theta}$ is a function of the data vector $\mathbf{x}$ as $\hat{\theta} = g(\mathbf{x})$, the mathematical definition of the unbiased estimator $g(\mathbf{x})$ can be expressed as:

$$E(\hat{\theta}) = \int g(\mathbf{x})\, p(\mathbf{x};\theta) d\mathbf{x} = \theta \qquad \textit{for all } \theta \tag{3.3}$$

Example of An Unbiased Estimator for Noise Variance

In practice, we need to estimate the unknown parameters without bias. In order to carry on the constant false alarm detection of the correlation peak of IS-95 pilot signal, we need to know the variance of the noise before despreading. Usually, the signal of input IS-95 pilot signals at the antenna elements can be as small as -120 dBm, thus the signal component $s[n]$ in the measured data $x[n]$ can be ignored, which can be expressed as:

$$x[n] = s[n] + w[n] \approx w[n] \qquad n = 1, 2, \cdots, N-1\,. \tag{3.4}$$

Assuming that the noise samples $\{w[0], w[1], \cdots, w[N-1]\}$ are independently and identically distributed (*iid*) Gaussian noise with zero mean as $\mathcal{N}(0,\ \sigma^2)$, the noise variance σ^2 can be estimated by:

$$\hat{\sigma^2} = \frac{1}{N}\sum_{n=0}^{N-1} x^2[n] = \frac{1}{N}\mathbf{x}^T\mathbf{x} \tag{3.5}$$

It can be easily proven that the estimator implemented by equation (3.5) is unbiased due to zero mean of $\mathbf{x}$. It will be shown later on in equations (3.6) and (3.12) that it is actually optimal.

In addition to the unbiasedness, we are also interested in the variance of the estimated parameter. The variance of the estimated parameter presents the degree of estimation error. The smaller the variance of the estimated parameter is, the larger the probability of obtaining the true value is. As $\mathbf{x}$ is zero mean, $E(x^4[n]) = 3\sigma^4$ (Kay 1998), the variance of $\hat{\sigma^2}$ can be derived as:

$$\begin{aligned}
\mathrm{var}(\hat{\sigma^2}) &= E[(\hat{\sigma^2} - \sigma^2)^2] \\
&= \int_{-\infty}^{\infty} \left(\frac{1}{N}\mathbf{x}^T\mathbf{x} - \sigma^2\right)^2 \frac{1}{\left(\sqrt{2\pi}\sigma\right)^N} \exp\left(-\frac{\mathbf{x}^T\mathbf{x}}{2\sigma^2}\right) d\mathbf{x} \\
&= \int_{-\infty}^{\infty} \left[\left(\frac{1}{N}\mathbf{x}^T\mathbf{x}\right)^2 - \frac{2\sigma^2}{N}\mathbf{x}^T\mathbf{x} + \sigma^4\right] \frac{1}{\left(\sqrt{2\pi}\sigma\right)^N} \exp\left(-\frac{\mathbf{x}^T\mathbf{x}}{2\sigma^2}\right) d\mathbf{x} \\
&= \frac{2}{N}\sigma^4
\end{aligned} \tag{3.6}$$

It shows that when $N \to \infty$, $\mathrm{var}(\hat{\sigma^2}) = 0$. Now the questions are: what is the minimum variance of the estimated parameter and can this estimator reach that minimum variance? To answer these questions, let us investigate the Cramer-Rao Lower Bound.

3.3 Cramer-Rao Lower Bound (CRLB)

3.3.1 Cramer-Rao Lower Bound – for a Scalar Parameter

If the PDF satisfies the "regularity" condition (Kay 1998) expressed as:

$$E\left[\frac{\partial \ln p(\mathbf{x};\theta)}{\partial \theta}\right] = 0 \quad for\ all\ \theta \tag{3.7}$$

where the expectation is taken with respect to the parameterized PDF $p(\mathbf{x};\theta)$, then the variance of any unbiased estimator $\hat{\theta}$ must satisfy the following CRLB:

$$\text{var}(\hat{\theta}) \geq \frac{1}{-E\left[\frac{\partial^2 \ln p(\mathbf{x};\theta)}{\partial \theta^2}\right]} \tag{3.8}$$

The expectation in (3.8) is also taken with respect to the parameterized PDF $p(\mathbf{x};\theta)$:

$$E\left[\frac{\partial^2 \ln p(\mathbf{x};\theta)}{\partial \theta^2}\right] = \int \frac{\partial^2 \ln p(\mathbf{x};\theta)}{\partial \theta^2} p(\mathbf{x};\theta)\, d\mathbf{x} \tag{3.9}$$

Now let us have a look at the Cramer-Rao Lower Bound for the above example of estimating the noise variance σ^2. The parameterized PDF $p(\mathbf{x};\theta)\Big|_{\theta=\sigma^2}$ can be written as:

$$p(\mathbf{x};\sigma^2) = \frac{1}{\left(\sqrt{2\pi\sigma}\right)^N} \exp\left(-\frac{\mathbf{x}^T\mathbf{x}}{2\sigma^2}\right). \tag{3.10}$$

The second derivative of the logarithm of $p(\mathbf{x};\sigma^2)$ can be expressed as:

$$\frac{\partial^2 \ln p(\mathbf{x};\sigma^2)}{\partial(\sigma^2)^2} = \frac{N}{2\sigma^4} - \frac{\mathbf{x}^T\mathbf{x}}{\sigma^6}. \tag{3.11}$$

Then the Cramer-Rao Lower Bound of estimating the noise variance σ^2 is:

$$\text{var}(\hat{\sigma^2}) \geq \frac{1}{-E\left[\frac{\partial^2 \ln p(\mathbf{x};\sigma^2)}{\partial(\sigma^2)^2}\right]} = \frac{2\sigma^4}{N}. \tag{3.12}$$

So, the unbiased estimator expressed by equation (3.5) is optimal because its estimated variance given in equation (3.6) reaches the above Cramer-Rao Lower Bound.

If the fundamental parameter is θ and the desired parameter is $\alpha = g(\theta)$, then the CRLB of the unbiased estimator is:

$$\text{var}(\hat{\alpha}) \geq \frac{\left(\frac{\partial g(\theta)}{\partial \theta}\right)^2}{-E\left[\frac{\partial^2 \ln p(\mathbf{x};\theta)}{\partial \theta^2}\right]}. \tag{3.13}$$

3.3.2 Cramer-Rao Lower Bound for a Vector Parameter

When there are p parameters $\{\theta_1, \theta_2, \cdots, \theta_p\}$ to be estimated, the Cramer-Rao Lower Bound should be extended to a vector parameter $\boldsymbol{\theta} = [\theta_1, \theta_2, \cdots, \theta_p]^T$. Assuming that the estimator $\hat{\boldsymbol{\theta}}$ is unbiased, i.e.,

$$E(\hat{\boldsymbol{\theta}}) = \begin{bmatrix} E(\hat{\theta}_1) \\ E(\hat{\theta}_2) \\ \vdots \\ E(\hat{\theta}_p) \end{bmatrix} = \begin{bmatrix} \theta_1 \\ \theta_2 \\ \vdots \\ \theta_p \end{bmatrix} = \boldsymbol{\theta} \tag{3.14}$$

and the "regularity" condition is satisfied (Kay 1998):

$$E\left[\frac{\partial \ln p(\mathbf{x};\boldsymbol{\theta})}{\partial \boldsymbol{\theta}}\right] = \mathbf{0} \quad or \quad E\begin{bmatrix} \frac{\partial \ln p(\mathbf{x};\boldsymbol{\theta})}{\partial \theta_1} \\ \frac{\partial \ln p(\mathbf{x};\boldsymbol{\theta})}{\partial \theta_2} \\ \vdots \\ \frac{\partial \ln p(\mathbf{x};\boldsymbol{\theta})}{\partial \theta_p} \end{bmatrix} = \begin{bmatrix} 0 \\ 0 \\ \vdots \\ 0 \end{bmatrix} \tag{3.15}$$

then the CRLB of the parameter θ_i is the $[i,i]$ element of the inverse of the *Fisher information matrix* $\mathbf{J}(\boldsymbol{\theta})$, which can be mathematically expressed as:

$$\text{var}(\hat{\theta}_i) \geq [\mathbf{J}^{-1}(\boldsymbol{\theta})]_{i\,i} \tag{3.16}$$

where $\mathbf{J}(\boldsymbol{\theta})$ is a $p \times p$ matrix, which is defined as:

$$[\mathbf{J}(\boldsymbol{\theta})]_{i\,j} = -E\left[\frac{\partial^2 \ln p(\mathbf{x};\boldsymbol{\theta})}{\partial \theta_i\, \partial \theta_j}\right] \quad for\ i = 1, 2, \cdots, p; \quad j = 1, 2, \cdots, p. \tag{3.17}$$

More generally, *the covariance matrix of the unbiased estimator* $\hat{\boldsymbol{\theta}}$ satisfies:

$$\mathbf{C}_{\hat{\boldsymbol{\theta}}} - \mathbf{J}^{-1}(\boldsymbol{\theta}) \geq \mathbf{0} \tag{3.18}$$

When r parameters to be estimated are the functions of p fundamental parameters $\boldsymbol{\theta} = [\theta_1, \theta_2, \cdots, \theta_p]^T$ as:

$$\begin{aligned} \boldsymbol{\alpha} &= [\alpha_1, \alpha_2, \cdots, \alpha_r]^T \\ &= \begin{bmatrix} g_1(\boldsymbol{\theta}) \\ g_2(\boldsymbol{\theta}) \\ \vdots \\ g_r(\boldsymbol{\theta}) \end{bmatrix} \\ &= \mathbf{g}(\boldsymbol{\theta}) \end{aligned}, \tag{3.19}$$

the CRLB of the unbiased estimator for $\boldsymbol{\alpha}$ is:

$$\begin{aligned} &\text{var}(\hat{\alpha}_i) \geq [\frac{\partial \mathbf{g}(\boldsymbol{\theta})}{\partial \boldsymbol{\theta}} \mathbf{J}^{-1}(\boldsymbol{\theta}) \frac{\partial \mathbf{g}(\boldsymbol{\theta})^T}{\partial \boldsymbol{\theta}}]_{i\,i} \quad (i = 1,2,\cdots r) \\ &or \\ &\mathbf{C}_{\hat{\boldsymbol{\alpha}}} - \frac{\partial \mathbf{g}(\boldsymbol{\theta})}{\partial \boldsymbol{\theta}} \mathbf{J}^{-1}(\boldsymbol{\theta}) \frac{\partial \mathbf{g}(\boldsymbol{\theta})^T}{\partial \boldsymbol{\theta}} \geq \mathbf{0} \end{aligned} \tag{3.20}$$

where $\mathbf{C}_{\hat{\boldsymbol{\alpha}}}$ is *the covariance matrix of the unbiased estimator* $\hat{\boldsymbol{\alpha}}$; and $\frac{\partial \mathbf{g}(\boldsymbol{\theta})}{\partial \boldsymbol{\theta}}$ is an $r \times p$ Jacobian matrix defined as:

$$\frac{\partial \mathbf{g}(\boldsymbol{\theta})}{\partial \boldsymbol{\theta}} = \begin{bmatrix} \frac{\partial g_1(\boldsymbol{\theta})}{\partial \theta_1} & \frac{\partial g_1(\boldsymbol{\theta})}{\partial \theta_2} & \cdots & \frac{\partial g_1(\boldsymbol{\theta})}{\partial \theta_p} \\ \frac{\partial g_2(\boldsymbol{\theta})}{\partial \theta_1} & \frac{\partial g_2(\boldsymbol{\theta})}{\partial \theta_2} & \cdots & \frac{\partial g_2(\boldsymbol{\theta})}{\partial \theta_p} \\ \vdots & \vdots & \ddots & \vdots \\ \frac{\partial g_r(\boldsymbol{\theta})}{\partial \theta_1} & \frac{\partial g_r(\boldsymbol{\theta})}{\partial \theta_2} & \cdots & \frac{\partial g_r(\boldsymbol{\theta})}{\partial \theta_p} \end{bmatrix}. \tag{3.21}$$

3.4 The Data Model for AOA and TOA Estimation

In this thesis, the estimation of signal parameters is focused on AOA and TOA with a uniform linear antenna array showed in Figure 3.1. The antenna array consists of M identical elements and receives K narrow-band signals that arrive at the array from directions $\beta_1,\ \beta_2,\ \cdots,\ \beta_K$.

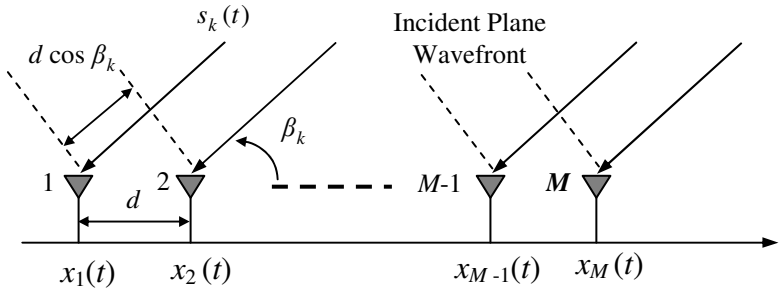

Figure 3.1: Uniform Linear Array

If the first element is taken as a reference point and K signals $s_1(t), s_2(t), \cdots, s_K(t)$ are complex, the output data of the array is an $M \times 1$ complex vector $\mathbf{x}(t)$. For the signal source $s_k(t)$, the array output vector $\mathbf{x}(t)$ can be expressed as:

$$\mathbf{x}(t) = \begin{bmatrix} x_1(t) \\ x_2(t) \\ \vdots \\ x_M(t) \end{bmatrix} = \begin{bmatrix} s_k(t) \\ s_k(t-\tau) \\ \vdots \\ s_k(t-(M-1)\tau) \end{bmatrix} + \begin{bmatrix} n_1(t) \\ n_2(t) \\ \vdots \\ n_M(t) \end{bmatrix} = \begin{bmatrix} 1 \\ e^{-j2\pi f_c \tau} \\ \vdots \\ e^{-j2\pi f_c (M-1)\tau} \end{bmatrix} s_k(t) + \begin{bmatrix} n_1(t) \\ n_2(t) \\ \vdots \\ n_M(t) \end{bmatrix}$$
$$= \mathbf{a}(\beta_k)\, s_k(t) + \mathbf{n}(t) \qquad (3.22)$$

where $\mathbf{a}(\beta_k) = \left[1,\ e^{-j2\pi f_c \tau}, \ldots, e^{-j2\pi f_c (M-1)\tau}\right]^T$ is an $M \times 1$ vector called the *direction vector*; the symbol (T) denotes transpose; f_c is the carrier frequency of the incident signals; $\tau = \dfrac{d * \cos(\beta_k)}{c}$ is the delay between two elements; d is the antenna element space; $\mathbf{n}(t)$ is the $M \times 1$ complex noise vector which comes from the devices in the receiver. The noise at different antenna elements can be assumed to be *iid* zero-mean Gaussian stationary random process. Meanwhile, the noises are uncorrelated with the impinging signals.

If d is equal to q times of the carrier wavelength λ, the direction vector can be written as:

$$\begin{aligned}
\mathbf{a}(\beta_k) &= \left[1,\ e^{-j2\pi\ q\cos\beta_k}, \ldots, e^{-j2\pi(M-1)\ q\cos\beta_k}\right]^T \\
&= \left[1,\ e^{-j\varphi_k}, \ldots, e^{-j_c(M-1)\ \varphi_k}\right]^T \\
&= \left[1, a_{\ k}, a_k^2, \cdots, a_k^{M-1}\right]^T \\
&= \{a_k^i\} \\
&\qquad i = 0, 2, \cdots, M-1
\end{aligned} \tag{3.23}$$

where $q = \dfrac{d}{\lambda}$; $a_k^i = e^{-j2\pi\ i\ q\ \cos\beta_k} = e^{-j\,i\,\varphi_k}$; $\varphi_k = 2\pi\ q\ \cos\beta_k$ which is called the phase delay with respect to the adjacent element.

For K signal sources, the $M \times 1$ array output vector can be expressed as:

$$\mathbf{x}(t) = \mathbf{a}(\beta_1)\, s_1(t) + \ldots + \mathbf{a}(\beta_K)\, s_K(t) + \mathbf{n}(t) = \sum_{i=1}^{K} \mathbf{a}(\beta_i)\, s_i(t) + \mathbf{n}(t)$$

$$= [\mathbf{a}(\beta_1), \mathbf{a}(\beta_2), \ldots, \mathbf{a}(\beta_K)] \begin{bmatrix} s_1(t) \\ s_2(t) \\ \vdots \\ s_K(t) \end{bmatrix} + \begin{bmatrix} n_1(t) \\ n_2(t) \\ \vdots \\ n_M(t) \end{bmatrix}$$

$$= \mathbf{A}\,\mathbf{s}(t) + \mathbf{n}(t)$$

and

$$\boldsymbol{\varphi} = [\varphi_1, \varphi_2, \cdots, \varphi_K]^T \tag{3.24}$$

where

$\varphi_k = 2\pi\, q \cos\beta_k$;

$M = No.\ of\ antenna\ elements; K = No.\ of\ source\ signals.$

where $\mathbf{A} = [\mathbf{a}(\beta_1), \mathbf{a}(\beta_2), \ldots, \mathbf{a}(\beta_K)]$ is an $M \times K$ direction matrix with a Vandermonde-structure (*columns are not linearly related if* $\beta_1, \beta_2, \cdots, \beta_K$ *are different*) and $\mathbf{s}(t) = [s_1(t), \ldots, s_K(t)]^T$ is a $K \times 1$ signal vector. The equation (3.24) is in continuous time. In the following Sections (3.5, 3.6 and 3.7) however, the discussions are all in discrete time.

Assuming that the *I* and *Q* base band outputs of the antenna array are corrupted by *iid* Gaussian noise with zero mean and known variance $\sigma^2/2$, $\mathcal{N}(0, \sigma^2/2)$, then the parameterized PDF $p(\mathbf{x};\boldsymbol{\theta})$ with *M* real and *M* imaginary random variables can be written as (Proakis 2001):

$$p(\mathbf{x};\boldsymbol{\theta}) = p\big(\mathrm{Re}(\mathbf{x}), \mathrm{Im}(\mathbf{x});\boldsymbol{\theta}\big)$$

$$= \frac{1}{\left(\sqrt{\pi\sigma^2}\right)^{2M}} \exp\left\{-\frac{[\mathbf{x}-\mathbf{A}\mathbf{s}]^H[\mathbf{x}-\mathbf{A}\mathbf{s}]}{\sigma^2}\right\} \tag{3.25}$$

The investigation of the CRLB for AOA and TOA is based on the above equation.

3.5 CRLB of AOA Estimation for a Single IS-95 Pilot Signal

In this section, one sample of single dispread IS-95 pilot signal is used to estimate AOA CRLB. The derivation is contributed by the author. The case of multiple samples of multi-sources is discussed in Section 3.6. Assume that the received dispread signal $\mathbf{x}(t)$ is a complex signal with I and Q components. If $\mathbf{x}(t)$ is sampled at one time point of t_0 and the source signal is $s(t)$ with the incident angle of β, then equation (3.24) can be simplified as:

$$\begin{aligned}\mathbf{x}(t_0) &= \mathbf{A}\, s(t_0) + \mathbf{n}(t_0) \\ &= \begin{bmatrix} 1 \\ e^{-j\varphi} \\ \vdots \\ e^{-j(M-1)\varphi} \end{bmatrix} s(t_0) + \begin{bmatrix} n_1(t_0) \\ n_2(t_0) \\ \vdots \\ n_M(t_0) \end{bmatrix}\end{aligned} \tag{3.26}$$

where

$$\varphi = 2\pi \frac{d}{\lambda} \cos\beta \quad \text{(referring to equation (3.23))} \tag{3.27}$$

$$\begin{aligned} s(t_0) &= \gamma[PN_I(t_0) + jPN_Q(t_0)]e^{j\phi}[PN_I(t_0) - jPN_Q(t_0)] \\ &= 2\gamma e^{j\phi} \\ n_m(t_0) &= [n_I(t_0) + jn_Q(t_0)][PN_I(t_0) - jPN_Q(t_0)] \quad m = 1, 2, ..., M \end{aligned} \tag{3.28a}$$

The signal to noise ratio of the dispread signal can be delivered as

$$SNR = \frac{|\, s(t_0)\,|^2}{E\{|\, n(t_0)\,|^2\}} = \frac{2\gamma^2}{\sigma^2} \quad note\ that\ E\{|\, n_I(t_0)\,|^2\} = E\{|\, n_I(t_0)\,|^2\} = \frac{\sigma^2}{2} \quad (3.28b)$$

It shows that, from equation (3.28b), the signal to noise ratio of the dispread signal is the same as the one before despreading.

Here γ and ϕ are the amplitude and the initial phase of the signal impinging on the first array element, respectively.

For simplicity, if only one snapshot is taken, t_0 can be ignored. Thus the array element outputs **x** can be expressed as:

$$\mathbf{x} = \begin{bmatrix} x_1 \\ x_2 \\ \vdots \\ x_M \end{bmatrix} = \mathbf{A}\, s + \mathbf{n} = \begin{bmatrix} 1 \\ e^{-j\varphi} \\ \vdots \\ e^{-j(M-1)\varphi} \end{bmatrix} s + \begin{bmatrix} n_1 \\ n_2 \\ \vdots \\ n_M \end{bmatrix} \quad (3.29)$$

Because **x** is a complex vector, the PDF $p(\mathbf{x};\boldsymbol{\theta})$ is defined as the joint PDF of its real and imaginary components as:

$$p(\mathbf{x};\boldsymbol{\theta}) = p\big(\mathrm{Re}(\mathbf{x}),\, \mathrm{Im}(\mathbf{x});\boldsymbol{\theta}\big). \quad (3.30)$$

In this case, the unknown parameter vector $\boldsymbol{\theta}$ is as follows:

$$\boldsymbol{\theta} = \begin{bmatrix} \theta_1 \\ \theta_2 \\ \theta_3 \end{bmatrix} = \begin{bmatrix} \gamma \\ \varphi \\ \phi \end{bmatrix}. \quad (3.31)$$

Here γ and ϕ are the amplitude and the initial phase of the signal impinging on the first array element; φ is the impinging signal phase delay between adjacent antenna elements.

Because $\varphi = 2\pi \frac{d}{\lambda} \cos\beta$ in equation (3.27), where β is the incident angle to be estimated, the transformation of parameters is:

$$\boldsymbol{\alpha} = \mathbf{g}(\boldsymbol{\theta}) = \begin{bmatrix} \gamma \\ \beta \\ \phi \end{bmatrix} = \begin{bmatrix} \gamma \\ arc\cos\left(\dfrac{\lambda \varphi}{2\pi d} \right) \\ \phi \end{bmatrix}. \tag{3.32}$$

Assuming that the *I* and *Q* outputs of the correlators are corrupted by Gaussian noise with zero mean and known variance $\sigma^2 / 2$, which are *iid* $\mathcal{N}(0, \sigma^2 / 2)$, the PDF $p(\mathbf{x}; \boldsymbol{\theta})$ with *M* real and *M* imaginary random variables is:

$$\begin{aligned} p(\mathbf{x}; \boldsymbol{\theta}) &= p\big(\mathrm{Re}(\mathbf{x}), \mathrm{Im}(\mathbf{x}); \boldsymbol{\theta}\big) \\ &= \frac{1}{\left(\sqrt{\pi\sigma^2}\right)^{2M}} \exp\left\{ -\frac{[\mathbf{x} - \mathbf{A}s]^H [\mathbf{x} - \mathbf{A}s]}{\sigma^2} \right\} \end{aligned} \tag{3.33}$$

The logarithm of $p(\mathbf{x}; \boldsymbol{\theta})$ can be derived as:

$$\begin{aligned} \ln p(\mathbf{x}; \boldsymbol{\theta}) &= -M \ln(\pi\sigma^2) - \frac{[\mathbf{x} - \mathbf{A}s]^H [\mathbf{x} - \mathbf{A}s]}{\sigma^2} \\ &= -M \ln(2\pi\sigma^2) - \frac{1}{\sigma^2} [\mathbf{x}^H \mathbf{x} - \mathbf{A}^H \mathbf{x}\, s^* - \mathbf{x}^H \mathbf{A}\, s + \mathbf{A}^H \mathbf{A}\, s^* s] \\ &= constant + \frac{2}{\sigma^2} \mathrm{Re}[\mathbf{A}^H \mathbf{x}\, s^*] - \frac{4M\, \gamma^2}{\sigma^2} \end{aligned} \tag{3.34}$$

Based on equation (3.17), one has the following equations:

$$[\mathbf{J}(\boldsymbol{\theta})]_{11} = -E\left[\frac{\partial^2 \ln p(\mathbf{x}; \boldsymbol{\theta})}{\partial \gamma^2} \right] = \frac{8M}{\sigma^2}$$

$$[\mathbf{J}(\boldsymbol{\theta})]_{12} = -E\left[\frac{\partial^2 \ln p(\mathbf{x};\boldsymbol{\theta})}{\partial\gamma\partial\varphi}\right] = \frac{4}{\sigma^2}E\left[\mathrm{Re}\left(\sum_{m=1}^{M} j(m-1)e^{j(m-1)\varphi}\, e^{-j\phi}x_m\right)\right]$$
$$= \frac{4}{\sigma^2}\mathrm{Re}\left(\sum_{m=1}^{M} j(m-1)e^{j(m-1)\varphi}\, e^{-j\phi}E(x_m)\right) = \frac{4\gamma}{\sigma^2}\mathrm{Re}\left[\sum_{m=1}^{M} j(m-1)\right] = 0$$

$$[\mathbf{J}(\boldsymbol{\theta})]_{13} = -E\left[\frac{\partial^2 \ln p(\mathbf{x};\boldsymbol{\theta})}{\partial\gamma\partial\phi}\right] = \frac{4}{\sigma^2}E\left[\mathrm{Re}\left(\sum_{m=1}^{M} je^{j(m-1)\varphi}\, e^{-j\phi}x_m\right)\right]$$
$$= \frac{4}{\sigma^2}\mathrm{Re}\left(\sum_{m=1}^{M} j(e^{j(m-1)\varphi}\, e^{-j\phi}E(x_m)\right) = \frac{4\gamma}{\sigma^2}\mathrm{Re}(j\,M) = 0$$

$$[\mathbf{J}(\boldsymbol{\theta})]_{22} = -E\left[\frac{\partial^2 \ln p(\mathbf{x};\boldsymbol{\theta})}{\partial\varphi^2}\right] = \frac{4\gamma}{\sigma^2}E\left[\mathrm{Re}\left(\sum_{m=1}^{M}(m-1)^2 e^{j(m-1)\varphi}\, e^{-j\phi}x_m\right)\right]$$
$$= \frac{4\gamma}{\sigma^2}\mathrm{Re}\left(\sum_{m=1}^{M}(m-1)^2 e^{j(m-1)\varphi}\, e^{-j\phi}E(x_m)\right) = \frac{8\gamma^2}{\sigma^2}\sum_{m=1}^{M-1} m^2$$
$$= \frac{4\gamma^2}{\sigma^2}\frac{(M-1)M(2M-1)}{3}$$

$$[\mathbf{J}(\boldsymbol{\theta})]_{23} = -E\left[\frac{\partial^2 \ln p(\mathbf{x};\boldsymbol{\theta})}{\partial\varphi\partial\phi}\right] = \frac{4\gamma}{\sigma^2}E\left[\mathrm{Re}\left(\sum_{m=1}^{M}(m-1)e^{j(m-1)\varphi}\, e^{-j\phi}x_m\right)\right]$$
$$= \frac{4\gamma}{\sigma^2}\mathrm{Re}\left(\sum_{m=1}^{M}(m-1)e^{j(m-1)\varphi}\, e^{-j\phi}E(x_m)\right) = \frac{8\gamma^2}{\sigma^2}\sum_{m=1}^{M-1} m$$

$$[\mathbf{J}(\boldsymbol{\theta})]_{33} = -E\left[\frac{\partial^2 \ln p(\mathbf{x};\boldsymbol{\theta})}{\partial\phi\partial\phi}\right] = \frac{4\gamma}{\sigma^2}E\left[\mathrm{Re}\left(\sum_{m=1}^{M} e^{j(m-1)\varphi}\, e^{-j\phi}x_m\right)\right]$$
$$= \frac{4\gamma}{\sigma^2}\mathrm{Re}\left(\sum_{m=1}^{M} e^{j(m-1)\varphi}\, e^{-j\phi}E(x_m)\right) = \frac{8\gamma^2}{\sigma^2}M$$

The *Fisher information matrix* $\mathbf{J}(\boldsymbol{\theta})$ can be derived as:

$$\mathbf{J}(\boldsymbol{\theta}) = \frac{8}{\sigma^2}\begin{bmatrix} M & 0 & 0 \\ 0 & \gamma^2 \sum_{m=1}^{M-1} m^2 & \gamma^2 \sum_{m=1}^{M-1} m \\ 0 & \gamma^2 \sum_{m=1}^{M-1} m & \gamma^2 M \end{bmatrix}. \tag{3.35}$$

From the above equation, it can be seen that the three unknown parameters $[\gamma\ \varphi\ \phi]$ have the following relationship in their estimation:

(1) No matter whether the γ is known or unknown, it will not affect the estimation accuracy of φ and ϕ, i.e., $\text{var}(\hat{\varphi})\big|_{\gamma=known} = \text{var}(\hat{\varphi})\big|_{\gamma=unknown}$ and $\text{var}(\hat{\phi})\big|_{\gamma=known} = \text{var}(\hat{\phi})\big|_{\gamma=unknown}$, because γ is independent of both φ and ϕ ($\mathbf{J}_{12}(\boldsymbol{\theta}) = \mathbf{J}_{13}(\boldsymbol{\theta}) = 0$).

(2) However, φ is not independent of ϕ ($\mathbf{J}_{23}(\boldsymbol{\theta}) = \mathbf{J}_{32}(\boldsymbol{\theta}) \neq 0$). So they will affect each other during the estimation.

In order to estimate the incident angle β which is the function of φ, the Jacobian matrix $\frac{\partial \mathbf{g}(\boldsymbol{\theta})}{\partial \boldsymbol{\theta}}$ is given as below:

$$\frac{\partial \mathbf{g}(\boldsymbol{\theta})}{\partial \boldsymbol{\theta}} = \begin{bmatrix} 1 & 0 & 0 \\ 0 & -\dfrac{\lambda}{2\pi d \sin\beta} & 0 \\ 0 & 0 & 1 \end{bmatrix} \qquad 0 < \beta < \pi. \tag{3.36}$$

Because the incident angles from π to 2 π are resolved as the values which are symmetric to the antenna array from 0 to π.

Based on equation (3.20), the error of the estimated parameter $\hat{\beta}$ is:

$$\mathrm{var}(\hat{\beta}) = [\mathbf{C}_{\hat{\boldsymbol{\alpha}}}]_{22}. \tag{3.37}$$

Meanwhile it is known that:

$$\left[\mathbf{C}_{\hat{\boldsymbol{\alpha}}} - \frac{\partial \mathbf{g}(\boldsymbol{\theta})}{\partial \boldsymbol{\theta}} \mathbf{J}^{-1}(\boldsymbol{\theta}) \frac{\partial \mathbf{g}(\boldsymbol{\theta})^T}{\partial \boldsymbol{\theta}}\right]_{22} \geq 0. \tag{3.38}$$

Because $\frac{\partial \mathbf{g}(\boldsymbol{\theta})}{\partial \boldsymbol{\theta}}$ is a diagonal matrix, it yields the following equation:

$$\mathrm{var}(\hat{\beta}) = [\mathbf{C}_{\hat{\boldsymbol{\alpha}}}]_{22} \geq \left[\frac{\partial \mathbf{g}(\boldsymbol{\theta})}{\partial \boldsymbol{\theta}}\right]_{22}^2 [\mathbf{J}^{-1}(\boldsymbol{\theta})]_{22}. \tag{3.39}$$

From equation (3.35), the following formula can be obtained:

$$[\mathbf{J}^{-1}(\boldsymbol{\theta})]_{22} = \frac{\left(\frac{8}{\sigma^2}\right)^2}{\left(\frac{8}{\sigma^2}\right)^3} \frac{M * \gamma^2 M}{\frac{\gamma^4 M^3 (M^2 - 1)}{12}} = \frac{3}{\frac{2\gamma^2}{\sigma^2} * M(M^2 - 1)} = \frac{3}{SNR * M(M^2 - 1)} \tag{3.40}$$

where $SNR = \frac{2\gamma^2}{\sigma^2}$ is the signal to noise ratio at the sampled point, seeing (3.28.b).

Therefore, the CRLB of the estimated parameter $\hat{\beta}$ can be derived as:

$$\begin{aligned}\mathrm{var}(\hat{\beta}) &\geq \frac{3}{M(M^2-1)\,SNR\left(2\pi\frac{d}{\lambda}\right)^2\sin^2\beta} \\ &= \frac{3}{(2\pi)^2 M(M^2-1)\,SNR\left(\frac{d}{\lambda}\right)^2\sin^2\beta}\ \text{(Radian}^2\text{)} \\ &\cong const.\frac{1}{SNR}\frac{1}{M^3}\frac{1}{\left(\frac{d}{\lambda}\right)^2}\frac{1}{\sin^2\beta}\end{aligned} \tag{3.41}$$

The above result is similar to that of Kay (1998). One difference is that the signal considered here is a complex signal, whereas in Kay's book, the signal is a real number. The other difference is that the data processed is sampled from the correlator output of the IS-95 pilot signal instead of a continuous wave signal. It can be seen from the above equation that (a) the higher *SNR* can result in a smaller error, which is evident; (b) a higher number of antenna elements *M* improves the estimation accuracy, because then it will have a higher number of samples for estimation. Intuitively more samples contain more information, so it is easier to estimate the unknown parameters; (c) the larger spacing d/λ can reduce the interference from element to element, which helps to reduce the estimation error; (d) the last term in equation (3.41) $\frac{1}{\sin^2\beta}$ has an interesting effect on the estimation error. When β is zero or $n\pi$, it cannot be estimated. However, this problem can be resolved by using a circular or a rectangular antenna array. The theoretical and physical explanation are as follows.

Let's investigate the sensitivity of the direction vector. The direction vector of the signal with an incident angle of β_k is the same as equation (3.22), which is expressed as:

$$\mathbf{a}(\beta_k) = \left[1,\ e^{-j2\pi\ q\cos\beta_k}, \ldots, e^{-j2\pi(M-1)\ q\cos\beta_k}\right]^T. \tag{3.42}$$

Then the direction vector at the *i*th antenna element is:

$$\mathbf{a}_k(\beta) = e^{-j2\pi(i-1)\ q\cos\beta} \tag{3.43}$$

The derivative of the direction vector $\mathbf{a}_k(\beta)$ is:

$$\mathbf{a}_k^{'}(\beta) = j\ 2\pi(i-1)\ q\sin(\beta)\ e^{-j2\pi(i-1)\ q\cos\beta}. \tag{3.44}$$

When $\beta = 90^\circ$, $\mathbf{a}_k^{'}(\beta) = j\ 2\pi(i-1)\ q$. That means in the array boresight area, the direction vector is the most sensitive to the change of incident angle value of β. So it will result in a smaller estimation error for the angle estimation. When $\beta = 0^\circ$, $\mathbf{a}_k^{'}(\beta) = 0$. That means far from the array boresight area (see Figure 3.2), the direction vector is the least sensitive to the change of incident angle of β. So the estimation error of β is larger. One solution to overcome this problem is proposed in Chapter 7 as future work. The present method is to block the signals from the endfires (see Figure 3.2) (Thompson 1995).

Physically speaking, if five antenna elements together with one BS are considered to construct the Geometric Dilution of Precision (GDOP) as shown in Figure 3.2, when the antenna array is parallel to the transmitting signal direction from BS2, i.e., $\beta = 0^\circ$, the GDOP is ∞ and so the angle estimation error is also ∞; On the other hand, when the antenna array is perpendicular to the transmitting signal direction from BS1, i.e., $\beta = 90^\circ$, the GDOP is small and so the angle estimation error is also small.

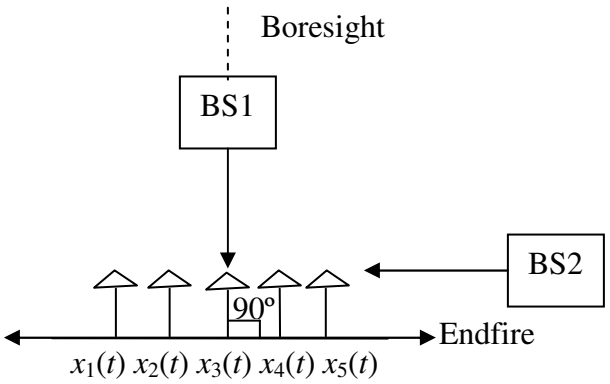

Figure 3.2: Construction of GDOP by Antenna Array and BS

Based on equation (3.41), Figure 3.3 is the CRLB for one source signal case under different *SNR*. It shows that when the incident signal is perpendicular to the antenna array ($\beta = 90^0$), the CRLB is the smallest. For example, when *SNR* = 10 dB, *M* = 5 and $\frac{d}{\lambda} = 0.7$ and

if $\beta = 90^0$, $\sqrt{\text{var}(\hat{\beta})} \geq 1^0$;

if $\beta = 30^0$, $\sqrt{\text{var}(\hat{\beta})} \geq 2^0$;

if $\beta = 5^0$, $\sqrt{\text{var}(\hat{\beta})} \geq 11.6^0$;

if $\beta = 1^0$, $\sqrt{\text{var}(\hat{\beta})} \geq 58^0$.

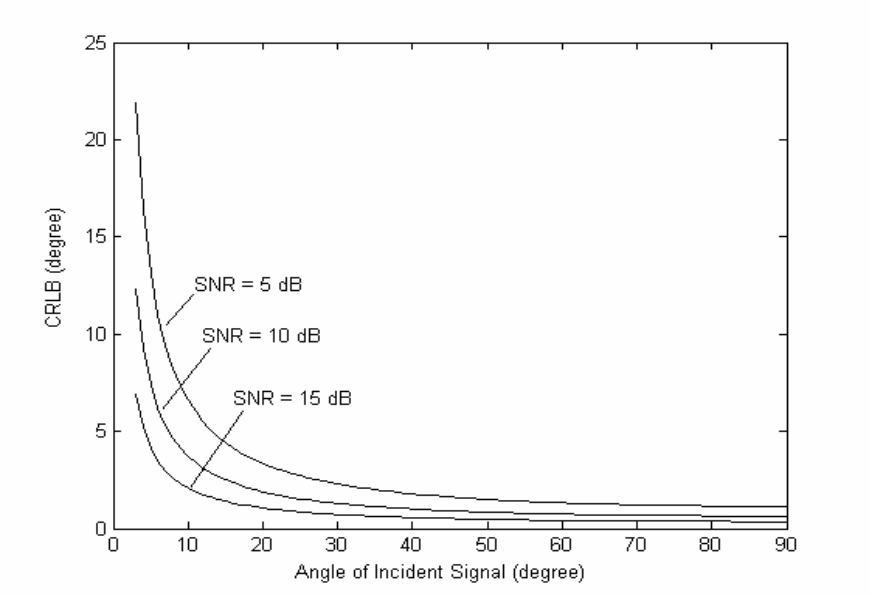

Figure 3.3: CRLB of AOA for One Source Signal

Based on the above analysis, we have the following useful conclusions about the unbiased AOA estimator's estimation error:

1) It is easiest to estimate AOA if $\beta = 90^0$ and impossible to estimate it if $\beta = 0^0$ or $\beta = 180^0$.
2) To decrease the variance of estimation error, it is helpful to increase *SNR*, the number of sensors, *M* and the ratio of antenna spacing to signal wavelength, $\frac{d}{\lambda}$.

3.6 CRLB of AOA Estimation for Multiple IS-95 Pilot Signals

The CRLB of AOA estimators for multiple sources is discussed in this section. Similarly to Section 3.5, it is still assumed that the *I* and *Q* outputs of the correlators are corrupted

by Gaussian noise with zero mean and variance $\sigma^2/2$, which are identically distributed $\mathcal{N}(0,\sigma^2/2)$ and independent from sensor to sensor. The variance σ^2 is taken as an unknown parameter.

Meanwhile, assuming that there are *N* snapshots, which are sampled at T_S, equation (3.24) can be expressed as:

$$\begin{aligned}&\mathbf{x}(n)=\mathbf{x}(t)\big|_{t=nT_s}=[\mathbf{A}\,\mathbf{s}(t)+\mathbf{n}(t)]\big|_{t=nT_s}\\&t=\{1,2,\ \ldots\ ,N\}\end{aligned}\quad . \tag{3.45}$$

Note that $\mathbf{x}(t)$ and $\mathbf{n}(t)$ are $M\times 1$ complex vectors and $\mathbf{s}(t)$ is a $K\times 1$ complex vector. M and K are the number of antenna elements and the number of source signals as defined in equation (3.24).

In Section 3.5, the impinging signal *s*(*t*) is described with its unknown amplitude γ and initial phase ϕ. Because the wanted parameter is the signal's incident angle, instead of the signal' amplitude and its initial phase, and for the convenience of derivation of multiple sources, the impinging signals are described with their real and imaginary components. Thus, the unknown parameter vector $\boldsymbol{\theta}$ can be taken as follows, which is a (1+*KN*+*K*) × 1 vector:

$$\boldsymbol{\theta}=\left[\sigma^2,\mathbf{s}_R^T(1),\mathbf{s}_I^T(1),\cdots,\mathbf{s}_R^T(N),\mathbf{s}_I^T(N),\boldsymbol{\varphi}^T\right]^T \tag{3.46}$$

where σ^2 is the noise variance; $\mathbf{s}_R(t)$ and $\mathbf{s}_I(t)$ are the real and imaginary components of $\mathbf{s}(t)$ $t\in\{1,2,\ \ldots\ ,N\}$ respectively:

$$\begin{aligned} \mathbf{s}_R(t) &= \mathrm{Re}[\mathbf{s}(t)] \\ \mathbf{s}_I(t) &= \mathrm{Im}[\mathbf{s}(t)] \quad t \in \{1, 2, \ldots, N\} \end{aligned} \tag{3.47}$$

and

$$\begin{aligned} \boldsymbol{\varphi} &= [\varphi_1, \varphi_2, \cdots, \varphi_K]^T \\ \varphi_k &= 2\pi \frac{d}{\lambda} \cos\beta_k \end{aligned} . \tag{3.48}$$

Under the above assumptions and definitions, the CRLB for $\hat{\boldsymbol{\varphi}}$ is obtained as follows (Stoica & Nehorai 1989) (The detailed proof is given in Appendix B):

$$\begin{aligned} &\mathrm{var}_{CRLB}(\hat{\boldsymbol{\varphi}}) = \frac{\sigma^2}{2}\left[\sum_{t=1}^{N} \mathrm{Re}\left\{\mathbf{S}^H(t)\mathbf{D}^H[\,\mathbf{I} - \mathbf{A}(\mathbf{A}^H\mathbf{A})^{-1}\mathbf{A}^H\,]\,\mathbf{D}\mathbf{S}(t)\right\}\right]^{-1} \\ &\textit{or} \\ &\mathrm{var}_{CRLB}(\hat{\boldsymbol{\varphi}}) = \frac{\sigma^2}{2}\left[\mathrm{Re}\left(\{\mathbf{D}^H[\,\mathbf{I} - \mathbf{A}(\mathbf{A}^H\mathbf{A})^{-1}\mathbf{A}^H\,]\,\mathbf{D}\} \odot \sum_{t=1}^{N} \mathbf{s}(t)\mathbf{s}^H(t)\right)\right]^{-1} \\ &\odot \textit{is the Hadamard product} \quad [\mathbf{A} \odot \mathbf{B}]_{ij} = \mathbf{A}_{ij}\mathbf{B}_{ij} \end{aligned} \tag{3.49}$$

where $\mathbf{S}(t)$ is a diagonal matrix expressed as:

$$\mathbf{S}(t) = \begin{bmatrix} s_1(t) & & \mathbf{0} \\ & \ddots & \\ \mathbf{0} & & s_K(t) \end{bmatrix} \tag{3.50}$$

and $\mathbf{D}$ is a differential matrix expressed as:

$$\begin{aligned} \mathbf{D} &= \left[\mathbf{d}(\varphi_1), \mathbf{d}(\varphi_2), \cdots, \mathbf{d}(\varphi_K)\right] \\ \mathbf{d}(\varphi_k) &= \frac{d\mathbf{a}(\varphi_k)}{d\varphi_k} \end{aligned} . \tag{3.51}$$

For large N, $\sum_{t=1}^{N}\mathbf{s}(t)\mathbf{s}^{H}(t) \approx N\mathbf{R}_S$, here $\mathbf{R}_S = E[\mathbf{s}(t)\mathbf{s}(t)^{H}]$ is signal correlation matrix, and the CRLB can be simplified as:

$$\mathrm{var}_{CRLB}(\hat{\varphi}) = \frac{\sigma^2}{2N}\left[\mathrm{Re}\left(\{\mathbf{D}^{H}[\mathbf{I}-\mathbf{A}(\mathbf{A}^{H}\mathbf{A})^{-1}\mathbf{A}^{H}]\mathbf{D}\}\odot\mathbf{R}_S\right)\right]^{-1} . \qquad (3.52a)$$

Equation (3.52a) is with N samples for multiple source signal environments. For a single source environment using N samples, it can be derived as follows:

Replace $\mathbf{A}$, $\mathbf{D}$, $\mathbf{R}_S$ with $\mathbf{a}(\varphi)$, $\mathbf{d}(\varphi) = \frac{d\mathbf{a}(\varphi)}{d\varphi}$, $\mathbf{R}_S = 4\gamma^2$, and equation (3.52a) can be simplified as:

$$\begin{aligned}
\mathrm{var}_{CRLB}(\hat{\varphi}) &= \frac{\sigma^2}{2N}\left\{\left[\mathbf{d}^{H}(\varphi)\mathbf{d}(\varphi) - \mathbf{d}^{H}(\varphi)\mathbf{a}(\varphi)(\mathbf{a}^{H}(\varphi)\mathbf{a}(\varphi))^{-1}\mathbf{a}^{H}(\varphi)\mathbf{d}(\varphi)\right] * 4\gamma^2\right\}^{-1} \\
&= \frac{\sigma^2}{2N}\left\{\sum_{i=0}^{M-1} i^2 - \left[(-j\sum_{i=0}^{M-1} i)\frac{1}{M}(-j\sum_{i=0}^{M-1} i)\right]\right\}^{-1} \frac{1}{4\gamma^2} \\
&= \frac{\sigma^2}{8N\gamma^2}\left\{\frac{1}{6}M(M-1)(2M-1) - \frac{1}{M}\left[\frac{(M-1)M}{2}\right]^2\right\}^{-1} \\
&= \frac{3}{N * \frac{2\gamma^2}{\sigma^2} * M(M^2-1)} = \frac{3}{N * SNR * M(M^2-1)}
\end{aligned}$$

(3.52b)

Here N is the number of sampled data; M is the number of antenna elements; SNR is the signal to noise ratio at the sampled point.

Both equation (3.52b) and equation (3.40) are for a single source signal case. But equation (3.52b) is based on *N* samples, so it is 1/*N* of a single sample case in equation (3.40). When the number of samples is one, it is the same as equation (3.40).

In equation (3.52a), if the angle of arrival β_k is the final estimated parameter, the CRLB of $\hat{\beta}_k$ can be expressed as:

$$\mathrm{var}_{CRLB}(\hat{\beta}_k) = \frac{[\mathrm{var}_{CRLB}(\hat{\boldsymbol{\beta}})]_{k\,k}}{\left(2\pi\frac{d}{\lambda}\right)^2 \sin^2\beta_k} \tag{3.53}$$

If the signal vector $\mathbf{s}(t)$ at the reference antenna is defined as:

$$\mathbf{s}(t) = [\gamma_1 \exp(j\phi_1(t)), \cdots, \gamma_K \exp(j\phi_K(t))]^T \quad \textit{where } \boldsymbol{\gamma} = [\gamma_1, \cdots, \gamma_K]^T, \boldsymbol{\phi} = [\phi_1, \cdots, \phi_K]^T$$

it can be seen that $\mathrm{var}_{CRLB}(\hat{\beta}_k)$ depends on N, $\frac{d}{\lambda}$, σ^2, $\boldsymbol{\gamma}$, $\boldsymbol{\phi}$ and $\boldsymbol{\beta} = [\beta_1, \cdots, \beta_K]^T$. A more practical analysis, which cannot be seen easily from equation (3.53), is provided in the ***case study of AOA CRLB*** below.

In equation (3.52b) for the single source signal case, the CRLB of angle of arrival β can be expressed as:

$$\begin{aligned}\mathrm{var}_{CRLB}(\hat{\beta}) &= \frac{[\mathrm{var}_{CRLB}(\hat{\varphi})]}{\left(2\pi\frac{d}{\lambda}\right)^2 \sin^2\beta_k} \\ &= \frac{3}{N*SNR*M(M-1)\left(2\pi\frac{d}{\lambda}\right)^2 \sin^2\beta_k}\end{aligned} . \tag{3.54}$$

It is worth mentioning that, from the Fisher information matrix in equation (B.24), no matter if the noise variance is known or unknown, the AOA estimation $\hat{\beta}$ is not affected by it because the noise variance σ^2 is not related to φ which is a function of β. So the following example is given based on that fact that the noise variance is known.

Definition

The correlation coefficient of a set of observations $\{(x_i, y_i): i = 1, \cdots, N\}$ for two signals x and y is defined by the following formula:

$$\rho_{xy} = \frac{\sum_{i=1}^{N}(x_i - \bar{x})(y_i - \bar{y})}{\sqrt{\sum_{i=1}^{N}(x_i - \bar{x})^2 \sum_{i=1}^{N}(y_i - \bar{y})^2}}$$

$$\text{or } \rho_{xy} = \frac{E[(x_i - \bar{x})(y_i - \bar{y})]}{\sqrt{E[|x_i - \bar{x}|^2]\, E[|y_i - \bar{y}|^2]}}$$

where $\bar{x}$ and $\bar{y}$ are the average values of x and y respectively.

The properties of the complex correlation coefficients are:

- $\left|\rho_{xy}\right| = 0$, which is when signals are uncorrelated.

- $0 < \left|\rho_{xy}\right| \le 1$, which is when signals are correlated.

The relationship between the correlation coefficient and the correlation matrix $\mathbf{R}_S$ in equation (3.52a) is that *the correlation coefficient is the normalized correlation function for each element in correlation matrix when the signal's expectation is zero*, i.e.

$\rho_{s_i s_j} = \dfrac{R_s(i,j)}{\sqrt{E\{\left|s_i\right|^2\}E\{\left|s_j\right|^2\}}}$. So in the following *case study*, the correlation coefficient is used to discuss the CRLB described by equation (3.52a).

Case Study of AOA CRLB

Assuming that the number of signal sources is $K \le 3$, the number of array sensors is M = 5, d/λ = 0.5 and the estimated LOS AOA is $\hat{\beta}_1$, the normalized CRLB $N\,\mathrm{var}_{CRLB}(\hat{\beta}_1)$ is investigated. These three practical factors are considered and shown in Figure 3.4.

1. The phase of the correlation coefficient ρ_{xy} of two signals

Different initial phase between two incident rays result in minimum and maximum boundaries of $\mathrm{var}_{CRLB}(\hat{\beta}_1)$ as shown in Figure 3.5. Stoica & Nehorai (1989) only discussed the case when the phase of correlation coefficient ρ_{xy} of two signals is zero,

so only one CRLB exists. The upper circled two lines are obtained from three source signals case and the lower circled two lines are obtained from two source signals case. The initial phases of incident rays also affect the singularity of the source signal matrix $\mathbf{R}_S^{f/b}$ when the forward/backward smooth MUSIC algorithm is applied, which is discussed in Section 4.5.3.

2. The AOA difference $\Delta\beta = | \beta_i - \beta_j |$

In this case, the LOS incident angle AOA1 is supposed to be at 90°; *SNR* and *SIR* are 14 dB; the absolute value of correlation coefficient is $| \rho_{xy} | = 0.8 \quad x \neq y$. It can be seen that as the $\Delta\beta$ increases, the $\text{var}_{CRLB}(\hat{\beta}_1)$ decreases. When AOA1 is from different angle, its CRLB also changes as shown in Figure 3.5.

3. The number of source signals K

When there are three source signals, $\text{var}_{CRLB}(\hat{\beta}_1)$ is much more than that of two source signals case within $\Delta\beta < 20^0$. Another simulation experiment is done, which is not displayed, to increase the *SNR* to 28 dB for the three source signals situation and it reaches the same $\text{var}_{CRLB}(\hat{\beta}_1)$ as that in the two source signals condition within $\Delta\beta < 20^0$. *It means that to achieve a small* $\text{var}_{CRLB}(\hat{\beta}_k)$*, decreasing the number of source signals K is more efficient than increasing SNR when the AOA difference* $\Delta\beta$ *is small.* This can be controlled through sampling the data at the correlation rising part where few multipath signals are added to LOS, which is implemented in this research described in Chapter 5.

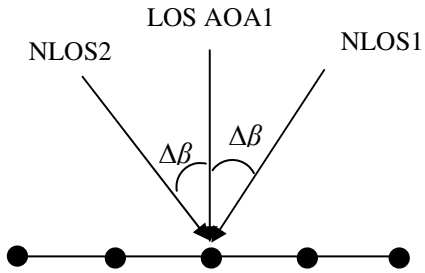

Figure 3.4: Geometry of Incident Signals

From the simulation results shown in Figure 3.5, for $\Delta\beta$ = 25º, the maximum CRLB values are obtained when the phase difference between LOS and NLOS1 is 164º and the phase difference between LOS and NLOS2 is 108º; the minimum CRLB values are obtained when the phase difference between LOS and NLOS1 is 29º and the phase difference between LOS and NLOS2 is 63º. No general formula was derived here to describe the phase difference condition for maximum or the minimum CRLB to hold because it is difficult to formulate. However through the simulation, it shows that the maximum or the minimum CRLB values do exist when the phase difference between two incident rays has a certain relationship.

Figure 3.5 also gives us a guide on how to apply MUSIC efficiently. It can be seen that the CRLB for three source signals are higher than that for two source signals. So even though MUSIC can resolve a certain number of incident signals only if the number of antenna array is large enough, **the best choice is to limit the number of incident signals**, which is presented in the proposed algorithm through using the data sampled at the correlation initial part. Another phenomena worth mentioning is that different LOS

AOA will result in different CRLB values. For example, if LOS AOA1 = 70º, the CRLB increases, as shown in Figure 3.5 (b).

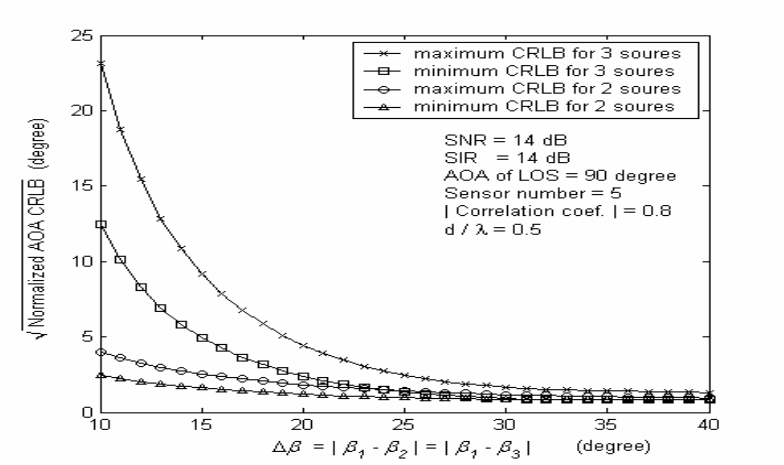

(a) CRLB of AOA for Multiple Sources Signals, LOS AOA = 90º

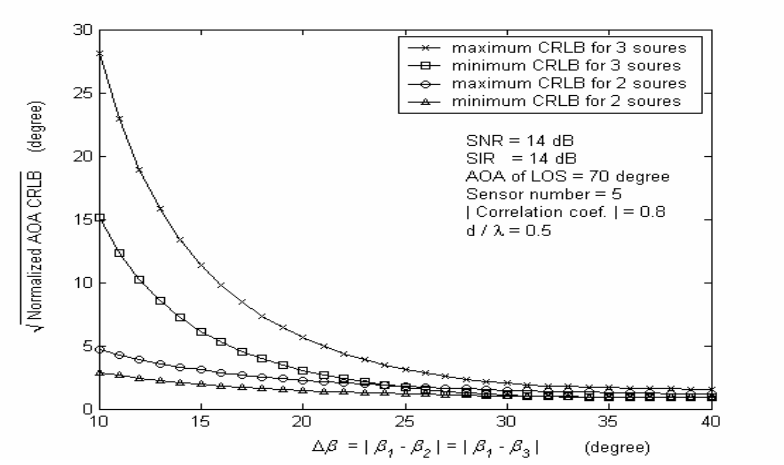

(b) CRLB of AOA for Multiple Sources Signals, LOS AOA = 70º

Figure 3.5: (a) CRLB of AOA for Multiple Sources Signals, LOS AOA = 90º;

(b) CRLB of AOA for Multiple Sources Signals, LOS AOA = 70º

3.7 CRLB of TOA Estimation for IS-95 Pilot Signal

The TOA of the LOS component of the received signal is estimated based on correlation functions, independently from the AOA estimation process, i.e., after the AOA is estimated in this approach, the AOA is a known parameter for the TOA estimation. Compared with the maximum likelihood–based optimal joint AOA/TOA estimation, this method is computationally more efficient to implement and sub-optimal when signal to noise ratio is large. When the AOAs are estimated, the LOS is strengthened and the multipath is mitigated through the beamformer. The performance of the beamformer is discussed in Section 5.4. After beamforming, the weak multipath signals are not considered. The following derivation of the CRLB for TOA is based on one source signal because after the correlation function has been compensated by the estimated AOA, the multipath signals can be treated as noise.

Assuming that the size of the linear antenna array is much less than cT_C (c is the velocity of light and T_C is the PN code chip period, so $cT_C = 3\times10^8\times800\times10^{-9} = 240$ m; whereas the size of antenna array with 5 elements = 30 cm), the relative time delays of the baseband signals at different elements of the antenna array can be ignored. It means that all time delays of PN code at different elements are the same. Thus the equation (3.22) can be modified as:

$$\mathbf{x}(t) = \begin{bmatrix} x_1(t) \\ x_2(t) \\ \vdots \\ x_M(t) \end{bmatrix} = \mathbf{a}(\beta)\, s(t) + \mathbf{n}(t) \qquad (3.55)$$
$$= \mathbf{a}(\beta)\gamma\, PN(t-\tau)\, e^{j\phi} + \mathbf{n}(t)$$

Here γ, τ and ϕ are the amplitude, time delay and initial phase of the IS-95 pilot signal before despreading, respectively. For the IS-95 pilot signal, $PN(t-\tau)$ can be defined as (referring to Chapter 2 for the IS-95 pilot signal correlation process):

$$PN(t-\tau) = PN_I(t-\tau) + jPN_Q(t-\tau)$$

Now the unknown parameter vector $\boldsymbol{\theta}$ is:

$$\boldsymbol{\theta} = \left[\sigma^2,\ \gamma, \phi, \tau\right]^T$$

where σ^2 is considered as the unknown noise variance; γ, τ and ϕ are the amplitude, time delay and initial phase of the IS-95 pilot signal, respectively.

The above assumes that the *I* and *Q* outputs of the demodulators are corrupted by *iid* Gaussian noises with zero mean and variance $\sigma^2/2$, $\mathcal{N}(0, \sigma^2/2)$. However it will be seen later on from the Fisher information matrix that the noise variance is not related with the other three parameters γ, ϕ and τ, which means that the noise variance can be treated as a known parameter for the TOA estimation or can be estimated independently.

If the number of snapshots is N, the parameterized PDF of the sampling data $\mathbf{x}(t)$ can be written as:

$$
\begin{aligned}
& p(\mathbf{x}(1), \mathbf{x}(2), \cdots, \mathbf{x}(N); \boldsymbol{\theta}) \\
&= \frac{1}{\left(\sqrt{\pi\sigma^2}\right)^{2MN}} \exp\left\{-\frac{1}{\sigma^2}\sum_{t=1}^{N}\mathbf{n}^H(t)\mathbf{n}(t)\right\} \\
&= \frac{1}{\left(\sqrt{\pi\sigma^2}\right)^{2MN}} \exp\left\{-\frac{1}{\sigma^2}\sum_{t=1}^{N}[\mathbf{x}(t)-\mathbf{a}(\beta)s(t)]^H[\mathbf{x}(t)-\mathbf{a}(\beta)s(t)]\right\} \\
&= \frac{1}{\left(\sqrt{\pi\sigma^2}\right)^{2MN}} \exp\left\{-\frac{\sum_{t=1}^{N}[\mathbf{x}(t)-\mathbf{a}(\beta)\gamma PN(t-\tau)e^{j\phi}]^H[\mathbf{x}(t)-\mathbf{a}(\beta)\gamma PN(t-\tau)e^{j\phi}]}{\sigma^2}\right\}
\end{aligned}
\tag{3.56}
$$

In the above equation, t is the discrete time and τ is the time delay normalized by T_S:

$$0 \le \tau < T/T_S$$

T is the period of PN sequence and T_S is the sampling period.

The logarithm of $p(\mathbf{x}(1), \mathbf{x}(2), \cdots, \mathbf{x}(N); \boldsymbol{\theta})$ can be derived as:

$$
\begin{aligned}
& \overset{\Delta}{L} = \ln p(\mathbf{x}(1), \mathbf{x}(2), \cdots, \mathbf{x}(N); \boldsymbol{\theta}) \\
&= const - MN\ln\sigma^2 - \frac{1}{\sigma^2}\sum_{t=1}^{N}[\mathbf{x}(t)-\mathbf{a}(\beta)\gamma PN(t-\tau)e^{j\phi}]^H[\mathbf{x}(t)-\mathbf{a}(\beta)\gamma PN(t-\tau)e^{j\phi}]
\end{aligned}
\tag{3.57}
$$

Based on equation (3.57), one can obtain the following equations:

$$\frac{\partial L}{\partial(\sigma^2)} = -\frac{MN}{\sigma^2} + \frac{1}{\sigma^4}\sum_{t=1}^{N}\mathbf{n}^H(t)\mathbf{n}(t) \tag{3.58}$$

$$\frac{\partial L}{\partial \gamma} = \frac{2}{\gamma\sigma^2}\sum_{t=1}^{N}\mathrm{Re}[\mathbf{n}^H(t)\mathbf{a}(\beta)s(t)] \tag{3.59}$$

$$\frac{\partial L}{\partial \phi} = \frac{2j}{\sigma^2}\sum_{t=1}^{N}\mathrm{Im}[\mathbf{n}^H(t)\mathbf{a}(\beta)s(t)] \tag{3.60}$$

$$\begin{aligned}\frac{\partial L}{\partial \tau} &= \frac{2}{\sigma^2}\sum_{t=1}^{N}\mathrm{Re}[\mathbf{n}^H(t)\mathbf{a}(\beta)\gamma\frac{\partial PN(t-\tau)}{\partial\tau}e^{j\phi}] \\ &= \frac{2}{\sigma^2}\sum_{t=1}^{N}\mathrm{Re}[\mathbf{n}^H(t)\,\mathbf{a}(\beta)\frac{\partial s(t,\tau)}{\partial\tau}]\end{aligned} \tag{3.61}$$

Based on the above partial differentials and equations B.9 -10, the elements in the Fisher Information matrix can be derived as:

$$[\mathbf{J}(\boldsymbol{\theta})]_{11} = -E\left[\frac{\partial^2 L}{\partial(\sigma^2)^2}\right] = \frac{MN}{\sigma^4}$$

$$[\mathbf{J}(\boldsymbol{\theta})]_{12} = -E\left[\frac{\partial^2 L}{\partial\sigma^2\partial\gamma}\right] = 0$$

$$[\mathbf{J}(\boldsymbol{\theta})]_{13} = -E\left[\frac{\partial^2 L}{\partial\sigma^2\partial\phi}\right] = 0$$

$$[\mathbf{J}(\boldsymbol{\theta})]_{14} = -E\left[\frac{\partial^2 L}{\partial\sigma^2\partial\tau}\right] = 0$$

$$[\mathbf{J}(\boldsymbol{\theta})]_{22} = -E\left[\frac{\partial^2 L}{\partial\gamma^2}\right] = \frac{2}{\gamma^2\sigma^2}\sum_{t=1}^{N}\mathrm{Re}[s^*(t)\mathbf{a}^H(\beta)\mathbf{a}(\beta)s(t)] = \frac{2M}{\sigma^2}\sum_{t=1}^{N}|\,PN(t-\tau)\,|^2 = \frac{4MN}{\sigma^2}$$

$$[\mathbf{J}(\boldsymbol{\theta})]_{23} = -E\left[\frac{\partial^2 L}{\partial\gamma\,\partial\phi}\right] = -E\left[\frac{\partial L}{\partial\gamma}\frac{\partial L}{\partial\phi}\right] = \frac{4j}{\gamma\sigma^4}E\left[\sum_{t=1}^{N}\mathrm{Re}[\mathbf{n}^H(t)\mathbf{a}(\beta)s(t)]\,\mathrm{Im}[\mathbf{n}^H(t)\mathbf{a}(\beta)s(t)]\right]$$

$$= \frac{2j}{\gamma\sigma^4}E\left[\sum_{t=1}^{N}\mathrm{Im}[\mathbf{n}^H(t)\mathbf{a}(\beta)s(t)]^2 - \mathrm{Im}[\mathbf{n}^H(t)\mathbf{a}(\beta)s(t)(\mathbf{n}^H(t)\mathbf{a}(\beta)s(t))^*]\right]$$

$$= 0$$

$$[\mathbf{J}(\boldsymbol{\theta})]_{24} = -E\left[\frac{\partial^2 L}{\partial\gamma\,\partial\tau}\right] = -E\left[\frac{\partial L}{\partial\gamma}\frac{\partial L}{\partial\tau}\right]$$

$$= -\frac{4}{\gamma\sigma^4}E\left[\sum_{t=1}^{N}\mathrm{Re}[\mathbf{n}^H(t)\mathbf{a}(\beta)s(t)]\,\mathrm{Re}[\mathbf{n}^H(t)\mathbf{a}(\beta)\frac{\partial s(t,\tau)}{\partial\tau}]\right]$$

$$= -\frac{2}{\gamma\sigma^4}E\left[\sum_{t=1}^{N}\mathrm{Re}[\mathbf{n}^H(t)\mathbf{a}(\beta)s(t)\mathbf{n}^H(t)\mathbf{a}(\beta)\frac{\partial s(t,\tau)}{\partial\tau}]\right.$$

$$\left. + \mathrm{Re}[\mathbf{n}^H(t)\mathbf{a}(\beta)s(t)(\mathbf{n}^H(t)\mathbf{a}(\beta)\frac{\partial s(t,\tau)}{\partial\tau})^*]\right]$$

$$= -\frac{2M\gamma}{\sigma^2}\sum_{t=1}^{N}\mathrm{Re}\left(PN(t-\tau)\frac{\partial PN^*(t-\tau)}{\partial\tau}\right)$$

$$= -\frac{2M\gamma}{\sigma^2}\sum_{t=1}^{N}PN_I(t-\tau)\frac{\partial PN_I(t-\tau)}{\partial\tau} + PN_Q(t-\tau)\frac{\partial PN_Q(t-\tau)}{\partial\tau}$$

$$= \frac{M\gamma}{\sigma^2}\sum_{n=1}^{N}\frac{dPN_I^2(v)}{dv}\Big|_{v=(n-1)T_S-\tau T_S} + \frac{dPN_Q^2(v)}{dv}\Big|_{v=(n-1)T_S-\tau T_S}$$

$$= 0$$

here T_S *is the sampling period and* $PN_I(t) = \pm 1,\ PN_Q(t) = \pm 1$

$$[\mathbf{J}(\boldsymbol{\theta})]_{33} = -E\left[\frac{\partial L}{\partial \phi}\frac{\partial L}{\partial \phi}\right] = \frac{4}{\sigma^4}E\left[\sum_{t=1}^{N}\mathrm{Im}[\mathbf{n}^H(t)\mathbf{a}(\beta)s(t)]\,\mathrm{Im}[\mathbf{n}^H(t)\mathbf{a}(\beta)s(t)]\right]$$

$$= -\frac{2}{\sigma^4}E\left[\sum_{t=1}^{N}\mathrm{Re}[\mathbf{n}^H(t)\mathbf{a}(\beta)s(t)]^2 - \mathrm{Re}[\mathbf{n}^H(t)\mathbf{a}(\beta)s(t)(\mathbf{n}^H(t)\mathbf{a}(\beta)s(t))^H]\right]$$

$$= \frac{2}{\sigma^4}E\left[\sum_{t=1}^{N}\mathrm{Re}[\mathbf{a}^T(\beta)\mathbf{n}^*(t)\mathbf{n}^T(t)\mathbf{a}^*(\beta)s(t)s^*(t)]\right]$$

$$= \frac{2M\gamma^2}{\sigma^2}\sum_{t=1}^{N}|\,PN(t-\tau)\,|^2 = \frac{4MN\gamma^2}{\sigma^2}$$

$$[\mathbf{J}(\boldsymbol{\theta})]_{34} = -E\left[\frac{\partial L}{\partial \phi}\frac{\partial L}{\partial \tau}\right] = -\frac{4j}{\sigma^4}E\left[\sum_{t=1}^{N}\mathrm{Im}[\mathbf{n}^H(t)\mathbf{a}(\beta)s(t)]\,\mathrm{Re}[\mathbf{n}^H(t)\mathbf{a}(\beta)\frac{\partial s(t,\tau)}{\partial \tau}]\right]$$

$$= -\frac{2j}{\sigma^4}E\Big[\mathrm{Im}[\mathbf{n}^H(t)\mathbf{a}(\beta)s(t)\mathbf{n}^H(t)\mathbf{a}(\beta)\frac{\partial s(t,\tau)}{\partial \tau}] + \mathrm{Im}[\mathbf{n}^H(t)\mathbf{a}(\beta)s(t)\mathbf{n}^T(t)\mathbf{a}^*(\beta)\frac{\partial s^*(t,\tau)}{\partial \tau}]\Big]$$

$$= -\frac{2jM\gamma^2}{\sigma^2}\sum_{t=1}^{N}\mathrm{Im}\left(PN(t-\tau)\frac{\partial PN^*(t-\tau)}{\partial \tau}\right) \approx 0 \quad (\textit{see Appendix F})$$

$$[\mathbf{J}(\boldsymbol{\theta})]_{44} = -E\left[\frac{\partial^2 L}{\partial \tau^2}\right]$$

$$= -\frac{2}{\sigma^2}E\left[\sum_{t=1}^{N}\mathrm{Re}[-\mathbf{a}^H(\beta)\frac{\partial s^*(t,\tau)}{\partial \tau}\mathbf{a}(\beta)\frac{\partial s(t,\tau)}{\partial \tau}] + \mathrm{Re}[\mathbf{n}^H(t)\mathbf{a}(\beta)\frac{\partial^2 s(t,\tau)}{\partial \tau^2}]\right]$$

$$= \frac{2M\gamma^2}{\sigma^2}\sum_{t=1}^{N}\left|\frac{\partial PN(t-\tau)}{\partial \tau}\right|^2$$

The Fisher information matrix is expressed as:

$$\mathbf{J}(\boldsymbol{\theta}) = \begin{bmatrix} [\mathbf{J}(\boldsymbol{\theta})]_{11} & 0 & 0 & 0 \\ 0 & [\mathbf{J}(\boldsymbol{\theta})]_{22} & 0 & 0 \\ 0 & 0 & [\mathbf{J}(\boldsymbol{\theta})]_{33} & [\mathbf{J}(\boldsymbol{\theta})]_{34} \\ 0 & 0 & [\mathbf{J}(\boldsymbol{\theta})]_{34} & [\mathbf{J}(\boldsymbol{\theta})]_{44} \end{bmatrix} \tag{3.62}$$

From the above matrix, it can be seen that the TOA estimation is only affected by the IS-95 signal initial phase ϕ, not by both the noise variance σ^2 and signal amplitude γ because the delay τ is not correlated with both σ^2 and γ.

Then the CRLB of the time delay or TOA for CDMA signal is given by:

$$\begin{aligned} \mathrm{var}_{CRLB}(\hat{\tau}) = [\mathbf{J}(\boldsymbol{\theta})]_{44}^{-1} &= \frac{\prod_{i=1}^{3}[\mathbf{J}(\boldsymbol{\theta})]_{ii}}{\prod_{i=1}^{4}[\mathbf{J}(\boldsymbol{\theta})]_{ii} - [\mathbf{J}(\boldsymbol{\theta})]_{11}[\mathbf{J}(\boldsymbol{\theta})]_{22}[\mathbf{J}(\boldsymbol{\theta})]_{34}^2} \\ &= \frac{1}{[\mathbf{J}(\boldsymbol{\theta})]_{44} - [\mathbf{J}(\boldsymbol{\theta})]_{34}^2 / [\mathbf{J}(\boldsymbol{\theta})]_{33}} \\ &= \frac{\sigma^2}{\gamma^2} \frac{1}{2M\sum_{t=1}^{N}\left|\frac{\partial PN(t-\tau)}{\partial \tau}\right|^2 - \left\{\mathrm{Im}\left[\frac{1}{\sqrt{N}}\sum_{t=1}^{N} PN(t-\tau)\frac{\partial PN^*(t-\tau)}{\partial \tau}\right]\right\}^2} \end{aligned} \quad . \tag{3.63}$$

To prove $\mathrm{Im}\left[\frac{1}{\sqrt{N}}\sum_{t=1}^{N} PN(t-\tau)\frac{\partial PN^*(t-\tau)}{\partial \tau}\right] \approx 0$ appeared in the above equation, a further investigation of equation (3.63) is given in Appendix F.

Thus CRLB of TOA for an IS-95 pilot signal is as follows:

$$\begin{aligned}
\mathrm{var}_{CRLB}(\hat{\tau}) &= \frac{\sigma^2}{\gamma^2}\frac{1}{2M\sum_{t=1}^{N}\left|\frac{\partial PN(t-\tau)}{\partial\tau}\right|^2 - \left\{\mathrm{Im}\left[\frac{1}{\sqrt{N}}\sum_{t=1}^{N}PN(t-\tau)\frac{\partial PN^*(t-\tau)}{\partial\tau}\right]\right\}^2} \\
&= \frac{\sigma^2}{\gamma^2}\frac{1}{2M\sum_{t=1}^{N}\left|\frac{\partial PN(t-\tau)}{\partial\tau}\right|^2} \qquad (3.64) \\
&= \frac{\sigma^2}{\gamma^2}\frac{T_S T_C}{16MK} \quad (T_S = T_C/2) \\
&= \frac{T_C^2}{32MK\cdot SNR}
\end{aligned}$$

where $SNR = \frac{\gamma^2}{\sigma^2}$ is the signal to noise ratio before despreading; $K = 2^{15}$ is the length of IS-95 PN sequences; M is the array elements and T_C is the chip period . It can be seen that the shorter the chip period is, the lower the CRLB is; the longer the length of the PN sequence is, the lower the CRLB is; the higher the *SNR* is, the lower the CRLB is; The higher the number of array elements is, the lower the CRLB is.

3.8 CRLB of Joint AOA and TOA Estimation for IS-95 Pilot Signal

For the joint AOA and TOA estimation, the parameter vector $\boldsymbol{\theta}$ is defined as:

$$\boldsymbol{\theta} = \left[\sigma^2,\ \gamma, \phi, \tau, \varphi\right]^T \qquad (3.65)$$

where σ^2 is considered an unknown noise variance; γ, τ and ϕ are the amplitude, time delay and initial phase of IS-95 pilot signal respectively; φ is the impinging signal's phase delay between adjacent antenna elements.

Compared with the unknown parameter vector $\boldsymbol{\theta}$ in Section 3.7 for the case of TOA estimation, here the added parameter is $\varphi = 2\pi \frac{d}{\lambda} \cos\beta$, which is defined in equations (3.23) and (3.27).

The direction vector $\mathbf{a}(\beta)$ can be expressed as:

$$\mathbf{a}(\beta) = \mathbf{a}(\varphi) = \left[1,\ e^{-j\varphi}, \ldots, e^{-j,(M-1)\ \varphi} \right]^T \tag{3.66}$$

Similar to equation (3.51), the differential vector $\mathbf{d}(\varphi)$ is defined as:

$$\mathbf{d}(\varphi) = \frac{d\mathbf{a}(\varphi)}{d\varphi} \tag{3.67}$$

Just as in the definition of log-likelihood L in equation (3.57), one can derive the following equation:

$$\frac{\partial L}{\partial \varphi} = \frac{2}{\sigma^2} \sum_{t=1}^{N} \mathrm{Re}[\mathbf{n}^H(t)\mathbf{d}(\varphi)s(t)] \tag{3.68}$$

Note that the elements $[\mathbf{J}(\boldsymbol{\theta})]_{ij}$ $i, j = 1, 2, \cdots, 4$ in the Fisher Information matrix are the same as those derived in Section 3.7. Only the new added parameter φ needs to be considered. The additional elements in the Fisher Information matrix can be derived as:

$$[\mathbf{J}(\boldsymbol{\theta})]_{15} = -E\left[\frac{\partial^2 L}{\partial\sigma^2\partial\varphi}\right] = \frac{2}{\sigma^4}E\left[\sum_{t=1}^{N}\mathrm{Re}[\mathbf{n}^H(t)\mathbf{d}(\varphi)s(t)]\right] = 0$$

$$[\mathbf{J}(\boldsymbol{\theta})]_{25} = -E\left[\frac{\partial^2 L}{\partial\gamma\partial\varphi}\right] = -\frac{2}{\gamma\sigma^2}E\left[\sum_{t=1}^{N}\mathrm{Re}[\mathbf{n}^H(t)\mathbf{d}(\varphi)s(t) - \mathbf{a}^H(\varphi)s^*(t)\mathbf{d}(\varphi)s(t)]\right]$$

$$= \frac{4N\gamma}{\sigma^2}\mathrm{Re}[\mathbf{a}^H(\varphi)\mathbf{d}(\varphi)] = \frac{2N\gamma}{\sigma^2}\mathrm{Re}[jM(M-1)] = 0$$

$$[\mathbf{J}(\boldsymbol{\theta})]_{35} = -E\left[\frac{\partial^2 L}{\partial\phi\partial\varphi}\right] = -\frac{2}{\sigma^2}E\left[\sum_{t=1}^{N}\mathrm{Re}[j\mathbf{n}^H(t)\mathbf{d}(\varphi)s(t) + j\mathbf{a}^H(\varphi)s^*(t)\mathbf{d}(\varphi)s(t)]\right]$$

$$= -\frac{4N\gamma^2}{\sigma^2}\mathrm{Re}[j\mathbf{a}^H(\varphi)\mathbf{d}(\varphi)] = \mathrm{Re}\left[\frac{2NM(M-1)\gamma^2}{\sigma^2}\right] = \frac{2NM(M-1)\gamma^2}{\sigma^2}$$

$$[\mathbf{J}(\boldsymbol{\theta})]_{45} = -E\left[\frac{\partial^2 L}{\partial\tau\partial\varphi}\right]$$

$$= -\frac{2}{\sigma^2}E\left[\sum_{t=1}^{N}\mathrm{Re}[\mathbf{n}^H(t)\mathbf{d}(\varphi)\gamma e^{j\phi}\frac{\partial PN(t-\tau)}{\partial\tau} - \mathbf{a}^H(\varphi)\gamma e^{-j\phi}\frac{\partial PN^*(t-\tau)}{\partial\tau}\mathbf{d}(\varphi)s(t)]\right]$$

$$= \frac{2\gamma^2}{\sigma^2}\sum_{t=1}^{N}\mathrm{Re}\left[\mathbf{a}^H(\varphi)\mathbf{d}(\varphi)\frac{\partial PN^*(t-\tau)}{\partial\tau}PN(t-\tau)\right]$$

$$= \frac{M(M-1)\gamma^2}{\sigma^2}\sum_{t=1}^{N}\mathrm{Re}\left[j\frac{\partial PN^*(t-\tau)}{\partial\tau}PN(t-\tau)\right]$$

$$= \frac{M(M-1)\gamma^2}{\sigma^2}\sum_{t=1}^{N}\left[\frac{\partial PN_Q(t-\tau)}{\partial\tau}PN_I(t-\tau) - \frac{\partial PN_I(t-\tau)}{\partial\tau}PN_Q(t-\tau)\right]$$

$$\approx -\frac{2M(M-1)\gamma^2}{T_S\sigma^2}\int_0^T \frac{dPN_I(t)}{dt}PN_Q(t)\,dt$$

$$\approx 0 \qquad (\textit{refering to Appendix F})$$

$$[\mathbf{J}(\boldsymbol{\theta})]_{55} = -E\left[\frac{\partial^2 L}{\partial\varphi^2}\right] = -\frac{2}{\sigma^2}E\left[\sum_{t=1}^{N}\mathrm{Re}[\mathbf{n}^H(t)\frac{\partial\mathbf{d}(\varphi)}{\partial\varphi}s(t) - \mathbf{d}^H(\varphi)s^*(t)\mathbf{d}(\varphi)s(t)]\right]$$

$$= \frac{4N\gamma^2}{\sigma^2}\sum_{m=1}^{M}(m-1)^2 = \frac{2NM(M-1)(2M-1)\gamma^2}{3\sigma^2}$$

(3.69)

Finally the Fisher information matrix for joint AOA and TOA estimation is obtained as:

$$\mathbf{J}(\boldsymbol{\theta}) = \begin{bmatrix} [\mathbf{J}(\boldsymbol{\theta})]_{11} & 0 & 0 & 0 & 0 \\ 0 & [\mathbf{J}(\boldsymbol{\theta})]_{22} & 0 & 0 & 0 \\ 0 & 0 & [\mathbf{J}(\boldsymbol{\theta})]_{33} & 0 & [\mathbf{J}(\boldsymbol{\theta})]_{35} \\ 0 & 0 & 0 & [\mathbf{J}(\boldsymbol{\theta})]_{44} & 0 \\ 0 & 0 & [\mathbf{J}(\boldsymbol{\theta})]_{35} & 0 & [\mathbf{J}(\boldsymbol{\theta})]_{55} \end{bmatrix} \tag{3.70}$$

Based on the above equation, the CRLB of joint AOA and TOA estimation is formed as follows:

1. The ***CRLB*** of AOA-joint TOA (τ) estimation for CDMA IS-95 pilot signal is:

$$\begin{aligned} \mathrm{var}_{CRLB}(\hat{\tau}) = [\mathbf{J}(\boldsymbol{\theta})]^{-1}_{44} &= \frac{\prod_{i=3}^{5}[\mathbf{J}(\boldsymbol{\theta})]_{ii} \Big/ [\mathbf{J}(\boldsymbol{\theta})]_{44} - [\mathbf{J}(\boldsymbol{\theta})]_{11}[\mathbf{J}(\boldsymbol{\theta})]_{22}[\mathbf{J}(\boldsymbol{\theta})]^2_{35}}{\prod_{i=3}^{5}[\mathbf{J}(\boldsymbol{\theta})]_{ii} - [\mathbf{J}(\boldsymbol{\theta})]^2_{35}\prod_{i=3}^{4}[\mathbf{J}(\boldsymbol{\theta})]_{ii} \Big/ [\mathbf{J}(\boldsymbol{\theta})]_{33}} \\ &= \frac{1}{[\mathbf{J}(\boldsymbol{\theta})]_{44}} \\ &= \frac{\sigma^2}{\gamma^2}\frac{1}{2M\sum_{t=1}^{N}\left|\frac{\partial PN(t-\tau)}{\partial \tau}\right|^2} \\ &= \frac{\sigma^2}{\gamma^2}\frac{T_S T_C}{16MK} \quad (T_S = T_C/2) \quad (\textit{referring to Appendix F}) \\ &= \frac{T_C^2}{32MK \cdot SNR} \end{aligned} \tag{3.71}$$

where T_C is the PN chip period; M is the number of antenna array; $K = 2^{15}$ is the length of PN sequence and SNR is the signal to noise ratio before despreading.

Comparing equation (3.71) with equation (3.64), it can be seen that the CRLB of the AOA-joint TOA estimator for the CDMA IS-95 pilot signal is the same as that of the independent TOA estimator. This can also be seen from equation (3.69) where $[\mathbf{J}(\boldsymbol{\theta})]_{45} \to 0$ because $\int_0^T \frac{dPN_I(t)}{dt} PN_Q(t)\, dt \to 0$ (see Appendix F), which means that the added unknown angle parameter φ in equation (5.32) affects little the TOA estimation.

2. The ***CRLB*** of TOA-joint AOA ($\varphi = 2\pi \frac{d}{\lambda} \cos\beta$) estimation for the CDMA IS-95 pilot signal is:

$$\begin{aligned} \mathrm{var}_{CRLB}(\hat{\varphi}) = [\mathbf{J}(\boldsymbol{\theta})]_{55}^{-1} &= \frac{\prod_{i=3}^{4} [\mathbf{J}(\boldsymbol{\theta})]_{ii}}{\prod_{i=3}^{5} [\mathbf{J}(\boldsymbol{\theta})]_{ii} - [\mathbf{J}(\boldsymbol{\theta})]_{35}^2 \prod_{i=3}^{4} [\mathbf{J}(\boldsymbol{\theta})]_{ii} \Big/ [\mathbf{J}(\boldsymbol{\theta})]_{33}} \\ &= \frac{1}{[\mathbf{J}(\boldsymbol{\theta})]_{55} - [\mathbf{J}(\boldsymbol{\theta})]_{35}^2 / [\mathbf{J}(\boldsymbol{\theta})]_{33}} \\ &= \frac{1}{\frac{2NM(M-1)(2M-1)\gamma^2}{3\sigma^2} - \left[\frac{2NM(M-1)\gamma^2}{\sigma^2}\right]^2 \Big/ \frac{4NM)\gamma^2}{\sigma^2}} \\ &= \frac{3}{N * SNR * M(M-1)^2} \end{aligned} \tag{3.72}$$

Here the SNR is the signal to noise ratio at the sampled point; N is the number of samples; and M is the number of antenna array elements.

Comparing equation (3.72) with (3.52b) shows that the CRLB of the TOA-joint AOA estimator for CDMA IS-95 pilot signal is larger than that of the independent AOA estimator because the latter estimator has fewer unknown parameters. However, when the number of antenna array *M* is large, their CRLBs are close.

3.9 Conclusions

Parameterized PDF and unbiased estimators were introduced followed by an example. The general estimation theory about CRLB was also described. Based on the linear uniform array, a data model and the corresponding parameterized PDF for AOA and TOA estimation were given. The CRLB of AOA estimation under one source signal was studied. From this simple case, we can see that the signal from the broadside of the antenna array has a smaller estimation error than that from the endfires. The larger the antenna spacing, the larger the number of antenna elements, and the higher *SNR* results in a smaller estimation error. The CRLB of AOA estimation under multiple source signals was also investigated. A simulation experiment result was given to explain the error factors from several more practical aspects. It shows that first, the phase of the correlation coefficient has a great impact on the value of CRLB; secondly, the larger AOA difference between two incident rays results in smaller CRLB values; thirdly, the number of source signals has a larger effect on the estimation accuracy than the *SNR* when the AOA difference between two incident rays is small. The CRLB of TOA for the IS-95 PN pilot signal was derived in terms of *SNR*, which is easier to be applied in practice. Finally, the

CRLBs of ***joint TOA and AOA estimation*** were derived and show a ***little bit worse performance than that of an independent AOA estimator, whereas for TOA estimation, both are the same***. The CRLBs of joint and independent AOA /TOA estimations for CDMA IS-95 pilot signals are summarized as Table 3.1.

Table 3:1: CRLB Comparison of Joint and Independent AOA/TOA Estimation

<table>
<tr><th></th><th>CRLBs of Joint AOA / TOA Estimation</th><th>CRLBs of AOA-assisted TOA Estimation</th></tr>
<tr><td rowspan="2">AOA</td><td rowspan="2">from equation (3.72) for single source signal:
$\mathrm{var}_{CRLB}(\hat{\varphi}) \approx \frac{3}{N * SNR * M(M-1)^2}$</td><td>from equation (3.52b) for single source signal:
$\mathrm{var}_{CRLB}(\hat{\varphi}) = \frac{3}{N * SNR * M(M^2-1)}$
It is the same as equation (3.40) when $N=1$.</td></tr>
<tr><td>from equation (3.52a) for multiple source signals:
$\mathrm{var}_{CRLB}(\hat{\ }) = \frac{\sigma^2}{2N}\left[\mathrm{Re}\left(\{\mathbf{D}^H[\,\mathbf{I}-\mathbf{A}(\mathbf{A}^H\mathbf{A})^{-1}\mathbf{A}^H\,]\,\mathbf{D}\}\odot\mathbf{R}_S\right)\right]^{-1}$
(Stoica & Nehorai 1989)</td></tr>
<tr><td>TOA</td><td>$\mathrm{var}_{CRLB}(\hat{\tau}) \approx \frac{T_C^2}{32MK \cdot SNR}$
from equation (3.71)</td><td>$\mathrm{var}_{CRLB}(\hat{\tau}) = \frac{T_C^2}{32MK \cdot SNR}$
from equation (3.64)</td></tr>
</table>

Chapter Four: AOA Estimation with the Forward/Backward Spatial Smoothing MUSIC Algorithm

4.1 Introduction

In Chapter 3, the CRLBs of the AOA-joint TOA method and AOA-assisted TOA method were derived. In this chapter, a specific estimator called the MUSIC (**MU**ltiple **SI**gnal **C**lassification) algorithm for AOA estimation is fully investigated followed by an error analysis. The variance expression for MUSIC AOA estimation is taken from Stoica & Nehorai (1989). Based on that, as in the case of the AOA CRLB, it is found that minimum and maximum variances exist and that the variance under more source signal environments is larger than that under fewer source signal environments, which is fundamental in this thesis. It will be seen that the unbiased MUSIC AOA estimator is suboptimal when the angle difference between two incident rays is large.

The *original* or *conventional* MUSIC algorithm was proposed by Schmidt (1979) to estimate the parameters of multiple uncorrelated or at most partially correlated signals arriving at an antenna array. It can provide asymptotically unbiased estimates of the following parameters (*ibid*):

1) The number of signals;
2) The angle of arrival;
3) The frequency.

Because the estimate resolution of the MUSIC algorithm exceeds the Rayleigh resolution criterion, it is classified as a high-resolution or super-resolution algorithm. The criteria were developed by Lord Rayleigh in 1879. It states that two arrivals are considered resolved when the first minimum angular spectrum value of one signal coincides with the maximum angular spectrum value of the other signal, as shown in Figure 4.1.

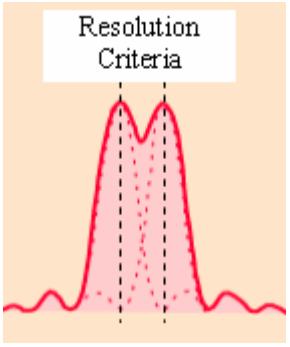

Figure 4.1: Rayleigh Resolution Criteria

Basically in the MUSIC algorithm, the measured data from M elements in the antenna array can be visualized as a vector in M dimensional space. It is fundamentally based on the eigen decomposition of the correlation matrix of the measured data. Assuming that there are K signals impinging on M elements ($M > K$) in the antenna array (otherwise, K signals cannot be resolved by an antenna array with M elements) and the correlation matrix of the signals is non-singular, M eigenvalues and the corresponding eigenvectors of the correlation matrix of the measured data can be obtained. These eigenvalues and eigenvectors can be grouped into two sets:

1. $M - K$ smallest eigenvalues and the corresponding eigenvectors that construct the noise subspace;

2. K largest eigenvalues and the corresponding eigenvectors that construct the signal subspace.

As a result, an M dimensional space can be spanned by M eigenvectors and partitioned into the above two subspaces, the noise and the signal subspace. Because the noise vectors and the signal vectors are orthogonal (Section 2.2.1), the inner product of the signal eigenvectors with the noise eigenvectors should be zero. Based on the above eigen decomposition technique and the partition of the orthogonal subspaces, the parameters of multiple signals can be estimated.

There are several MUSIC algorithms for different situations. Among them, the forward/backward MUSIC algorithm is suitable for AOA estimation under multipath environments (Pillai & Kwon 1989). In order to understand the application of the forward/backward MUSIC algorithm on the AOA estimation of IS-95 pilot signals, the fundamental characteristics of the algorithm are discussed in detail in the following sections.

4.2 Data Model for AOA Estimation

The data is received from a uniform linear array with M identical elements, as shown in Figure 3.1. Here is a brief review of Section 3.4. The K signals $s_1(t), s_2(t), \cdots, s_K(t)$ are

complex, the output data from the array is an $M \times 1$ complex vector $\mathbf{x}(t)$. For a single signal source $s_k(t)$, the array output vector $\mathbf{x}(t)$ can be expressed as

$$\begin{aligned}\mathbf{x}(t) &= \begin{bmatrix} x_1(t) \\ x_2(t) \\ \vdots \\ x_M(t) \end{bmatrix} = \begin{bmatrix} s_k(t) \\ s_k(t-\tau) \\ \vdots \\ s_k(t-(M-1)\tau \end{bmatrix} + \begin{bmatrix} n_1(t) \\ n_2(t) \\ \vdots \\ n_M(t) \end{bmatrix} = \begin{bmatrix} 1 \\ e^{-j2\pi f_c \tau} \\ \vdots \\ e^{-j2\pi f_c (M-1)\tau} \end{bmatrix} s_k(t) + \begin{bmatrix} n_1(t) \\ n_2(t) \\ \vdots \\ n_M(t) \end{bmatrix} \\ &= \mathbf{a}(\beta_k)\, s_k(t) + \mathbf{n}(t)\end{aligned} \tag{4.1}$$

where $\mathbf{a}(\beta_k) = \left[1,\ e^{-j2\pi f_c \tau}, \ldots, e^{-j2\pi f_c (M-1)\tau}\right]^T$ is an $M \times 1$ vector called the *direction vector*; the symbol (T) denotes transpose; f_c is the carrier frequency of the incident signals; $\tau = \dfrac{d * \cos(\beta_k)}{c}$ is the delay between two elements; d is the antenna element space; and $\mathbf{n}(t)$ is the $M \times 1$ complex noise vector. The noise at different antenna elements can be assumed to be zero-mean Gaussian stationary random processes and independent from element to element. Meanwhile, the noise is uncorrelated with the impinging signals.

If d equals to q times the carrier wavelength λ, the direction vector can be written as:

$$\begin{aligned}\mathbf{a}(\beta_k) &= \left[1,\ e^{-j2\pi\ q\cos\beta_k}, \ldots, e^{-j2\pi(M-1)\ q\cos\beta_k}\right]^T \\ &= \left[1,\ e^{-j\varphi_k}, \ldots, e^{-j_c(M-1)\ \varphi_k}\right]^T \\ &= \left[1, a_{\ k}, a_k^2, \cdots, a_k^{M-1}\right]^T \\ &= \{a_k^i\} \\ &\qquad i = 0, 2, \cdots, M-1\end{aligned} \tag{4.2}$$

where $\varphi_k = 2\pi\ q\ \cos\beta_k;\quad q = \dfrac{d}{\lambda};\quad a_k^i = e^{-j2\pi\ i\ q\ \cos\beta_k} = e^{-j\ i\ \varphi_k}$.

For K source signals, the $M \times 1$ array output vector can be expressed as

$$\begin{aligned}\mathbf{x}(t) &= \mathbf{a}(\beta_1)\, s_1(t) + \ldots + \mathbf{a}(\beta_K)\, s_K(t) + \mathbf{n}(t) = \sum_{i=1}^{K} \mathbf{a}(\beta_i)\, s_i(t) + \mathbf{n}(t) \\ &= [\mathbf{a}(\beta_1), \mathbf{a}(\beta_2), \ldots, \mathbf{a}(\beta_K)] \begin{bmatrix} s_1(t) \\ s_2(t) \\ \vdots \\ s_K(t) \end{bmatrix} + \begin{bmatrix} n_1(t) \\ n_2(t) \\ \vdots \\ n_M(t) \end{bmatrix} \\ &= \mathbf{A}\,\mathbf{s}(t) + \mathbf{n}(t)\end{aligned} \tag{4.3}$$

where $\mathbf{A} = [\mathbf{a}(\beta_1), \mathbf{a}(\beta_2), \ldots, \mathbf{a}(\beta_K)]$ is the *direction matrix* with Vandermonde-structure (*linearly independent columns if* $\beta_1, \beta_2, \cdots, \beta_K$ *are different*) and $\mathbf{s}(t) = [s_1(t), \ldots, s_K(t)]^T$ is a $K \times 1$ source signal vector.

In the above assumption, the noise at the antenna elements is mutually uncorrelated and also uncorrelated with the signals. Thus the $M \times M$ auto-correlation matrix of the array output vector $\mathbf{x}(t)$, which plays an important role in the MUSIC algorithm, can now be expressed as:

$$\begin{aligned}\mathbf{R} &= E\{\mathbf{x}(t)\mathbf{x}^H(t)\} \\ &= \mathbf{A}E\{\mathbf{s}(t)\mathbf{s}^H(t)\}\mathbf{A}^H + E\{\mathbf{n}(t)\mathbf{n}^H(t)\} + \mathbf{A}E\{\mathbf{s}(t)\mathbf{n}^H(t)\} + E\{\mathbf{n}(t)\mathbf{s}^H(t)\}\mathbf{A}^H \\ &= \mathbf{A}\,\mathbf{R}_S\,\mathbf{A}^H + \sigma^2\,\mathbf{I}_M\end{aligned} \tag{4.4}$$

where the symbol (H) denotes the Hermitian transpose; $\mathbf{R}_S = E\{\mathbf{s}(t)\mathbf{s}^H(t)\}$ denotes the $K \times K$ auto-correlation matrix for source signals; σ^2 is the variance of the additive noise; and $\mathbf{I}_M$ is the identity matrix.

Notice that if $\sigma^2 \neq 0$, $\mathbf{R}$ is positive definite, which means that all of its eigenvalues are greater than zero; if $\sigma^2 = 0$, $\mathbf{R}$ is positive semidefinite, which means that its eigenvalues are not less than zero In addition, $\mathbf{R}_S$ can be classified as three cases (Shan 1985):

1. Diagonal, non-singular and positive definite when the signals are uncorrelated;
2. Non-diagonal, non-singular and positive definite when some signals are partially correlated;
3. Non-diagonal, singular and nonnegative when some signals are correlated, which means that some eigenvalues are equal to zero.

In practice, *N* data samples from different snapshots can be used to approximate the covariance matrix of the array output as follows:

$$\hat{\mathbf{R}} = \frac{1}{N}\sum_{i=1}^{N} \mathbf{x}(t_i)\mathbf{x}^H(t_i) \tag{4.5}$$

The above approximation by time averaging is close to the expectation of the measured signal in equation (4.4) when *N* is large. If *N* is small, the accuracy of the AOA estimates will be degraded. If the vehicle is moving, when *N* is large, the information contained in the data changes as the time goes by. Then the data needs to be modified.

4.3 Eigen Analysis of Array Data Space

4.3.1 Array Signal Space

Before discussing the eigenanalysis of array data space, it is necessary to figure out the array data space and the relationship between array signal vector $\mathbf{x}(t)$ and *direction*

matrix $\mathbf{A}$ or *direction vector* $\mathbf{a}(\beta_k)$. The expression of the array signal vector $\mathbf{x}(t)$ is rewritten as:

$$\begin{aligned}\mathbf{x}(t) &= [\mathbf{a}(\beta_1), \mathbf{a}(\beta_2), \ldots, \mathbf{a}(\beta_K)] \begin{bmatrix} s_1(t) \\ s_2(t) \\ \vdots \\ s_K(t) \end{bmatrix} + \begin{bmatrix} n_1(t) \\ n_2(t) \\ \vdots \\ n_M(t) \end{bmatrix} \\ &= \begin{bmatrix} u_1(t) \\ u_2(t) \\ \vdots \\ u_M(t) \end{bmatrix} + \begin{bmatrix} n_1(t) \\ n_2(t) \\ \vdots \\ n_M(t) \end{bmatrix} = \mathbf{u}(t) + \mathbf{n}(t) = \mathbf{A}\,\mathbf{s}(t) + \mathbf{n}(t)\end{aligned} \tag{4.6}$$

where $\mathbf{A} = [\mathbf{a}(\beta_1)\ \mathbf{a}(\beta_2)\ \cdots\ \mathbf{a}(\beta_K)]$ has a Vandermonde structure; the vector $\mathbf{u}(t)$ represents the noise free *array signal space*. It can be seen that $\mathbf{u}(t)$ is the linear combination of the direction vectors $\mathbf{a}(\beta_i)$ and the coefficients of the combination are the source signals $\mathbf{s}_i(t)$. The concepts of the *array signal space* and the corresponding vectors $\mathbf{u}(t)$ are illustrated geometrically in Figure 4.2(a). There are two source signals impinging on an antenna array with three elements, i.e., the array signal space is two dimensions because it is constructed by the combination of two signal vectors $\mathbf{a}(\beta_1)$ and $\mathbf{a}(\beta_2)$. The correlation matrix $\mathbf{R}$ of $\mathbf{x}(t)$ can be written as:

$$\begin{aligned}\mathbf{R} &= E\{\mathbf{x}(t)\mathbf{x}^H(t)\} \\ &= \mathbf{A}\,\mathbf{R}_S\,\mathbf{A}^H + \sigma^2\mathbf{I} \\ &= \mathbf{R}_u + \sigma^2\mathbf{I}_M\end{aligned} \tag{4.7}$$

The constant complex matrix $\mathbf{A}$ reflects the relative locations between the antenna array and the signal sources. The K direction vectors in $\mathbf{A}$ are visualized as a K dimensional

signal subspace within the array signal space and the source signal vector $\mathbf{s}(t)$ lies in the subspace.

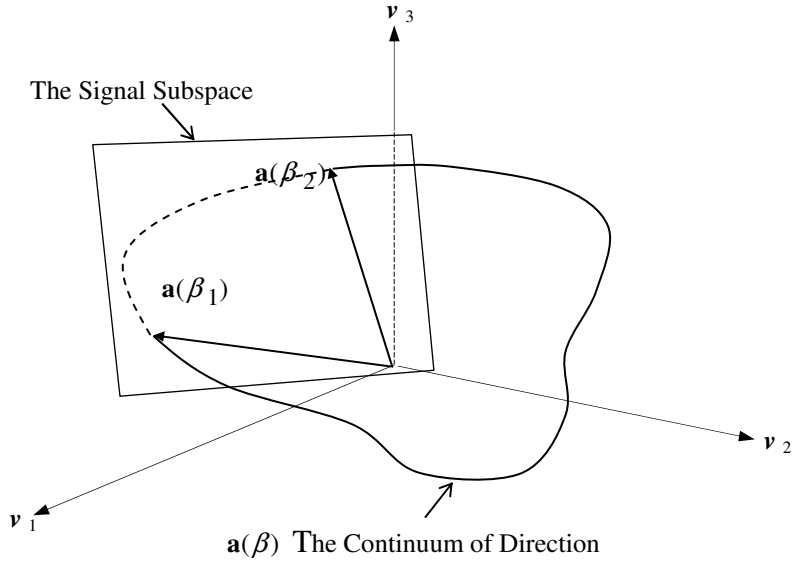

(a) Space for Two Signals and a Three-Element Antenna Array

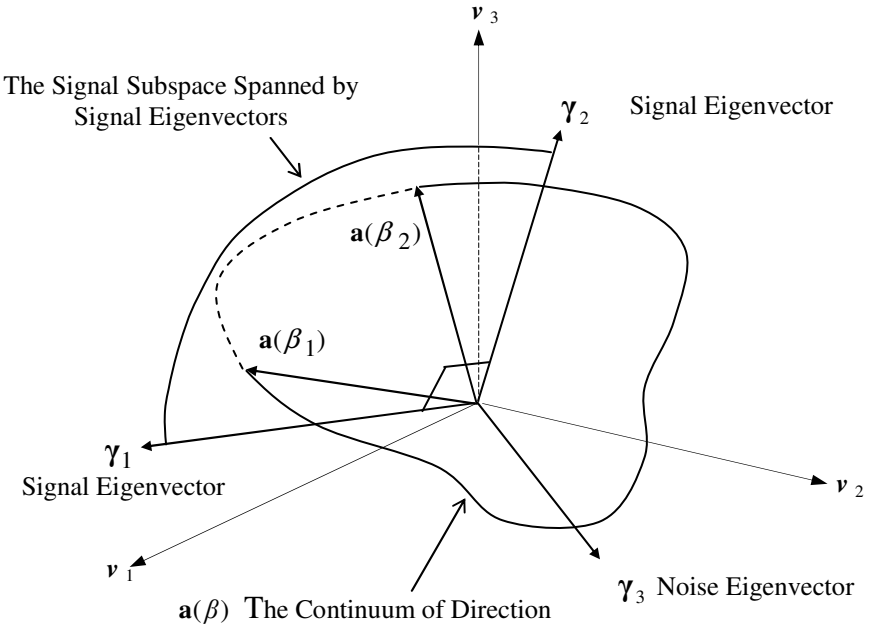

(b) Eigen Space for Two Signals and a Three-Element Antenna Array

Figure 4.2: (a) Space for Two Signals and a Three-Element Antenna Array; (b) Eigen Space for Two Signals and a Three-Element Antenna Array (Schmidt 1979)

4.3.2 Eigen Analysis of Array Signal Space with Spatially Uncorrelated or Partially Correlated Signals

Without loss of generalization, it can be assumed that the eigenvalues and the corresponding $M\times 1$ eigenvectors of $\mathbf{R}$ can be expressed as:

$$\begin{matrix}\{\lambda_1, \lambda_2, \cdots, \lambda_M\} & (\lambda_1 \geq \lambda_2 \geq \cdots \geq \lambda_M > 0) \\ \{\boldsymbol{\gamma}_1, \boldsymbol{\gamma}_2, \cdots, \boldsymbol{\gamma}_M\} & \end{matrix}. \tag{4.8}$$

The corresponding eigenvectors have the property of Hermitian matrices as follows:

$$\begin{matrix}\boldsymbol{\gamma}_i \perp \boldsymbol{\gamma}_j \quad or \quad \boldsymbol{\gamma}_i{}^H \boldsymbol{\gamma}_j = \mathbf{0} \\ (i, j = 1, 2, \cdots M \ \ and \ \ i \neq j)\end{matrix} \tag{4.9}$$

That is all eigenvectors of any correlation matrix are always *orthogonal.* When the signals impinging on the antenna array are uncorrelated or partially correlated, $\mathbf{R}_S = E\{\mathbf{s}(t)\mathbf{s}^H(t)\}$ is nonsingular with $rank(\mathbf{R}_S) = K$. After $\mathbf{R}_S$ is multiplied by the Vandermonde-structure direction matrix $\mathbf{A}_{M\times K}$, the matrix $\mathbf{R}_u = \mathbf{A}\,\mathbf{R}_S\,\mathbf{A}^H$ has a rank of:

$$rank(\mathbf{A}\,\mathbf{R}_S\,\mathbf{A}^H) = K \tag{4.10}$$

Based on Equation (4.7), (4.8) and (4.9), the following results can be obtained:

$$\begin{matrix}\lambda_1 \geq \lambda_2 \geq \cdots \geq \lambda_K > \sigma^2 \\ \lambda_{K+1} = \lambda_{K+2} = \cdots = \lambda_M = \sigma^2\end{matrix} \tag{4.11}$$

$$\mathbf{A}\,\mathbf{R}_S\,\mathbf{A}^H\boldsymbol{\gamma}_i = 0 \qquad i = K+1,\, K+2, \cdots, M \tag{4.12}$$

which results in the following equations:

$$\begin{aligned} &\mathbf{A}^H\boldsymbol{\gamma}_i = 0 \qquad i = K+1,\, K+2, \cdots, M \\ &or \\ &\mathbf{a}^H(\beta_j)\boldsymbol{\gamma}_i = 0 \quad or \quad \boldsymbol{\gamma}_i^H\mathbf{a}(\beta_j) = 0 \quad \begin{cases} j = 1, 2, \cdots, K \\ i = K+1,\, K+2, \cdots, M \end{cases} \end{aligned} \tag{4.13}$$

***Derivation of Equation* (4.13):**

By multiplying $\mathbf{A}^H$ to equation (4.12) and continuously multiplying $(\mathbf{A}^H\mathbf{A})^{-1}$ to the equation, one can get the following expression:

$$\begin{aligned} &(\mathbf{A}^H\mathbf{A})^{-1}(\mathbf{A}^H\mathbf{A})\,\mathbf{R}_S\,\mathbf{A}^H\boldsymbol{\gamma}_i = 0 \qquad i = K+1,\, K+2, \cdots, M \\ &or \\ &\mathbf{R}_S\,\mathbf{A}^H\boldsymbol{\gamma}_i = 0 \qquad i = K+1,\, K+2, \cdots, M \end{aligned} \tag{4.14}$$

By multiplying $\mathbf{R}^{-1}{}_S$ to the above equation, one can obtain equation (4.13).

Equations (4.11) - (4.13) state the following important facts:

1. There are *M-K* minimal eigenvalues that are equal to σ^2;
2. All direction vectors $\mathbf{a}(\beta_j)$ ($j = 1, 2, \cdots, K$) in the Vandermonde-structure direction matrix $\mathbf{A}$ are *orthogonal* to *M-K* noise eigenvectors corresponding to the *M-K* minimal eigenvalues.

As a result, the *M* dimensional array data space can be decomposed into two subspaces:

1. The noise subspace constructed by *M–K* noise eigenvectors;
2. The signal subspace constructed by *K* signal eigenvectors.

The concept of eigen analysis-based signal space is explained in Figure 4.2 (b). There are also two signals impinging on an antenna array with three elements. The two dimensional signal subspace can be visualized as a plane spanned by the signal eigenvectors, $\boldsymbol{\gamma}_1$ and $\boldsymbol{\gamma}_2$ ($\boldsymbol{\gamma}_1 \perp \boldsymbol{\gamma}_2$). The noise eigenvector $\boldsymbol{\gamma}_3$ is orthogonal to the signal eigenvectors.

4.4 AOA Estimation with the Conventional MUSIC Algorithm for Spatially Uncorrelated or Partially Correlated Signals

4.4.1 Conventional MUSIC Algorithm

As discussed in section 4.3, there are (*M-K*) noise eigenvectors. If $\mathbf{V}_N$ denotes the $M \times$ (*M-K*) matrix whose columns are the noise eigenvectors as follows:

$$\mathbf{V}_N = [\boldsymbol{\gamma}_{K+1}, \boldsymbol{\gamma}_{K+2}, \ldots, \boldsymbol{\gamma}_M] \tag{4.15}$$

and if any vector $\mathbf{Y}$ with *M* elements is orthogonal to the noise eigenvectors in matrix $\mathbf{V}_N$, then the multiplication of vector $\mathbf{Y}$ by matrix $\mathbf{V}_N$ yields:

$$\begin{aligned} &\mathbf{V}_N^H \mathbf{Y} = 0 \\ &or \\ &\mathbf{Y}^H \mathbf{V}_N \mathbf{V}_N^H \mathbf{Y} = 0 \end{aligned} \tag{4.16}$$

Based on the above equations, the conventional MUSIC algorithm is similar in the equation below because the direction vectors $\mathbf{a}(\beta_j)$ ($j = 1, 2, \cdots, K$) are orthogonal to all the noise eigenvectors in matrix $\mathbf{V}_N$ (Section 4.3.2):

$$\mathbf{a}^H(\beta_j)\mathbf{V}_N\mathbf{V}_N^H\mathbf{a}(\beta_j) = 0 \quad (j = 1, 2, \cdots, K) \tag{4.17}$$

By using a steering vector $\mathbf{a}(\beta)$, the AOAs of signals can be determined by searching through all angles β in the "MUSIC spatial spectrum" $P(\beta)$, expressed as:

$$P(\beta) = \frac{1}{\mathbf{a}^H(\beta)\mathbf{V}_N\mathbf{V}_N^H\mathbf{a}(\beta)}. \tag{4.18}$$

When $\mathbf{a}(\beta)$ is equal to any one of the direction vectors $\mathbf{a}(\beta_j)$ ($j = 1, 2, \cdots, K$), i.e., $\mathbf{a}(\beta)$ is perpendicular to the noise eigenvectors in matrix $\mathbf{V}_N$, and the denominator of $P(\beta)$ is zero. So the AOAs are estimated by locating the peaks of a "MUSIC spatial spectrum" $P(\beta)$. The relationship between the number *M* of linear array elements and the number *K* of uncorrelated signals should be as follows:

$$M \geq K + 1 \tag{4.19}$$

This is because there should be at least one vector space for noise among *M* eigenvectors to scan out $K = M - 1$ signals. If the number of noise vectors is *i*, then the number of signals is $K = M - i$.

The steps in the conventional MUSIC algorithm are summarized as follows:

1. Choose *M* (the number of linear array elements) $\geqq$ *K*+1 (*K* is the number of

uncorrelated signals);

2. Calculate the correlation matrix **R** of the measured data;
3. Calculate the eigenvalues of the correlation matrix **R**;
4. Construct the noise matrix $\mathbf{V}_N$ based on noise eigenvectors;
5. Evaluate the "spatial spectrum" $P(\beta) = \dfrac{1}{d^2(\beta)} = \dfrac{1}{\mathbf{a}^H(\beta)\mathbf{V}_N\mathbf{V}_N^H\mathbf{a}(\beta)}$;
6. Pick *K* peaks of $P(\beta)$ and obtain AOAs.

4.4.2 Failure of the Conventional MUSIC Algorithm

If some signals impinging on the antenna array are spatially correlated, the conventional MUSIC algorithm cannot be used to estimate the AOAs of the signals. The following example shows how the conventional MUSIC fails under correlated signals.

***Example 1*:**

Assuming that there are two correlated CW signals $s_1(t)$ and $s_2(t)$ impinging on a linear antenna array with three elements and the antenna spacing is $d = \lambda/2$. $s_1(t)$ is a LOS signal and $s_2(t)$ is an NLOS signal. If their impinging angles are $\beta_1 = 90^0$ and $\beta_2 = 60^0$ respectively, the direction vectors and matrix can be expressed as:

$$\mathbf{a}(\beta_1) = [1, 1, 1]^T, \quad \mathbf{a}(\beta_2) = [1, e^{-j\varphi_2}, e^{-j2\varphi_2}]^T = [1, -j, -1]^T$$

$$\textit{here} \quad \varphi_2 = 2\pi\frac{d}{\lambda}\cos\beta_2 = \pi/2 \quad \textit{and} \qquad \mathbf{A} = [\mathbf{a}(\beta_1) \quad \mathbf{a}(\beta_2)].$$

Because the NLOS signal $s_2(t)$ is the replica of the LOS signal $s_1(t)$, the relationship between two signals can be written as:

$$s_2(t) = ws_1(t)$$

where w is the complex weight coefficient, which represents the time delay and amplitude attenuation with respect to the LOS signal. Suppose that the independent noise $\mathbf{n}(t)_{3\times 1}$ at different antenna elements is a zero-mean Gaussian stationary random process with variance σ^2 and uncorrelated with the impinging signals. Then the correlation matrix $\mathbf{R}$ of the measured array data $\mathbf{x}(t)_{3\times 1} = [\mathbf{a}(\beta_1)s_1(t) + \mathbf{a}(\beta_2)s_2(t)] + \mathbf{n}(t)$, if $|s_1(t)|^2 = 1$, can be expressed as follows:

$$\begin{aligned}\mathbf{R} &= E\{\mathbf{x}(t)\mathbf{x}^H(t)\} \\ &= \mathbf{A}\begin{bmatrix} 1 & w^* \\ w & w^2 \end{bmatrix}\mathbf{A}^H + \sigma^2\mathbf{I} = \begin{bmatrix} |1+w|^2+\sigma^2 & (1+w)(1+jw^*) & (1+w)(1-w^*) \\ (1+w^*)(1-jw) & |j+w|^2+\sigma^2 & (1-w^*)(1-jw) \\ (1+w^*)(1-w) & (1-w)(1+jw^*) & |1-w|^2+\sigma^2 \end{bmatrix}\end{aligned}$$

It is evident that $\mathbf{R}_S$ is not a full rank matrix with rank($\mathbf{R}_S$) = 1. A further analysis is worth doing for understanding the limitation of the "MUSIC spatial spectrum". Substituting $w = e^{j\pi/4}$, which means that there is a $\pi/4$ phase delay for the NLOS signal $s_2(t)$, into the above equation, the correlation matrix $\mathbf{R}$ is obtained as:

$$\mathbf{R} = \begin{bmatrix} 2+\sqrt{2}+\sigma^2 & (1+\sqrt{2})(1+j) & j\sqrt{2} \\ (1+\sqrt{2})(1-j) & 2+\sqrt{2}+\sigma^2 & 1+j \\ -j\sqrt{2} & 1-j & 2-\sqrt{2}+\sigma^2 \end{bmatrix}$$
$$= \begin{bmatrix} 2+\sqrt{2}+\sigma^2 & \sqrt{2}(1+\sqrt{2})\,e^{j\pi/4} & \sqrt{2}e^{j\pi/2} \\ \sqrt{2}(1+\sqrt{2})\,e^{-j\pi/4} & 2+\sqrt{2}+\sigma^2 & \sqrt{2}\,e^{j\pi/4} \\ \sqrt{2}e^{-j\pi/2} & \sqrt{2}\,e^{-j\pi/4} & 2-\sqrt{2}+\sigma^2 \end{bmatrix}$$

Three eigenvalues of $\mathbf{R}$ are $\lambda_1 = 6+\sqrt{2}+\sigma^2$, $\lambda_2 = \lambda_3 = \sigma^2$. The corresponding eigenvectors of the eigenvalues are calculated as:

$$\gamma_1 = [\ 1,\quad \frac{\sqrt{2}}{2} - j\frac{\sqrt{2}}{2},\quad -j(\sqrt{2}-1)\ ]^T,\quad \gamma_2 = [\ \frac{\sqrt{2}}{2} + j\frac{\sqrt{2}}{2},\quad -1,\quad 0\ ]^T$$
$$\gamma_3 = [\ -j(\sqrt{2}-1),\quad 0,\quad 1\ ]^T$$

It is clear that the noise space eigenvectors γ_2 and γ_3 are orthogonal to the combined direction vector $\mathbf{a}(\beta_1) + w\mathbf{a}(\beta_2)$, but not orthogonal to the original direction vectors, either $\mathbf{a}(\beta_1)$ or $\mathbf{a}(\beta_2)$. Therefore, AOAs cannot be estimated by "MUSIC spatial spectrum" of equation (4.18). The extension of this example, *Example 2*, is continued in Section 4.5.3 for the explanation of the successful use of forward/backward smoothing MUSIC technique.

In terms of matrix algebra theory, the following more general example is given to prove that the rank of the covariance matrix of the correlated signals is not full and not orthogonal to the noise eigenvectors. Assume that the multipath environment consists of *K* correlated signals from the same CW source (perfectly correlated) and the number of

array elements is *M*. The correlated signals $s_1(t), s_2(t), \cdots, s_K(t)$, from the directions of $\beta_1, \beta_2, \cdots, \beta_K$ respectively, are phase-delayed amplitude-weighted replicas of the source signal and expressed as:

$$s_k(t) = w_k s_1(t) \qquad k = 1, 2, \cdots, K \tag{4.20}$$

here w_k represents the complex weight coefficient of the k^{th} signal $s_k(t)$ with respect to the source signal $s_1(t)$.

By defining **w** to be the weight coefficient vector as follow:

$$\mathbf{w} = [w_1, w_2, \ldots, w_K]^T, \tag{4.21}$$

the signal vector can be written as:

$$\mathbf{s}(t) = \mathbf{w} s_1(t) \tag{4.22}$$

and the expression for the measured data vector can be written as:

$$\begin{aligned} \mathbf{x}(t) &= [\mathbf{a}(\theta_1), \mathbf{a}(\theta_2), \ldots, \mathbf{a}(\theta_K)]\, \mathbf{w}\, s_1(t) + \begin{bmatrix} n_1(t) \\ n_2(t) \\ \vdots \\ n_M(t) \end{bmatrix} \\ &= \mathbf{A}\, \mathbf{w} s_1(t) + \mathbf{n}(t) \end{aligned} . \tag{4.23}$$

Thus, the covariance or correlation matrix $\mathbf{R}_S$ of $\mathbf{s}(t)$ is as follows:

$$\mathbf{R}_S = E\{\mathbf{s}(t)\mathbf{s}^H(t)\} = |s_1(t)|^2 \mathbf{w}\mathbf{w}^H \tag{4.24}$$

Now the covariance or correlation matrix **R** of $\mathbf{x}(t)$ is modified as:

$$\begin{aligned}\mathbf{R} &= E\{\mathbf{x}(t)\mathbf{x}^H(t)\} \\ &= |s_1(t)|^2\ \mathbf{A}\,\mathbf{w}\mathbf{w}^H\,\mathbf{A}^H + \sigma^2\,\mathbf{I}_M\end{aligned} \tag{4.25}$$

Because the rank of the $K \times K$ Hermitian matrix $\mathbf{w}\mathbf{w}^H$ is equal to 1 (singular) expressed as:

$$rank(\mathbf{w}\mathbf{w}^H) = 1\ , \tag{4.26}$$

according to matrix algebra theory (Abadir & Magnus 2005), the rank of $\mathbf{A}\,\mathbf{w}\mathbf{w}^H\,\mathbf{A}^H$ is also equal to 1 as follow:

$$rank(\mathbf{A}\,\mathbf{w}\mathbf{w}^H\,\mathbf{A}^H) = 1\,. \tag{4.27}$$

It means that there is only one independent source signal. Therefore there are M-1 noise eigenvectors orthogonal to $\mathbf{A}\,\mathbf{w}\mathbf{w}^H\,\mathbf{A}^H$, which can be expressed as follows:

$$\mathbf{A}\,\mathbf{w}\mathbf{w}^H\,\mathbf{A}^H\boldsymbol{\gamma}_i = 0 \qquad i = 2, 3, \cdots, M\ . \tag{4.28}$$

Based on the fact that the inverse of matrix $\mathbf{w}\mathbf{w}^H$ does not exist, the above formula can be simplified as:

$$\mathbf{w}^H\,\mathbf{A}^H\boldsymbol{\gamma}_i = 0 \quad or \quad (\mathbf{A}\mathbf{w})^H\boldsymbol{\gamma}_i = 0 \quad i = 2, 3, \cdots, M \tag{4.29}$$

where $\mathbf{A}\mathbf{w}$ is an $M\times1$ column vector which is the linear combination of all of direction mode vectors. It can be defined as:

$$\mathbf{b} = \mathbf{A}\mathbf{w} = \sum_{i=1}^{K}\mathbf{a}(\beta_i)w_i \qquad . \tag{4.30}$$

It can be seen from equations (4.29) and (4.30) that only the linear combination of all of direction vectors **b,** which is no longer of the Vandermonde structure, is orthogonal to the noise eigenvectors. So when the Vandermonde-structure steering vector $\mathbf{a}(\beta)$ scans the all possible angles, it will never match non-Vandermonde structure direction vector $\mathbf{b}=\mathbf{Aw}$ in the newly generated direction matrix $\mathbf{A}\,\mathbf{w}\mathbf{w}^H\,\mathbf{A}^H$ to estimate the AOAs of the correlated signals.

The limitations of the conventional MUSIC algorithm application in correlated signal AOA finding can be summarized as:

If m out of K signals are fully correlatetd, only the K-m uncorrelated signals can be resolved using the conventional MUSIC algorithm.

4.5 AOA Estimation with the Forward/Backward Smoothing MUSIC Algorithm for Spatially Correlated Signals

In practice, multipath signals exit in most wireless systems, which motivated people to improve the conventional MUSIC algorithm to find the AOAs of correlated signals. Evans et al (1981) and Shan et al (1985) proposed and demonstrated the effectiveness of the forward smoothing MUSIC algorithm. Pillai et al (1989) then proposed the backward smoothing MUSIC algorithm and combined the two algorithms into one

Forward/Backward Smoothing MUSIC algorithm to resolve the AOAs of correlated signals.

4.5.1 Forward Smoothing MUSIC Algorithm for Spatially Correlated Signals

Assume that a linear uniform array consists of M elements that are divided into L overlapping subarrays, each with m elements, as shown in Figure 4.3. Thus, the elements $\{1, 2, \ldots, m\}$ are grouped as the first forward subarray; the elements $\{2, 3, \ldots, m+1\}$ as the second forward subarray and so on. The number of forward subarrays is defined as:

$$L = M - m + 1 \tag{4.31}$$

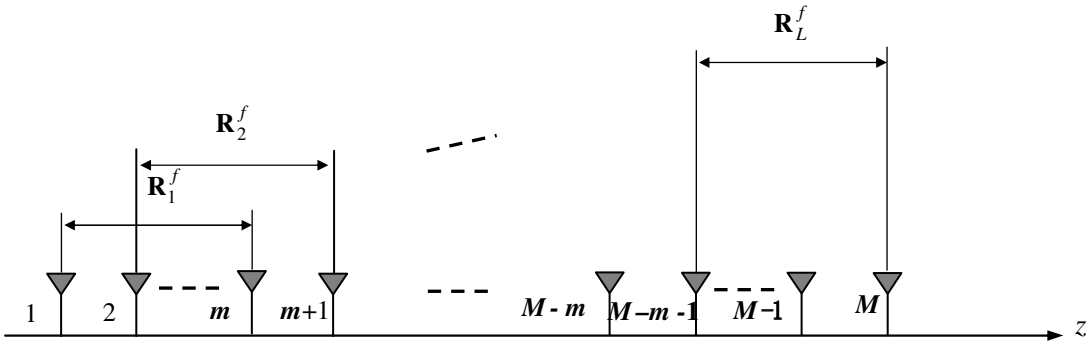

Figure 4.3: Forward Spatial Smoothing Scheme

Let $\mathbf{x}_l^f(t)$ be the measured data vector of the l^{th} forward subarray (l = 1, 2, … , L). Based on equations (4.1) - (4.3), $\mathbf{x}_l^f(t)$ can be expressed as follows:

$$\begin{aligned}\mathbf{x}_l^f(t) &= [x_l(t), x_{l+1}(t), \ldots, x_{l+m-1}(t)]^T \\ &= [a_1^{l-1}\mathbf{a}(\beta_1), a_2^{l-1}\mathbf{a}(\beta_2), \ldots, a_K^{l-1}\mathbf{a}(\beta_K)]\begin{bmatrix} s_1(t) \\ s_2(t) \\ \vdots \\ s_K(t) \end{bmatrix} + \begin{bmatrix} n_l(t) \\ n_{l+1}(t) \\ \vdots \\ n_{l+m-1}(t) \end{bmatrix} \\ &= \mathbf{A}\,\mathbf{B}^{l-1}\mathbf{s}(t) + \mathbf{n}_l^f(t)\end{aligned} \tag{4.32}$$

where $\mathbf{A}$ is an $m \times K$ direction matrix defined in equation (4.3); $\mathbf{B}^{l\text{-}1}$ is the $(l\text{-}1)^{\text{th}}$ power of the $K \times K$ diagonal matrix $\mathbf{B}$ and it has the following expression:

$$\mathbf{B} = diag\,[a_1, a_2, \ldots, a_K]; \qquad a_i = e^{-j2\pi q \cos\beta_i} \qquad i = 1, 2, \cdots, K\,. \tag{4.33}$$

Consequently, the auto-correlation matrix of the l^{th} forward subarray can be derived as:

$$\begin{aligned}\mathbf{R}_l^f &= E\{\mathbf{x}_l^f(t)(\mathbf{x}_l^f(t))^H\} \\ &= \mathbf{A}\mathbf{B}^{l-1}\mathbf{R}_S\,(\mathbf{B}^{l-1})^H\mathbf{A}^H + \sigma^2\mathbf{I}_m\end{aligned} \tag{4.34}$$

Here $\mathbf{I}_m$ is an m-dimensional identity matrix.

The forward spatial smoothing scheme is to obtain the mean of all forward subarray covariance matrices and then implement eigendecomposition of the smoothed covariance matrix. Thus, the forward smoothed auto-correlation matrix $\mathbf{R}^f$ for all subarrays can be written as:

$$\begin{aligned}\mathbf{R}^f &= \frac{1}{L}\sum_{l=1}^{L}\mathbf{R}_l^f = \mathbf{A}\left(\frac{1}{L}\sum_{l=1}^{L}\mathbf{B}^{l-1}\mathbf{R}_S\,(\mathbf{B}^{l-1})^H\right)\mathbf{A}^H + \sigma^2\mathbf{I}_m \\ &= \mathbf{A}\mathbf{R}_S^f\mathbf{A}^H + \sigma^2\mathbf{I}_m\end{aligned} \tag{4.35}$$

where $\mathbf{R}_S^f$ is the forward smoothed source signal auto-correlation matrix of the signal, which is expressed as:

$$\begin{aligned}
\mathbf{R}_S^f &= \frac{1}{L}\sum_{l=1}^{L}\mathbf{B}^{l-1}\mathbf{R}_S\ (\mathbf{B}^{l-1})^H \\
&= \frac{1}{L}\sum_{l=1}^{L}\mathbf{B}^{l-1}\mathbf{R}_S\ \mathbf{B}^{-(l-1)} \\
&= \frac{1}{L}\mathbf{R}_S \odot \sum_{l=1}^{L} diag(\mathbf{B}^{l-1})[diag(\ \mathbf{B}^{-(l-1)})]^T
\end{aligned}$$

where

$$\begin{aligned}
&\mathbf{B}^{(l-1)} = diag\ [a_1^{(l-1)}, a_2^{(l-1)}, \ldots, a_K^{(l-1)}]; \\
&diag(\mathbf{B}^{(l-1)}) = [a_1^{(l-1)}, a_2^{(l-1)}, \ldots, a_K^{(l-1)}]^T; \\
&\mathbf{B}^{-(l-1)} = diag\ [a_1^{-(l-1)}, a_2^{-(l-1)}, \ldots, a_K^{-(l-1)}]; \\
&diag(\mathbf{B}^{-(l-1)}) = [a_1^{-(l-1)}, a_2^{-(l-1)}, \ldots, a_K^{-(l-1)}]^T; \\
&\quad a_i = e^{-j2\pi q \cos\beta_i} \qquad i = 1, 2, \cdots, K
\end{aligned} \tag{4.36}$$

Based on the conventional MUSIC algorithm of Section 4.4.1, if only $\mathbf{R}_S^f$ in equation (4.35) is a full rank matrix, i.e. $rank(\mathbf{R}_S^f) = K$, then all AOAs can be estimated even if the impinging signals are correlated. In fact, $\mathbf{R}_S^f$ is a full rank matrix, only if $L \geq K$. This property is demonstrated below.

Assuming that the impinging signals are all correlated, the signal vector has the expression of equation (4.22) with $|s_1(t)|^2 = 1$, and the $K \times K$ source auto-correlation matrix $\mathbf{R}_S^f$ of the forward smoothing scheme has the following form:

$$\begin{aligned}\mathbf{R}_S^f &= \frac{1}{L}\sum_{l=1}^{L}\mathbf{B}^{l-1}\mathbf{w}\,(\mathbf{B}^{l-1}\mathbf{w})^H \\ &= \frac{1}{L}[\mathbf{w}, \mathbf{Bw}, \mathbf{B}^2\mathbf{w}, \cdots, \mathbf{B}^{L-1}\mathbf{w}][\mathbf{w}, \mathbf{Bw}, \mathbf{B}^2\mathbf{w}, \cdots, \mathbf{B}^{L-1}\mathbf{w}]^H \\ &= \frac{1}{L}\mathbf{C}\mathbf{C}^H\end{aligned} \tag{4.37}$$

where $\mathbf{C}$ is a $K\times L$ matrix, which is expressed as:

$$\begin{aligned}\mathbf{C} &= [\mathbf{w}, \mathbf{Bw}, \mathbf{B}^2\mathbf{w}, \cdots, \mathbf{B}^{L-1}\mathbf{w}] \\ &= \begin{bmatrix} w_1 & & & \mathbf{0} \\ & w_2 & & \\ & & \ddots & \\ \mathbf{0} & & & w_K \end{bmatrix}\begin{bmatrix} 1 & a_1 & a_1^2 & \cdots & a_1^{L-1} \\ 1 & a_2 & a_2^2 & \cdots & a_2^{L-1} \\ \vdots & \vdots & \vdots & \ddots & \vdots \\ 1 & a_K & a_K^2 & \cdots & a_K^{L-1} \end{bmatrix} \\ &= \mathbf{D}\boldsymbol{\Lambda}\end{aligned} \tag{4.38}$$

where $\mathbf{D}$ is a diagonal matrix and $\boldsymbol{\Lambda}$ has a Vandermonde structure.

Based on equation (4.37) and (4.38), the following relationship between the ranks of $\mathbf{R}_S^f$, $\mathbf{C}$, $\mathbf{D}$ and $\boldsymbol{\Lambda}$ is obtained:

$$rank(\mathbf{R}_S^f) = rank(\mathbf{C}) = \min\left(rank(\mathbf{D}), rank(\boldsymbol{\Lambda})\right). \tag{4.39}$$

Note that the rank of the $K\times K$ diagonal matrix $\mathbf{D}$ is K. Thus, if $L \geq K$, the rank of the Vandermonde matrix $\boldsymbol{\Lambda}$ is also K. As a result, $\mathbf{R}_S^f$ is a full rank covariance matrix, $rank(\mathbf{R}_S^f) = K$, only if $L \geq K$. It means that even when the impinging signals are all correlated, their AOAs can be resolved by the forward smoothing MUSIC algorithm. The above result is obtained when $a_1 \neq a_2 \neq a_3 \cdots \neq a_K$. When $a_1 = a_2 = a_3 \cdots = a_K$, i.e. all K signals are from the same incident angle, then the MUSIC algorithm cannot resolve them.

Based on the above discussion and Figure 4.3, the minimum number of antenna array elements for the forward smoothing MUSIC algorithm should meet the following equation:

$$M_{\min} = L_{\min} + m_{\min} - 1 = K + (K+1) - 1 = 2K \,. \tag{4.40}$$

Compared with K+1 elements for the conventional MUSIC algorithm, the forward smoothing MUSIC algorithm sacrifices more antenna elements to overcome the correlated signal problems that occur in the conventional MUSIC algorithm.

4.5.2 Backward Smoothing MUSIC Algorithm for Spatially Correlated Signals

The backward subarrays are also generated from the linear uniform array, as shown in Figure 4.3.

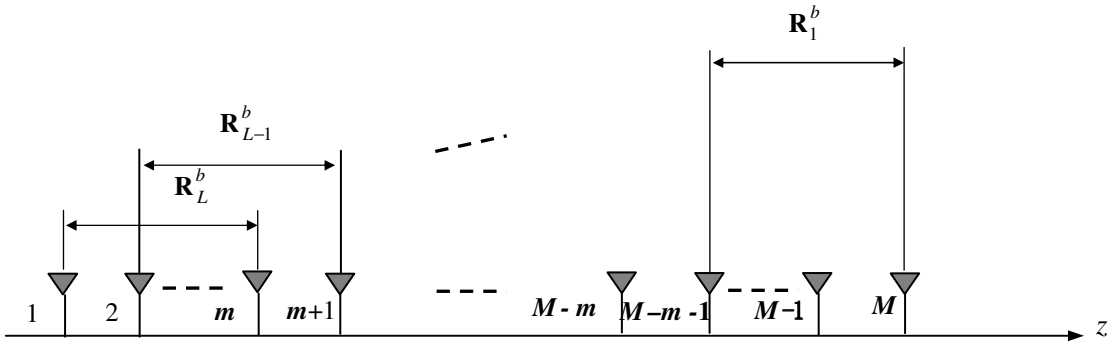

Figure 4.4: Backward Spatial Smoothing Scheme

Based on Figure 4.4, the elements {M, M-1, … , M-m+1} are grouped as the first backward subarray; the elements { M-1, M-2, … , M-m } as the second backward

subarray and so on. Thus, the number of the backward subarrays is the same as the forward smoothing case, which is $L = M - m + 1$ as in equation (4.31).

Let $\mathbf{x}_l^b(t)$ be the measured data vector of the l^{th} backward subarray (l = 1, 2, … , L). Based on equations (4.1) - (4.3), it has the following expression:

$$\begin{aligned}
\mathbf{x}_l^b(t) &= [x_{M-l+1}^*(t),\, x_{M-l}^*(t),\, \ldots,\, x_{L-l+1}^*(t)]^T \\
&= \left([a_1^{M-l+1}\mathbf{a}^*(\beta_1),\, a_2^{M-l+1}\mathbf{a}^*(\beta_2),\, \ldots,\, a_K^{M-l+1}\mathbf{a}^*(\beta_K)] \begin{bmatrix} s_1(t) \\ s_2(t) \\ \vdots \\ s_K(t) \end{bmatrix} \right)^* + \begin{bmatrix} n_{M-l+1}^*(t) \\ n_{M-1}^*(t) \\ \vdots \\ n_{L-l+1}^*(t) \end{bmatrix} \\
&= \mathbf{A}\left(\mathbf{B}^{M-l+1}\mathbf{s}(t)\right)^* + \tilde{\mathbf{n}}_l(t) = \mathbf{A}\mathbf{B}^{l-1}\left(\mathbf{B}^{M-1}\mathbf{s}(t)\right)^* + \mathbf{n}_l^b(t) \\
&= \mathbf{A}\mathbf{B}^{l-1}\mathbf{r}(t) + \mathbf{n}_l^b(t) \qquad l = 1, 2, \cdots, L
\end{aligned} \tag{4.41}$$

where $\mathbf{r}(t) = \left(\mathbf{B}^{M-1}\mathbf{s}(t)\right)^*$. Then the auto-correlation matrix of the l^{th} backward subarray can be derived as:

$$\begin{aligned}
\mathbf{R}_l^b &= E\{\mathbf{x}_l^b(t)(\mathbf{x}_l^b(t))^H\} \\
&= \mathbf{A}\mathbf{B}^{l-1}\mathbf{R}_{\mathbf{r}}\,(\mathbf{B}^{l-1})^H\mathbf{A}^H + \sigma^2\mathbf{I}_m
\end{aligned} \tag{4.42}$$

where

$$\begin{aligned}
\mathbf{R}_{\mathbf{r}} &= E\{\mathbf{r}(t)\mathbf{r}(t)^H\} \\
&= \mathbf{B}^{-(M-1)}E\{\mathbf{s}^*(t)\mathbf{s}^T(t)\}\,(\mathbf{B}^{-(M-1)})^H \\
&= \mathbf{B}^{-(M-1)}\left(E[\mathbf{s}(t)\mathbf{s}^H(t)]\right)^*(\mathbf{B}^{-(M-1)})^H \\
&= \mathbf{B}^{-(M-1)}\mathbf{R}_S^*\,\mathbf{B}^{(M-1)} \\
\mathbf{B}^{-(M-1)} &= diag\,[a_1^{-(M-1)},\, a_2^{-(M-1)},\, \ldots,\, a_K^{-(M-1)}]; \\
a_i &= e^{-j2\pi q\cos\beta_i} \qquad i = 1, 2, \cdots, K
\end{aligned} \tag{4.43}$$

Similarly, the backward spatial smoothing scheme is to obtain the mean of all backward subarray covariance matrices and then implement the eigen decomposition of the smoothed covariance matrix. Thus, the backward smoothed auto-correlation matrix $\mathbf{R}^b$ for all subarrays can be written as:

$$\begin{aligned}\mathbf{R}^b &= \frac{1}{L}\sum_{l=1}^{L}\mathbf{R}_l^b = \mathbf{A}\left(\frac{1}{L}\sum_{l=1}^{L}\mathbf{B}^{l-1}\mathbf{R}_{\mathbf{r}}\,(\mathbf{B}^{l-1})^H\right)\mathbf{A}^H + \sigma^2\mathbf{I} \\ &= \mathbf{A}\mathbf{R}_S^b\mathbf{A}^H + \sigma^2\mathbf{I}_m\end{aligned} \tag{4.44}$$

where $\mathbf{R}_S^b$ is the backward smoothed source signal auto-correlation matrix, which is written as:

$$\begin{aligned}\mathbf{R}_S^b &= \frac{1}{L}\sum_{l=1}^{L}\mathbf{B}^{l-1}\mathbf{R}_{\mathbf{r}}\,(\mathbf{B}^{l-1})^H \\ &= \frac{1}{L}\sum_{l=1}^{L}\mathbf{B}^{-(M-l)}\mathbf{R}_S^*\,\mathbf{B}^{(M-l)} \\ &= \frac{1}{L}\mathbf{R}_S^* \odot\sum_{l=1}^{L} diag(\mathbf{B}^{-(M-l)})[diag(\,\mathbf{B}^{(M-l)})]^T\end{aligned} \tag{4.45}$$

where $diag(\,\mathbf{B}^{(M-l)}) = [a_1^{(M-1)}, a_2^{(M-1)}, \ldots, a_K^{(M-1)}]^T$.

Considering the completely correlated situation (referring to equation (4.24)) and assuming that $|\,s_1(t)\,|^2 = 1$, $\mathbf{R}_{\mathbf{r}}$ in equation (4.43) can be modified as:

$$\begin{aligned}\mathbf{R}_{\mathbf{r}} &= \mathbf{B}^{-(M-1)}\mathbf{R}_S^*\,(\mathbf{B}^{-(M-1)})^H \\ &= \mathbf{B}^{-(M-1)}\mathbf{w}^*\,(\mathbf{B}^{-(M-1)}\mathbf{w}^*)^H \\ &= \boldsymbol{\delta}\,\boldsymbol{\delta}^H\end{aligned} \tag{4.46}$$

where (refer to equation (4.2))

$$\begin{aligned}
&\boldsymbol{\delta} = [\,\delta_1, \delta_2, \cdots, \delta_K\,]^T; \\
&\delta_k = w_k^* \, a_k^{-(M-1)}; \quad a_k^{-(M-1)} = e^{j2\pi(M-1)\ q\cos\beta_k} \qquad k = 1, 2, \cdots, K
\end{aligned} \tag{4.47}$$

As a result, the $K\times K$ source auto-correlation matrix $\mathbf{R}_S^b$ of the backward smoothing scheme has the following form:

$$\begin{aligned}
\mathbf{R}_S^b &= \frac{1}{L}\sum_{l=1}^{L} \mathbf{B}^{l-1}\mathbf{R}_{\mathbf{r}}\ (\mathbf{B}^{l-1})^H \\
&= \frac{1}{L}\sum_{l=1}^{L} \mathbf{B}^{l-1}\boldsymbol{\delta}\ \boldsymbol{\delta}^H\ (\mathbf{B}^{l-1})^H \\
&= \frac{1}{L}[\boldsymbol{\delta}, \mathbf{B}\boldsymbol{\delta}, \mathbf{B}^2\boldsymbol{\delta}, \cdots, \mathbf{B}^{L-1}\boldsymbol{\delta}][\boldsymbol{\delta}, \mathbf{B}\boldsymbol{\delta}, \mathbf{B}^2\boldsymbol{\delta}, \cdots, \mathbf{B}^{L-1}\boldsymbol{\delta}]^H \\
&= \frac{1}{L}\mathbf{E}\mathbf{E}^H
\end{aligned} \tag{4.48}$$

where $\mathbf{E}$ is a $K\times L$ matrix, which is formed as:

$$\begin{aligned}
\mathbf{E} &= [\boldsymbol{\delta}, \mathbf{B}\boldsymbol{\delta}, \mathbf{B}^2\boldsymbol{\delta}, \cdots, \mathbf{B}^{L-1}\boldsymbol{\delta}] \\
&= \begin{bmatrix} \delta_1 & & & \mathbf{0} \\ & \delta_2 & & \\ & & \ddots & \\ \mathbf{0} & & & \delta_K \end{bmatrix} \begin{bmatrix} 1 & a_1 & a_1^2 & \cdots & a_1^{L-1} \\ 1 & a_2 & a_2^2 & \cdots & a_2^{L-1} \\ \vdots & \vdots & \vdots & \ddots & \vdots \\ 1 & a_K & a_K^2 & \cdots & a_K^{L-1} \end{bmatrix} \\
&= \mathbf{F}\boldsymbol{\Lambda}
\end{aligned} \tag{4.49}$$

where $\boldsymbol{\Lambda}$ is the same as that of equation (4.38) and $\mathbf{F}$ is a diagonal matrix.

Similar to the forward smoothing scheme, if $L \geq K$, then $rank(\mathbf{R}_S^b) = K$ can be satisfied and the AOAs of all correlated signals can be estimated. It follows that the backward smoothing scheme also requires at least $2K$ elements in the uniform linear array and works for correlated signals.

4.5.3 Forward/Backward Smoothing MUSIC Algorithm for Spatially Correlated Signals

The following shows that, by simultaneous use of the forward and backward smoothing schemes, it is possible to reduce the number of elements required in the antenna array (Pillai & Kwon 1989).

Firstly, one defines the forward/backward smoothed auto-correlation matrix $\mathbf{R}^{f/b}$ as the mean of $\mathbf{R}^{f}$ and $\mathbf{R}^{b}$. In completely correlated situations, $\mathbf{R}^{f/b}$ can be written as:

$$\begin{aligned}\mathbf{R}^{f/b} &= \frac{1}{2}(\mathbf{R}^{f} + \mathbf{R}^{b}) \\ &= \mathbf{A}\left[\frac{1}{2L}(\mathbf{C}\mathbf{C}^{H} + \mathbf{E}\mathbf{E}^{H})\right]\mathbf{A}^{H} + \sigma^{2}\mathbf{I} \\ &= \mathbf{A}\mathbf{R}_{S}^{f/b}\mathbf{A}^{H} + \sigma^{2}\mathbf{I}_{m}\end{aligned} \tag{4.50}$$

where $\mathbf{R}_{S}^{f/b}$ is the $K\times K$ source auto-correlation matrix of the forward/backward smoothing scheme, which is written as:

$$\begin{aligned}\mathbf{R}_{S}^{f/b} &= \frac{1}{2}\left[\mathbf{R}_{S}^{f} + \mathbf{R}_{S}^{b}\right] \\ &= \frac{1}{2L}(\mathbf{C}\mathbf{C}^{H} + \mathbf{E}\mathbf{E}^{H}) \\ &= \frac{1}{2L}\mathbf{G}\mathbf{G}^{H}\end{aligned} \tag{4.51}$$

The analysis of the rank of **G**, which determines the singularity of $\mathbf{R}_{S}^{f/b}$, is based on equation (4.51). The matrix **G** can be derived as:

$$\begin{aligned}\mathbf{G} &= [\mathbf{w}, \mathbf{B}\mathbf{w}, \mathbf{B}^{2}\mathbf{w}, \cdots, \mathbf{B}^{L-1}\mathbf{w}, \quad \boldsymbol{\delta}, \mathbf{B}\boldsymbol{\delta}, \mathbf{B}^{2}\boldsymbol{\delta}, \cdots, \mathbf{B}^{L-1}\boldsymbol{\delta}] \\ &= [\mathbf{D}\boldsymbol{\Lambda} \vdots \mathbf{F}\boldsymbol{\Lambda}] = \mathbf{D}[\boldsymbol{\Lambda} \vdots \mathbf{D}^{-1}\mathbf{F}\boldsymbol{\Lambda}] \quad = \mathbf{D}[\boldsymbol{\Lambda} \vdots \mathbf{J}\boldsymbol{\Lambda}] = \mathbf{D}\mathbf{G}_{0} \\ \mathbf{G}_{0} &= [\boldsymbol{\Lambda} \vdots \mathbf{J}\boldsymbol{\Lambda}]\end{aligned} \tag{4.52}$$

where $\mathbf{D}$ and Λ are the same as that in equation (4.38) and $\mathbf{J}$ is a diagonal matrix as (refer to equation (4.38) and (4.49)):

$$\begin{aligned} &\mathbf{J} = \mathbf{D}^{-1}\mathbf{F} = diag[\varepsilon_1, \varepsilon_2, \cdots, \varepsilon_K]; \\ &\varepsilon_k = \frac{\delta_k}{w_k} = \frac{w_k^* a_k^{-(M-1)}}{w_k}, \quad a_k^{-(M-1)} = e^{j2\pi(M-1)\ q\ \cos\beta_k}, \quad k = 1, 2, \cdots, K \end{aligned} \tag{4.53}$$

Considering that $\mathbf{D}$ is a $K \times K$ diagonal matrix, if the rank of $\mathbf{G}_0$ is kept as K, the following relationships can be obtained:

$$rank(\mathbf{R}_S^{f/b}) = rank(\mathbf{G}) = rank(\mathbf{G}_0) = K \tag{4.54}$$

As a result, AOAs of all impinging signals can be estimated. Now the key point is to analyze the rank of $\mathbf{G}_0$. The rank of $K \times 2L$ matrix $\mathbf{G}_0$ as in equation (4.52) is mainly determined by the variables ε_k and the total number of subarrays, $2L$. The following analysis of the $rank(\mathbf{G}_0)$ is based on Figure 4.5.

1. $L \geq K$

   In this situation, $rank(\mathbf{G}_0)$ is always equal to K because the $\mathbf{\Lambda}$ with Vandermonde structure is always a full rank matrix, so the AOAS of all impinging signals can be estimated. However, the number of elements in the antenna array is not reduced and it is still $2K$.

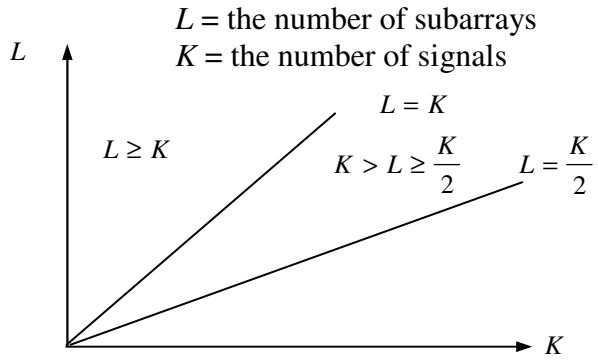

Figure 4.5: Relationship between *L* and *K*

2. $K > L \geq K/2$

In this case, a subset is considered. Any $\{\varepsilon_k : k = 1, 2, \cdots, K\}$ can be divided into several subsets according to their equality. For example, if $K = 6$ and $\varepsilon_2 = \varepsilon_3, \varepsilon_4 = \varepsilon_5 = \varepsilon_6$, then there are three subsets, $\{\varepsilon_1\}$, $\{\varepsilon_2, \varepsilon_3\}$ and $\{\varepsilon_4, \varepsilon_5, \varepsilon_6\}$.

If the largest size of the subset is of *L* ***at most*** and $\{a_k\}$ of this largest subset are not equal to each other, the rank of $K \times 2L$ matrix $\mathbf{G}_0$ can be kept as *K*, because of the Vandermonde structure Λ in $\mathbf{G}_0$, as defined in equations (4.38, 4.52). If the above condition cannot be satisfied, $rank(\mathbf{G}_0)$ will be less than *K*. For example, if all of ε_k are equal, $rank(\mathbf{G}_0)$ is *L* which is less than *K*. Fortunately the above requirement is easily satisfied in practice because each $\varepsilon_k (k = 1, 2, \cdots, K)$ are different most of the time, which can be seen from the following equation:

$$\varepsilon_k = \frac{\delta_k}{w_k} = \frac{w_k^* \, a_k^{-(M-1)}}{w_k} = \exp\{ j \, [2\pi (M-1) \; q \cos\beta_k + 2 \, \phi(w_k^*)] \} \qquad (4.55)$$
$$k = 1, 2, \cdots, K$$

where $\phi(w_k^*)$ is the phase angle of the complex weight w_k^* as defined in equation (4.20). It is clear that ε_k is the function of the impinging angle β_k and weight w_k of the k^{th} signal. Therefore, each $\varepsilon_k (k = 1, 2, \cdots, K)$ rarely has the same value.

Thus, in any situations, if $L \geq K/2$ is satisfied, AOAs of all correlated signals can be estimated with the forward/backward smoothing MUSIC algorithm. The minimum number of elements in the antenna array for the forward/backward smoothing scheme should meet the following equation:

$$M_{\min} = L_{\min} + m_{\min} - 1 = K/2 + (K+1) - 1 = 3K/2 \; . \qquad (4.56)$$

***Example 2*:**

Now we apply the forward/backward smoothing MUSIC algorithm to *example 1* given in section 4.4.2. In this case, the size of subarray $m = M = 3$ and the number of subarrays $L = 1$, i.e., one forward subarray and one backward subarray. According to equations (4.36), (4.43), (4.45) and (4.51), $\mathbf{R}_S^{f/b}$ can be derived as:

$$\mathbf{R}_S^{f/b} = \frac{1}{2}[\mathbf{R}_S + \mathbf{B}^{-(M-1)} \mathbf{R}_S^* \, \mathbf{B}^{(M-1)}] = \frac{1}{2}[\mathbf{R}_S + \mathbf{B}^{-2} \mathbf{R}_S^* \, \mathbf{B}^2]$$
$$= \frac{1}{2}\begin{bmatrix} 1 & w^* \\ w & |w|^2 \end{bmatrix} + \frac{1}{2}\begin{bmatrix} 1 & 0 \\ 0 & -1 \end{bmatrix}\begin{bmatrix} 1 & w \\ w^* & |w|^2 \end{bmatrix}\begin{bmatrix} 1 & 0 \\ 0 & -1 \end{bmatrix} = \begin{bmatrix} 1 & 0 \\ 0 & |w|^2 \end{bmatrix}$$

After forward and backward smoothing, $\mathbf{R}_S^{f/b}$ is a full rank matrix with rank($\mathbf{R}_S$) = 2. According to equation (4.50), the auto-correlation matrix of the received signal is expressed as:

$$\mathbf{R}^{f/b} = \mathbf{A}\mathbf{R}_S^{f/b}\mathbf{A}^H + \sigma^2\mathbf{I} = \begin{bmatrix} 1+|w|^2+\sigma^2 & 1+j|w|^2 & 1-|w|^2 \\ 1-j|w|^2 & 1+|w|^2+\sigma^2 & 1+j|w|^2 \\ 1-|w|^2 & 1-j|w|^2 & 1+|w|^2+\sigma^2 \end{bmatrix}$$

Substituting $w = e^{j\pi/4}$ into the above equation, one obtains the following expression:

$$\mathbf{R}^{f/b} = \begin{bmatrix} 2+\sigma^2 & 1+j & 0 \\ 1-j & 2+\sigma^2 & 1+j \\ 0 & 1-j & 2+\sigma^2 \end{bmatrix}.$$

Three eigenvalues of $\mathbf{R}$ are $\lambda_1 = 4+\sigma^2, \lambda_2 = 2+\sigma^2, \lambda_3 = \sigma^2$. The corresponding eigenvectors to eigenvalues can be derived as:

$$\boldsymbol{\gamma}_1 = [\,1,\ \ 1-j,\ \ -j\,]^T, \quad \boldsymbol{\gamma}_2 = [\,1,\ \ 0,\ \ j\,]^T \quad \text{and} \quad \boldsymbol{\gamma}_3 = [\,1,\ \ -(1-j),\ \ -j\,]^T$$

From the above results, it is clear that the eigenvector $\boldsymbol{\gamma}_3$ belonging to the noise space are orthogonal to the original direction vectors because $\mathbf{a}^H(\beta_1)\boldsymbol{\gamma}_3 = \mathbf{a}^H(\beta_2)\boldsymbol{\gamma}_3 = 0$. Therefore, after the forward/backward smoothing, the AOAs of the correlated signals can be estimated by equation (4.18). Meanwhile, it can be easily seen that the original signal direction vectors $\mathbf{a}(\beta_1)$ and $\mathbf{a}(\beta_2)$ can be spanned linearly with signal space eigenvectors $\boldsymbol{\gamma}_1$ and $\boldsymbol{\gamma}_2$ as $\mathbf{a}(\beta_1) = \frac{1+j}{2}\boldsymbol{\gamma}_1 + \frac{1-j}{2}\boldsymbol{\gamma}_2$ and $\mathbf{a}(\beta_2) = \frac{1-j}{2}\boldsymbol{\gamma}_1 + \frac{1+j}{2}\boldsymbol{\gamma}_2$.

4.6 AOA Estimation Variance of MUSIC Estimator and Comparison with CRLB

In practice, the auto-correlation matrix $\mathbf{R}$ is replaced by its estimate $\hat{\mathbf{R}}$ in equation (4.5). Because MUSIC algorithms are based on eigenanalysis of the auto-correlation matrix $\hat{\mathbf{R}}$, then only the estimates $\{\hat{\beta}_i\}$ of AOAs can be obtained, not the true values. An estimation variance therefore occurs.

The MUSIC estimation error $\{\hat{\beta}_i - \beta_i\}$ are asymptotically (for large number of snapshots) jointly Gaussian distributed with zero means. Its variance is given by Stoica & Nehorai (1989) as follows:

$$\begin{aligned}
\mathrm{var}_{MUSIC}(\hat{\beta}_i) &= E[(\hat{\beta}_i - \beta_i)^2] \\
&= \frac{\sigma^2}{2N}\left[\sum_{k=1}^{K}\frac{\lambda_k}{(\sigma^2-\lambda_k)^2}\left|\mathbf{a}^H(\beta_i)\boldsymbol{\gamma}_k\right|^2\right]\Bigg/\left\{\left[\frac{d\mathbf{a}(\beta_i)}{d\beta_i}\right]^H \mathbf{V}_N\mathbf{V}_N^H\,\frac{d\mathbf{a}(\beta_i)}{d\beta_i}\right\} \qquad (4.57a)\\
&= \frac{\sigma^2}{2N}\frac{\mathbf{a}^H(\beta_i)[\mathbf{V}_S(\overline{\boldsymbol{\Gamma}}_S^{-1}+\sigma^2\overline{\boldsymbol{\Gamma}}_S^{-2})\mathbf{V}_S^H]\mathbf{a}(\beta_i)}{\left[\frac{d\mathbf{a}(\beta_i)}{d\beta_i}\right]^H \mathbf{V}_N\mathbf{V}_N^H\,\frac{d\mathbf{a}(\beta_i)}{d\beta_i}}
\end{aligned}$$

where N is the number of snapshots; $\mathbf{a}(\beta_i)$ is the direction vector defined in equation (4.2); $\mathbf{V}_N$ is the noise eigen vectors defined in equation (4.15); and $\overline{\boldsymbol{\Gamma}}_S$ and $\mathbf{V}_S$ are defined as:

$$\overline{\boldsymbol{\Gamma}}_S = diag[\lambda_1-\sigma^2, \lambda_2-\sigma^2, \cdots, \lambda_K-\sigma^2] \quad and \quad \mathbf{V}_S = [\boldsymbol{\gamma}_1, \boldsymbol{\gamma}_2, \cdots, \boldsymbol{\gamma}_K].$$

Based on (4.57a), the MUSIC error variance may have large values in the following situations:

(1) When signal eigenvalues $\{\lambda_k : k \in [1, 2, \cdots, K]\}$ are close to σ^2. It means that the signal auto-correlation matrix $\mathbf{R}_S$ is nearly singular. This situation may occur when the directions of signals are close in space or signals are highly correlated and when the signal-to-noise ratio is low.

(2) When the vector $\frac{d\mathbf{a}(\beta_i)}{d\beta_i}$ is close to a zero vector. Based on equation (4.2), this situation occurs when $\beta_i \to 0^0 \quad or \quad 180^0$. The explanation was given in Section 3.5.

For convenience of calculation, equation (4.57a) can be modified to (*ibid*):

$$\begin{aligned} &\mathrm{var}_{MUSIC}(\hat{\beta}_i) \\ &= \frac{\sigma^2}{2N} \frac{\{[\mathbf{R}_S^{-1}]_{ii} + \sigma^2 [\mathbf{R}_S^{-1}(\mathbf{A}^H\mathbf{A})\mathbf{R}_S^{-1}]_{ii}\}}{\left[\frac{d\mathbf{a}(\beta_i)}{d\beta_i}\right]^H [\mathbf{I} - \mathbf{A}(\mathbf{A}^H\mathbf{A})^{-1}\mathbf{A}^H] \frac{d\mathbf{a}(\beta_i)}{d\beta_i}}. \end{aligned} \tag{4.57b}$$

In the single source signal case, the MUSIC estimator's variance becomes:

$$\mathrm{var}_{MUSIC}(\hat{\beta}) = \frac{3}{(2\pi)^2 N * M (M^2 - 1)\, SNR \left(\frac{d}{\lambda}\right)^2 \sin^2\beta} \left(1 + \frac{1}{M * SNR}\right) \ (\mathrm{Radian}^2)$$

(4.57c)

where N is the number of sampled data; M is the number of antenna elements; and SNR is signal to noise ratio at the sampled point.

Comparing equation (4.57c) with equation (3.54) shows that, when *M* and *SNR* are very large, it reaches the CRLB. Figure 4.6 shows the AOA variance of the F/B MUSIC estimator under different *SNRs* for single source signal case.

It should be mentioned that when using the F/B MUSIC estimator, the parameters in equations (4.57a) to (4.57c) should be related to the subarray scheme, e.g. the size of antenna array is referred to the size of subarray antenna elements.

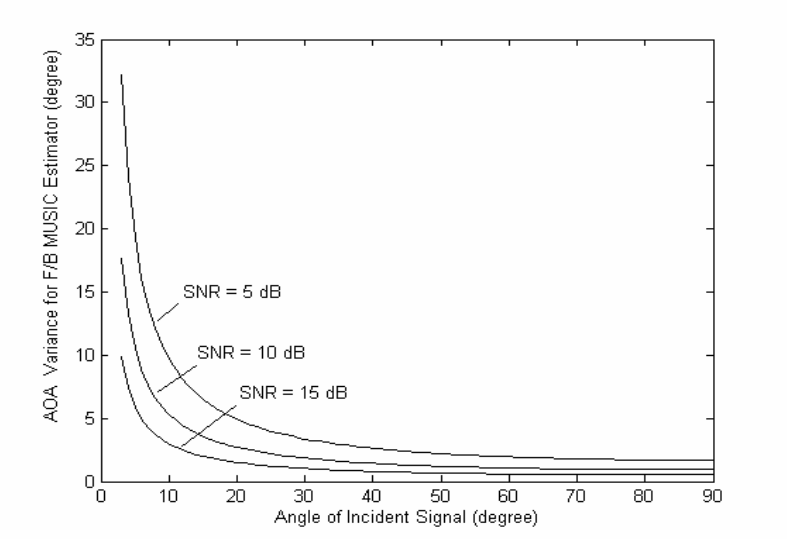

Figure 4.6: AOA Variance of F/B MUSIC Estimator for One Source Signal

Case Study of F/B Smooth MUSIC Estimator for Multiple Source Signals

Similar to Section 3.6, assuming that the number of source signals is $K \le 3$, the number of array sensors is $M = 5$. The difference is that the number of subarray sensors to be considered, which is $m = 4$. The number of forward and backward subarrays is $2L = 4$.

The number of samples $N = 1$ and the estimated LOS AOA is $\hat{\beta}_1$. Then the CRLB of the independent AOA estimator, $\text{var}_{CRLB}(\hat{\beta}_1)$ as expressed in equation (3.53) for multiple source signals situation and the MUSIC AOA estimator error $\text{var}_{MUSIC}(\hat{\beta}_1)$ as expressed in equation (4.57b) are compared, as shown in Figure 4.7. In this case, the LOS is s_1 and its AOA1 is supposed to be at 80^0; *SNR* and *SIR* are 14 dB. It can be seen that the MUSIC estimator error is larger than the CRLB given in equation (3.53) and the variance of two source signals is much smaller than that of three source signals. In addition, considering the phase of the correlation coefficient ρ_{xy} of two signals, it is found that the MUSIC estimator also exist maximum and minimum variances, which is similar to the existence of maximum and minimum CRLB described in Chapter 3.

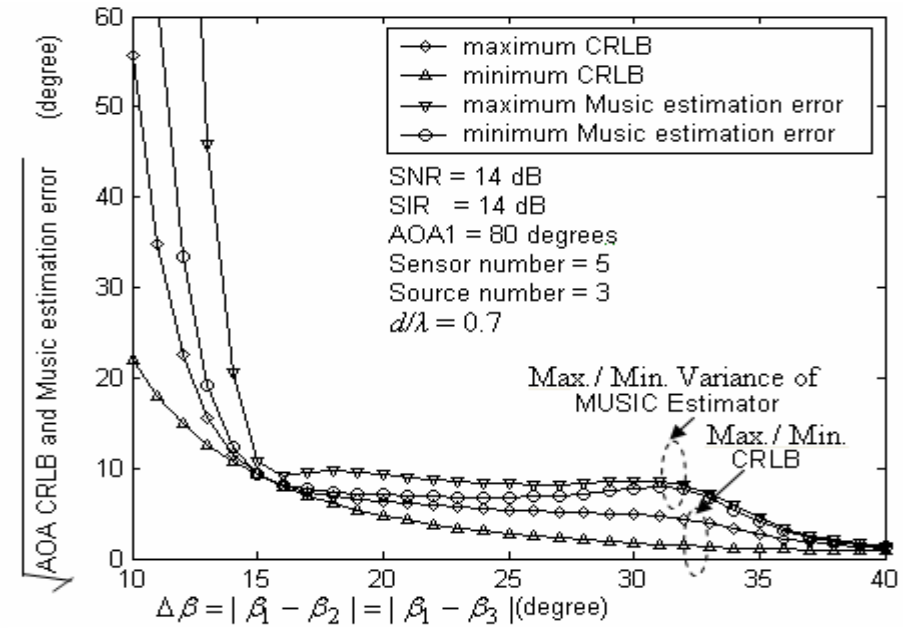

(a) Comparison of MUSIC AOA Variance with CRLB for Three Source Signals

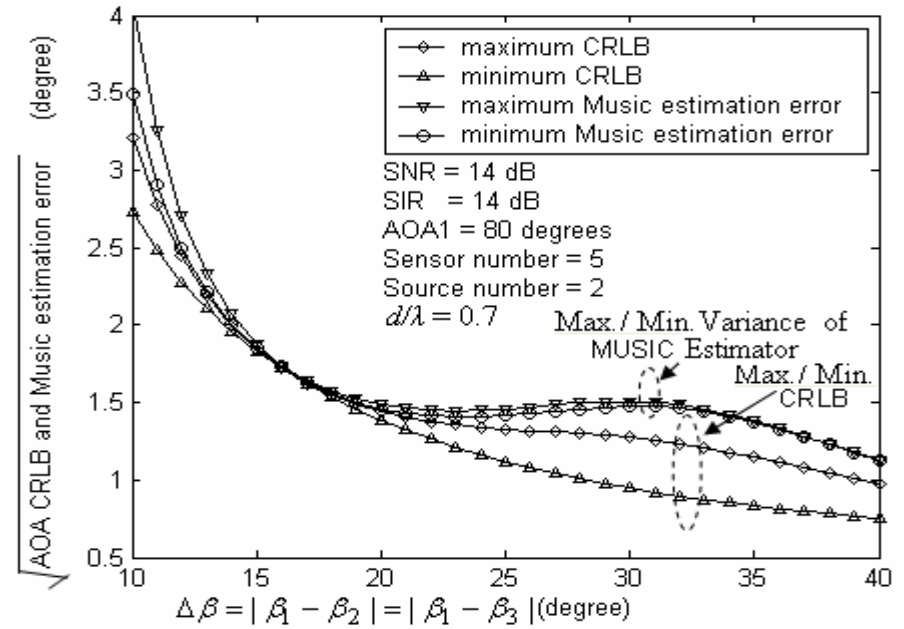

(b) Comparison of MUSIC AOA Variance with CRLB for Two Source Signals

Figure 4.7 (a) Comparison of MUSIC AOA Variance with CRLB for Three Source Signals; (b) Comparison of MUSIC AOA Variance with CRLB for Two Source Signals

Comparison with AOA CRLB

Table 4.1 summarizes the expressions of AOA estimation variances of the MUSIC estimator and compares them with its CRLB. ***For single source signals***, it is easy to compare according to the formula. ***When M and SNR are very large, the MUSIC estimator reaches CRLB***. However, ***for multiple source signals***, it is hard to compare based on the formula. It is easier to compare through the simulation results as shown in Figure 4.7. It shows that ***when the angles of incident signals are far apart, the MUSIC estimator reaches CRLB***.

Table 4:1: Comparison of CRLBs with Specific Estimator Variances for the CDMA IS-95 Pilot Signal

CRLBs of AOA-assisted TOA Estimation	Variances of Specific Estimator
AOA: from equation (3.54) for single source signal: $\mathrm{var}_{CRLB}(\hat{\beta}) = \frac{3}{N*SNR*M(M^2-1)\left(2\pi\frac{d}{\lambda}\right)^2 \sin^2\beta}$ Simulation result is shown in Figure 3.3.	*MUSIC AOA Estimator* from equation (4.57c) for single source signal: $\mathrm{var}_{CRLB}(\hat{\beta}) = \frac{3(1+\frac{1}{M*SNR})}{N*SNR*M(M^2-1)\left(2\pi\frac{d}{\lambda}\right)^2 \sin^2\beta}$ Simulation result is shown in Figure 4.6.

from equation (3.53) for multiple source signals (Stoica & Nehorai 1989): $\text{var}_{CRLB}(\hat{\beta}_i)$ $= \frac{\frac{\sigma^2}{2N}\left[\text{Re}\left(\{\mathbf{D}^H[\mathbf{I}-\mathbf{A}(\mathbf{A}^H\mathbf{A})^{-1}\mathbf{A}^H]\mathbf{D}\}\odot\mathbf{R}_S\right)\right]^{-1}}{\left(2\pi\frac{d}{\lambda}\right)^2\sin^2\beta}$ Simulation result is shown in Figure 3.5.	from equation (4.57a) for multiple source signals (Stoica & Nehorai 1989): $\text{var}_{MUSIC}(\hat{\beta}_i)$ $= \frac{\sigma^2}{2N}\frac{\mathbf{a}^H(\beta_i)[\mathbf{V}_S(\overline{\mathbf{\Gamma}}_S^{-1}+\sigma^2\overline{\mathbf{\Gamma}}_S^{-2})\mathbf{V}_S^H]\mathbf{a}(\beta_i)}{\left[\frac{d\mathbf{a}(\beta_i)}{d\beta_i}\right]^H\mathbf{V}_N\mathbf{V}_N^H\frac{d\mathbf{a}(\beta_i)}{d\beta_i}}$ Simulation result is shown in Figure 4.7.
TOA: $\text{var}_{CRLB}(\hat{\tau}) = \frac{T_C^2}{32MK\cdot SNR}$ from equation (3.64)	*Correlation Function Rising Slope-based TOA Estimator* to be discussed in Chapter 5

4.7 Application of MUSIC AOA Estimator for IS-95 Pilot Signal

In Section 4.6, the MUSIC estimator for AOA estimation is based on continuous wave (CW) signals. In this section, the AOA estimation of IS-95 pilot signals with ***Forward/Backward Smoothing MUSIC algorithm*** is discussed. Figure 4.8 shows that the data for IS-95 pilot signal AOA estimation is from I&Q correlator outputs.

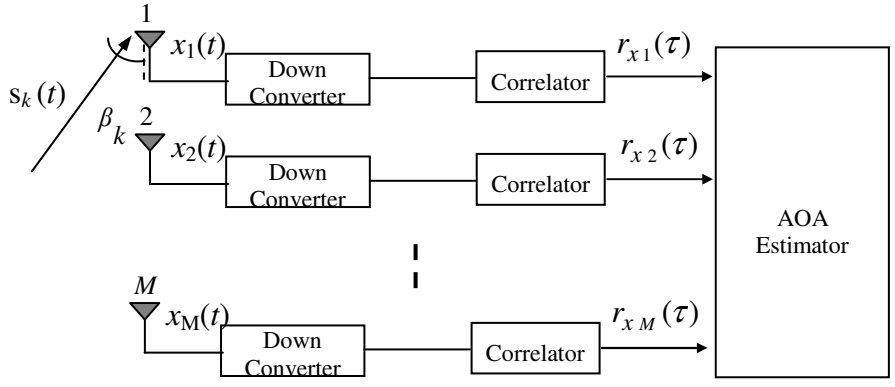

Figure 4.8: IS-95 Pilot Signal AOA Estimation from Correlator Outputs

Assuming that there are M sensors and K impinging signals, the baseband complex signals are still denoted by $s_1(t), s_2(t), \cdots, s_K(t)$ and they can be defined as follows for the first channel (the reference channel in the array) after the down converter:

$$s_k(t) = w_k s(t - t_{dk}) \quad k = 1, 2, \cdots, K \tag{4.59}$$

where $s(t)$ is the IS-95 pilot baseband complex signal transmitted at the base station; w_k is the complex attenuation coefficient; t_{dk} ($t_{d1} < t_{d2} < \cdots < t_{dK}$) is the time delay and $s_1(t)$ is the LOS signal.

Based on equations (2.4) to (2.12) and (3.22) to (3.24), the output of the *i*th correlator $r_{xi}(\tau, \mathbf{t}_d)$ for K impinging signals is redefined as:

$$r_{xi}(\tau, \mathbf{t}_d) = r_{si}(\tau, \mathbf{t}_d) + r_{ni}(\tau) \quad i = 1, 2, \cdots, M; \quad \mathbf{t}_d = [t_{d1}, t_{d2}, \cdots, t_{dK}] \tag{4.60}$$

$$\begin{aligned} r_{si}(\tau, \mathbf{t}_d) &= \sum_{k=1}^{K} \int_0^T s_k(t) \exp[-j(i-1)\varphi_k] s_l(t-\tau)\, dt \\ &= \sum_{k=1}^{K} \int_0^T w_k\, s(t - t_{dk}) \exp[-j(i-1)\varphi_k] s_l(t-\tau)\, dt \\ &= \sum_{k=1}^{K} r_k(\tau - t_{dk}) \exp[-j(i-1)\varphi_k] \end{aligned} \tag{4.61}$$

where

$$\begin{aligned} r_k(\tau - t_{dk}) &= \int_0^T s_k(t) s_l(t-\tau)\, dt \\ &= \int_0^T w_k\, s(t - t_{dk})\, s_l(t-\tau)\, dt \quad k = 1, 2, \cdots, K \end{aligned}$$

$$r_{ni}(\tau) = \int_0^T n_k(t) s_l(t-\tau)\, dt \tag{4.62}$$

where $r_{si}(\tau,\mathbf{t}_d)$ and $r_{ni}(\tau)$ are the signal and noise parts of $r_{xi}(\tau,\mathbf{t}_d)$, respectively; $s_l(t)$ is the local IS-95 pilot base band complex signal; $\varphi_k = 2\pi\, q \cos\beta_k$ is defined in equation (3.23).

Based on equations (4.60) to (4.62), the matrix format $\mathbf{r}_x(\tau,\mathbf{t}_d)$ of the outputs of the correlators can be written as:

$$\begin{aligned}
&\mathbf{r}_x(\tau,\mathbf{t}_d) = [r_{x1}(\tau,\mathbf{t}_d),\, r_{x2}(\tau,\mathbf{t}_d),\cdots,\, r_{xM}(\tau,\mathbf{t}_d)]^T \\
&\qquad = \mathbf{A}\mathbf{r}_S(\tau,\mathbf{t}_d) + \mathbf{r}_n(\tau) \\
&\textit{where} \\
&\mathbf{r}_S(\tau,\mathbf{t}_d) = [r_1(\tau - t_{d1}),\, r_2(\tau - t_{d2}),\cdots,\, r_K(\tau - t_{dK})]^T \\
&\mathbf{r}_n(\tau) = [r_{n1}(\tau),\, r_{n2}(\tau),\cdots,\, r_{nM}(\tau)]^T
\end{aligned} \tag{4.63}$$

where **A** is the direction matrix defined in (3.24) and $r_{ni}(\tau)$ $(i = 1, 2, \cdots, M)$ is *iid* Gaussian noise.

Comparing equation (4.63) with equation (3.24) or (4.3), all of them have the same formats. It means that MUSIC algorithm can still be used for the IS-95 pilot signal AOA estimation through the IS-95 pilot signal correlator output data and the IS-95 pilot signal AOA estimation error can be calculated through equation (4.57b).

4.8 Comparison of the MUSIC with the ML Method for AOA Estimation

In order to compare the MUSIC with the ML, the formulas for AOA estimation are written as follows:

MUSIC: $P_{MU}(\beta) = \dfrac{1}{\mathbf{a}^H(\beta)\mathbf{V}_N\mathbf{V}_N^H\mathbf{a}(\beta)}$ (same as equation (4.18))

ML (Schmidt 1979): $P_{ML}(\beta) = \dfrac{1}{\mathbf{a}^H(\beta)\mathbf{R}^{-1}\mathbf{a}(\beta)}$ (for single source signal)

$$P_{ML}(\beta) = \frac{1}{\mathbf{A}^H(\beta)\mathbf{R}^{-1}\mathbf{A}} \quad \text{(for multiple source signals)}$$

where $\mathbf{a}(\beta)$ is the direction vector defined in equation (4.2), $\mathbf{V}_N$ is the noise matrix defined in equation (4.15), $\mathbf{A} = [\mathbf{a}(\beta_1)\ \mathbf{a}(\beta_2)\ \cdots\ \mathbf{a}(\beta_K)]$ is the direction matrix, and $\mathbf{R}$ is the correlation matrix of the received signal defined in equation (4.7).

It can be seen that for single source signal, the ML has the same computation load as the MUSIC. Both of them are one dimensional search. However, for *K* source signals, the ML searches in *K* dimensions.

4.9 Conclusions

The conventional MUSIC algorithm, which works under uncorrelated or partially correlated signals, was discussed in this chapter. However, in multipath environments, it fails. An example was given to help understanding that failure. The forward-only smoothing MUSIC algorithm overcomes that limitation, i.e., it can resolve the AOAs of fully correlated signals. However, it sacrifices more array elements. The Forward/backward smoothing MUSIC algorithm improves the efficiency of the use of

array elements. An example is given to show how the forward/backward smoothing MUSIC algorithm resolves the AOAs of fully correlated signals. The theoretical performance analysis compared with CRLB followed. Finally, the practical consideration of sampling data from the correlator output for CDMA IS-95 pilot signal AOA estimation with MUSIC algorithm was explained and the comparison with the ML method is explained briefly.

Chapter Five: AOA-assisted TOA/TDOA Method for Multipath Mitigation

5.1 Introduction

In this chapter, the proposed AOA-assisted approach for TOA estimation for multipath propagation environments is described. The limitation of the conventional TOA estimator based on the beamforming technique is also discussed. It can be seen that through the use of AOA information, multipath can be mitigated efficiently. The formulas for the correlation function initial rising part-based TOA estimator and its predicted error are derived based on the linearized vector parameter transformation of more fundamental parameters of the correlation function initial rising slope and its intercept through coordinate transformation. It is shown that the proposed TOA estimator is asymptotically unbiased and the estimated standard deviation is about 37 m when the SNR after despreading is 15 dB. The actual estimated variance is given in Chapter 6, as a function of SNR. Finally the comparison between AOA-assisted TOA and AOA-join TOA method is given.

5.2 Multipath Effect on the Correlation Functions of CDMA Signals

In spread spectrum radiolocation systems, TOAs can be obtained from the peaks of the correlation function. Here the effect of multipath on the peaks of the correlation function is discussed. In an urban canyon, the average multipath delay is about 400 ns (Turin 1972). Based on this assumption, a simulation is carried out under the following

conditions, which are also described by Figure 5.1 and Table 5.1. It is noted that the parameter selection is somewhat arbitrary because Figure 5.1 is only the summation of five correlation functions to show multipath and it does not involve any proposed algorithm yet.

(1) linear uniform array of $M = 5$ antenna elements with half wavelength spacing (The RF frequency is 1.9475 GHz, $\lambda = 15.4\ cm$);

(2) number of the incident rays $K = 4$;

(3) signal to noise ratio before despreading (SNR) is –30 dB and multipath to noise ratio before despreading (INR) is –20 dB.

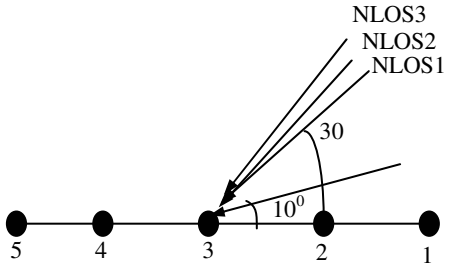

Figure 5.1: LOS and NLOS Signals with Different AOAs

Table 5:1: Parameters of Multipath on Correlation Functions

Received Signals	(dB)	AOA (º)	Delay (ns)
LOS	- 30 (SNR)	10	0
NLOS 1	- 20 (INR)	30	400
NLOS 2	- 20 (INR)	35	450
NLOS 3	- 20 (INR)	40	500

These IS-95 pilot signals with different time delays are down converted to baseband signals and sampled at a 2 MHz rate. The data snapshot is three pilot PN periods, which is 0.08 seconds. Similar to Chapter 3 and 4, it is assumed that each element of the antenna array generates one channel complex signal containing source signals and complex Gaussian noise.

The simulation results are shown in Figure 5.2. The peak of the LOS correlation function of the first channel is shifted by multipath signals from 0 to $T_C/2$, where T_C is the PN chip period which is 800 ns. For the summation of the five correlation functions in five channels, the correlation peak is also shifted by about 400 ns. This matches the given simulation conditions for the delayed signals, which have 400 ns or more delays. That is, the inter-chip multipath (less than 800 ns) in CDMA IS-95 systems cannot be resolved by CDMA signal's correlation peak, which can also be explained by PN sequence's correlation function shown in Figure 2.2. When the multipath delay is over one chip period, its effect on the LOS signal correlation function is close to zero; when the multipath delay is within one chip period, it has an effect on the LOS signal correlation function and that effect increases as the multipath delay decreases. Figure 5.3 is the result from the measured data. It shows that, due to inter-chip multipath, the LOS correlation function has been distorted at the correlation peak. However, the initial rising part still has a good linear shape, which means that multipath occurred after the first LOS signal. Therefore the initial part of the correlation function has not been distorted by multipath. Based on this, the proposed method focuses on the correlation rising slope estimation.

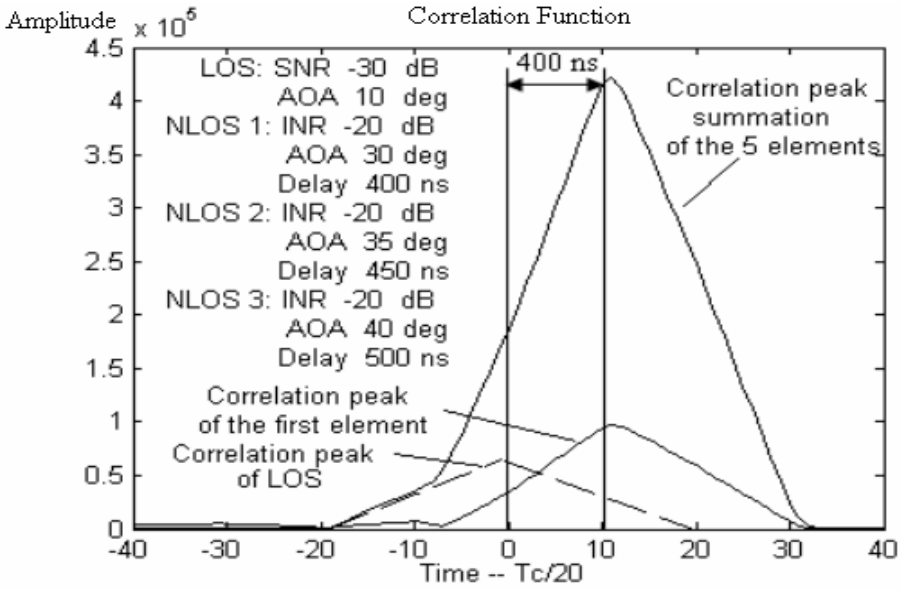

Figure 5.2: Correlation Functions of the Simulated Data in Multipath Environments

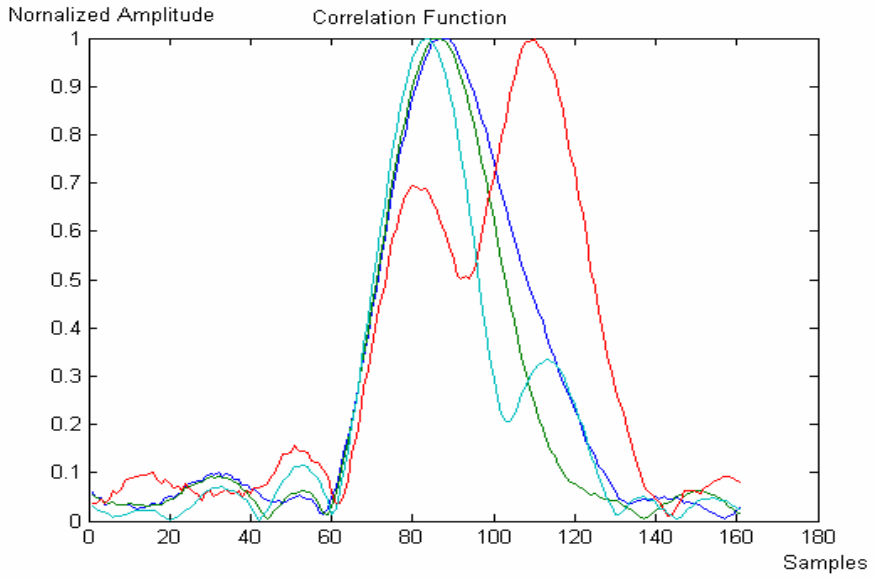

Figure 5.3: Correlation Functions of Four Channels in Real Multipath Environments

5.3 Limitations of Correlation Peak-based TOA Estimation in Multipath Environments

At present, most GPS receivers use multiple DLLs (Delay Lock Loops) to estimate TOA based on the correlation function peak position in the time domain. However, when multipath interference exists, the peak of the correlation function is shifted, shown in Figure 5.2 from simulated data and Figure 5.3 from real data. Due to limited bandwidth of the filter in the receiver, the shape of the correlation function in Figure 5.3 is not a triangle any more. Its bottom has been widened smoothly. The beamforming technique can be used to mitigate multipath, which is explained briefly below.

Suppose that the output vector of *M* channel correlators (correlating the same signals) is

$$\mathbf{r}_x(\tau,\mathbf{t}_d) = \mathbf{r}(\tau) + \mathbf{r}_n(\tau)$$
$$\mathbf{r}(\tau) = [r_1(\tau,\mathbf{t}_d),\, r_2(\tau,\mathbf{t}_d),\cdots,\, r_M(\tau,\mathbf{t}_d)]^T$$
$$\mathbf{r}_n(\tau) = [r_{n1}(\tau,\mathbf{t}_d),\, r_{n2}(\tau,\mathbf{t}_d),\cdots,\, r_{nM}(\tau,\mathbf{t}_d)]^T$$

where $\mathbf{r}(\tau)$ is the signal component including LOS and NLOS, $\mathbf{r}_n(\tau)$ is the noise component; $\mathbf{t}_d = [t_1, t_2, \cdots, t_k]$ is the time delay vector.

If the AOA of the LOS signal is β_{LOS}, after beamforming the LOS correlation function is enhanced as follows:

$$r_\Sigma(\tau) = \mathbf{a}^H(\beta_{LOS})\,\mathbf{r}_x(\tau,\mathbf{t}_d) \tag{5.1}$$

where $\mathbf{a}(\beta_{LOS}) = \left[1,\ e^{-j\varphi}, \ldots, e^{-j(M-1)\varphi}\right]^T$ is the direction vector of the LOS signal as defined in equations (4.2) and (3.23), and $\varphi = \frac{2\pi f_0 d * \cos(\beta_{LOS})}{c}$, where d is the antenna spacing, f_0 is the carrier frequency and c, the light velocity. Equation (5.1) means that the LOS parts in the correlation functions from five channels are summated coherently to enhance the LOS component and suppress multipath components coming from different angles.

However, when NLOS signals are stronger than LOS signals, multipath cannot be mitigated efficiently through equation (5.1), so the peak of the summated correlation function will still be shifted. The following section describes a new approach to mitigate multipath for TOA estimation.

5.4 AOA-based Multipath Mitigation Approach for TOA Estimation

The CRLB of the AOA-joint TOA approach is derived in Chapter 3, which can be used as a reference to evaluate a specific estimator for AOA and TOA estimations. As it is described by Kay (1998), the Maximum Likelihood (ML) estimator is optimal for both AOA and TOA estimation. However, its computation load increases exponentially as the number of multipath increases and it still cannot distinguish which is related to the LOS signal. The proposed method is to estimate AOA and TOA separately in order to filter out multipath based on estimated AOA and then to estimate TOA. Even though, as it is

discussed in Chapter 3, the CRLB of the proposed AOA-assisted TOA method is non-optimal in AOA estimation but optimal in TOA estimation, it is a practical way to mitigate multipath. Under this separate AOA and TOA estimation scheme, specific estimators for AOA and TOA estimations need to be created. Again, the ML estimator can be considered for AOA estimation. However, it still has the drawback of heavy computational load. For example, when there is only one source signal, it is the same complexity as the MUSIC because they are all one dimensional search. However, when there are two source signals, ML is a 2D search. When there are N source signals, it is N dimensional search. So the suboptimal MUSIC algorithm is applied, whose computation load does not increase as the number of multipath signals increase. For TOA estimation, the correlation function peak-based method is optimal (Kay 1998). However, it is suitable for clean LOS environment. In multipath environments, it causes large errors. Therefore one needs to create a new TOA estimator for multipath environments. It can be seen that although the correlation peak is distorted under multipath environments, fortunately the initial rising part still has a good linear shape, as shown in Figure 5.2 and Figure 5.3. The proposed AOA-based multipath mitigation approach for TOA estimation is based on the estimated AOAs obtained from the modified forward/backward smoothing MUSIC algorithm (Ch 4) to apply beamforming technique to improve the linearity of the initial rising part of the correlation function and enhance the LOS SNR of that part. Then by determining the correlation function rising slope and starting point, the TOA/TDOA can be estimated. This approach is described in detail as follows:

Step 1: Sample Data Generation from M Channels

The first step is to obtain the correlation functions of five channels and the data are generated by sampling the correlation function rising parts. The data is used to estimate the received signals' AOAs by MUSIC as intermediate values for further TOA estimation.

Step 2: Application of F/B Smoothing MUSIC for AOA Estimation in Multipath Environment

The second step is to estimate AOAs using the data obtained in *Step 1*. As discussed in Chapter 4, the conventional MUSIC algorithm works well when the signals are uncorrelated. However, it fails when the signals are highly correlated which is common in multipath environments. The F/B smoothing MUSIC algorithm can solve this problem. But the resolvable number of the incident signals on the antenna array is (2*M*/3) where *M* is the number of elements of the array. Based on the prototype IS-95 receiver used herein that has five antenna elements, the F/B smoothing MUSIC can only resolve three signals. To solve this problem, the data used to estimate AOA can be obtained by sampling the outputs of correlators at the initial rising part of the correlation function to reduce the number of incident signals.

Step 3: Improvement of LOS SNR at the Correlation Function Rising Part

Based on the AOAs estimated from the second step, the extraction of the LOS AOA is based on a beamforming technique. Suppose that β_i is the estimated AOA by step 2, the one resulting in the largest $r_{\Sigma}(\tau) = \left| \mathbf{a}^H(\beta_i)\mathbf{r}_x(\tau, \mathbf{t}_d) \right|$ is the LOS AOA. After beamforming based on LOS AOA, the LOS component of the correlation function is

enhanced and at the same time the multipath is suppressed. Assume that the AOA and TOA of the LOS s_1 is $\beta_{LOS} = \beta_1$ and t_{d1} respectively, then the correlator output after beamforming becomes

$$\begin{aligned} r_{\Sigma}(\tau) &= \mathbf{a}^H(\beta_{LOS})\mathbf{r}_x(\tau, \mathbf{t}_d) = \mathbf{a}^H(\beta_1)\mathbf{r}_x(\tau, \mathbf{t}_d) \\ &= \mathbf{a}^H(\beta_1)\mathbf{A}\mathbf{r}(\tau, \mathbf{t}_d) + \mathbf{a}^H(\beta_1)\mathbf{r}_n(\tau) \\ &= M\, r_1(\tau - t_{d1}) + \sum_{k=2}^{K} \mathbf{a}^H(\beta_1)\mathbf{a}(\beta_k)\, r_k(\tau - t_{dk}) + \mathbf{a}^H(\beta_1)\mathbf{r}_n(\tau) \\ &= r_{\Sigma LOS}(\tau) + r_{\Sigma NLOS}(\tau) + r_{\Sigma n}(\tau) \end{aligned} \tag{5.2}$$

where

$$r_{\Sigma LOS}(\tau) = M\, r_1(\tau - t_{d1})$$

$$r_{\Sigma NLOS}(\tau) = \sum_{k=2}^{K} \mathbf{a}^H(\beta_1)\mathbf{a}(\beta_k)\, r_k(\tau - t_{dk})$$

$$r_k(\tau - t_{dk}) = \sum_{k=0}^{N-1} s(k) s_l^*(k - \tau + t_{dk}) \quad \textit{for one channel}$$

$s(k)$ *is the received signal*

$s_l(k)$ *is the local generated signal* (*see Appendix C*)

$k = 1, 2, \cdots, K (k = 1$ *is for LOS signal*);

K *is the number of incident rays*;

N *is the number of samples*

$$r_{\Sigma n}(\tau) = \mathbf{a}^H(\beta_1)\mathbf{r}_n(\tau) = \sum_{m=1}^{M} \exp[j(m-1)\varphi_1]\, r_{nm}(\tau)$$

$$r_{nm}(\tau) = \sum_{k=0}^{N-1} n_m(k) s_l^*(k - \tau) \quad n_m(k) \text{ is the } m^{th} \text{ channel noise}$$

$$\varphi_1 = \frac{2\pi f_0 d * \cos(\beta_1)}{c} \tag{5.3}$$

d *is the antenna spacing,* f_0 *is the carrier frequency,* c *is the light velocity.*

Because the noise between each correlator output $r_{nm}(\tau)$ is *iid* Gaussian noise with zero mean, the noise variance of $r_{\Sigma n}(\tau)$ at the correlator output after beamforming can be derived as:

$$\sigma_{\Sigma n}^2 = E[r_{\Sigma n}(\tau) r_{\Sigma n}^*(\tau)\} = \sum_{m=1}^{M}\sum_{l=1}^{M} \exp[j(m-1)\varphi_1]\exp[-j(l-1)\varphi_1]\, E[r_{nm}(\tau) r_{nl}^*(\tau)] \\ = M\sigma_r^2 \tag{5.4}$$

where σ_r^2 is the noise variance at each correlator output $r_{nm}(\tau) \quad (m = 1, 2, \cdots, M)$.

Thus, the LOS signal to noise ratio $SNR_{\Sigma LOS}$ of the correlation function rising part after beamforming is as follow:

$$SNR_{\Sigma LOS} = \frac{|r_{\Sigma LOS}(\tau)|^2}{\sigma_{\Sigma n}^2} = M\frac{|r_1(\tau - t_{d1})|^2}{\sigma_r^2} \tag{5.5}$$

Here $r_1(\tau - t_{d1})$ is the LOS signal correlation function at one channel.

Equation (5.5) means that after beamforming, the LOS signal to noise ratio at the correlation function output increases *M* times.

Step 4: Correlation Function Slope Estimation based on Linear Model

After beamforming, the correlation function's shape is improved, i.e. its initial rising part is less distorted by multipath. The next step is to estimate the correlation function initial rising slope *a* and its intercept b. Suppose that *L* data samples $r_\Sigma(\tau_1)$, $r_\Sigma(\tau_2)$ … $r_\Sigma(\tau_L)$ are taken from the rising part, as shown in Figure 5.4. Even though the practical correlation function for IS-95 signals is more like a smoothened triangle as in Figure 5.3,

the triangle shape of correlation function in Figure 5.4 doesn't affect the generality of the analysis because the focus is on the rising linear part of the correlation function which can also be found in the real case from Figure 5.3. Also, these data are considered to be contaminated by noise only because multipath is suppressed significantly in Step 3.

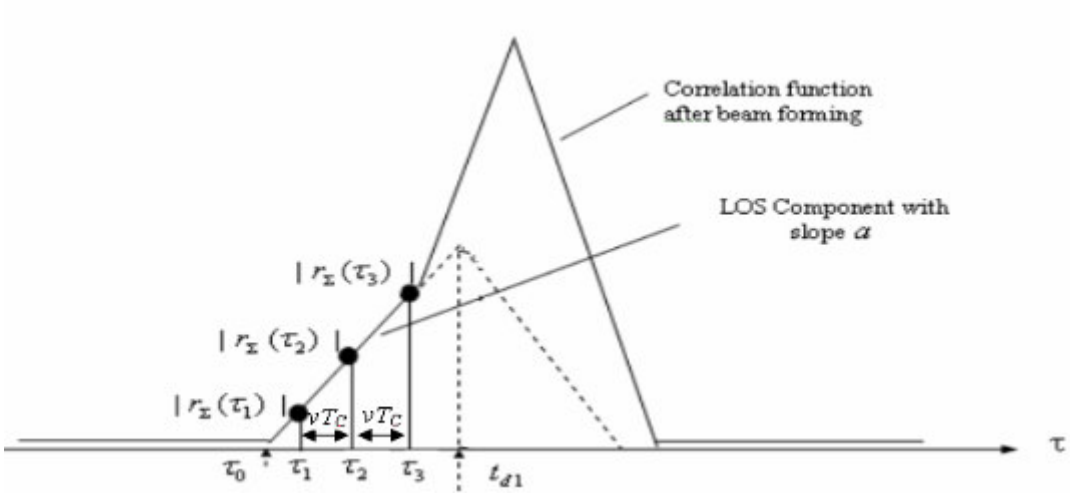

Figure 5.4: Correlation Function Slope Estimation

Considering that $r_{\Sigma LOS}(\tau)$ is a complex function, it can be written as:

$$\begin{aligned} r_{\Sigma LOS}(\tau) &= | r_{\Sigma LOS}(\tau) | \exp(j\phi) \\ &= (b + a\tau)\exp(j\phi) \\ &= b_R + jb_I + (a_R + ja_I)\tau \\ &= B + A\tau \end{aligned} \tag{5.6}$$

where

$$
\begin{aligned}
&a > 0;\\
&b > 0 \quad if \quad \tau_0 < 0;\\
&b \le 0 \quad if \quad \tau_0 \ge 0;\\
&A = a\exp(j\phi); \quad B = b\exp(j\phi) = |b|\exp[j(\phi + \phi(b))];\\
&\phi(b) = \begin{cases} 0 & b \ge 0 \\ \pi & b < 0 \end{cases}\\
&\phi(A) = \phi; \quad \phi(B) = \phi + \phi(b)\\
&a_R = \mathrm{Re}(A) = a\cos\phi; \quad a_I = \mathrm{Im}(A) = a\sin\phi;\\
&b_R = \mathrm{Re}(B) = b\cos\phi; \quad b_I = \mathrm{Im}(B) = b\sin\phi.
\end{aligned}
\tag{5.7}
$$

Thus, the complex number format and the real number format of the unknown parameters $\boldsymbol{\theta}$ and $\boldsymbol{\xi}$ can be defined respectively as (Kay 1998):

$$
\boldsymbol{\theta} = \begin{bmatrix} B \\ A \end{bmatrix} \quad and \quad \boldsymbol{\xi} = \begin{bmatrix} b_R \\ a_R \\ b_I \\ a_I \end{bmatrix}
\tag{5.8}
$$

Based on the sampled data $r_\Sigma(\tau_1)$, $r_\Sigma(\tau_2)$, …, $r_\Sigma(\tau_L)$, a linear model can be expressed as:

$$
\begin{aligned}
r_\Sigma(\tau_1) &= r_{\Sigma LOS}(\tau_1) + r_{\Sigma n}(\tau_1) = B + A\tau_1 + r_{\Sigma n}(\tau_1)\\
r_\Sigma(\tau_2) &= r_{\Sigma LOS}(\tau_2) + r_{\Sigma n}(\tau_2) = B + A\tau_2 + r_{\Sigma n}(\tau_2)\\
&\vdots\\
r_\Sigma(\tau_L) &= r_{\Sigma LOS}(\tau_L) + r_{\Sigma n}(\tau_L) = B + A\tau_L + r_{\Sigma n}(\tau_L)
\end{aligned}
\tag{5.9}
$$

The matrix expression of equation (5.9) can be written as:

$$\mathbf{r}_\Sigma = \mathbf{r}_{\Sigma LOS} + \mathbf{r}_{\Sigma n} = \mathbf{H}\boldsymbol{\theta} + \mathbf{r}_{\Sigma n}$$

where

$$\mathbf{r}_\Sigma = [r_\Sigma(\tau_1), r_\Sigma(\tau_2), \cdots, r_\Sigma(\tau_L)]^T$$

$$\mathbf{r}_{\Sigma LOS} = [r_{\Sigma LOS}(\tau_1), r_{\Sigma LOS}(\tau_2), \cdots, r_{\Sigma LOS}(\tau_L)]^T \tag{5.10}$$

$$\mathbf{r}_{\Sigma n} = [r_{\Sigma n}(\tau_1), r_{\Sigma n}(\tau_2), \cdots, r_{\Sigma n}(\tau_L)]^T$$

$$\mathbf{r}_{\Sigma LOS} = \mathbf{H}\boldsymbol{\theta}$$

$$\mathbf{H} = \begin{bmatrix} 1 & \tau_1 \\ 1 & \tau_2 \\ \vdots & \vdots \\ 1 & \tau_L \end{bmatrix} \qquad \boldsymbol{\theta} = \begin{bmatrix} B \\ A \end{bmatrix}$$

From the above equation, it can be seen that at least two samples are needed to determine A and B, i.e. $L \geq 2$.

The relationship between $\boldsymbol{\theta} = \begin{bmatrix} B \\ A \end{bmatrix}$ and the starting point τ_0 of the correlation function in Figure 5.4 is as follows:

$$\tau_0 = -\frac{b_R}{a_R} = -\frac{b_I}{a_I}, \quad \textit{that means} \quad a_R b_I - a_I b_R = 0$$

or

$$\tau_0 = g(\boldsymbol{\theta}) = -\frac{B}{A} = -\frac{A^* B}{|A|^2} \tag{5.11}$$

or

$$\tau_0 = g(\boldsymbol{\xi}) = -\frac{b_R + jb_I}{a_R + ja_I} = -\frac{a_R b_R + a_I b_I}{a_R^2 + a_I^2}$$

The true values for the unknown parameter $\boldsymbol{\theta}$ without noise corruption can be calculated by:

$$\boldsymbol{\theta} = (\mathbf{H}^H \mathbf{H})^{-1} \mathbf{H}^H \mathbf{r}_{\Sigma LOS} \,. \tag{5.12}$$

The analysis is based on the following two different noise conditions. It can be seen that from equation (5.18) the noise from the correlation function initial part discussed herein are correlated.

1. The estimated values of $\boldsymbol{\theta}$ under ***non "white" Gaussian noises*** can be obtained by (Kay 1998):

$$\hat{\boldsymbol{\theta}} = \begin{bmatrix} \hat{B} \\ \hat{A} \end{bmatrix} = (\mathbf{H}^T \mathbf{C}^{-1} \mathbf{H})^{-1} \mathbf{H}^T \mathbf{C}^{-1} \mathbf{r}_\Sigma \tag{5.13a}$$

where $\mathbf{C}^{-1}$ is the covariance matrix of the noise.

2. If the signal contains only ***"white" Gaussian noises***, i.e. $C^{-1} = \sigma_{\Sigma\,n}^2 I$, the above formula reduces as:

$$\hat{\boldsymbol{\theta}} = \begin{bmatrix} \hat{B} \\ \hat{A} \end{bmatrix} = (\mathbf{H}^T \mathbf{H})^{-1} \mathbf{H}^T \mathbf{r}_\Sigma \tag{5.13b}$$

The covariance matrix of $\boldsymbol{\theta}$ under non "white" Gaussian noise can be expressed in both complex numbers and real numbers as (*ibid*):

$$\begin{aligned} &\mathbf{C}_{\hat{\boldsymbol{\theta}}} = \mathbf{J}^{-1}(\boldsymbol{\theta}) = (\mathbf{H}^H \mathbf{C}^{-1} \mathbf{H})^{-1} \\ &\textit{and} \\ &\mathbf{C}_{\hat{\boldsymbol{\xi}}} = \mathbf{J}^{-1}(\boldsymbol{\xi}) \\ &\quad = \frac{1}{2}\begin{bmatrix} \mathrm{Re}[(\mathbf{H}^H \mathbf{C}^{-1} \mathbf{H})^{-1}]_{2\times 2} & -\mathrm{Im}[(\mathbf{H}^H \mathbf{C}^{-1} \mathbf{H})^{-1}]_{2\times 2} \\ \mathrm{Im}[(\mathbf{H}^H \mathbf{C}^{-1} \mathbf{H})^{-1}]_{2\times 2} & \mathrm{Re}[(\mathbf{H}^H \mathbf{C}^{-1} \mathbf{H})^{-1}]_{2\times 2} \end{bmatrix} \\ &\quad = \frac{1}{2}\begin{bmatrix} (\mathbf{H}^H \mathbf{C}^{-1} \mathbf{H})^{-1} & \mathbf{0} \\ \mathbf{0} & (\mathbf{H}^H \mathbf{C}^{-1} \mathbf{H})^{-1} \end{bmatrix}_{4\times 4} \end{aligned} \tag{5.14a}$$

In the above equation, $\mathbf{H}$ and $\mathbf{C}$ are both real numbered, so $\mathrm{Im}[(\mathbf{H}^H \mathbf{C}^{-1} \mathbf{H})^{-1}]_{2\times 2} = 0$.

The covariance matrix of $\boldsymbol{\theta}$ under "white" Gaussian noise can be expressed in both complex numbers and real numbers as (*ibid*):

$$\mathbf{C}_{\hat{\boldsymbol{\theta}}} = \mathbf{J}^{-1}(\boldsymbol{\theta}) = \sigma_{\Sigma\, n}^2 (\mathbf{H}^{\,H}\mathbf{H})^{-1}$$

and

$$\begin{aligned}\mathbf{C}_{\hat{\boldsymbol{\xi}}} &= \mathbf{J}^{-1}(\boldsymbol{\xi}) \\ &= \frac{1}{2}\sigma_{\Sigma\, n}^2 \begin{bmatrix} \mathrm{Re}[(\mathbf{H}^{\,H}\mathbf{H})^{-1}]_{2\times 2} & -\mathrm{Im}[(\mathbf{H}^{\,H}\mathbf{H})^{-1}]_{2\times 2} \\ \mathrm{Im}[(\mathbf{H}^{\,H}\mathbf{H})^{-1}]_{2\times 2} & \mathrm{Re}[(\mathbf{H}^{\,H}\mathbf{H})^{-1}]_{2\times 2} \end{bmatrix} \\ &= \frac{1}{2}\sigma_{\Sigma\, n}^2 \begin{bmatrix} (\mathbf{H}^{\,H}\mathbf{H})^{-1} & \mathbf{0} \\ \mathbf{0} & (\mathbf{H}^{\,H}\mathbf{H})^{-1} \end{bmatrix}_{4\times 4}\end{aligned} \tag{5.14b}$$

where $\sigma_{\Sigma\, n}^2$ is the noise variance at the correlator output after beamforming as defined in equation (5.4).

The assumption that samples are on the linear part of the correlation slope can be met. Because e***ven though the shape of the correlation function from real multipath environments is a smoothened triangle, there is still a linear segment, which can be seen in Figure 5.3.***

The estimation of $\hat{\boldsymbol{\theta}} = \begin{bmatrix} \hat{B} \\ \hat{A} \end{bmatrix}$ is based on a linear model. It is known that *for a linear model, the MVU (minimum variance unbiased) estimator attains the CRLB and an estimator*

which reaches its CRLB is called efficient (*ibid*). So the estimation of $\hat{\boldsymbol{\theta}} = \begin{bmatrix} \hat{B} \\ \hat{A} \end{bmatrix}$ is efficient.

Step 5: Correlation Slope-based TOA/TDOA Estimation in Multipath Environments

In order to estimate the TOA, which is t_{d1} as shown in Figure 5.4, one needs to estimate the correlation function starting point $\hat{\tau}_0$. Because the starting point is a real value, it can be expressed as:

$$\begin{aligned} \hat{\tau}_0 &= \mathrm{Re}[g(\hat{\boldsymbol{\theta}})] = -\mathrm{Re}\left[\frac{\hat{B}}{\hat{A}}\right] = -\frac{\mathrm{Re}[\hat{A}^* \hat{B}]}{|\hat{A}|^2} \\ &= -\mathrm{Re}\left[\frac{\hat{b}_R + j\hat{b}_I}{\hat{a}_R + j\hat{a}_I}\right] = -\frac{\hat{a}_R \hat{b}_R + \hat{a}_I \hat{b}_I}{\hat{a}_R^2 + \hat{a}_I^2} \end{aligned} \tag{5.15}$$

This equation shows that in order to estimate the correlation function starting point $\hat{\tau}_0$, one needs to estimate the correlation function slope $\hat{A}$ and its intercept $\hat{B}$.

Estimation of $\hat{A}$ and $\hat{B}$

$\hat{A}$ and $\hat{B}$ can be estimated through equation (5.13a) under non "white" Gaussian noise or equation (5.13b) under "white" Gaussian noise. One needs to figure out the correlation properties of the noise at the summated correlator output.

Suppose that the sampling rate for I/Q baseband signals is $2/T_c$ (two times the PN chip rate) and the noise in the sampled baseband signals is a "white" Gaussian noise, the

correlation characteristics of the noise in the correlation function after despreading, shown in Figure 5.4, is investigated as follows.

Suppose that the sampling rate for the correlation function is $vT_C \quad (0 < v < 1/2)$ and three samples are taken in the rising part of the correlation function. Equation (5.10) is changed to

$$
\begin{aligned}
&\mathbf{r}_\Sigma = \mathbf{r}_{\Sigma LOS} + \mathbf{r}_{\Sigma n} = \mathbf{H}\boldsymbol{\theta} + \mathbf{r}_{\Sigma n} \\
&\textit{where} \\
&\mathbf{r}_\Sigma = [r_\Sigma(\tau_1),\, r_\Sigma(\tau_2),\, r_\Sigma(\tau_3)]^T \\
&\mathbf{r}_{\Sigma LOS} = [r_{\Sigma LOS}(\tau_1),\, r_{\Sigma LOS}(\tau_2),\, r_{\Sigma LOS}(\tau_3)]^T \\
&\mathbf{r}_{\Sigma n} = [r_{\Sigma n}(\tau_1),\, r_{\Sigma n}(\tau_2),\, r_{\Sigma n}(\tau_3)]^T \\
&\mathbf{r}_{\Sigma LOS} = \mathbf{H}\boldsymbol{\theta} \\
&\mathbf{H} = \begin{bmatrix} 1 & \tau_1 \\ 1 & \tau_2 \\ 1 & \tau_3 \end{bmatrix} = \begin{bmatrix} 1 & \tau_1 \\ 1 & \tau_1 + vT_C \\ 1 & \tau_1 + 2vT_C \end{bmatrix} \quad 0 < v < 1/2 \\
&\boldsymbol{\theta} = \begin{bmatrix} B \\ A \end{bmatrix}
\end{aligned}
\tag{5.16}
$$

The above equation is based on three samples $[r_\Sigma(\tau_1), r_\Sigma(\tau_2), r_\Sigma(\tau_3)]$. In order to estimate the unknown parameter $\boldsymbol{\theta}$ using equation (5.13), the noise characteristics needs to be figured out.

Derivation of noise covariance matrix C

Based on (5.3), the correlation property between $r_{\Sigma n}(\tau_i)$ and $r_{\Sigma n}(\tau_j)$, $i, j = 1, 2, 3$ can be derived as (samples are still from the correlation function initial part):

$$
\begin{aligned}
E[r_{\Sigma n}(\tau_i) r^*_{\Sigma n}(\tau_j)] &= E\left\{ \mathbf{a}^H(\beta_1)\, \mathbf{r}_n(\tau_i) [\mathbf{a}^H(\beta_1)\, \mathbf{r}_n(\tau_j)]^H \right\} \\
&= \mathbf{a}^H(\beta_1)\, E[\mathbf{r}_n(\tau_i) \mathbf{r}_n^H(\tau_j)] \mathbf{a}(\beta_1) \\
&= \sum_{m=1}^{M} E[r_{nm}(\tau_i) r^*_{nm}(\tau_j)] \\
&(M \text{ is the number of array sensors}) \\
&= ME[r_{n1}(\tau_i) r^*_{n1}(\tau_j)] \\
&= ME\left\{ \left[\sum_{k=0}^{N-1} n_1(kT_S) s_l(kT_S - \tau_i) \right] \left[\sum_{k=0}^{N-1} n_1(kT_S) s_l(kT_S - \tau_j) \right]^* \right\} \\
&= ME\left[\sum_{k=0}^{N-1} |\, n_1(kT_S)\,|^2\, s_l(kT_S - \tau_i) s_l^*(kT_S - \tau_j) \right] \\
&= M\sigma^2 \sum_{k=0}^{N-1} s_l(kT_S - \tau_i) s_l^*(kT_S - \tau_j) = MN\sigma^2 (1 - |\, i - j\, | v) \qquad (5.17) \\
&= 2M\sigma_r^2 (1 - |\, i - j\, | v)
\end{aligned}
$$

where σ^2 is the noise variance at each channel before despreading and σ_r^2 is the noise variance at each channel after despreading.

Based on equation (5.17), the covariance matrix of the sampled noise on the rising edge of the correlation function can be written as:

$$
\mathbf{C} = 2M\sigma_r^2 \begin{bmatrix} 1 & 1-v & 1-2v \\ 1-v & 1 & 1-v \\ 1-2v & 1-v & 1 \end{bmatrix} \qquad (5.18)
$$

This equation means that the noise in the correlator output is correlated if the sampling rate for the correlation function is $vT_C \quad (0 < v < 1/2)$. That is the unknown parameter $\boldsymbol{\theta} = [B \quad A]^T$ should be estimated under non "white" Gaussian noise using equation (5.13a) as follows:

$$(\mathbf{H}^T\mathbf{C}^{-1}\mathbf{H})^{-1}\mathbf{H}^T\mathbf{C}^{-1} = \frac{1}{2vT_C}\begin{bmatrix} \tau_1 + 2vT_C & 0 & -\tau_1 \\ -1 & 0 & 1 \end{bmatrix}$$

$$= \frac{1}{2vT_C}\begin{bmatrix} \tau_3 & 0 & -\tau_1 \\ -1 & 0 & 1 \end{bmatrix}$$

$$\hat{\boldsymbol{\theta}} = \begin{bmatrix} \hat{B} \\ \hat{A} \end{bmatrix} = (\mathbf{H}^T\mathbf{C}^{-1}\mathbf{H})^{-1}\mathbf{H}^T\mathbf{C}^{-1}\mathbf{r}_\Sigma$$

$$= \frac{1}{2vT_C}\begin{bmatrix} \tau_3\, r_\Sigma(\tau_1) - \tau_1\, r_\Sigma(\tau_3) \\ r_\Sigma(\tau_3) - r_\Sigma(\tau_1) \end{bmatrix} \tag{5.19}$$

that is

$$\hat{B} = \frac{1}{2vT_C}[\tau_3\, r_\Sigma(\tau_1) - \tau_1\, r_\Sigma(\tau_3)] = B + \frac{1}{2vT_C}[\tau_3\, r_{\Sigma n}(\tau_1) - \tau_1\, r_{\Sigma n}(\tau_3)]$$

$$\hat{A} = \frac{1}{2vT_C}[r_\Sigma(\tau_3) - r_\Sigma(\tau_1)] = A + \frac{1}{2vT_C}[r_{\Sigma n}(\tau_3) - r_{\Sigma n}(\tau_1)]$$

Conclusions:

1. *The "white" Gaussian noise becomes non "white" Gaussian after it goes through □ispreading process. Because the noise at the correlator output is generated by multiplying the baseband noise with the local PN code, so the noise characteristics at the correlator output are related to the local PN code's properties. As it is known that within one PN chip, the samples of PN code are*

correlated. So at the correlation function rising slope side, which is within one PN chip, the samples are all correlated.

2. *Only two samples on the rising edge of the correlation function are needed to estimate the intercept A and the slope B because the samples are correlated as described in equation (5.18).*

It can also be proven that the estimation of $\boldsymbol{\theta} = [B \quad A]^T$ is unbiased as follows:

Because $E[r_{\Sigma_n}(\tau)] = 0$, the following expressions exist:

$$\begin{aligned} E(\hat{B}) &= E\left\{\frac{1}{2vT_C}[\tau_3\, r_\Sigma(\tau_1) - \tau_1\, r_\Sigma(\tau_3)]\right\} = \frac{1}{2vT_C}[\tau_3\, r_{\Sigma LOS}(\tau_1) - \tau_1\, r_{\Sigma LOS}(\tau_3)] = B \\ E(\hat{A}) &= E\left\{\frac{1}{2vT_C}[\, r_\Sigma(\tau_3) - r_\Sigma(\tau_1)]\right\} = \frac{1}{2vT_C}[r_{\Sigma LOS}(\tau_3) - r_{\Sigma LOS}(\tau_1)] = A \end{aligned} \tag{5.20}$$

The covariance matrix of the estimated parameters can be obtained as:

$$\begin{aligned} \mathbf{C}_{\hat{\boldsymbol{\theta}}} &= \mathbf{J}^{-1}(\boldsymbol{\theta}) = (\mathbf{H}^H \mathbf{C}^{-1} \mathbf{H})^{-1} \\ &= \frac{M\sigma_r^2}{vT_C^2}\begin{bmatrix} \tau_1^2 + 2v\tau_1 T_C + vT_C^2 & -(\tau_1 + vT_C) \\ -(\tau_1 + vT_C) & 1 \end{bmatrix} \\ &\textit{that is} \\ \mathrm{var}(\hat{B}) &= \frac{M\sigma_r^2}{vT_C^2}(\tau_1^2 + 2v\tau_1 T_C + vT_C^2) \\ \mathrm{var}(\hat{A}) &= \frac{M\sigma_r^2}{vT_C^2} \end{aligned} \tag{5.21}$$

It can be seen from the above expression that the accuracy of the estimates $\hat{A}$ and $\hat{B}$ affects each other because $\mathbf{J}^{-1}(\boldsymbol{\theta})_{12} = \mathbf{J}^{-1}(\boldsymbol{\theta})_{21} = -(\tau_1 + vT_C) \neq 0$. It will be shown later

on in Section 5.5 that after coordinate transformation, the estimation of $\hat{A}$ and $\hat{B}$ does not affect each other.

Estimation of correlation function starting point $\hat{\tau}_0$

The estimated correlation function starting point $\hat{\tau}_0$ described in equation (5.15) is derived based on the estimated $\hat{A}$ and $\hat{B}$ from equation (5.19) as follows:

$$\begin{aligned}\hat{\tau}_0 &= \mathrm{Re}[g(\hat{\boldsymbol{\theta}})] = -\mathrm{Re}\left[\frac{\hat{B}}{\hat{A}}\right] = -\frac{\mathrm{Re}(\hat{A}^{*}\hat{B})}{|\hat{A}|^2} \\ &= -\mathrm{Re}\left[\frac{\tau_3\, r_{\Sigma}(\tau_1) - \tau_1\, r_{\Sigma}(\tau_3)}{r_{\Sigma}(\tau_3) - r_{\Sigma}(\tau_1)}\right] \\ &= -\frac{\mathrm{Re}\{[r_{\Sigma}^{*}(\tau_3) - r_{\Sigma}^{*}(\tau_1)][\tau_3\, r_{\Sigma}(\tau_1) - \tau_1\, r_{\Sigma}(\tau_3)]\}}{|r_{\Sigma}(\tau_3) - r_{\Sigma}(\tau_1)|^2}\end{aligned} \tag{5.22}$$

The estimated variance of $\hat{\tau}_0$ is discussed in the next section.

Finally, the estimation of the LOS TOA $\hat{t}_{d1}$ is obtained as:

$$\hat{t}_{d1} = \hat{\tau}_0 + T_C \tag{5.23}$$

where T_C is the chip period of the PN code. In practice, T_C needs to be modified, because the bottom width of the correlation function of the real data is different from the theoretical value of one chip T_C due to the bandwidth of the baseband filter used. It will be obtained based on the real bandwidth of the received signal. However for TDOA estimation, the value of T_C is not required because it disappears when differencing two

TOA values, i.e. $TDOA = \hat{t}_{d1} - \hat{t}_{d2} = \hat{\tau}_{0,1} - \hat{\tau}_{0,2}$, where $\hat{\tau}_{0,1}$ and $\hat{\tau}_{0,2}$ are the starting points of two correlation functions related to two different base stations.

Summary

In this thesis, instead of trying to mitigate all inter-chip multipath, the proposed method attempts to mitigate multipath at the initial rising part of the correlation function by enhancing the LOS SNR based on the estimated AOAs from the F/B smoothing MUSIC algorithm.

The conventional F/B smoothing MUSIC is limited by the number of incident rays due to the limited antenna elements. For this purpose the new data set with less signal sources is generated by sampling the beginning part of the correlation function where fewer multipath components are included. After using the modified F/B smoothing MUSIC, the AOAs of the signals can be estimated. Then the spatial addition of the five channels' signals in the direction of the LOS is applied to enhance the strength of the LOS and at the same time mitigate the multipath efficiently at the rising edge of the correlation function even though the peak is still distorted by the same multipath. Then the focus is on the rising edge which has a good linear shape to detect the correlation function *linear slope* and, sequentially, the starting point is obtained. Finally the multipath mitigated TOA/TDOA measurement can be obtained. Figure 5.5 shows the flow chart for this algorithm.

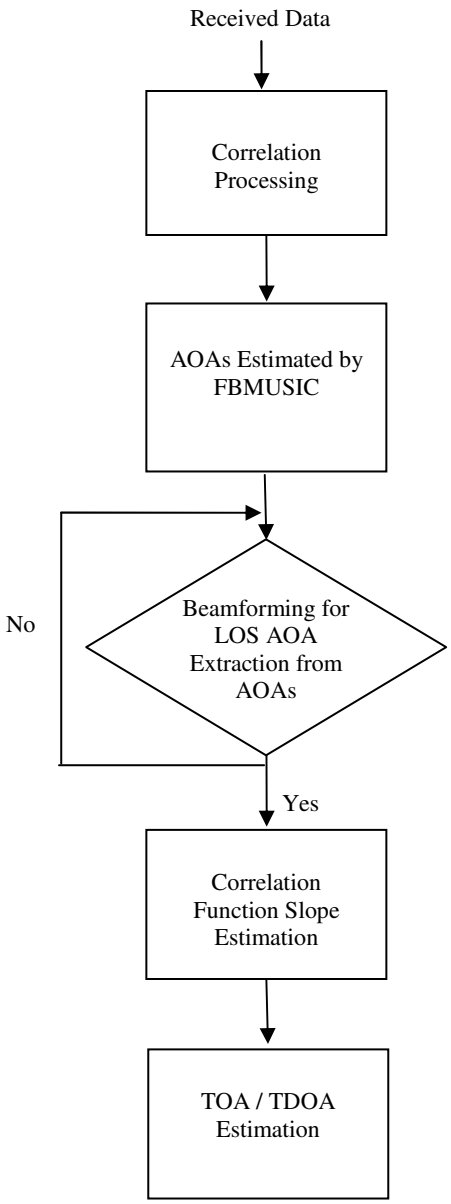

Figure 5.5: Flow Chart of Proposed Algorithm

5.5 Error Analysis of the AOA-assisted TOA Estimator Using Coordinate Transformation

Based on equation (5.23), it can be seen that the variance of TOA ($\hat{t}_{d1}$) is the same as that of the correlation function starting point ($\hat{\tau}_0$). So the variance of $\hat{\tau}_0$ is discussed here. As the expression in equation (5.22), the starting point $\hat{\tau}_0$ is the nonlinear transformation of the fundamental parameter $\hat{\boldsymbol{\theta}}$, so it is not possible to derive the variance $\text{var}(\hat{\tau}_0)$ directly by linear model. However, as discussed in Chapter 3, any unbiased estimator's variance can be obtained by equation (3.20). In this section, two tasks are carried on:

1. Prove that the non-linear estimator for $\hat{\tau}_0$ is unbiased under certain condition
2. Derive the variance of estimator for $\hat{\tau}_0$

Proof of unbiased estimator for $\hat{\tau}_0$

Intuitively, if there is a larger signal to noise ratio, then $|\hat{A}|^2 \approx |A|^2$ and equation (5.22) can be simplified as

$$\begin{aligned}\hat{\tau}_0 = \text{Re}[g(\hat{\boldsymbol{\theta}})] = -\text{Re}\left[\frac{\hat{B}}{\hat{A}}\right] = -\frac{\text{Re}(\hat{A}^*\hat{B})}{|\hat{A}|^2} \\ \approx -\frac{\text{Re}(\hat{A}^*\hat{B})}{|A|^2}\end{aligned} \tag{5.24}$$

Based on equation (5.19), the condition for $|\hat{A}|^2 \approx |A|^2$ is derived as follows:

$$
\begin{aligned}
|\hat{A}|^2 &= \frac{1}{(2vT_C)^2}\,|\,r_{\Sigma}(\tau_3)-r_{\Sigma}(\tau_1)\,|^2 \\
&= \frac{1}{(2vT_C)^2}\,|\,r_{\Sigma\,LOS}(\tau_3)-r_{\Sigma\,LOS}(\tau_1)+r_{\Sigma n}(\tau_3)-r_{\Sigma n}(\tau_1)\,|^2 \\
&= \left|A+\frac{r_{\Sigma n}(\tau_3)-r_{\Sigma n}(\tau_1)}{2vT_C}\right|^2 \\
&= \frac{1}{(2vT_C)^2}\,|\,2v\,r_{\Sigma\,LOS\ peak}(\tau)+r_{\Sigma n}(\tau_3)-r_{\Sigma n}(\tau_1)\,|^2 \\
&\quad (r_{\Sigma\,LOS\ peak}(\tau)\ \textit{is the peak value of the correlation function}) \\
&= \frac{1}{(2vT_C)^2}\{\ \left|2v\,r_{\Sigma\,LOS\ peak}(\tau)\right|^2+2\,\mathrm{Re}\{2v\,r_{\Sigma\,LOS\ peak}(\tau)\,[r^*_{\Sigma n}(\tau_3)-r^*_{\Sigma n}(\tau_1)]\} \\
&\qquad\qquad +\ \left|r_{\Sigma n}(\tau_3)\right|^2+\left|r_{\Sigma n}(\tau_1)\right|^2-2\,\mathrm{Re}[r^*_{\Sigma n}(\tau_1)r^*_{\Sigma n}(\tau_3)]\ \} \\
&= |\,A\,|^2+|\,A_n\,|^2
\end{aligned}
\tag{5.25}
$$

where

$$
|\,A\,|^2=\frac{(2v)^2}{(2vT_C)^2}\,|\,r_{\Sigma\,LOS\ peak}(\tau)\,|^2=\left|\frac{r_{\Sigma\,LOS\ peak}(\tau)}{T_C}\right|^2
$$

$$
\begin{aligned}
|\,A_n\,|^2 = \frac{1}{(2vT_C)^2}\{\ & 2\,\mathrm{Re}\{2v\,r_{\Sigma\,LOS\ peak}(\tau)[r^*_{\Sigma n}(\tau_3)-r^*_{\Sigma n}(\tau_1)]\} \\
& +|\,r_{\Sigma n}(\tau_3)\,|^2+|\,r_{\Sigma n}(\tau_1)\,|^2-2\,\mathrm{Re}[r_{\Sigma n}(\tau_1)\,r^*_{\Sigma n}(\tau_3)]\ \}
\end{aligned}
$$

Evidently, $|\,A_n\,|^2$ is introduced due to noise. Based on (5.17) and $E[r_{\Sigma_n}(\tau)]=0$, the expectation of $|\,A_n\,|^2$ can be derived as:

$$
E(|\,A_n\,|^2)=\frac{M\sigma_r^2}{vT_C^2} \tag{5.26}
$$

In order to find the condition for $|\hat{A}|^2 \approx |\,A\,|^2$, the probability of false alarm P_{fa} is introduced (Barton & Leonov 1997) as:

$$P_{fa} = \exp(\frac{-A^2}{2\sigma^2}) = \exp(\frac{-SNR}{2}) \tag{5.27a}$$

If $P_{fa} = 0.01 \sim 0.001$, then the required threshold to detect the signal is *SNR* = 9.6 ~ 11.4 dB; Usually the threshold is 5 dB below the signal peak, so the SNR_{paek} can reach 14.6 to 16.4 dB. For an array with 5 elements, the signal to noise ratio at the peak will be increased five times (7 dB), i.e. $SNR_{\Sigma\, peak} = 21.6dB \sim 23.4dB$.

For example, if it the required threshold is $SNR_{\Sigma\, peak} \geq 14.8\, dB$ and v = 1/6, i.e.

$$\frac{|A|^2}{E(|A_n|^2)} = \frac{\frac{|r_{\Sigma\, LOS\, peak}(\tau)|^2}{T_C^2}}{\frac{M\sigma_r^2}{vT_C^2}} = v\ SNR_{\Sigma\, peak} \geq \frac{1}{6} * 10^{1.48} = 5 \tag{5.27b}$$

Thus, the condition for $|\hat{A}|^2 \approx |A|^2$ is:

$$\frac{|A|^2}{E(|A_n|^2)} \geq 5 \tag{5.27c}$$

When $SNR_{\Sigma\, peak} \geq 14.8\, dB$, based on equation (5.19), the estimation of $\hat{\tau}_0$ in equation (5.24) becomes:

$$\hat{\tau}_0 \approx -\frac{\mathrm{Re}(\hat{A}^*\hat{B})}{|A|^2} = -\frac{1}{|A|^2}\mathrm{Re}\left\{\left[A^* + \frac{r_{\Sigma n}^*(\tau_3) - r_{\Sigma n}^*(\tau_1)}{2vT_C}\right]\left[B + \frac{\tau_3 r_{\Sigma n}(\tau_1) - \tau_1 r_{\Sigma n}(\tau_3)}{2vT_C}\right]\right\}$$

$$= \tau_0 - \frac{1}{|A|^2}\mathrm{Re}\left\{A^*\frac{\tau_3 r_{\Sigma n}(\tau_1) - \tau_1 r_{\Sigma n}(\tau_3)}{2vT_C} + B\frac{r_{\Sigma n}^*(\tau_3) - r_{\Sigma n}^*(\tau_1)}{2vT_C} + \frac{[r_{\Sigma n}^*(\tau_3) - r_{\Sigma n}^*(\tau_1)][\tau_3 r_{\Sigma n}(\tau_1) - \tau_1 r_{\Sigma n}(\tau_3)]}{(2vT_C)^2}\right\}$$

(5.28a)

Based on equation (5.17), the expectation of $\hat{\tau}_0$ can be derived as:

$$E(\hat{\tau}_0) \approx \tau_0 + \frac{1}{(2vT_C)^2|A|^2}\left\{\tau_1|r_{\Sigma n}(\tau_3)|^2 + \tau_3|r_{\Sigma n}(\tau_1)|^2 - \tau_3 E[r_{\Sigma n}^*(\tau_3)r_{\Sigma n}(\tau_1)] - \tau_1 E[r_{\Sigma n}^*(\tau_1)r_{\Sigma n}(\tau_3)]\right\}$$

$$= \tau_0 + \frac{1}{(2v)^2|r_{\Sigma LOS\ peak}(\tau)|^2}[\tau_1 M\sigma_r^2 + \tau_3 M\sigma_r^2 - (1-2v)\tau_3 M\sigma_r^2 - (1-2v)\tau_1 M\sigma_r^2]$$

$$= \tau_0 - \frac{2v(\tau_1+\tau_3)M\sigma_r^2}{(2v)^2|r_{\Sigma LOS\ peak}(\tau)|^2}$$

$$= \tau_0 - \frac{4v\tau_2 M\sigma_r^2}{(2v)^2|r_{\Sigma LOS\ peak}(\tau)|^2}$$

$$= \tau_0 - \frac{\tau_2}{vSNR_{\Sigma\ peak}}$$

(5.28b)

It can be seen that the ***unbiased estimator*** for $\hat{\tau}_0$ should meet the following conditions:

1. Large $SNR_{\Sigma\ peak}$, e.g. $SNR_{\Sigma\ peak} \geq 14.8dB$

2. $\tau_2 = 0$, otherwise a bias of $\frac{\tau_2}{vSNR_{\Sigma\ peak}}$ in equation (5.28b) will be introduced.

That is the origin of the coordinate in Figure 5.4 needs to move to the position of τ_2

Modification of estimator for $\hat{\tau}_0$ based on coordinate transformation

Based on the above conclusion, after coordinate transformation, the time axis τ is changed to:

$$\tau' = \tau - \tau_2 \tag{5.29}$$

Thus, three samples located in τ' the time axis are

$$\tau_1' = -vT_C, \quad \tau_2' = 0, \quad \tau_3' = vT_C \tag{5.30}$$

Here vT_C is the interval between two samples as shown in Figure 5.4 and $0 < v < \frac{1}{2}$

Under a new coordinate system, the linear model in equation (5.16) is modified as:

$$\begin{aligned}
&\mathbf{r}_\Sigma = \mathbf{r}_{\Sigma LOS} + \mathbf{r}_{\Sigma n} = \mathbf{H\theta} + \mathbf{r}_{\Sigma n} \\
&\textit{where} \\
&\mathbf{r}_\Sigma = [r_\Sigma(\tau_1'), r_\Sigma(\tau_2'), r_\Sigma(\tau_3')]^T \\
&\mathbf{r}_{\Sigma LOS} = [r_{\Sigma LOS}(\tau_1'), r_{\Sigma LOS}(\tau_2'), r_{\Sigma LOS}(\tau_3')]^T \\
&\mathbf{r}_{\Sigma n} = [r_{\Sigma n}(\tau_1'), r_{\Sigma n}(\tau_2'), r_{\Sigma n}(\tau_3')]^T \\
&\mathbf{r}_{\Sigma LOS} = \mathbf{H\theta} \\
&\mathbf{H} = \begin{bmatrix} 1 & \tau_1' \\ 1 & \tau_2' \\ 1 & \tau_3' \end{bmatrix} = \begin{bmatrix} 1 & -vT_C \\ 1 & 0 \\ 1 & vT_C \end{bmatrix} \quad 0 < v < 1/2 \\
&\mathbf{\theta} = \begin{bmatrix} B \\ A \end{bmatrix}
\end{aligned} \tag{5.31}$$

Accordingly, equation (5.19) for the estimates of $\hat{A}$ and $\hat{B}$ is modified as:

$$(\mathbf{H}^T\mathbf{C}^{-1}\mathbf{H})^{-1}\mathbf{H}^T\mathbf{C}^{-1} = \frac{1}{2vT_C}\begin{bmatrix} \tau_3' & 0 & -\tau_1' \\ -1 & 0 & 1 \end{bmatrix}$$

$$= \frac{1}{2vT_C}\begin{bmatrix} vT_C & 0 & vT_C \\ -1 & 0 & 1 \end{bmatrix}$$

$$\hat{\boldsymbol{\theta}} = \begin{bmatrix} \hat{B} \\ \hat{A} \end{bmatrix} = (\mathbf{H}^T\mathbf{C}^{-1}\mathbf{H})^{-1}\mathbf{H}^T\mathbf{C}^{-1}\mathbf{r}_\Sigma$$

$$= \frac{1}{2vT_C}\begin{bmatrix} vT_C[r_\Sigma(\tau_1') + r_\Sigma(\tau_3')] \\ r_\Sigma(\tau_3') - r_\Sigma(\tau_1') \end{bmatrix} \tag{5.32}$$

that is

$$\hat{B} = \frac{1}{2}[r_\Sigma(\tau_1') + r_\Sigma(\tau_3')] = \frac{1}{2}[r_\Sigma(-vT_C) + r_\Sigma(vT_C)]$$

$$\hat{A} = \frac{1}{2vT_C}[r_\Sigma(\tau_3') - r_\Sigma(\tau_1')] = \frac{1}{2vT_C}[r_\Sigma(vT_C) - r_\Sigma(-vT_C)]$$

Equation (5.21) for the estimated variance is modified as:

$$\mathbf{C}_{\hat{\boldsymbol{\theta}}} = \mathbf{J}^{-1}(\boldsymbol{\theta}) = (\mathbf{H}^H\mathbf{C}^{-1}\mathbf{H})^{-1}$$

$$= \frac{M\sigma_r^2}{vT_C^2}\begin{bmatrix} v(1-v)T_C^2 & 0 \\ 0 & 1 \end{bmatrix}$$

that is

$$\mathrm{var}(\hat{B}) = v(1-v)M\sigma_r^2$$

$$\mathrm{var}(\hat{A}) = \frac{M\sigma_r^2}{vT_C^2}$$

and

$$\mathbf{C}_{\hat{\boldsymbol{\xi}}} = \mathbf{J}^{-1}(\boldsymbol{\xi})$$

$$= \frac{1}{2}\begin{bmatrix} (\mathbf{H}^H\mathbf{C}^{-1}\mathbf{H})^{-1} & \mathbf{0} \\ \mathbf{0} & (\mathbf{H}^H\mathbf{C}^{-1}\mathbf{H})^{-1} \end{bmatrix}_{4\times4}$$

$$= \frac{1}{2}\frac{M\sigma_r^2}{vT_C^2}\begin{bmatrix} v(1-v)T_C^2 & 0 & 0 & 0 \\ 0 & 1 & 0 & 0 \\ 0 & 0 & v(1-v)T_C^2 & 0 \\ 0 & 0 & 0 & 1 \end{bmatrix} \tag{5.33}$$

It can be seen that, from equation (5.33), after coordinate transformation, the accuracies

of the estimates $\hat{A}$ and $\hat{B}$ do not affects each other because $\mathbf{J}^{-1}(\boldsymbol{\theta})_{12} = \mathbf{J}^{-1}(\boldsymbol{\theta})_{21} = 0$. This can be understood easily because when the origin of the time axis is moved to τ_2, the change of the correlation slope *A* will not result in the change of intercept *B*. Whereas, before coordinate transformation, they affects each other as expressed in equation (5.21) because the change of correlation slope *A* will result in the change of intercept *B*.

Finally, based on equation (5.32), the correlation starting point estimation expressed in equation (5.22) is modified as:

$$\begin{aligned}
\hat{\tau}_0^{'} &= \mathrm{Re}[g(\hat{\boldsymbol{\theta}})] = -\mathrm{Re}\left[\frac{\hat{B}}{\hat{A}}\right] = -\frac{\mathrm{Re}(\hat{A}^{*}\hat{B})}{|\hat{A}|^2} \\
&= -vT_C\,\mathrm{Re}\left[\frac{r_\Sigma(\tau_1)+r_\Sigma(\tau_3^{'})}{r_\Sigma(\tau_3^{'})-r_\Sigma(\tau_1^{'})}\right] \\
&= -vT_C\,\frac{\mathrm{Re}\{[r_\Sigma^{*}(\tau_3^{'})-r_\Sigma^{*}(\tau_1^{'})][r_\Sigma(\tau_1^{'})+r_\Sigma(\tau_3^{'})]\}}{|r_\Sigma(\tau_3^{'})-r_\Sigma(\tau_1^{'})|^2} \\
&= -vT_C\,\frac{\mathrm{Re}\{|r_\Sigma(\tau_3^{'})|^2-|r_\Sigma(\tau_1^{'})|^2+2j\,\mathrm{Im}[r_\Sigma^{*}(\tau_3^{'})r_\Sigma(\tau_1^{'})]\}}{|r_\Sigma(\tau_3^{'})-r_\Sigma(\tau_1^{'})|^2} \\
&= -vT_C\,\frac{|r_\Sigma(\tau_3^{'})|^2-|r_\Sigma(\tau_1^{'})|^2}{|r_\Sigma(\tau_3^{'})-r_\Sigma(\tau_1^{'})|^2}
\end{aligned} \tag{5.34}$$

Equation (5.34) can be used practically for the measured data. It is a simplified version of equation (5.22). One needs to remember that only when $SNR_{\Sigma\,peak} \geq 14.8\,dB$, is the estimate of $\hat{\tau}_0^{'}$ unbiased, which is shown below.

The true value of the correlation starting point in the new coordinate system $\tau_0^{'}$ is

formulated as follows:

$$\begin{aligned}
\tau_0^{'} &= g(\boldsymbol{\theta}) = -\frac{B}{A} = -\frac{A^{*}B}{|A|^2} \\
&= -\frac{\tau_3^{'} r_{\Sigma LOS}(\tau_1) - \tau_1^{'} r_{\Sigma LOS}(\tau_3^{'})}{r_{\Sigma LOS}(\tau_3^{'}) - r_{\Sigma LOS}(\tau_1^{'})} \\
&= -\frac{[r_{\Sigma LOS}^{*}(\tau_3^{'}) - r_{\Sigma LOS}^{*}(\tau_1^{'})][\tau_3^{'} r_{\Sigma LOS}(\tau_1^{'}) - \tau_1^{'} r_{\Sigma LOS}(\tau_3^{'})]}{|r_{\Sigma LOS}(\tau_3^{'}) - r_{\Sigma LOS}(\tau_1^{'})|^2} \\
&= -vT_C \frac{[r_{\Sigma LOS}^{*}(\tau_3^{'}) - r_{\Sigma LOS}^{*}(\tau_1^{'})][r_{\Sigma LOS}(\tau_1^{'}) + r_{\Sigma LOS}(\tau_3^{'})]}{|r_{\Sigma LOS}(\tau_3^{'}) - r_{\Sigma LOS}(\tau_1^{'})|^2} \\
&= -vT_C \frac{|r_{\Sigma LOS}(\tau_3^{'})|^2 - |r_{\Sigma LOS}(\tau_1^{'})|^2 + 2j\,\mathrm{Im}[r_{\Sigma LOS}^{*}(\tau_3^{'}) r_{\Sigma LOS}(\tau_1^{'})]}{|r_{\Sigma}(\tau_3^{'}) - r_{\Sigma}(\tau_1^{'})|^2} \\
&\quad (Note: \mathrm{Im}(\tau_0^{'}) = 0) \\
&= -vT_C \frac{|r_{\Sigma LOS}(\tau_3^{'})|^2 - |r_{\Sigma LOS}(\tau_1^{'})|^2}{|r_{\Sigma LOS}(\tau_3^{'}) - r_{\Sigma LOS}(\tau_1^{'})|^2}
\end{aligned} \tag{5.35.a}$$

When $SNR_{\Sigma\,peak} \geq 14.8\,dB$, the estimate of $\tau_0^{'}$ is

$$\hat{\tau}_0^{'} \approx -\frac{E[\mathrm{Re}(\hat{A}^{*}\hat{B})]}{|A|^2} = -vT_C \frac{|r_{\Sigma}(\tau_3^{'})|^2 - |r_{\Sigma}(\tau_1^{'})|^2}{|r_{\Sigma LOS}(\tau_3^{'}) - r_{\Sigma LOS}(\tau_1^{'})|^2} \tag{5.35.b}$$

Based on the above equation, the expectation of $\hat{\tau}_0^{'}$ is expressed as:

$$
\begin{aligned}
E(\hat{\tau}_0^{'}) &\approx -vT_C \frac{E(|r_{\Sigma}(\tau_3^{'})|^2) - E(|r_{\Sigma}(\tau_1^{'})|^2)}{|r_{\Sigma LOS}(\tau_3^{'}) - r_{\Sigma LOS}(\tau_1^{'})|^2} \\
&= -vT_C \frac{E(|r_{\Sigma LOS}(\tau_3^{'}) + r_{\Sigma n}(\tau_3^{'})|^2) - E(|r_{\Sigma LOS}(\tau_1^{'}) + r_{\Sigma n}(\tau_1^{'})|^2)}{|r_{\Sigma LOS}(\tau_3^{'}) - r_{\Sigma LOS}(\tau_1^{'})|^2} \\
&= -\frac{vT_C}{|r_{\Sigma LOS}(\tau_3^{'}) - r_{\Sigma LOS}(\tau_1^{'})|^2} \{ |r_{\Sigma LOS}(\tau_3^{'})|^2 - |r_{\Sigma LOS}(\tau_1^{'})|^2 \\
&\qquad + 2E[\mathrm{Re}(r_{\Sigma LOS}(\tau_3^{'}) r_{\Sigma n}^{*}(\tau_3^{'}))] + E[|r_{\Sigma n}(\tau_3^{'})|^2] \\
&\qquad - 2E[\mathrm{Re}(r_{\Sigma LOS}(\tau_1^{'}) r_{\Sigma n}^{*}(\tau_1^{'}))] - E[|r_{\Sigma n}^{*}(\tau_1^{'})|^2] \} \\
&= -\frac{-vT_C}{|r_{\Sigma LOS}(\tau_3^{'}) - r_{\Sigma LOS}(\tau_1^{'})|^2} \{ |r_{\Sigma LOS}(\tau_3^{'})|^2 - |r_{\Sigma LOS}(\tau_1^{'})|^2 + M\sigma_r^2 - M\sigma_r^2 \} \\
&= -vT_C \frac{|r_{\Sigma LOS}(\tau_3^{'})|^2 - |r_{\Sigma LOS}(\tau_1^{'})|^2}{|r_{\Sigma LOS}(\tau_3^{'}) - r_{\Sigma LOS}(\tau_1^{'})|^2} = \tau_0^{'}
\end{aligned}
\tag{5.36}
$$

So the estimator for the correlation starting point in the new coordinate system $\hat{\tau}_0^{'}$ is unbiased. After $\tau_0^{'}$ is estimated, the final estimated correlation starting point $\hat{\tau}_0$ in the original coordinate system can be obtained by:

$$\hat{\tau}_0 = \hat{\tau}_0^{'} + \tau_2 \tag{5.37}$$

Where τ_2 corresponds to the middle sample position which can be located by the local code shift during the correlation process.

Derivation of the variance of $\hat{\tau}_0^{'}$

Based on equation (3.20), the variance of the unbiased estimator $\hat{\tau}_0^{'}$ can be expressed as

$$\begin{aligned}\mathrm{var}(\hat{\tau}_0^{'}) &= \frac{\partial \mathbf{g}(\xi)}{\partial \xi}\mathbf{J}^{-1}(\xi)\frac{\partial \mathbf{g}^T(\xi)}{\partial \xi} \\ &= \frac{\partial \mathbf{g}(\xi)}{\partial \xi}\mathbf{C}_{\hat{\xi}}\frac{\partial \mathbf{g}^T(\xi)}{\partial \xi}\end{aligned} . \tag{5.38}$$

where $\mathbf{C}_{\hat{\xi}}$ is given in equation (5.33) and the 1×4 Jacobian matrix $\frac{\partial \mathbf{g}(\xi)}{\partial \xi}$ is defined as:

$$\begin{aligned}&\frac{\partial \mathbf{g}(\xi)}{\partial \xi} = \left[\frac{\partial g(\xi)}{\partial b_R} \quad \frac{\partial g(\xi)}{\partial a_R} \quad \frac{\partial g(\xi)}{\partial b_I} \quad \frac{\partial g(\xi)}{\partial a_I}\right] \\ &\textit{based on } (5.11) \textit{ and } (5.6), \\ &\frac{\partial g(\xi)}{\partial b_R} = -\frac{a_R}{a_R^2 + a_I^2} = -\frac{\cos\phi}{a}, \\ &\frac{\partial g(\xi)}{\partial a_R} = \frac{a_R^2 b_R - a_I^2 b_R + 2a_R a_I b_I}{\left(a_R^2 + a_I^2\right)^2} = \frac{b\cos\phi}{a^2} = -\frac{\tau_0^{'}\cos\phi}{a} \\ &\frac{\partial g(\xi)}{\partial b_I} = -\frac{a_I}{a_R^2 + a_I^2} = -\frac{\sin\phi}{a}, \\ &\frac{\partial g(\xi)}{\partial a_I} = \frac{a_I^2 b_I - a_R^2 b_I + 2a_R a_I b_I}{\left(a_R^2 + a_I^2\right)^2} = \frac{b\sin\phi}{a^2} = -\frac{\tau_0^{'}\sin\phi}{a}\end{aligned} \tag{5.39}$$

Because $\mathbf{C}_{\hat{\xi}}$ is a diagonal matrix, $\mathrm{var}(\hat{\tau}_0^{'})$ can be written as

$$
\begin{aligned}
\mathrm{var}(\hat{\tau}_0^{'}) &= \frac{\partial \mathbf{g}(\xi)}{\partial \xi}\mathbf{C}_{\hat{\xi}}\frac{\partial \mathbf{g}^T(\xi)}{\partial \xi} \\
&= \left[\frac{\partial g(\xi)}{\partial b_R}\right]^2\left[\mathbf{C}_{\hat{\xi}}\right]_{11} + \left[\frac{\partial g(\xi)}{\partial a_R}\right]^2\left[\mathbf{C}_{\hat{\xi}}\right]_{22} + \left[\frac{\partial g(\xi)}{\partial b_I}\right]^2\left[\mathbf{C}_{\hat{\xi}}\right]_{33} + \left[\frac{\partial g(\xi)}{\partial a_I}\right]^2\left[\mathbf{C}_{\hat{\xi}}\right]_{44} \\
&= \frac{1}{2}\frac{M\sigma_r^2}{vT_C^2}\left[\frac{v(1-v)T_C^2}{a^2} + \frac{(\tau_0')^2}{a^2}\right] = \frac{1}{2}\frac{M\sigma_r^2}{r_{\Sigma\,LOS\;peak}(\tau)}\left[(1-v)T_C^2 + \frac{(\tau_0')^2}{v}\right] \\
&= \frac{1}{2SNR_{\Sigma\;peak}(\tau)}\left[(1-v)T_C^2 + \frac{(\tau_0')^2}{v}\right] \\
&= \frac{1}{2SNR_{\Sigma\;peak}(\tau)}\left[T_C^2 - \frac{(\tau_1'-\tau_0')(\tau_1'+\tau_0')}{v}\right] \\
&= \frac{1}{2SNR_{\Sigma\;peak}(\tau)}\left[T_C^2 - 2T_C(\tau_1'-\tau_0') + \frac{(\tau_1'-\tau_0')^2}{v}\right]
\end{aligned}
\tag{5.40}
$$

where T_C is the PN chip period; $0 < v < ½$ and $0 < (\tau_1' - \tau_0') < (1-2v)T_C$.

Equation (5.40) shows that $\mathrm{var}(\hat{\tau}_0^{'})$ is related with three parameters: $SNR_{\Sigma\;peak}(\tau)$, the sample interval vT_C, and the first sample position with respect to the position of the starting point $(\tau_1' - \tau_0')$. It can be seen that, from equation (5.18), the closer the samples are, the more correlated the noise is. Therefore, Figure 5.6 shows that a smaller v results in a larger variance (dashed line). For example, when v = 1/6, $\tau_1' - \tau_0' = 0.15T_C$ and $SNR_{\Sigma\;peak}(\tau) = 15dB$, the estimation standard deviation is 36.8 m. It can also be seen that the closer to the starting point the first sample is, the smaller the variance $\mathrm{var}(\hat{\tau}_0^{'})$ is. Because any vibration of the samples due to noise will cause the error of the estimated starting point and that error decreases if the first sample is closer to the stating point. So the variance $\mathrm{var}(\hat{\tau}_0^{'})$ is also reduced.

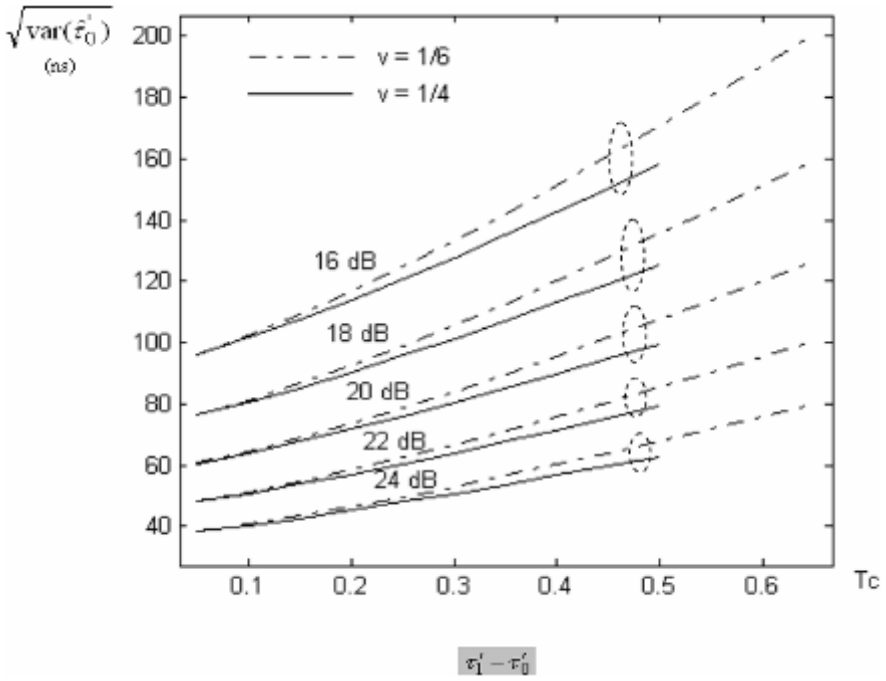

Figure 5.6: Square Root of var($\hat{\tau}_0'$)

5.6 Comparison of the AOA-Assisted TOA Estimation Variance with TOA CRLB

Based on equations (5.40) and (C.11), when $\tau_0' = 0$ and v = ½, the minimum variance of $\hat{\tau}_0'$ or $\hat{\tau}_0$ or $\hat{\tau}$ is obtained as:

$$\mathrm{var}(\hat{\tau}_0')_{\min} = \mathrm{var}(\hat{\tau}_0)_{\min} = \mathrm{var}(\hat{\tau})_{\min} = \frac{T_C^2}{4SNR_{\Sigma\ peak}(\tau)} = \frac{T_C^2}{16MK \cdot SNR} \tag{5.41}$$

where $\hat{\tau}_0' = \hat{\tau}_0 - \tau_2$; $\hat{\tau} = \hat{\tau}_0 + T_C$ (T_C is the chip period of PN code).

Based on equation (3.64), the CRLB of the estimated TOA can rewritten as follows:

$$\text{var}_{CRLB}(\hat{\tau}) = \frac{T_C^2}{32MK \cdot SNR} \tag{5.42}$$

where T_C is the PN chip period; M is the number of antenna array; $K = 2^{15}$ is the length of the PN sequence and SNR is the signal to noise ration before despreading.

Comparing equation (5.42) with equation (5.41) shows that the ***minimum variance of AOA-assisted TOA estimation is twice that of the TOA CRLB***. Table 5.2 summarizes the expressions of AOA estimated variance of the MUSIC estimator, the TOA estimated variance of the proposed method and their CRLBs.

Table 5:2: Comparison of CRLBs with Specific Estimator Variances for the CDMA IS-95 Pilot Signal

CRLBs of AOA-assisted TOA Estimates	Variances of Specific AOA and TOA Estimators
AOA: from equation (3.54) for single source signal: $\mathrm{var}_{CRLB}(\hat{\beta}) = \dfrac{3}{N*SNR*M(M^2-1)\left(2\pi\dfrac{d}{\lambda}\right)^2\sin^2\beta}$ Simulation result is shown in Figure 3.3.	*MUSIC AOA Estimator* from equation (4.57c) for single source signal: $\mathrm{var}_{CRLB}(\hat{\beta}) = \dfrac{3(1+\dfrac{1}{M*SNR})}{N*SNR*M(M^2-1)\left(2\pi\dfrac{d}{\lambda}\right)^2\sin^2\beta}$ Simulation result is shown in Figure 4.7.
from equation (3.53) for multiple source signals: $\mathrm{var}_{CRLB}(\hat{\beta}_i) = \dfrac{\dfrac{\sigma^2}{2N}\left[\mathrm{Re}\left(\{\mathbf{D}^H[\mathbf{I}-\mathbf{A}(\mathbf{A}^H\mathbf{A})^{-1}\mathbf{A}^H]\mathbf{D}\}\odot\mathbf{R}_S\right)\right]^{-1}}{\left(2\pi\dfrac{d}{\lambda}\right)^2\sin^2\beta}$ (Stoica & Nehorai 1989) Simulation result is shown in Figure 3.5.	from equation (4.57a) for multiple source signals: $\mathrm{var}_{MUSIC}(\hat{\beta}_i) = \dfrac{\sigma^2}{2N}\dfrac{\mathbf{a}^H(\beta_i)[\mathbf{V}_S(\overline{\mathbf{\Gamma}}_S^{-1}+\sigma^2\overline{\mathbf{\Gamma}}_S^{-2})\mathbf{V}_S^H]\mathbf{a}(\beta_i)}{\left[\dfrac{d\mathbf{a}(\beta_i)}{d\beta_i}\right]^H\mathbf{V}_N\mathbf{V}_N^H\dfrac{d\mathbf{a}(\beta_i)}{d\beta_i}}$ (Stoica & Nehorai 1989) Simulation result is shown in Figure 4.7.
TOA: $\mathrm{var}_{CRLB}(\hat{\tau}) = \dfrac{T_C^2}{32MK\cdot SNR}$ from equation (3.64)	*Correlation Rising Slope-based TOA* *Estimator*: $\mathrm{var}(\hat{\tau})_{\min} = \dfrac{T_C^2}{16MK\cdot SNR}$ from equation (5.41)

5.7 Conclusions

The effect of multipath on correlation peaks was discussed by using both simulated and measured data. The results show that the position of the peak is shifted, which results in a TOA estimation error. By using a beamforming technique, multipath can be mitigated. But when the multipath is much stronger than the LOS signal, the multipath effect on the correlation peak cannot be suppressed efficiently. The proposed approach focused on the correlation function initial rising part because multipath arrives after the LOS signal and it will not affect the correlation function initial rising shape theoretically. Even though in real IS-95 system, due to limited bandwidth of the filter, the side lobe of multipath correlation function affects LOS correlation function initial rising part a little bit, after beamformer is used along the direction of LOS, the side lobe of multipath correlation function is suppressed because the random phase in each antenna cancel out that side lobe signal and whereas the LOS signal strength is enhanced. Section 5.4 proved that the SNR for the LOS signal has increased M (number of array elements) times after beamforming. Its TOA estimation error is therefore M times less than that of a single antenna-based TOA estimator. The TOA estimator is based on the estimates of the correlation function rising slope and its intercept, which has a non linear relationship. So the coordinate transform is introduced. The correlation function initial rising slope and its intercept are estimated by a linear model under non “white” Gaussian noise. The TOA estimated variance is derived. Even though the proposed unbiased TOA estimator does not reach the CRLB, the estimated variance is 36.8 m when the SNR after despreading is 15 dB. It will be seen in Chapter 6 that the actual estimation error is much smaller than that due to

the high SNR after despreading. The advantage of the proposed AOA-assisted TOA method is that it is more practical due to its light computational burden and it can be used in multipath environments.

Chapter Six: System Hardware Implementation and Experimental Results

6.1 Introduction

In this chapter, a hardware platform developed to collect IS-95 data is described together with experiments based on real data collected under various environments with the above platform. The results are compared with the theoretically estimated values of AOA and TOA derived in Chapter 4 and Chapter 5, respectively. It can be seen that the experimental AOA estimation results are unbiased and the estimated standard deviation is less than 3º. The final estimated TOA values has a constant offset of about 200 metres due to an unknown but deterministic parameter. The theoretical value is asymptotically unbiased when the signal to noise ratio at the correlation peak is more than 15 dB (Section 5.5, equation 5.27). The practical TDOA standard deviation is 8 m in the real environment, where the signal to noise ratio after despreading is 30 dB, meeting the FCC requirements of 50 to 150 metres. The practical errors are uncontrollable systematic errors due to receiver transfer function uncertainties, timing offsets in ADC sampling and base station timing uncertainties.

6.2 General Description of the System

The hardware platform was developed in PLAN (Positioning, Location and Navigation) group of the Department of Geomatics Engineering. The system consists of an antenna array, RF & baseband circuit, FPGA-based digital circuit and data collection control

software (e.g. Lopez et al 2005). The developed prototype CDMA receiver receives the real time pilot signals from IS-95 CDMA base stations. The data is used to verify the proposed algorithm. The diagram of the system is shown in Figure 6.1. The detail description of each part is given in the following subsections.

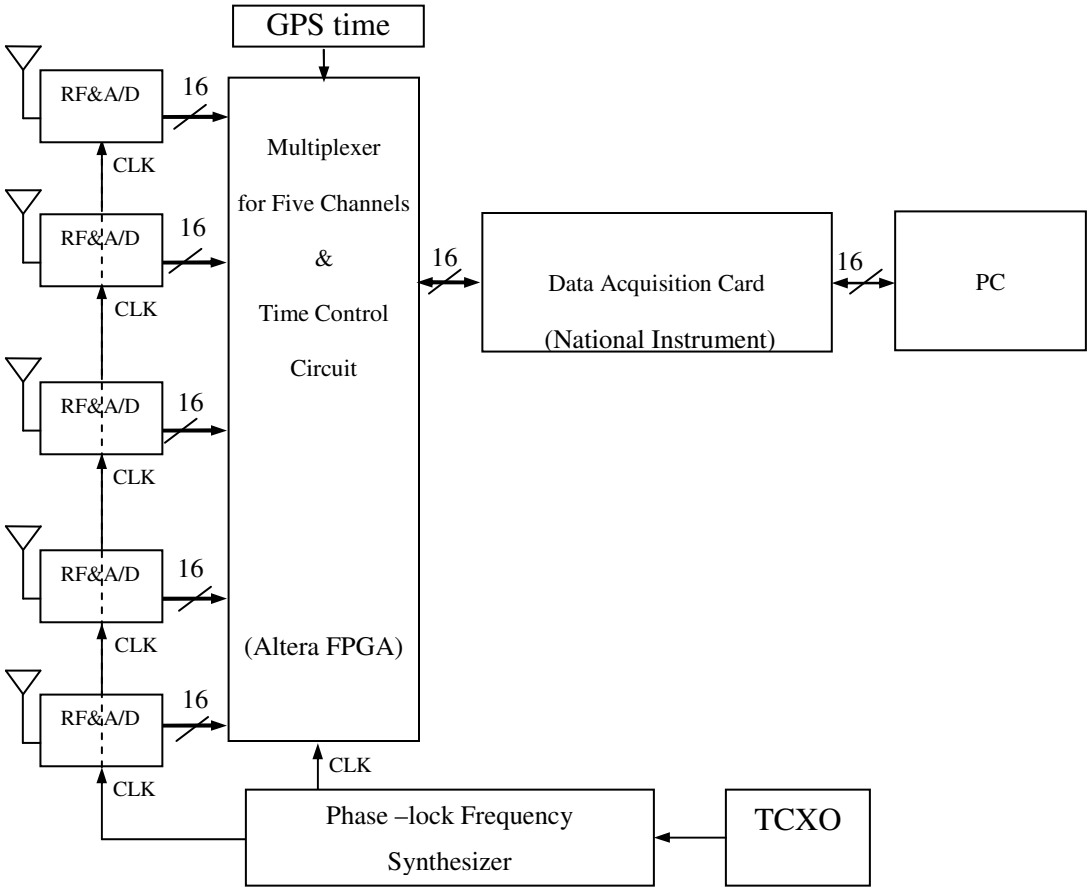

Figure 6.1: Hardware System Diagram

6.2.1 Directional and Omni-directional Antenna Array Design and Development

A uniform linear antenna array with five elements is connected to the five-channel input of RF circuits. The antenna element spacing is 0.7λ. The RF frequency is 1.9475 GHz.

The antenna array is put on a turntable to adjust the array's direction for receiving base station signals from different angles as shown in Figure 6.2 (a), installed on the roof of the CCIT building on the University of Calgary campus. Figure 6.2 (b) is the directional antenna's pattern, which has a high antenna gain in a range of about 120° in azimuth and 20° in elevation. This is suitable for receiving the CDMA base station signals, which are usually from low elevation. Because the directional antenna limits the number of multipath and the number of available base station signals, it is helpful to identify the signals at the initial research experiment stage. However in order to verify the proposed algorithm for multipath mitigation, in the later experiment, the omni-directional antenna is used to receive more multipath and the antenna spacing changes to 0.5λ for another test as shown in Figure 6.2 (c). The omni-directional antenna pattern is in Figure 6.2 (d), which has full gain in azimuth and a range of about 30° in elevation.

(a) Linear Uniform Array with Directional Antenna

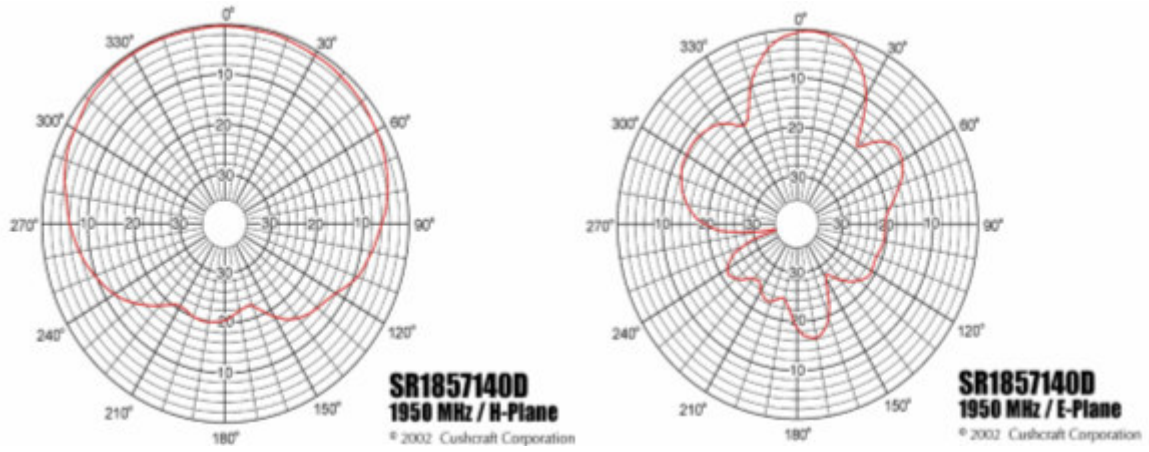

(b)) Single Directional Antenna Patterns (E & H Plane)

(c) Linear Uniform Array with Omni-directional Antenna

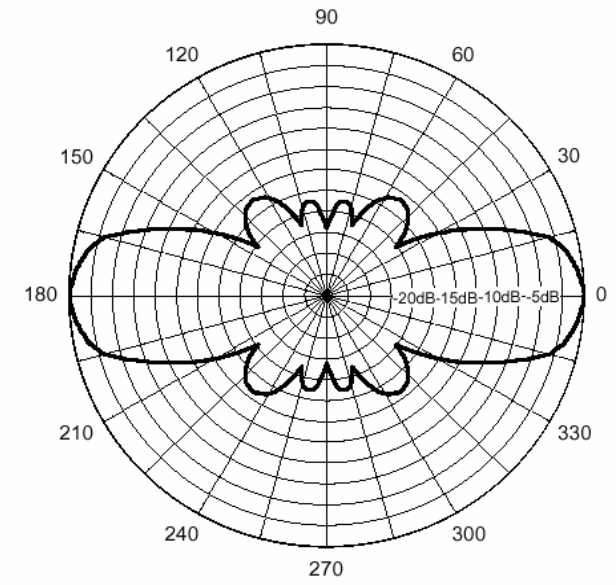

(d) Single Omni-directional Antenna Pattern (E-Plane) from Specification Sheet

Figure 6.2: (a) Linear Uniform Array with Directional Antenna; (b) Directional Antenna Patterns (E & H Plane); (c) Linear Uniform Array with Omni-directional Antenna (d) Omni-directional Antenna Pattern (E-Plane)

6.2.2 RF & Baseband Circuit Design and Development

Figure 6.3 is the RF superheterodyne receiver block diagram. It contains the functions of amplification, filtering, mixing and demodulation. The RF LO converts the incoming signal first to IF at a relatively high frequency, and then the IF LO converts the IF signal into baseband. The demodulated I & Q signals are fed to the following baseband circuit as shown in Figure 6.4. The stability of the sampling frequency for ADC is affected by the stability of TCXO, which is described by its Allan variance in Appendix D. The unstable sampling frequency will affect the acquisition process for the CDMA signal despreading processing. The identity of the sampling frequency of 10 MHz for each channel ADC will not introduce an extra phase difference between antenna elements. The AGC control signal is generated separately for each channel to adjust the signal amplitude of each channel efficiently.

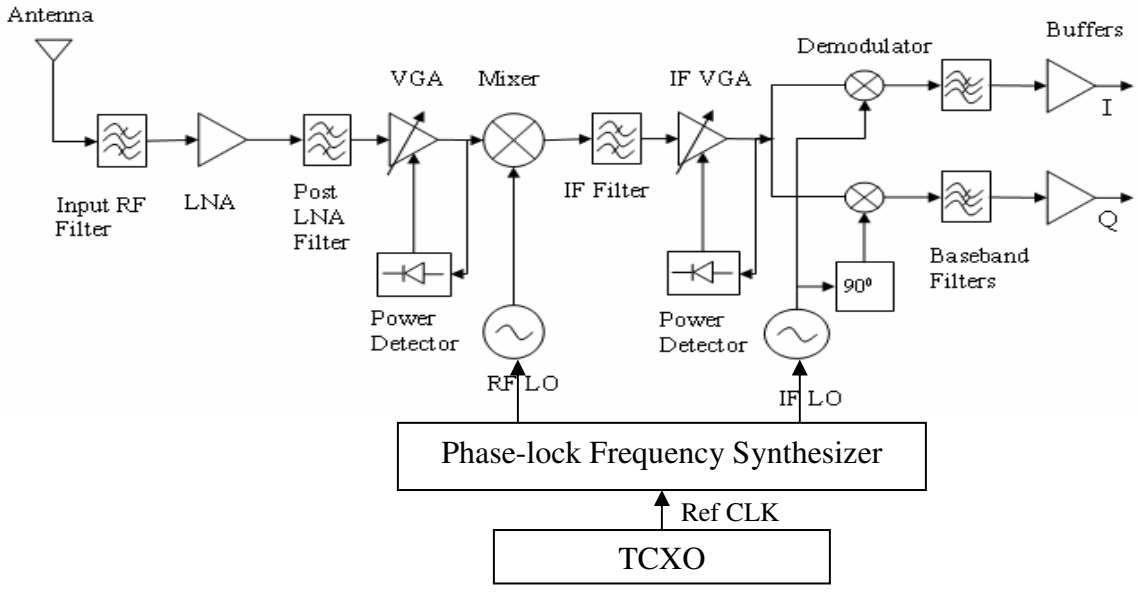

Figure 6.3: RF Circuit Diagram for One Channel

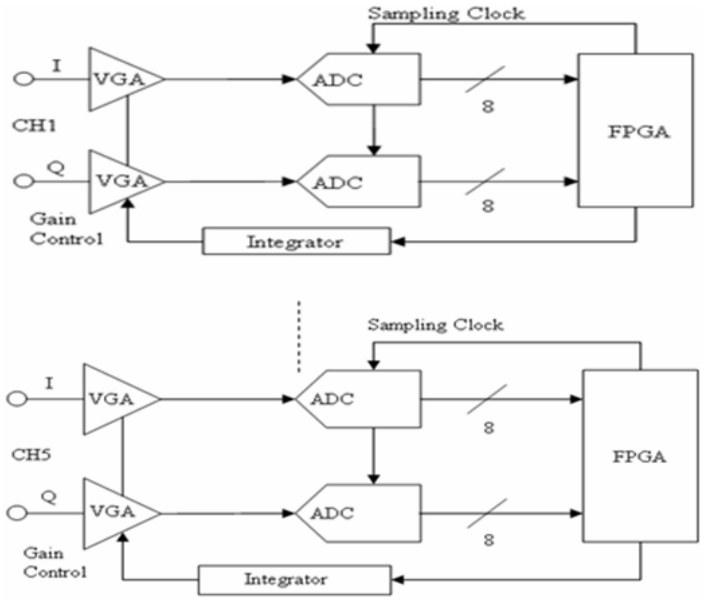

(a) Baseband Circuit Diagram for Five Channels

(b) **Baseband with Five Channels & Altera FPGA (1st Generation Receiver)**

Figure 6.4: (a) Baseband Circuit Diagram for Five Channels; (b) Baseband with Five Channels & Altera FPGA (1st Generation Receiver)

6.2.3 FPGA-based Digital Circuit Design and Development

In order to collect the data stream from the five RF channels to the computer correctly, a strict time control circuit is required. The Altera FPGA shown in Figure 6.4 multiplexes five-channel data into a PC via a National Instrument Data Acquisition Card. The data is triggered by a 1pps (1 pulse per second) GPS signal to synchronize the local receiver time to GPS time. The diagram is shown in Figure 6.5. $I(t)$ and $Q(t)$ are the input five-channel data from the ADC outputs. Each ADC output is 8-bit, so for five channels I(t) and Q(t), the total number of data bits is 80-bit while the NI DAQ (Data Acquisition Card) data width is 16-bit. Thus it requires that the data transfer frequency for DAQ be five times of the parallel five channels data samples. The sampling frequency for ADC is 10 MHz and then the data is decimated to reduce the data rate to 2 MHz. The data transfer frequency for DAQ (REQ Φ_2) is therefore 10 MHz. The 1pps GPS signal is fed in as a trigger signal (Trig) for DAQ to make the collected data synchronized to GPS time. There is a fixed data delay of 200 ns after the 1pps appears. The uncertainty of the 1pps appearance at the rising edge of the 10 MHz clock signal Φ_1 is 100 ns. The possible maximum data delay with respect to the GPS time is therefore 300 ns. The data stored in the PC is in a 16-bit format with the most significant 8-bit for the I channel and the least significant 8-bit for the Q channel and the data obtained from the ADC output is a sign data. The data to be transferred to the DAQ is also fed into the VGA control signal generator, whose outputs are sent to the VGA device located on the digital board.

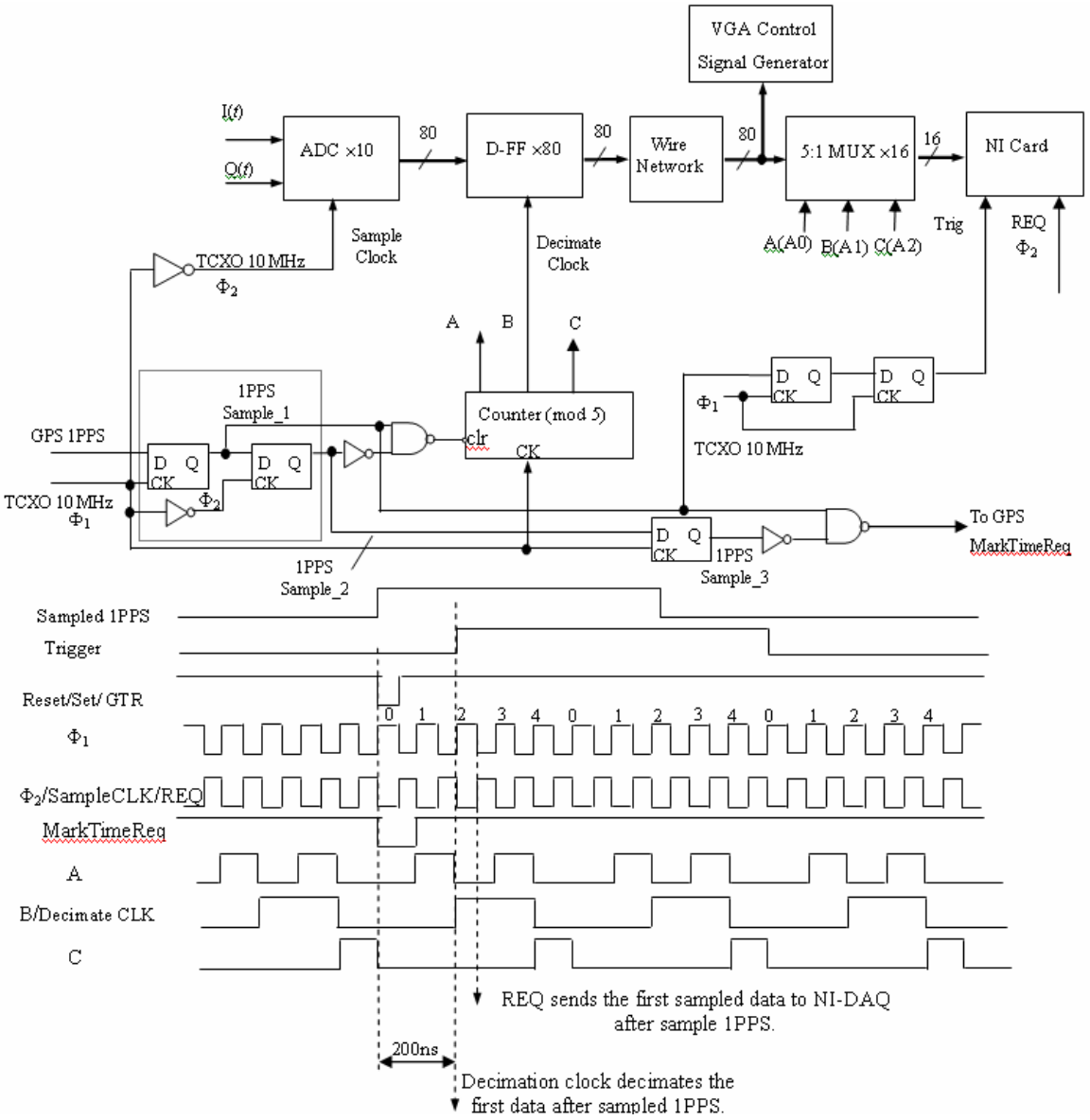

Figure 6.5: FPGA Design for Five-Channel Data Collection

6.2.4 Control Software Development

In order to implement the GPS synchronized data transfer from the FPGA to PC via DAQ, the related control software is developed in the C language. Because the IS-95 pilot signal is transmitted at GPS even seconds, it needs the receiver to collect the data in GPS even seconds. Once the 1pps signal from the NovAtel OEM4 GPS receiver is decoded as an even second, the generated trigger signal in FPGA is used to activate the DAQ to receive the data at each rising edge of the FPGA generated REQ signal as shown in Figure 6.5.

6.2.5 The Second Generation of CDMA Receiver

The first generation receiver is suitable for data collection when the Doppler frequency does not change significantly during the long integration time. However, it is not applicable when the Doppler frequency changes significantly during the integration time, such as in the case of dynamic movement of the receiver or the use of the crystal oscillator with low stability. So in the second generation CDMA receiver, the frequency de-rotation circuit was added in the Xilinx FPGA as shown in Figure 6.6 to detect the Doppler frequency and remove it before the data is transferred to the computer. The design of the second generation receiver is given in Appendix E.

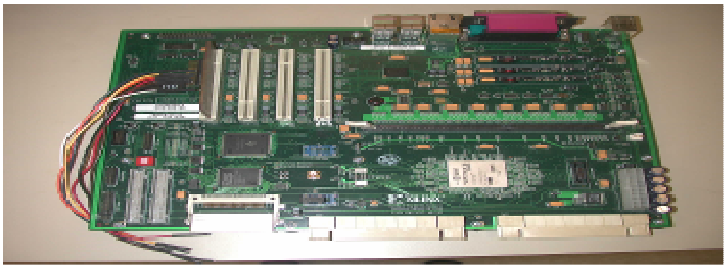

Figure 6.6: Xilinx FPGA Board for the 2nd Generation Receiver

6.3 Experiment and Performance Analysis

In this section, the field experiment is described. A group of data is measured by the CDMA prototype receiver when the SmartMotor™ controls the turntable with steps of 2.5º. The receiver is treated as a user. The measured data from the nearby CDMA base stations is used to estimate the AOA and TOA of the user based on the approach proposed in this thesis.

6.3.1 Experiment Setup

The diagram of the data collection system and the real field measurement system are shown in Figure 6.7 (a) and (b) respectively. For calibration purpose, the first spot to collect should be a LOS signal environment, such as a building roof or an open area. The antenna array should be set perpendicular to the signal from a nearby base station. The turntable in Figure 6.7 (a) is to collect the data at different antenna angles in order to verify the AOA algorithm. After this process, the data can be collected in various locations without the turntable.

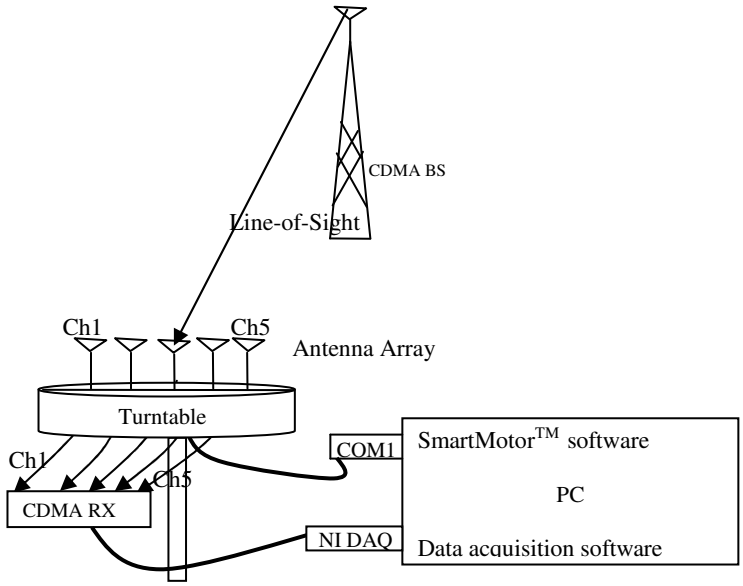

(a) Diagram of Data Measurement

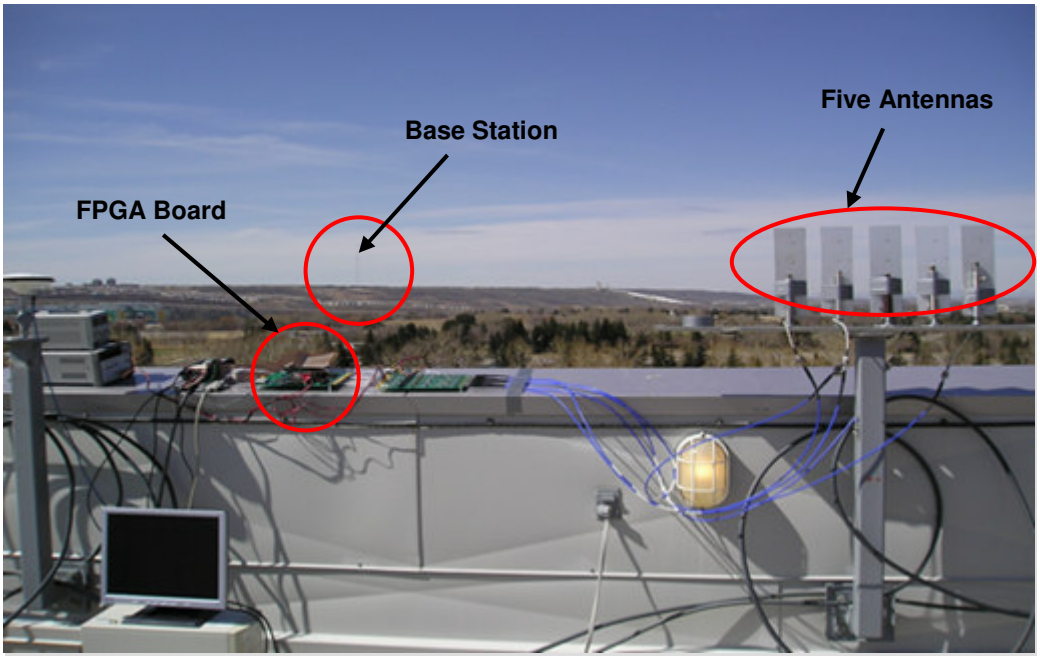

(b) Field Measurement on the Roof of CCIT Building, University of Calgary

Figure 6.7: (a) Diagram of Data Measurement; (b) Field Measurement on the Roof of CCIT Building, University of Calgary

Here are the data processing steps:

Step 1: adjust the antenna array orthogonal to the incident ray from the base station nearby through geomatic measurement to get channel phase calibration data.

Step 2: Apply the calibration data to the data measured under different incident angles to compensate for the channel phase error in order to apply the MUSIC algorithm

Step 3: Use MUSIC to estimate AOAs for different raw data sets. The results are shown later in this chapter.

Channel Phase Calibration

The channel phase calibration is important because the F/B Smoothing MUSIC algorithm is based on all the antenna elements and their corresponding channels having the same channel properties. For example each channel phase characteristics is supposed to be the same. However it is impossible to manufacture the hardware of each channel to have the same channel phase. So channel calibration is necessary before using MUSIC. Without phase calibration, the AOA estimation using the Forward/backward Smoothing MUSIC algorithm would result in a large error. The channel phase calibration is carried out by putting the antenna array perpendicular to the signal ray coming from the nearby visible CDMA BS which, in this case, is located on the West Campus of the University of Calgary, as shown in Figure 6.7 and on the diagram shown in Figure 6.8 (a). In this case the phase of each channel reflects hardware phase shift and the phase shift of an array element with respect to the reference element (first element) will not be counted. Suppose that one snapshot data is collected and the autocorrelation functions of five channels are $R_1(t), R_2(t), R_3(t), R_4(t), R_5(t)$, respectively, as shown in Figure 6.8 (b). Then five

samples from five correlation functions respectively are obtained, namely $R_1(\tau_1), R_2(\tau_1), R_3(\tau_1), R_4(\tau_1), R_5(\tau_1)$, to calculate the phase of each channel as $\varphi_i = atan\dfrac{\mathrm{Im}(R_i(\tau_1))}{\mathrm{Re}(R_i(\tau_1))}$ $i = 1, 2, ..., 5$ *represents the* i^{th} *antenna element*. In order to get a better average channel phase, *N* samples are used. Then the phase angle becomes

$\varphi_i = \dfrac{1}{N}\sum_{k=1}^{N} atan\dfrac{\mathrm{Im}(R_i(\tau_k))}{\mathrm{Re}(R_i(\tau_k))}$ $i = 1, 2, ..., 5$ *represents the* i^{th} *antenna element*, where τ_k is selected from the correlation function initial rising linear part in which multipath has been supposed to be suppressed.

These phase corrections are multiplied by the corresponding five autocorrelation functions for phase compensation, resulting in $R_1(t)e^{-j\varphi_1}, R_2(t)e^{-j\varphi_2}, R_3(t)e^{-j\varphi_3}, R_4(t)e^{-j\varphi_4}, R_5(t)e^{-j\varphi_5}$. The phase-compensated auto-correlation functions are then sampled at the initial rising part to construct a data matrix processed by MUSIC for further AOA estimation, which is expressed by equation (4.4).

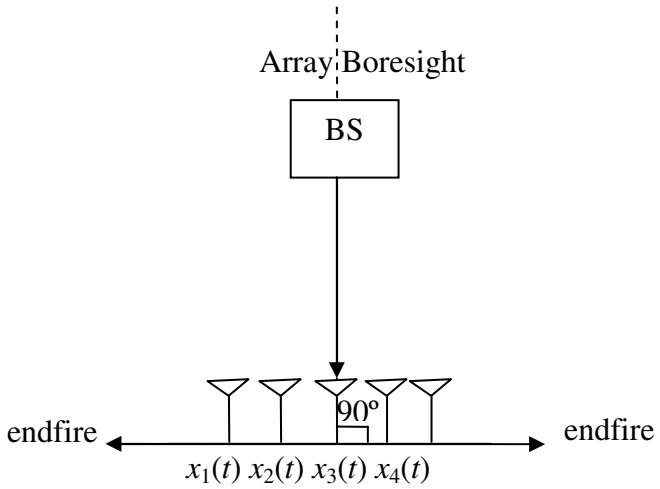

(a) Channel Phase Calibration Diagram

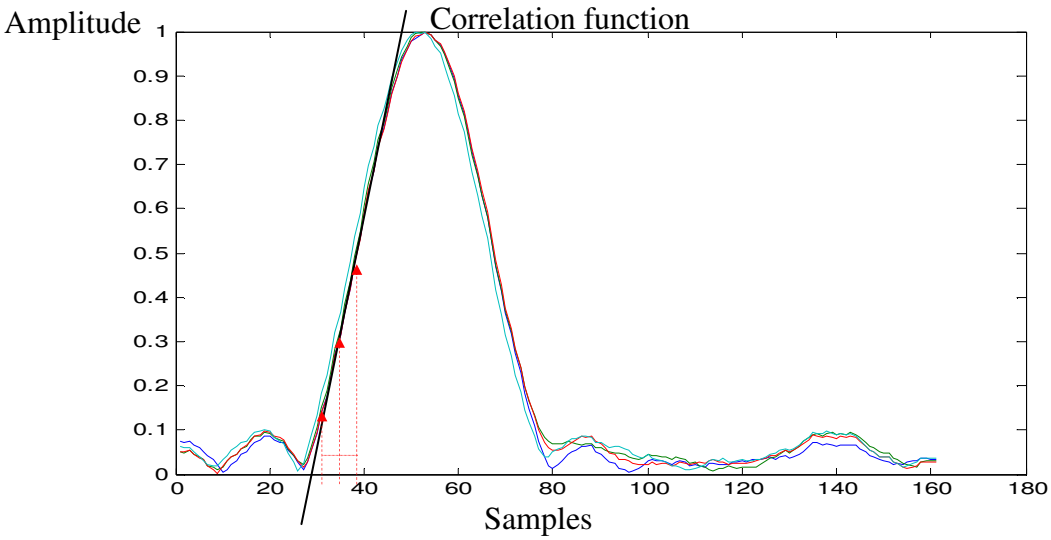

(b) Autocorrelation Function of LOS Signal from Soccer Field at the Univ. of Calgary

Figure 6.8: (a) Channel Phase Calibration Diagram; (b) Autocorrelation Function of LOS Signal from Soccer Field at the Univ. of Calgary

6.3.2 Multipath Effect on the Measured Data

Figure 6.9 (a) shows the correlation functions of several base stations for one antenna

element (one channel) after the coarse acquisition process. The integration time is 3 PN epochs (80 ms), and the peak pattern therefore repeats three times. Figure 6.9 (b) shows the detail shapes of the correlation functions of the five channels from the strongest correlation peak, BS1. The strongest peak is from the nearest base station. The resolution for the correlation function is determined by the correlation process in the time domain, which is chosen to be (1/20) chip, equal to 40 ns because one chip is 800 ns. The resolution level affects the processing time required. The higher resolution, the more time required. It can be seen that from Figure 6.9 (b) due to the multipath, the width of the correlation peak has been enlarged to around 2000 ns, whereas the theoretical width should be 2 chips (1600 ns). This results in a shift of the correlation peak. So the correlation peak based TOA method will fail in multipath situations. However the correlation function's rising part has not been distorted significantly, because the multipath always arrives after the LOS. So the data to be processed by the F/B Smoothing MUSIC for AOA estimation is sampled on the correlation function initial part, which reduces the impact of multipath. Figure 6.9 (c) shows the correlation functions of five channels from another base station, namely BS2, which have smaller correlation peaks. It can be seen that the bottom width of the correlation functions have also increased and the correlation peaks have been destroyed significantly while the initial part still has a good linearity. Due to low signal to noise ratio, the five correlation functions from different channels do not align closely.

The above multipath effect from actual data matches the theoretical analysis based on the simulated results shown in Section 5.2. An AOA-assisted TOA/TDOA method to

mitigate multipath has been proposed and described in Section 5.4.

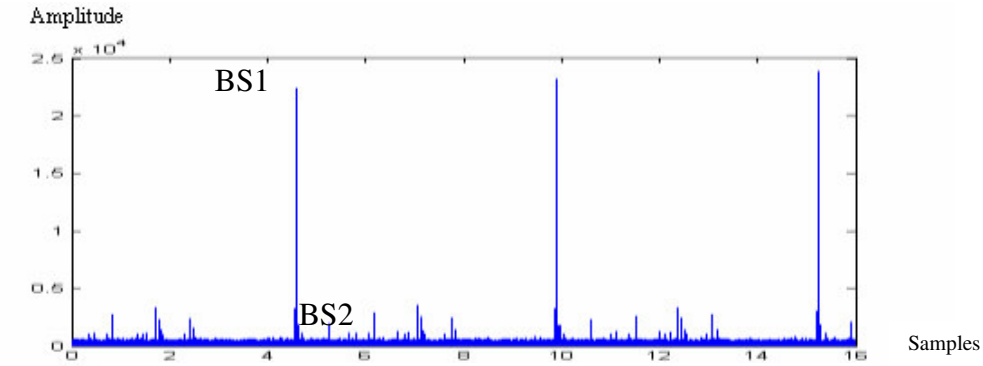

(a) Correlation Functions Obtained in One Channel

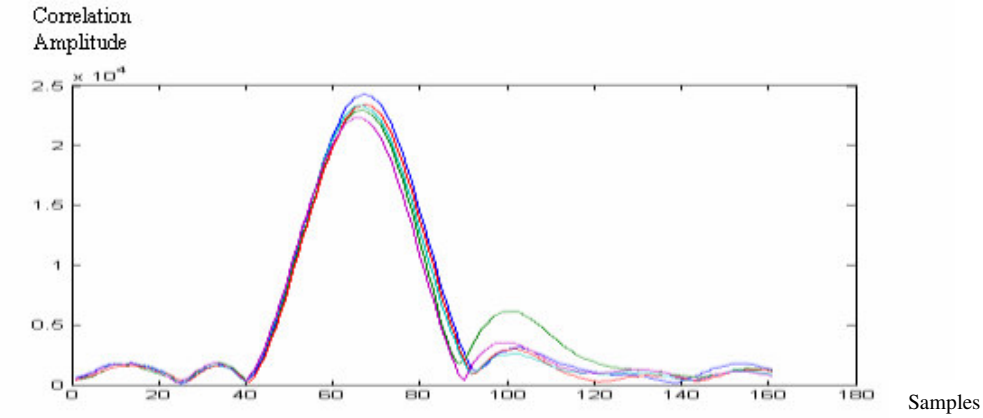

(b) Superimposed Correlation Functions of Five Channels from a Strong Signal

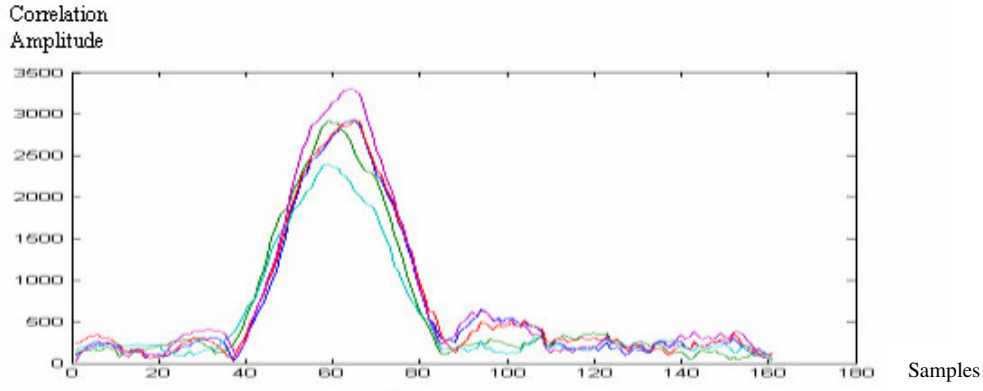

(c) Superimposed Correlation Functions of Five Channels from a Weak Signal

Figure 6.9: (a) Correlation Functions Obtained in One Channel; (b) Superimposed Correlation Functions of Five Channels from a Strong Signal; (c) Superimposed Correlation Functions of Five Channels from a Weak Signal

6.3.3 AOA Estimation Results and Error Analysis

Figure 6.10 (a) is the AOA estimation based on equation (4.18) for the strongest signal (from BS1) in Figure 6.9 (a) without phase calibration. It is supposed to be at 115º. But now it is estimated at 87º and the error is therefore 28º. Figure 6.10 (b) is for the same incident ray, but with phase calibration. The estimated AOA is 114º which is a remarkable improvement. The small peak in Figure 6.10 (b) is due to 0.7 λ antenna spacing. If the antenna spacing is 0.5 λ, there will be no ambiguity. Large antenna spacing has weak coupling interference from adjacent antenna, but introduces ambiguity, which can be seen from direction vector $a(\beta_k) = e^{-j2\pi \frac{d}{\lambda} \cos\beta_k}$. If $d = 0.5\lambda$, then $a(\beta_k) = e^{-j\pi \cos\beta_k}$ which has no ambiguity; If $d = \lambda$, then $a(\beta_k) = e^{-j2\pi \cos\beta_k}$ which has ambiguity.

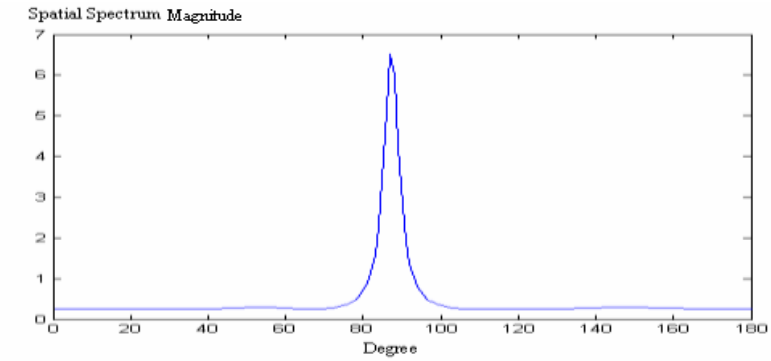

(a) AOA Estimation Spectrum without Phase Compensation

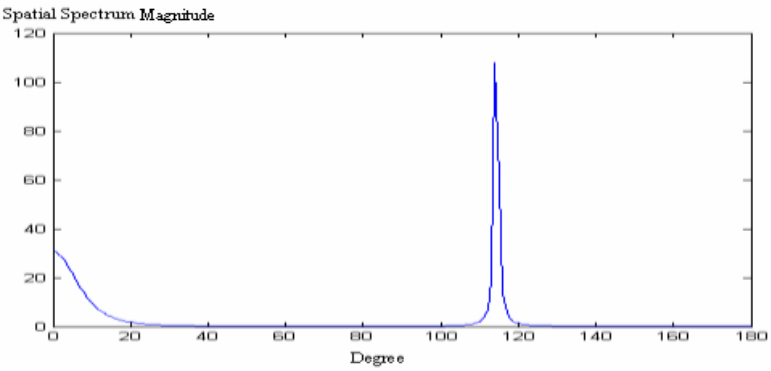

(b) AOA Estimation Spectrum with Phase Compensation

Figure 6.10: (a) AOA Estimation Spectrum without Phase Compensation

(b) AOA Estimation Spectrum with Phase Compensation

In order to get the directional antenna-based AOA estimations from 0º to 180º, a step motor provided by Servo Systems is applied to adjust the angle of the antenna array. Figure 6.11 shows the estimated AOAs from 0 to 180 degree. Figure 6.12 shows the error curve. It can be seen that when the incident ray is between 45º and 170º, the error ranges from +2º to -3º. Beyond that, the error increases to 20º. This is due to the insensitivity of the antenna array at the endfires, as explained in Section 3.5.

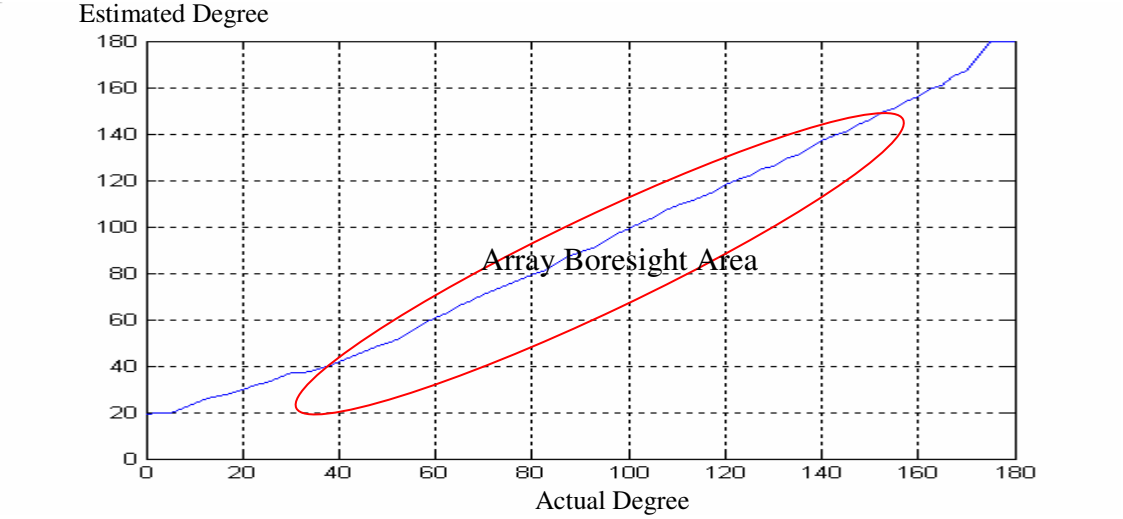

Figure 6.11: AOA Estimation Using F/B Smoothing MUSIC

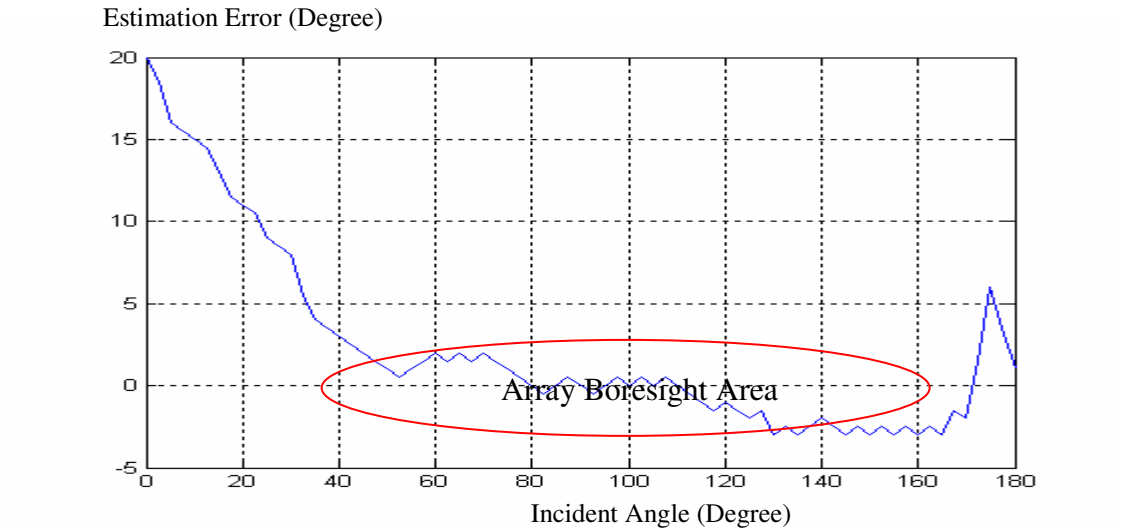

Figure 6.12: AOA Estimation Error Using F/B Smoothing MUSIC

6.3.4 Multipath Mitigation through the AOA Compensation

As a result of multipath, the shape of each autocorrelation function from four omni-directional antennas is different as shown in Figure 6.13 (a), for data collected on the roof of the CCIT building. After beamforming using the estimated LOS AOA, which is

denoted by β_{LOS}, the summation of the four correlation function, $R_{\sum}(\tau) = \sum_{i=1}^{4} e^{-j(i-1)\frac{2\pi f_0 d * \cos(\beta_{LOS})}{c}} R_i(\tau)$, is plotted in Figure 6.13 (b). It shows that multipath has been suppressed significantly. It also shows that the amplitude is increased, which is helpful for determining the slope of the correlation function rising part. So the benefit of using estimated AOA is to filter out some multipath and enhance the SNR of the correlation function.

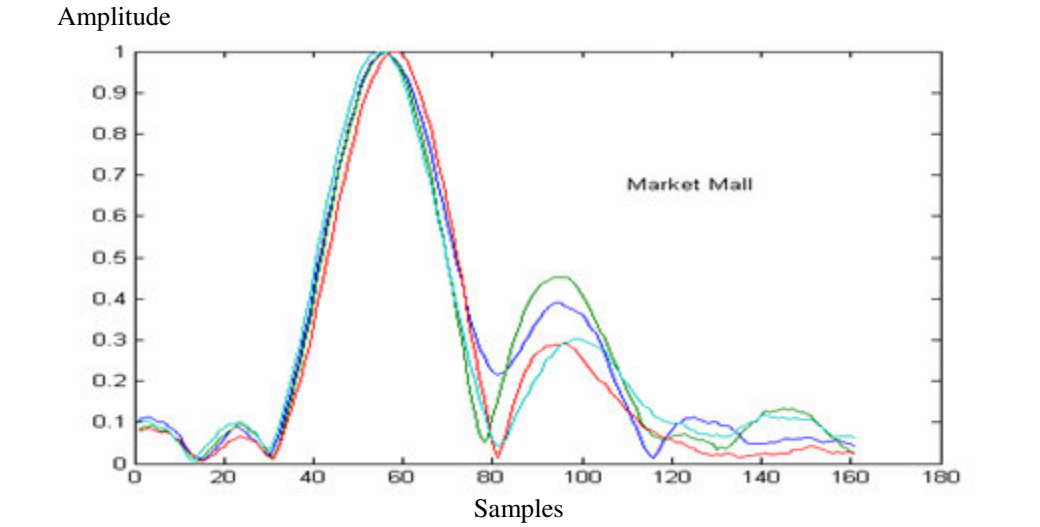

(a) IS-95 Signal Autocorrelation in Each Antenna Element

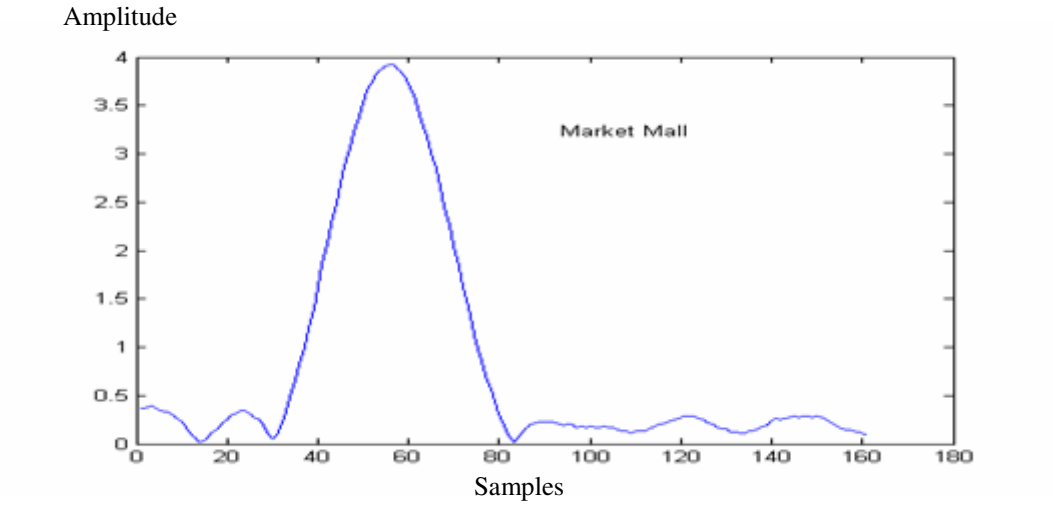

(b) Summation of Four Autocorrelations after Beamforming

Figure 6.13: (a) IS-95 Signal Autocorrelation in Each Antenna Element (b) Summation of Four Autocorrelation after Beamforming

6.3.5 AOA-Assisted TOA Results and Error Analysis

(*The antenna used is a BNF1905S (1850 – 1990 MHz) omni-directional antenna*)

The experiment data is obtained from the four locations shown in Figure 6.14, which is on the campus of the University of Calgary. The results are described in the four scenarios below. The proposed correlation slope-based method is compared with the correlation peak-based method, which is also based on multiple channels. The comparison with the one-channel correlation peak-based method is also given for Scenario 2.

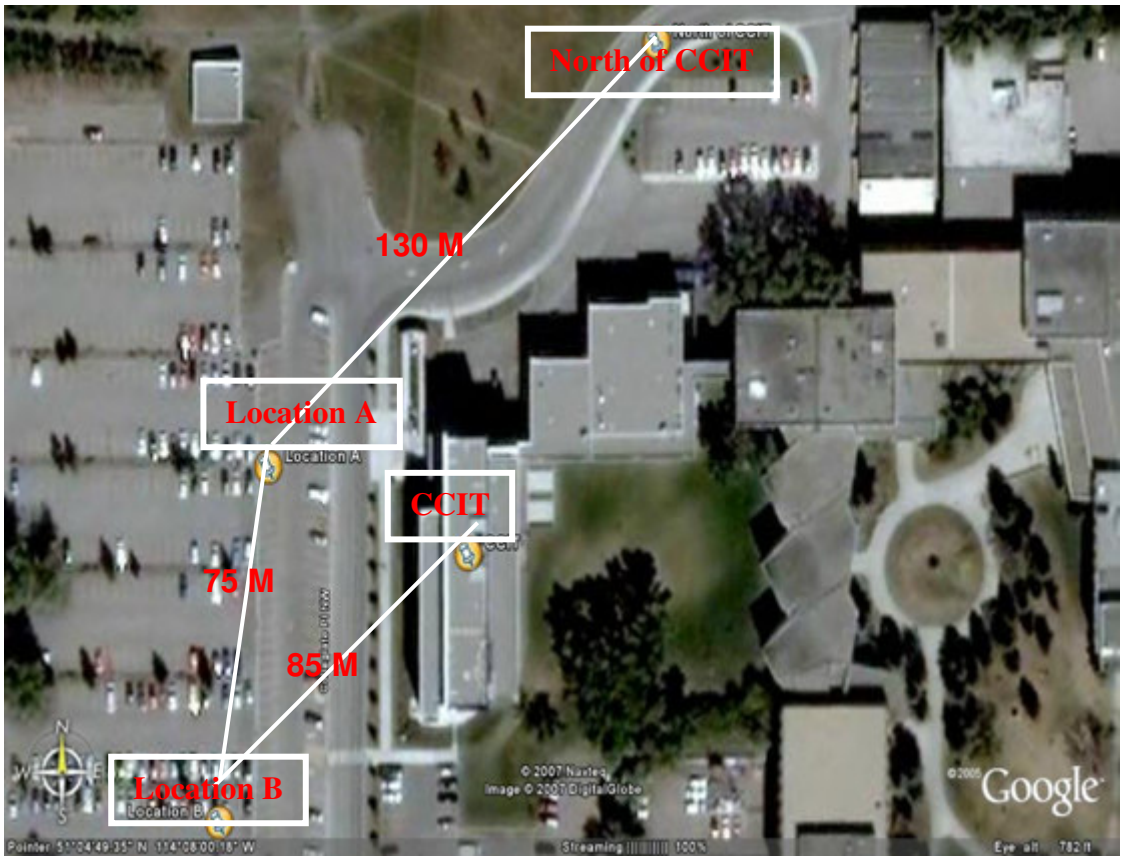

Figure 6.14: Measurement Locations of AOA-Assisted TOA Test

Scenario 1. Data collected in LOS under low multipath effect environment

Roof of CCIT building, University of Calgary

In this environment, multipath is reflected from surrounding high buildings, as can be seen in Figure 6.15. The side lobe of the correlation function on the falling side is different from that on the rising side due to multipath. However the rising part still has a good linear shape, which is suitable for the use of the method proposed herein.

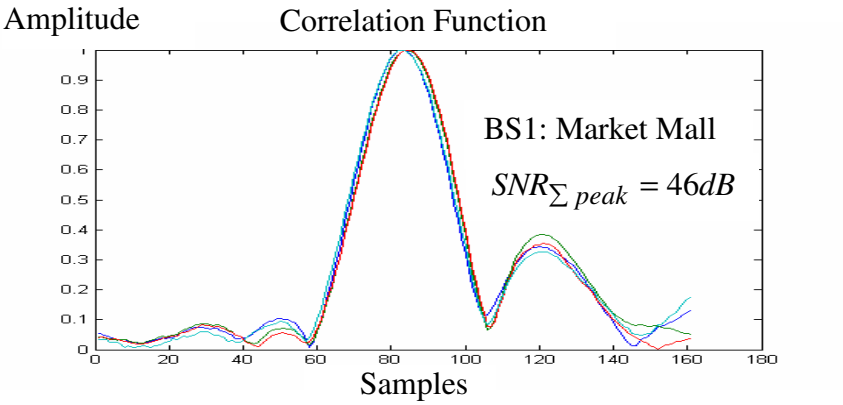

(a) Correlation Functions from Market Mall Base Station

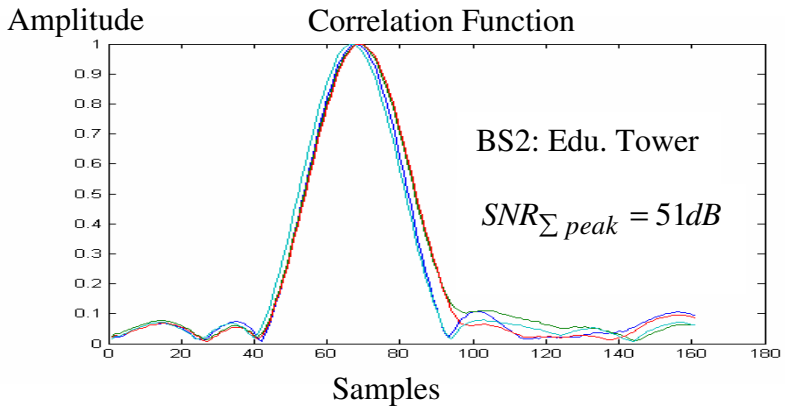

(b) Correlation Functions from Education Tower Base Station

Figure 6.15: Correlation Functions from Different Base Stations - Roof of CCIT Building

Based on the above correlation functions from two base stations, after calibration and beamforming for each of them, two correlation functions like those of Figure 6.13 (b) can be obtained. Then two data segment in the linear part are selected (the principle is described in Chapter 5) to estimate the slope and hence the starting point of each correlation function. Then the subtraction of these two starting points is the TDOA value which is provided in the second column of Table 6.1. This is the process of the proposed algorithm.

Another method called the correlation peak-based method is used for comparison. It is also based on antenna array process and AOAs are used to sum four correlation functions in the direction of LOS to locate the peak position of the summated correlation function instead of estimating the correlation function starting point proposed in this dissertation. The subtraction of the peak position is a TDOA value, which is provided in the first column of Table 6.1. The correlation peak-based method is also subject to calibration and beamforming, but no samples at the correlation rising part are needed and that is the difference from the method proposed herein.

It can be seen from table 6.1 that under a comparatively clean LOS environment, the results from the correlation peak-based and the proposed correlation slope-based methods are quite close. This verifies that the proposed method operates well under this condition. In order to compare performance, the surveyed value is provided. However the two methods have large biases of 217 m and 215 m respectively, with respect to the surveyed value. This may be due to synchronization errors among base stations in the CDMA

network (Iltis & Mailaender 1996). It can be seen from Table 6.9 that each base station is quite stable because this bias remains constant.

Table 6:1: TDOA Estimation Comparison - Roof of CCIT Building

Correlation Peak-based	Correlation Slope-based	Survey Reference
130.9 m	133.4 m	348.0 m

In order to calculate the variance based on the real data, eight mega samples are collected which is under 2.5 MHz sampling rate within 3.2 seconds. The variance is computed based on 40 groups of data and each group of data is 0.08 seconds which contain three epochs of IS-95 PN sequences. It can be seen from Table 6.2 that the actual TDOA standard deviation of the proposed method is close to the theoretical standard deviation discussed in Section 5.5. The practical standard deviation is a little bit larger than theoretical value because the accuracy of the estimated LOS AOA and the linearity of the correlation function initial rising part will affect the final TOA /TDOA estimation accuracy.

Table 6:2: Correlation Slope-based TDOA Standard Deviation - Roof of CCIT Building

Practical Standard Deviation (8 mega samples)	Theoretical Standard Deviation
3.4 m	1.3 m

Front of CCIT building (Location A)

In this environment, multipath is reflected from the wall of the building as shown in Figure 6.16. The multipath effect is low, which can be seen from the correlation function shown in Figure 6.17. In such an environment, the proposed method does not show a significant advantage over the correlation peak-based method because the peak is not significantly shifted. So the TDOA values are very close as shown in Table 6.3. The bias is still about 200 m but the standard deviation is still small as shown in Table 6.4.

Figure 6.16: Field Measurement - Front of CCIT Building (Location A)

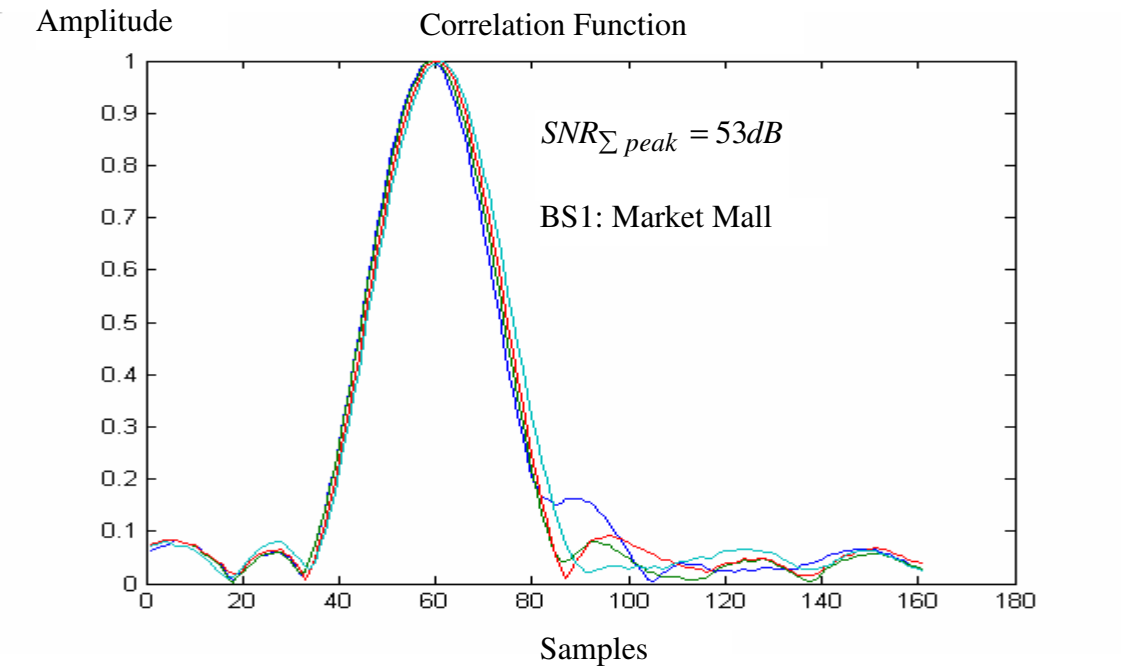

(a) Correlation Functions from Market Mall Base Station

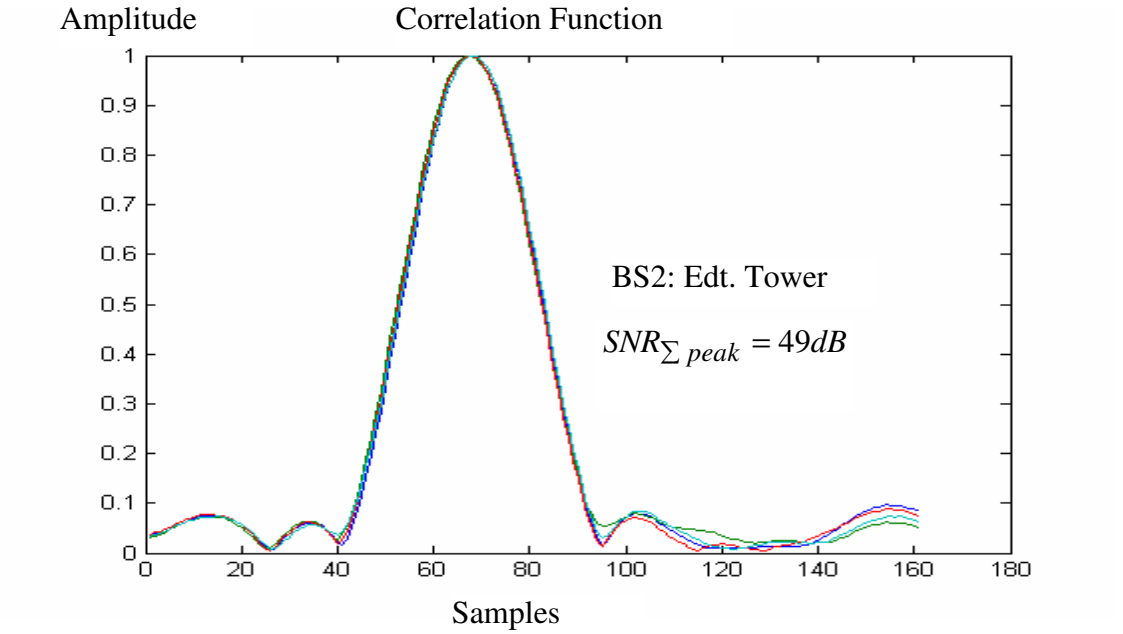

(b) Correlation Functions from Education Tower Base Station

Figure 6.17: Correlation Functions from Different Base Stations - Front of CCIT Building (Location A)

Table 6:3: TDOA Estimation Comparison - Location A

Correlation Peak-based	Correlation Slope-based	Survey Reference
56.7 m	66.3 m	281.9 m

Table 6:4: Correlation Slope-based TDOA Standard Deviation - Location A

Practical Standard Deviation (8 mega samples)	Theoretical Standard Deviation
1.3 m	0.9 m

Scenario 2. Data collected in LOS under high multipath effect environment

Front of CCIT building (Location B)

In this environment, multipath is reflected from the wall of several buildings as shown in Figure 6.18. The multipath effect is significant as shown in Figure 6.19(a), where the correlation peak has shifted significantly. In this case, the proposed method should have better performance than the correlation peak-based method, which can be seen from Table 6.12.

Figure 6.18: Field Measurement - Front of CCIT Building (Location B)

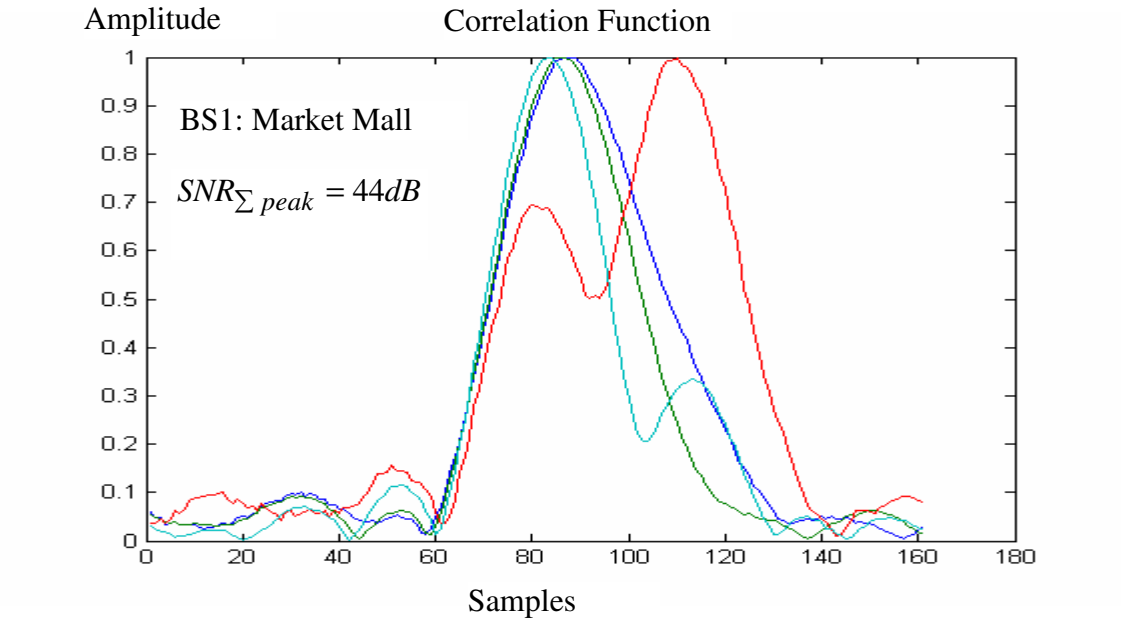

(a) Correlation Functions from Market Mall Base Station

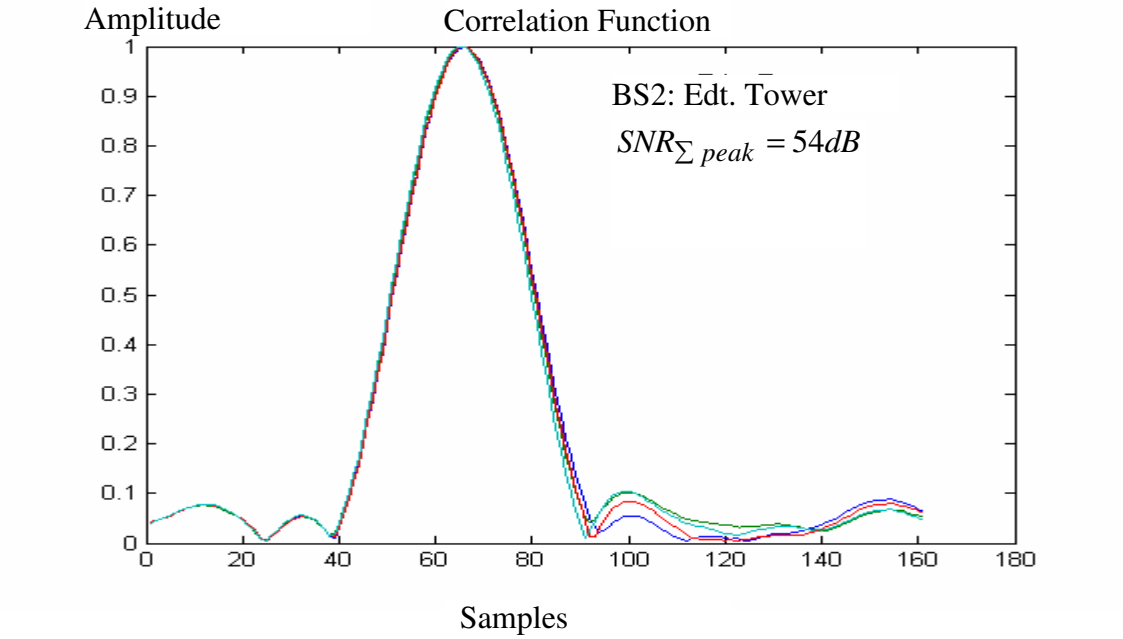

(b) Correlation Functions from Education Tower Base Station

Figure 6.19: Correlation Functions from Different Base Stations - Front of CCIT Building (Location B)

Table 6:5: TDOA Estimation Comparison - Location B

Correlation Peak-based	Correlation Slope-based	Survey Reference
25.6 m	41.6 m	266.9 m

Table 6:6: Correlation Slope-based TDOA Standard Deviation - Location B

Practical Standard Deviation (8 mega samples)	Theoretical Standard Deviation
3.9 m	1.5 m

Scenario 3. Data collected under LOS and weak signal environment

Roof of CCIT building

In this case, a comparatively weak signal from the Varsity Tower base station, which is far away, is measured. It can be seen that the proposed method still works well. It can also be seen that the CDMA IS-95 signals are quite strong even though the base station is far away.

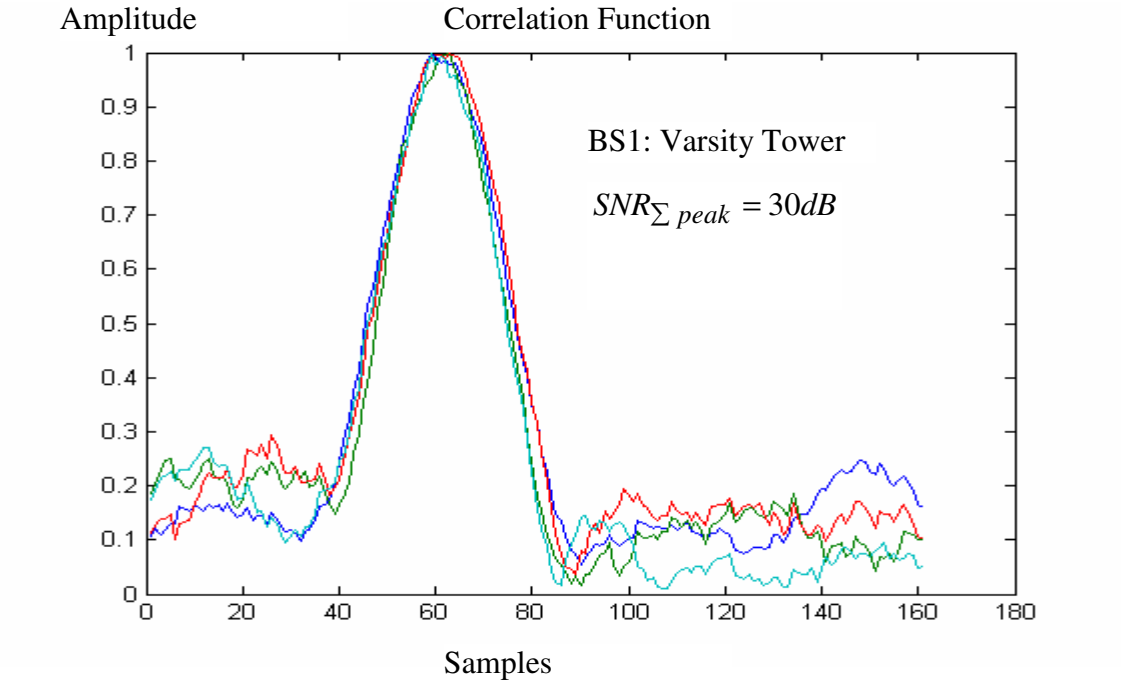

(a) Correlation Functions from Varsity Tower Base Station

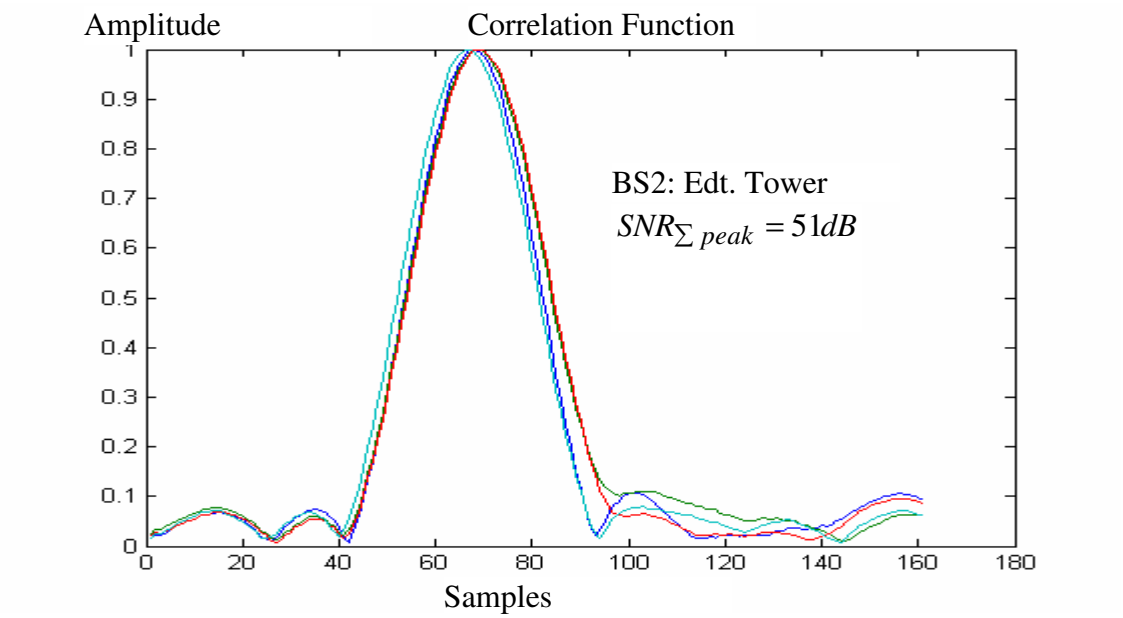

(b) Correlation Functions from Education Tower Base Station

Figure 6.20: Correlation Functions from Different Base Stations - Roof of CCIT Building

Table 6:7: TDOA Estimation Comparison - Roof of CCIT Building

Correlation Peak-based	Correlation Slope-based	Survey Reference
933.4 m	934.0 m	1151.0 m

Table 6:8: Correlation Slope-based TDOA Standard Deviation - Roof of CCIT Building

Practical Standard Deviation (8 mega samples)	Theoretical Standard Deviation
7.8 m	7.1 m

Scenario 4. Data collected under non-LOS multipath environment

North of CCIT Building

In the previous scenarios, LOS signals exist and multipath delay was more than 200 ns, so the correlation function rising part had not been distorted. The correlation functions, as shown in Figure 6.21, are separated because of random NLOS signal delays, incident angles and phase on each antenna array. In this case, the proposed method does not work properly because MUSIC works only when each incident signal on each antenna element has close amplitude characteristics. From Figure 6.21, it can be seen that the amplitude of each channel at the sampling point is quite different because of multipath effect on each channel. As an auxiliary method, the first correlation peak can be considered the peak for LOS signal because it can be treated as the peak of the earliest NLOS signal.

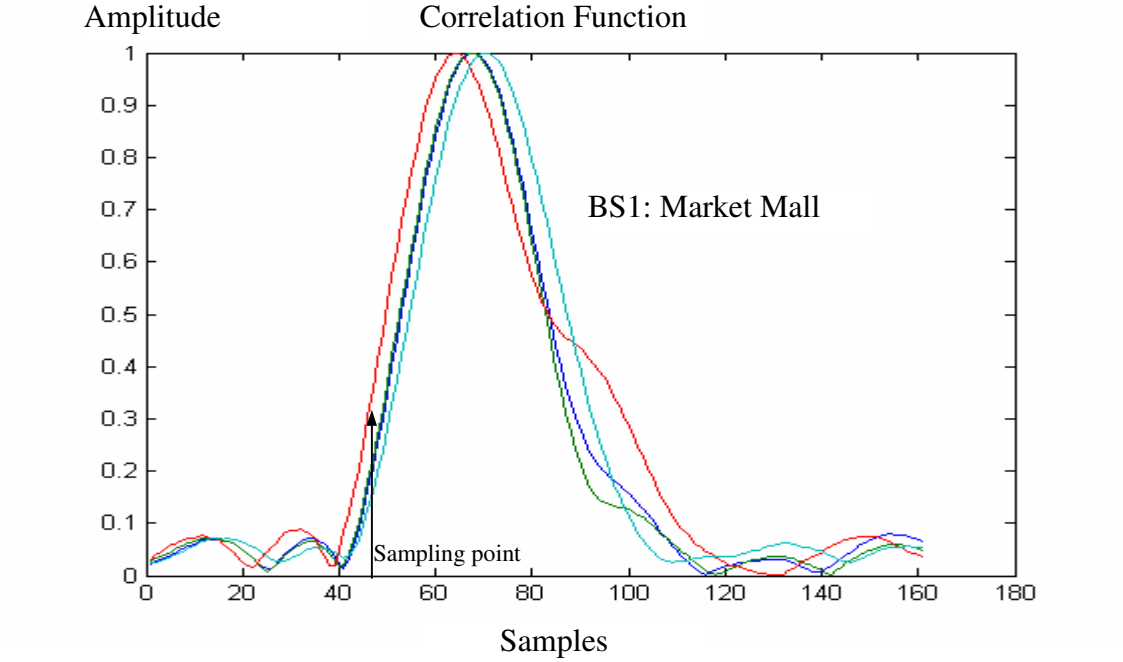

(a) Correlation Functions from Market Mall Base Station

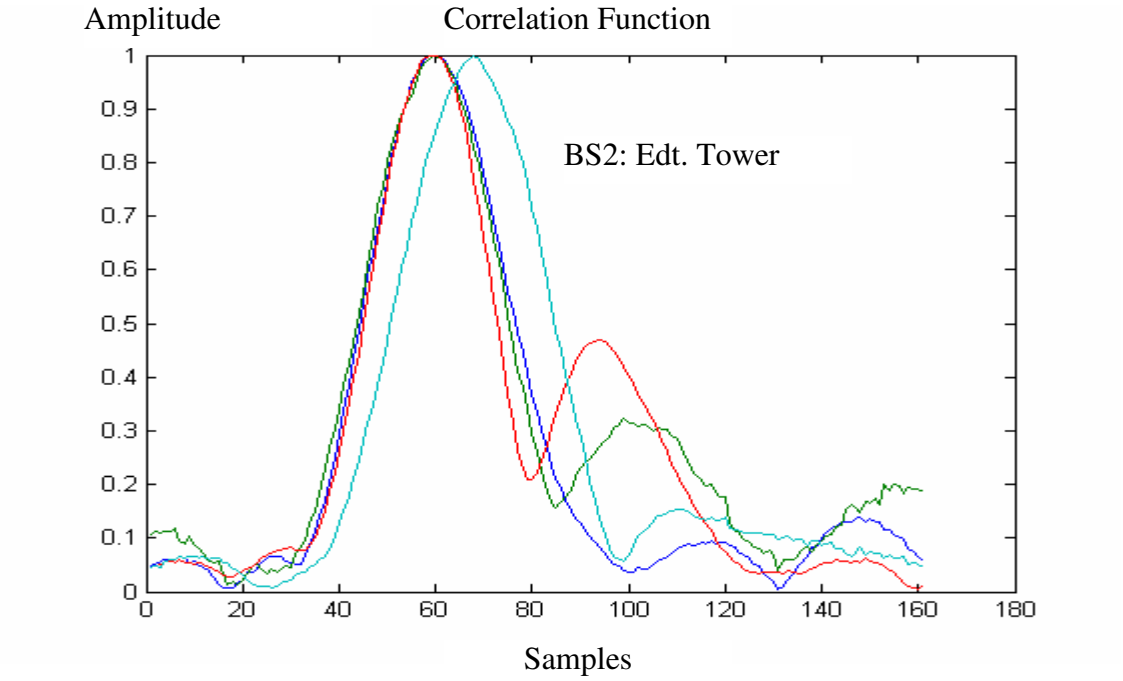

(b) Correlation Functions from Education Tower Base Station

Figure 6.21: Correlation Functions from Different Base Stations - North of CCIT Building

Stability Analysis

Scenario 1: One location at different time periods

The data use here is collected on the roof of CCIT building on May 7, 2007, at about every one hour interval. The system setup and the calibration of five antennas is the same as the previous description in Section 6.3.1. The results are shown in Table 6.9. It can be seen from the third column that the TDOA bias varies by about 6 m within the four hours, which is the stability of the system including the receiver and the transmitters at the base stations. The bias of about 220 m in the third column is due to unknown system offset. The survey values were provided by Tellus Mobility, Canada and some of them were re-measured by Geomatics Engineering department, University of Calgary.

Table 6:9: Stability Analysis of TDOA Bias for Scenario 1 (Roof of CCIT Building)

Time Slot	TDOA Measurement (m) (BSs: Market Mall & Edt. Tower)	TDOA Bias with Survey Reference (m)
12:31 pm	125.4	222.6
2:16 pm	125.4	222.6
3:26 pm	120.5	227.5
4:00 pm	126.4	221.6
4:47 pm	120.0	228.0

Scenario 2: Different locations measured on different days

This data is collected at different locations on the University of Calgary campus on different days. The results are shown in Table 6.10. The TDOA biases with respect to the survey reference at different locations, as shown in the second column, are at the same level of about 220 m, which means that the bias is about the same at the different locations; as shown in the third column, the measurements on the other day is similar, which is reassuring from a consistency point of view.

Table 6:10: Stability Analysis of TDOA Bias for Scenario 2 (Different Locations)

Locations	TDOA Bias with Survey Reference (m) Day 1	TDOA Bias with Survey Reference (m) Day 2
Roof of CCIT Building (BSs: Market Mall & Edt. Tower)	214.6	216.8
Roof of CCIT Building (BSs: Varsity & Edt. Tower)	217.0	215.4
Front of CCIT Building (Location A) (BSs: Market Mall & Edt. Tower)	215.6	214.7
Front of CCIT Building (Location B) (BSs: Market Mall & Edt. Tower)	225.3	221.9

Error Analysis

One reason for the above constant bias of about 220 m in the TDOA measurements may be due to the CDMA network time synchronization accuracy of 1 μs (Iltis & Mailaender

1996). As discussed in Section 2.2.2, the TDOA technique does not require synchronization of the mobile user to the network because the timing error cancels out. So the error from the non perfect GPS synchronized data in the receiver board will not contribute to the TDOA error. However the TDOA technique requires that the network should be precisely synchronized for high location performance. This constant bias can be compensated at the CDMA base stations. The measured TDOA standard deviation under different environments discussed previously may be due to uncontrollable systematic errors, e.g. receiver transfer function uncertainty, timing offsets in ADC sampling and base station timing uncertainty, etc.

Comparison with Single Antenna-based Correlation Peak Method

In Table 6.1, 6.3, 6.5 and 6.7, the correlation peak-based method uses the antenna array to estimate the correlation peak, which requires calibration and beamforming process and then locates the correlation peak position. Here the comparison with the single antenna-based correlation peak method, which is the conventional correlation peak-based method without calibration and beamforming process, is given. Table 6.11 shows the result obtained from a low multipath environment from ***Scenario 1***, which is on the roof of CCIT building. It can be seen that, in this environment, the single antenna-based correlation function peak method produces stable results from one antenna to another, which means that each channel is working properly and the correlation slope-based method also has similar TDOA value. In this case, the proposed method does not show a significant advantage over the correlation peak method.

Table 6:11: TDOA Estimation - Roof of CCIT building (Scenario 1)

Method	Correlation Peak-based Method (BSs: Market Mall & Edt. Tower)				Correlation Slope-based Method (BSs: Market Mall & Edt. Tower)
	Ch1	Ch2	Ch3	Ch4	using antenna array
TDOA (m)	109.2	102.5	112.9	117.8	119.9

Table 6.12 shows the results from an environment with strong multipath (***Scenario 2***), which is in front of CCIT building. It can be seen that the single antenna-based correlation function peak method produces unstable results from one antenna to another, whereas the correlation slope-based method overcomes this effect through array processing using estimated LOS AOAs. In this case, the proposed method shows a more dependable result.

Table 6:12: TDOA Estimation - Front of CCIT building (Location B)

Method	Correlation Peak-based Method (BSs: Market Mall & Edt. Tower)				Correlation Slope-based Method (BSs: Market Mall & Edt. Tower)
	Ch1	Ch2	Ch3	Ch4	using antenna array
TDOA (m)	106.8	51.8	340.5	22.5	41.6

6.4 Conclusions

A CDMA receiver with multiple channels is described, including the RF front end and the digital circuit. The multiplexer is implemented by an Altera FPGA to transfer the five channels data to a PC via a NI DAQ. The related control software is developed using the C language. The experiment is based on measured data from actual CDMA base stations at different time periods and locations on the campus of the University of Calgary. The data is processed with the proposed AOA-assisted TOA / TDOA algorithm. The results show that the proposed method is working in both LOS and multipath environments. In LOS environments, the proposed method produces similar TDOA results to those obtained from using the correlation peak method. However, in multipath environments the correlation slope-based method shows a more dependable result than that of the correlation peak-based method (Table 6.12).

Chapter Seven: Conclusions and Recommendations for Future Work

7.1 Research Summary

In a positioning system, the AOA and TOA parameters are the major values for position estimation. The accuracy of AOA / TOA estimates and the GDOP affect the location accuracy significantly. When the signal is strong and multipath is weak, the AOA / TOA can be estimated correctly through various methods as discussed in Chapter 2. However under multipath environments, the accurate estimations of AOA and TOA become difficult because the correlation function of the line-of-sight signals is corrupted by multipath.

In this research, a new approach for TOA estimation under multipath environment through the use of AOA information was proposed. It is suitable for user-based wireless location systems. The test measurement data is from CDMA IS-95 downlink pilot signals.

Conventional TOA estimators based on correlation function peak for CDMA signals can mitigate multipath with over one chip delay. However the inter-chip multipath cannot be resolved efficiently, which results in the shift of the peak especially when the multipath signal is strong. As a consequence, the estimation of TOAs based on the correlation function peak method is inaccurate in multipath environments. Fortunately, the initial rising part of the correlation function still has a good linear shape without distortion by

multipath because the latter always arrives later than LOS signal. Usually, the multipath delay is larger than 200 ns (in urban areas it is typically larger than 400 ns (Turin 1972)). Based on this condition, which is also valid from the experiment results in Chapter 6, the estimation of the initial rising slope was investigated to determine TOA. The problem is that low SNR at the initial rising part of the correlation function affects performance. Then the beamforming technique based on an antenna array is applied to improve SNR. In order to enhance the LOS signal strength and mitigate NLOS signals at the same time efficiently through the beamformer, the AOA of LOS signals needs to be estimated. This is the process that was investigated to make use of the AOA information for the proposed AOA-assisted TOA estimation algorithm.

In this approach, the AOA estimation is an important step. The forward/backward smoothing MUSIC algorithm is applied to estimate AOA in multipath environments because the conventional MUSIC algorithm is not suitable for fully correlated signals which exist in such environments. The computational effort using MUSIC is low with one dimension search no matter how high the number of source signals is, whereas the Maximum Likelihood method needs N dimension search if the number of signals is N and other parameters, such as signals' amplitude and phase are known. One of the limitations of the F/B smoothing MUSIC algorithm is that the number of source signals cannot be over $2M/3$ (M is the number of antenna array elements), otherwise the angles of the signals cannot be resolved. This problem is overcome in a CDMA IS-95 system by sampling the data at the correlation function initial rising part, where fewer source signals are contained.

The CRLBs of the AOA-joint TOA method and the proposed AOA-assisted TOA method were investigated in Chapter 3. One interesting phenomena that was found for multiple source signals is that the AOA CRLB of the AOA-assisted TOA method exists maximum and minimum values due to different initial phases of the incident rays. Stoica & Nehorai (1989) only discussed the case when the phase of the correlation coefficient ρ_{xy} of two signals is zero, so only one CRLB exists. Compared with AOA-joint TOA estimation, ***the AOA-assisted TOA method is a suboptimal method***. The advantage of the proposed method is that the computation is much less than the Maximum Likelihood method because it only needs to search the signal incident angle within 180º; whereas the ML method needs to search in multiple dimensions including the signal amplitude, phase, incident angle and time delay.

In Chapter 4, a specific AOA estimator called MUSIC estimator was analyzed and compared with its CRLB. It can be seen that the unbiased MUSIC-based AOA estimator is suboptimal when the angle difference between two incident rays is large. Similar to the discussion of the maximum and minimum CRLB in Chapter 3, the MUSIC estimator also exist maximum and minimum variances when the phase of correlation coefficient ρ_{xy} of two signals is considered.

In Chapter 5, a specific TOA estimator using a multipath mitigated correlation function rising slope is analyzed theoretically and compared with its CRLB. It can be seen that the asymptotically unbiased TOA estimator exists when the SNR after despreading is

more than 15 dB but its variance increases with the decrement of SNR after despreading. For example, when SNR after despreading is 15 dB, the TOA standard deviation is 36.8 m. The advantage to process data in the correlation function initial rising part is that fewer multipath components were contained in that range. The conventional correlation peak-based TOA method fails in multipath environments even if is optimal (Kay 1998).

The experiment described in Chapter 6 is based on data measured by a CDMA receiver prototype. The results show that:

1. The proposed method works in both clean LOS environment (open air area without multipath) and multipath environments.
2. AOA estimates are close to the theoretical values which are accurate to about 1º to 2º when the angle of incident ray is perpendicular to the array line; whereas when the incident angle is parallel to antenna array, the AOA estimates have large error, in which case other suitable base stations needs to be choosen.
3. TDOA estimates are biased. Theoretically when the SNR after despreading is more than 15 dB, it will be unbiased.However, when the practical SNR after despreading is more than 30 dB, other practical factors such as the non-synchronization of the CDMA network base stations may cause a bias. The TDOA standard deviation is small and close to the theoretical value of 8 m when the SNR after despreading is 30 dB.
4. A stability test shows that the TDOA measurements vary by 10 m during a one hour interval.

From several scenarios described in Chapter 6, it can be seen that:

1. In open air areas with LOS signals without or little multipath effect as in *Scenario 1* of Section 6.3.5, both the correlation peak-based method and the correlation slope-based method yield similar results. In this case, the latter one has no significant advantage.
2. In LOS environments with strong multipath as in *Scenario 2* of Section 6.3.5, the proposed method shows a significant advantage over the correlation peak-based method.
3. In LOS environments with weak signal strength as in *Scenario 3* of Section 6.3.5, the proposed method still works with standard deviation less than 10 m .
4. In non- LOS environments with multipath as in *Scenario 4* of Section 6.3.5, the proposed method deteriorates because the earliest NLOS is treated as LOS, resulting in five channel correlation functions separated from one another as shown in Figure 6.21. In that case, the MUSIC algorithm cannot resolve the incident signals' angles.

7.2 Limitations of the Proposed Algorithm and Recommended Future Work

Limitations

Short Delayed Multipath Results in Low SNR at the Correlation Function Rising Part

The proposed algorithm is based on that the correlation function initial rising part has little distortion by multipath due to the certain delay of multipath in city canyon environment. The statistical delay value is more than 200 ns (Turin 1972). If the delay is

very small, less than 100 ns, the correlation function initial part will have a small segment without distortion, in which area the SNR is small resulting in performance degradation.

The More the Number of Short Delayed Multipath, the Worse the AOA Estimation

The AOA estimation performance is affected by the number of antenna array elements. More array elements results in smaller estimation error. In this research, we use five antenna elements which have the ability to resolve three source signals. If the synthetic array technique is used, the number of array elements can be increased. The synthetic array can be applied in MUSIC algorithm by constructing a new antenna array output vector and its auto-correlation matrix by equation (4.4). Then the contents in Chapter 4 can be used. However during the construction of the new array output vector, it needs to determine the phase change in the antenna array which is related with the movement of the array. If the movement of the array in a vehicle is random, then it will be difficult to parameterize the change of the array phase. So an inertial device will be helpful to apply the synthetic array technique for AOA estimation (Ali et al 2007).

AOA Estimation Accuracy Decreases if Signals Come Parallel with Antenna Array

From the experiment results, it can be seen that the accuracy of the AOA estimation is related with the geometric angle between the antenna array line and the base stations. If the signal from the base station is perpendicular to the array line, the AOA estimation error will be small. If the signal from the base station is parallel to the array line, the AOA estimation error will be large. To solve this problem, one possible solution is to add

one more linear uniform array orthogonal to the previous one. So when the signal is parallel to one ULA, it is orthogonal to the other ULA. This will increase the complexity of the algorithm which can be studied in the future.

Without LOS, the Earliest NLOS is Treated as LOS, Resulting in Estimation Error

The proposed algorithm is on the condition that the LOS exists. In the paper by Qi (2003), it proposed a method to estimate TOA based on the NLOS with prior PDF by subtracting the NLOS delay from the total time delay. However it still needs to know if the received signal is LOS or NLOS which is hard to determine. So in this research, the first arrival signal is used as the LOS signal.

Future Work

More Field Testing

The experiment is based on the limited measured data. More field testing under a wider range of conditions (different environments such as down town areas, different antenna spacing and different number of antenna elements) is needed to fully validate the approach designed herein.

The Application of the Proposed Algorithm in Tracking Process

The proposed method is verified through the acquisition process for CDMA IS-95 pilot signals. However it can also be applied in tracking process, in which Kalman filter technique can be used to predict new AOA estimates based on the previous AOA values from MUSIC estimator and the updated AOA estimates will be sent to the adaptive

beamformer to enhance LOS SNR and mitigate multipath. Then TOA can be determined using the proposed method. The proposed method is also suitable for GPS signal and the steps also go from AOA estimation, beamforming for multipath mitigation and then correlation function rising slope estimation for TOA determination. The difference is that the GPS signal is weaker than CDMA signal, which can be improved through long integration and antenna array to increase SNR after beamforming.

Application to Dynamic Cases

For dynamic application, the impact of coherent integration time on the overall performance should be studied. The clock stability, the Doppler shift during the coherent integration time will all affect the data collected and cause the signal processing more complicated.

Requirements for the CDMA Network

From the experiment results it can be seen that the synchronization among the base stations is very important for location accuracy using TDOA technique because 1 μs time offset between two base stations will result in a bias of about 300 metres. The bandwidth of the filter before despreading will affect the correlation function's shape significantly. The larger bandwidth, the correlation function will be closer to be like a triangle, which is helpful for determining the rising linear part.

Requirements for the Antenna Size

The antenna array used herein is suitable for amounting on vehicles. For handset application, it requires smaller size of antenna which can be distributed around the circumference of handset. In that case, the MUSIC algorithm is not applied in a uniform linear array. It needs to figure out the phase difference between each antenna element.

References

Abadir, K. M. and J. R. Magnus (2005) *Matrix Algebra*, Cambridge University Press, NY, USA

Ali, Broumandan, T. Lin, A. Moghaddam, D. Lu, J. Nielsen and G. Lachapelle (2007) "Direction of Arrival Estimation of GNSS Signals Based on Synthetic Antenna Array," *Proceedings of GNSS07, The Institute of Navigation,* Forth Worth, TX, US *(accepted)*

Lopez, Alfredo, Dingchen Lu, S.K. Shanmugam, H. Agus, N. Salimi, A.R. Moghaddam, N. John, G. Lachapelle, "Tactical Outdoor Positioning System (TOPS) Technology Demonstration – Stage 3", Progress Report, Department of National Defence, Ottawa, Pages 137, Mar. 2006.

Barton, D.K. and S.A. Leonov (1997) *Radar Technology Encyclopedia*, Artech House, Inc., Boston, London

Caffery, J.J. Jr. and G.L. Stuber (1998) "Overview of Radiolocation in CDMA Cellular Systems," *IEEE Communications Magazine*, April

Chan, Y.T. (1994) "A Simple and Efficient Estimation for Hyperbolic Location," *IEEE Trans. on Signal Processing*, vol. 42, no. 8, pp. 1905-1915, August

Dempster A.G. (2006) "Dilution of Precision in Angle-Of-Arrival Positioning Systems," *Electronics Letters*, vol. 42, no. 5, 2nd March

Dovis, F., M, Pini, and P. Mulassano (2004) "Multiple DLL Architecture for Multiple Recovery in Navigation Receiver," *IEEE 59th Vehicular Technology Conference*, Spring, Volume 5, May 17-19, pp. 2848 – 2851

Dumont, L.R., (1994) *Super-Resolution of Discrete Arrivals in a Spread Spectrum System*, M.Sc. Thesis, Department of Electrical and Computer Engineering, The University of Calgary, Calgary, Alberta, Canada

EI-Behery, I.N. and R.H. Macphie (1977) "Maximum Likelihood Estimation of Source Parameters from Time-Sampled Outputs of a Linear Array," *J. Acoustic Soc. Am.*, vol 62, no. 1, July

Ertel, R.B., P. Cardieri, K.W. Sowerby, T.S. Rappaport, and J.H. Reed (1998) "Overview of Spatial Channel Models for Antenna Array Communication Systems," *IEEE Wireless Communications*, Personal Communications, Volume 5, Issue 1, Feb., pp. 10 – 22

Evans, J.E., J.R. Johnson, and D.F. Sun (1981) "High Resolution Angular Spectrum Estimation Techniques for Terrian Scattering Analysis and Angle of Arrival Estimation," *Proc. 1st ASSP Workshop Spectrum Estimation*, Hamilton, Ont., Canada, pp. 134-139

Falletti, E., L.L. Presti, and F. Sellone (2006) "SAMLOST Smart Antenna-Based Movable Localization System," *IEEE Trans. on Vehicular Technology*, vol. 55, no. 1, January

FCC (2001) *Fact sheet: FCC wireless 911 requirements*, http://www.fcc.gov/911/enhanced/releases/factsheet_requirements_012001.pdf

Figel,W., N. Shepherd, and W. Trammell (1969) "Vehicle Location by Signal Attenuation Method," *IEEE Trans. On Vehicular Technology*, Vol. VT-18, pp. 105-109

Friedlander, B. and B. Porat (1989) "Performance Analysis of a Null-steering Algorithm Based on Direction-of-Arrival Estimation" *IEEE Trans. Acoustic, Speech, Signal Processing*, Vol. 37, pp. 461-466

Fruehauf, Hugo (1991) *Precision Time and Frequency Handbook,* Ball Efraton Division

Gans, M.J. (1972) "A Power-spectral Theory of Propagation in the Mobile Radio Environment," IEEE Thans., VT (21), (1), pp. 27-38

Goud, P, A. Sesay, and M. Fattouche (1991) "A Spread Spectrum Radiolocation Technique and its Application to Cellular Radio," *IEEE Pacific Rim Conf. Communication, Computers, and Signal Processing*, pp. 661-664

Hou, Haiying (2004) Chapter 4: *Allan Variance Definition and property*, MSc thesis, (http://www.geomatics.ucalgary.ca/links/GradTheses.html)

Iltis, R. A. and L. Mailaender (1996) "Multiuser Detection of Quasisynchronous CDMA Signals Using Linear Decorrelators," *IEEE Trans. On Communications*, Vol. 44, No. 11, Nov.

Jakes, W.C. (1993) *Microwave Mobile Communications*, New York, IEEE Press

Jekeli, C. (2000) Inertial *Navigation Systems with Geodetic Applications*, Walter de Gruyter, New York, NY., USA

Kay, S.M. (1998) *Fundamentals of Statistical Signal Processing*, Prentice-Hall PTR

Kaplan, E.D. and C.J. Hegarty (2005) *Understanding GPS*: *Principles and Applications*, Artech House

Kim, M., K. Ichige, and H. Arai (2003) "Implementation of FPGA based Fast DOA Estimation Using Unitary MUSIC Algorithm," Proc. IEEE Vehicle Tech. Conf., Orlando, FL, USA, October

Kim, S. (2004) "Improved MUSIC Algorithm for the Code-Timing Estimation of DS-CDMA Multipath-Fading Channels in Multiantenna Systems" *IEEE Trans. On Vehicular*

Technology, vol. 53, no. 5, September

Klukas, R. (1997) *A Superresolution Based Cellular Positioning System Using GPS Time Synchronization*, PhD Thesis, published as Report No. 20114, Department of Geomatics Engineering, University of Calgary

Krizman, K.J., T.E. Biedka, and T.S. Rappaport (1997) "Wireless Position Location: Fundamentals, Implementation Strategies, and Sources of Error," *Vehicular Technology Conference, 1997 IEEE 47th*, Volume 2, 4-7 May, Page(s):919 - 923

Lachapelle, G. and M.E. Cannon (2004) "Global Navigation Satellite Systems – Capabilities and Opportunities," *Canadian Aeronautics and Space Journal*, 50, 1, 49-59

Lachapelle, G. (1998) *Hydrography*, ENGO 545 Lecture Notes, Department of Geomatics Engineering, University of Calgary, Canada

Ma, C. (2003) *Techniques to Improve Ground-Based Wireless Location Performance Using a Cellular Telephone Network*, PhD thesis, Department of Geomatics Engineering Report No. 20177

Messier, G.G. and J.S. Nielsen (1999) "An Analysis of TOA-Based Location for IS-95 Mobiles," *IEEE VTC-Fall, IEEE VTS 50th*, Vol.2, 19-22 Sept., pp. 1067-1071

Petovello, M. G. (2003) *Real-Time Integration of a Tactical-Grade IMU and GPS for High Accuracy Positioning and Navigation*, Ph.D. Thesis

Phillips, C.L. (2003) *Signals, Systems, and Transforms*, Third Edition

Pillai, S.U. and B.H. Kwon (1989) "Forward/Backward Spatial Smoothing Techniques for Coherent Signal Identification," *IEEE Trans. on Acoustics, Speech, and Signal Processing*, Vol. 37, No. 1, Jan

Proakis, J.G. (2001) *Digital Communications*, McGraw-Hill

Qi, Y. (2003) *Wireless Geolocation in a None-Line-Of-Sight Environment*, Ph.D. Thesis, Department of Electrical Engineering, Princeton University

Qualcomm (2006) *Qualcomm History*, **http://www.qualcomm.com/about/history.html**, last accessed August 23, 2006

Rappaport, T.S., S.Y. Seidel, and K. Takamizawa (1991) "Statistical Channel Model for Factory and Open Plan Building Radio Communication System Design," *IEEE Trans. Commun*., vol. 34, pp. 794-807, May

Reed, J.H., K.J. Krizman, B.D. Woerner, and T.S. Rappaport (1998) "An Overview of the Challenges and Progress in Meeting the E-911 Requirement for Location Service," *Communications Magazine, IEEE*, Volume 36, Issue 4, April, Page(s):30 – 37

Roth, P.R. (1971) "Effective Measurements using Digital Signal Analysis," *IEEE Spectrum*, Vol. 8, pp. 62-70, April

Roy, R. and T. Kailath (1989) "ESPRIT-Estimation of Signal Parameters via Rotational Invariance Techniques," *IEEE Trans. on Acoustic, Speech, and Signal Processing*, vol. 37, no. 7, July

Sakagami, S., S. Aoyama, K. Kuboi, S. Shirota, and A. Akeyama (1992) "Vehicle position Estimates by Multi-beam Antennas in Multipath Environments," *IEEE Trans. On Vehicular Technology*, Vol. 41, pp. 63-67

Shanmugam, S., A. Lopez, D. Lu, N. Luo, J. Nielsen, G. Lachapelle, R. Klukas, and A. Taylor (2005) "Wireless Location in IS-95 CDMA Cellular Radio Systems," *TRLab Wireless 2005 Conference*, Calgary 11-13 July, 10 pages

Schmidt, R.O. (1986) "Multiple Emitter Location and Signal Parameter Estimation," *Trans. On Antenna and Propagation*, Vol. AP-34, No. 3, March

Schmidt, R.O. (1979) "Multiple Emitter Location and Signal Parameter Estimation," *Proc. RADC Spectral Estimation Workshop*, pp. 243-258

Shan, T.J., M.Wax, and T. Kailath (1985) "On Spatial Smoothing for Direction-of-Arrival Estimation of Coherent Signals," *IEEE Trans. on Acoustics, Speech, and Processing*, Vol.33, No. 4, Aug

Smith, Jr. (1991) "Passive Location of Mobile Cellular Telephone Terminals," *25th Int. Carnahan Conf. on Security Technology*, pp. 221-225

So, H.C. and P.C.Ching (1993) "Target Localization in the Presence of Multipaths," *Electronics Letters*, vol.29, no.3, pp.293-294, February

Svantesson, T. (2001) *Antennas and Propagation from a Signal Processing Perspective*, Ph.D. Thesis

Stoica, P. and A. Nehorai (1989) "MUSIC, Maximum Likelihood, and Cramer-Rao Bound," *IEEE Trans. on ASSP*, vol. 37, no. 5, May

Tarighat, A., N. Khajehnouri, and A.H. Sayed (2003) "CDMA Location Using Multiple Antennas and Interference Cancellation," *Vehicular Technology Conference, Spring, The 57th IEEE Semiannual*, Volume 4, 22-25 April, Page(s):2711 – 2715

Thomas, N.J., D.G.M. Cruickshank, and D.I. Laurenson (2001) "Performance of a TDOA-AOA Hybrid Mobile Location System," *The Second International Conference on 3G Mobile Communication Technologies*, 26-28 March, Page(s):216 – 220

Thompson J.S. (1995) *Bearing Estimation Techniques for Improved Performance Spread Spectrum Receivers*, Ph.D. Dissertation, Department of Electrical Engineering, University of Edinburgh, UK

Turin, G.L., F.D. Clapp, T.L. Johnston, S.B. Fine, and D. Lavry (1972) "A Statistical Model of Urban Multipath Propagation," *IEEE Transactions on Vehicular Technology,* Vol. VT-21, No. 1, pp. 1-9, February

Van der Veen, A.-J., M.C. Vanderveen, and A. Paulraj (1997) "SI-JADE: An Algorithm for Joint Angle and Delay Estimation Using Shift-invariance Properties," *First IEEE Signal Processing Workshop on Signal Processing Advances in Wireless Communications*, pp. 161-164

Wang, F., T. Lo, J. Litva, W. Tead (1994) "VHF Antenna Array Processing: High Accuracy Direction Finding and Performance Evaluation with Real Data" *IEE Proc., Sonar Navigation*, vol. 141, no. 3, June

Wang, Y.Y., J. T. Chen, and W. H. Fang (2001) "TST-MUSIC for joint DOA-delay Estimation," *IEEE Trans. on Signal Processing*, Vol. 49(4), pp. 721-729

Yoo, S., S. Kim, D.H. Youn, and C. Lee (2003) "Multipath Mitigation Technique Using Null-Steering Beamformer for Positioning System," *The 57th IEEE Semiannual Vehicular Technology Conference*, Volume 1, 22-25 April, pp. 602 – 605

Yousef, N.R., A.H. Sayed, and L.M.A. Jalloul (2003) "Robust Wireless Location over Fading Channels," *IEEE Transactions on Vehicular Technology*, Volume 52, Issue 1, Jan. Page(s):117 – 126

Zoltowski, M. D., M. Haardt, and C. P. Mathews (1996) "Closed-form 2-D Angle Estimation with Rectangular Arrays in Element Space or Beamspace via Unitary ESPRIT," *IEEE Trans. on Signal Processing*, vol. 44, pp. 316-328, February

Zoltowski, M. D., G.M. Kautz, and S.D. Silverstein (1993) "Beamspace Root-MUSIC," *IEEE Trans. Signal Processing*, vol. 41, no. 7, pp. 2502-2507, January

APPENDIX A: IS-95 SIGNAL PROCESSING IN FREQUENCY DOMAIN

The relationship between the linear convolution and the Fourier transform of the discrete signals $\tilde{s}_3[n]$ and $\tilde{s}_l[n]$ in Section 2.2.2 is:

$$\tilde{s}_3(n) * \tilde{s}_l(n) = \sum_{m=-\infty}^{\infty} \tilde{s}_3(m)\tilde{s}_l(n-m) \quad \longleftrightarrow \quad \tilde{S}_3(\Omega)\tilde{S}_l(\Omega). \tag{A.1}$$

where symbol (*) denotes the linear convolution, $\tilde{S}_3(\Omega)$ and $\tilde{S}_l(\Omega)$ denote the Fourier transform of the signals $\tilde{s}_3(n)$ and $\tilde{s}_l[n]$ respectively. If $\tilde{s}_3[n]$ and $\tilde{s}_l[n]$ are the periodic discrete signals, the relationship between the circular convolution and the DFT of the signals $\tilde{s}_3[n]$ and $\tilde{s}_l[n]$ is:

$$\tilde{s}_3(n) \otimes \tilde{s}_l(n) = \sum_{m=0}^{N-1} \tilde{s}_3(m)\tilde{s}_l(n-m) \quad \longleftrightarrow \quad \tilde{S}_3(k)\tilde{S}_l(k) \tag{A.2}$$

where symbol ($\otimes$) denotes the circular convolution, $\tilde{S}_3(k)$ and $\tilde{S}_l(k)$ denote the discrete Fourier transform of the signals $\tilde{s}_3(n)$ and $\tilde{s}_l[n]$ respectively.

Based on $\tilde{s}_l(-n) \longleftrightarrow \tilde{S}_l(-k)$, $\tilde{s}_l^*(n) \longleftrightarrow \tilde{S}_l^*(-k)$ and equation (A.2), the correlation between $\tilde{s}_3[n]$ and $\tilde{s}_l[n]$ can be implemented in the frequency domain by:

$$r(m) = \tilde{s}_3(m) \otimes \tilde{s}_l^*(-m) = \sum_{n=0}^{N-1} \tilde{s}_3(n)\tilde{s}_l^*(n-m) \quad \longleftrightarrow \quad \tilde{S}_3(k)\tilde{S}_l^*(k). \tag{A.3}$$

Because $\tilde{s}_3[n]$ contains the estimated carrier frequency difference $\hat{f}_{error}$, equation (A.3) can also be written as:

$$r(m,\hat{f}_{error}) = \sum_{n=0}^{N-1} \tilde{s}_3(n)\tilde{s}_l(n-m) = \mathrm{DF}^{-1}\,[\tilde{S}_3(k)\tilde{S}_l^{*}(k)] \tag{A.4}$$

Equation (A.3) can be proved generally as follows:

Considering two sampled signals $x[n]$ and $y[n]$, the cross correlation function is given by:

$$r_{y,x}[m] = \frac{1}{N}\sum_{n=0}^{N-1} y[n]\,x^{*}\,[n-m] \tag{A.5}$$

Both $x[n]$ and $y[n]$ may be written as:

$$x[n] = \sum_{f=0}^{N-1} X[f]\,e^{j\frac{2\pi n f}{N}} \tag{A.6}$$

$$y[n] = \sum_{f=0}^{N-1} Y[f^{'}]\,e^{j\frac{2\pi n f^{'}}{N}} \tag{A.7}$$

where $X[f]$ and $Y[f^{'}]$ are the DFT of $x[n]$ and $y[n]$ respectively. Substituting (A.6) and (A.7) to (A.5), we obtain the following expression:

$$\begin{aligned}
r_{y,x}[m] &= \frac{1}{N}\sum_{n=0}^{N-1}\left(\sum_{f'=0}^{N-1} Y[f^{'}]\,e^{j\frac{2\pi n f^{'}}{N}}\right)\left(\sum_{f=0}^{N-1} X^{*}[f]\,e^{-j\frac{2\pi(n-m)f}{N}}\right)\\
&= \frac{1}{N}\sum_{n=0}^{N-1}\left(\sum_{f'=0}^{N-1} Y[f^{'}]\,e^{j\frac{2\pi n f^{'}}{N}}\right)\left(\sum_{f=0}^{N-1} X^{*}[f]\,e^{-j\frac{2\pi n f}{N}}\,e^{j\frac{2\pi m f}{N}}\right)\\
&= \frac{1}{N}\sum_{n=0}^{N-1}\sum_{f^{'}=0}^{N-1}\sum_{f=0}^{N-1} Y[f^{'}]X^{*}[f]\,e^{j\frac{2\pi n f^{'}}{N}}\,e^{-j\frac{2\pi n f}{N}}\,e^{j\frac{2\pi m f}{N}}\\
&= \frac{1}{N}\sum_{f^{'}=0}^{N-1}\sum_{f=0}^{N-1}\left(Y[f^{'}]X^{*}[f]\,e^{j\frac{2\pi m f}{N}}\sum_{n=0}^{N-1} e^{j\frac{2\pi n(f^{'}-f)}{N}}\right)
\end{aligned} \tag{A.8}$$

Considering that $(f' - f)$ is an integer and $-(N-1) \le (f' - f) \le N-1$, we can derive

$$\sum_{n=0}^{N-1} e^{j\frac{2\pi n(f'-f)}{N}} = \frac{1-e^{j2\pi n(f'-f)}}{1-e^{j\frac{2\pi (f'-f)}{N}}} = N\,\delta(f' - f) = \begin{cases} N & f' - f = 0 \\ 0 & f' - f \neq 0 \end{cases} \tag{A.9}$$

Substituting (A.9) to (A.8), the correlation function of signals $x[n]$ and $y[n]$ can be expressed as follow:

$$\begin{aligned} r_{y,x}[m] &= \frac{1}{N} \sum_{f'=0}^{N-1} \sum_{f=0}^{N-1} \left(Y[f']X^*[f]\, e^{j\frac{2\pi mf}{N}} N\,\delta(f' - f) \right) \\ &= \sum_{f=0}^{N-1} Y[f]X^*[f]\, e^{j\frac{2\pi mf}{N}} \\ &= \mathrm{DF}^{-1}\,[Y(f)X^*(f)] \end{aligned} \tag{A.10}$$

APPENDIX B: CRLB DERIVATION FOR AOA ESTIMATION UNDER MULTIPLE SOURCE SIGNALS

For convenience, the real and imaginary components of a complex vector or matrix $\mathbf{y}(t)$ are defined as:

$$\overline{\mathbf{y}}(t) \stackrel{\Delta}{=} \mathrm{Re}[\mathbf{y}(t)], \quad \tilde{\mathbf{y}}(t) \stackrel{\Delta}{=} \mathrm{Im}[\mathbf{y}(t)]$$

The fundamental parameter vector in equation (3.46) is expressed as:

$$\boldsymbol{\theta} = \left[\sigma^2, \overline{\mathbf{s}}^T(1), \tilde{\mathbf{s}}^T(1), \cdots, \overline{\mathbf{s}}^T(N), \tilde{\mathbf{s}}^T(N), \boldsymbol{\varphi}^T\right]^T \quad (1+2KN+K)\times 1 \quad \textit{vector}$$

$$\boldsymbol{\varphi} = [\varphi_1, \varphi_2, \cdots, \varphi_K]^T$$
$$\varphi_k = 2\pi \frac{d}{\lambda} \cos\beta_k \qquad k = 1, 2, \cdots, K$$

Assuming that the complex measured data $x_i(t)$ is corrupted by Gaussian complex noise $n_i(t)$, which is identically distributed $\mathcal{N}(0, \sigma^2/2)$, and the noises are independent from sensor to sensor, the parameterized PDF $p(\mathbf{x}(1), \mathbf{x}(2), \cdots, \mathbf{x}(N); \boldsymbol{\theta})$ can be expressed as:

$$\begin{aligned} p(\mathbf{x}(1), \mathbf{x}(2), \cdots, \mathbf{x}(N); \boldsymbol{\theta}) &= p\left(\overline{\mathbf{x}}(1), \tilde{\mathbf{x}}(1), \cdots, \overline{\mathbf{x}}(N), \tilde{\mathbf{x}}(N); \boldsymbol{\theta}\right) \\ &= \frac{1}{\left(\sqrt{\pi\sigma^2}\right)^{2MN}} \exp\left\{-\frac{1}{\sigma^2}\sum_{t=1}^{N} \mathbf{n}^H(t)\mathbf{n}(t)\right\} \\ &= \frac{1}{\left(\sqrt{\pi\sigma^2}\right)^{2MN}} \exp\left\{-\frac{1}{\sigma^2}\sum_{t=1}^{N} [\mathbf{x}(t) - \mathbf{A}\mathbf{s}(t)]^H [\mathbf{x}(t) - \mathbf{A}\mathbf{s}(t)]\right\} \end{aligned} \tag{B.1}$$

The logarithm of $p(\mathbf{x}(1), \mathbf{x}(2), \cdots, \mathbf{x}(N); \boldsymbol{\theta})$ can be derived as:

$$
\begin{aligned}
L &\stackrel{\Delta}{=} \ln p(\mathbf{x}(1), \mathbf{x}(2), \cdots, \mathbf{x}(N); \boldsymbol{\theta}) \\
&= const - MN \ln \sigma^2 - \frac{1}{\sigma^2} \sum_{t=1}^{N} [\mathbf{x}^H(t) - \mathbf{s}^H(t)\mathbf{A}^H][\mathbf{x}(t) - \mathbf{A}\mathbf{s}(t)]
\end{aligned} \tag{B.2}
$$

For obtaining the Fisher information matrix $\mathbf{J}(\boldsymbol{\theta}) = E\left[\frac{\partial L}{\partial \boldsymbol{\theta}}\left(\frac{\partial L}{\partial \boldsymbol{\theta}}\right)^T\right]$ or CRLB covariance matrix $\mathbf{J}^{-1}(\boldsymbol{\theta})$, the derivations of the parameterized PDF logarithm with respect to σ^2, $\bar{\mathbf{s}}(t)$, $\tilde{\mathbf{s}}(t)$ and φ_k should be obtained.

Noting that

$$
\frac{\partial \mathbf{s}^H(t)\mathbf{A}^H}{\partial \bar{\mathbf{s}}(t)} = \begin{bmatrix} \frac{\partial \mathbf{s}^H(t)}{\partial \bar{s}_1(t)} \\ \frac{\partial \mathbf{s}^H(t)}{\partial \bar{s}_2(t)} \\ \vdots \\ \frac{\partial \mathbf{s}^H(t)}{\partial \bar{s}_N(t)} \end{bmatrix} \mathbf{A}^H = \mathbf{A}^H; \quad \frac{\partial \mathbf{A}\mathbf{s}(t)}{\partial \bar{\mathbf{s}}(t)} = \mathbf{A}\left[\frac{\partial \mathbf{s}(t)}{\partial \bar{s}_1(t)} \quad \frac{\partial \mathbf{s}(t)}{\partial \bar{s}_2(t)} \quad \cdots \quad \frac{\partial \mathbf{s}(t)}{\partial \bar{s}_N(t)}\right] = \mathbf{A}
$$

$$
\frac{\partial \mathbf{s}^H(t)\mathbf{A}^H}{\partial \tilde{\mathbf{s}}(t)} = \begin{bmatrix} \frac{\partial \mathbf{s}^H(t)}{\partial \tilde{s}_1(t)} \\ \frac{\partial \mathbf{s}^H(t)}{\partial \tilde{s}_2(t)} \\ \vdots \\ \frac{\partial \mathbf{s}^H(t)}{\partial \tilde{s}_N(t)} \end{bmatrix} \mathbf{A}^H = -j\mathbf{A}^H; \quad \frac{\partial \mathbf{A}\mathbf{s}(t)}{\partial \bar{\mathbf{s}}(t)} = \mathbf{A}\left[\frac{\partial \mathbf{s}(t)}{\partial \tilde{s}_1(t)} \quad \frac{\partial \mathbf{s}(t)}{\partial \tilde{s}_2(t)} \quad \cdots \quad \frac{\partial \mathbf{s}(t)}{\partial \tilde{s}_N(t)}\right] = j\mathbf{A}
$$

the derivations of the parameterized PDF logarithm with respect to σ^2, $\bar{\mathbf{s}}(t)$, $\tilde{\mathbf{s}}(t)$ and φ_k can be written as:

$$\frac{\partial L}{\partial(\sigma^2)} = -\frac{MN}{\sigma^2} + \frac{1}{\sigma^4}\sum_{t=1}^{N}\mathbf{n}^H(t)\mathbf{n}(t) \tag{B.3}$$

$$\frac{\partial L}{\partial \bar{\mathbf{s}}(t)} = \frac{1}{\sigma^2}[\mathbf{A}^H\mathbf{n}(t) + \mathbf{n}^H(t)\mathbf{A}] = \frac{2}{\sigma^2}\mathrm{Re}[\mathbf{A}^H\mathbf{n}(t)] \quad t = 1, 2, \cdots, N \tag{B.4}$$

$$\frac{\partial L}{\partial \tilde{\mathbf{s}}(t)} = \frac{1}{\sigma^2}[-j\mathbf{A}^H\mathbf{n}(t) + j\mathbf{n}^H(t)\mathbf{A}] = \frac{2}{\sigma^2}\mathrm{Im}[\mathbf{A}^H\mathbf{n}(t)] \quad t = 1, 2, \cdots, N \tag{B.5}$$

$$\begin{aligned}\frac{\partial L}{\partial \varphi_k} &= \frac{1}{\sigma^2}\left[\sum_{t=1}^{N}\mathbf{s}^H(t)\frac{\partial \mathbf{A}^H}{\partial \varphi_k}\mathbf{n}(t) + \mathbf{n}^H(t)\frac{\partial \mathbf{A}}{\partial \varphi_k}\mathbf{s}(t)\right] \\ &= \frac{1}{\sigma^2}\left[\sum_{t=1}^{N}s_k^*(t)d^H(\varphi_k)\mathbf{n}(t) + \mathbf{n}^H(t)d(\varphi_k)s_k(t)\right] \\ &= \frac{2}{\sigma^2}\sum_{t=1}^{N}\mathrm{Re}\left[s_k^*(t)d^H(\varphi_k)\mathbf{n}(t)\right] \qquad k = 1, 2, \cdots, K\end{aligned} \tag{B.6}$$

Based on (3.44) and (3.45), the vector expression of (B.6) can be formulated as:

$$\frac{\partial L}{\partial \boldsymbol{\varphi}} = \frac{2}{\sigma^2}\sum_{t=1}^{N}\mathrm{Re}\left[\mathbf{S}^H(t)\mathbf{D}^H\mathbf{n}(t)\right] \tag{B.7}$$

Now some pre-results for CRLB covariance matrix $\mathbf{J}^{-1}(\boldsymbol{\theta})$ are needed, which are stated and proven in the following:

$$1)\ E\left[\mathbf{n}^H(t)\mathbf{n}(t)\mathbf{n}^H(\tau)\mathbf{n}(\tau)\right] = \begin{cases} M^2\sigma^4 & t \neq \tau \\ M(M+1)\sigma^4 & t = \tau \end{cases} \tag{B.8}$$

For $t \neq \tau$,

$$E[\mathbf{n}^H(t)\mathbf{n}(t)\mathbf{n}^H(\tau)\mathbf{n}(\tau)] = E[\mathbf{n}^H(t)\mathbf{n}(t)]E[\mathbf{n}^H(\tau)\mathbf{n}(\tau)] = M\sigma^2 * M\sigma^2 = M^2\sigma^4$$

For $t = \tau$, note that $\overline{\mathbf{n}}^T(t)\tilde{\mathbf{n}}(t) = \tilde{\mathbf{n}}^T(t)\overline{\mathbf{n}}(t)$

$$\begin{aligned}
&E[\mathbf{n}^H(t)\mathbf{n}(t)\mathbf{n}^H(t)\mathbf{n}(t)] = E\{[\mathbf{n}^H(t)\mathbf{n}(t)]^2\} \\
&= E\{[\,\overline{\mathbf{n}}^T(t)\overline{\mathbf{n}}(t) - j\tilde{\mathbf{n}}^T(t)\mathbf{n}(t) + j\overline{\mathbf{n}}^T(t)\mathbf{n}(t) + \tilde{\mathbf{n}}^T(t)\tilde{\mathbf{n}}(t)]^2\} \\
&= E\{[\overline{\mathbf{n}}^T(t)\overline{\mathbf{n}}(t) + \tilde{\mathbf{n}}^T(t)\tilde{\mathbf{n}}(t)]^2\} \\
&= E\{[\overline{\mathbf{n}}^T(t)\overline{\mathbf{n}}(t)]^2\} + 2E\{\overline{\mathbf{n}}^T(t)\overline{\mathbf{n}}(t)\tilde{\mathbf{n}}^T(t)\tilde{\mathbf{n}}(t)\} + E\{[\tilde{\mathbf{n}}^T(t)\tilde{\mathbf{n}}(t)]^2\} \\
&= 2E\{[\overline{\mathbf{n}}^T(t)\overline{\mathbf{n}}(t)]^2\} + 2E\{\overline{\mathbf{n}}^T(t)\overline{\mathbf{n}}(t)\}E\{\tilde{\mathbf{n}}^T(t)\tilde{\mathbf{n}}(t)\} \\
&= 2E\{[\overline{\mathbf{n}}^T(t)\overline{\mathbf{n}}(t)]^2\} + \frac{1}{2}M^2\sigma^4
\end{aligned}$$

Since

$$E\{[\overline{\mathbf{n}}^T(t)\overline{\mathbf{n}}(t)]^2\} = E\left\{\left[\sum_{i=1}^{M}\overline{n}_i^2(t)\right]^2\right\} = E\left[\sum_{i=1}^{M}\sum_{j=1}^{M}\overline{n}_i^2(t)\overline{n}_j^2(t)\right]$$

$$= \sum_{\substack{i=1\\ i\neq j}}^{M}\sum_{j=1}^{M}E[\overline{n}_i^2(t)] * E[\overline{n}_j^2(t)] + \sum_{i=1}^{M}E[\overline{n}_i^4(t)] = (M^2 - M)\frac{\sigma^4}{4} + 3M\frac{\sigma^4}{4}$$

$$= (M^2 + 2M)\frac{\sigma^4}{4}$$

thus $\quad E[\mathbf{n}^H(t)\mathbf{n}(t)\mathbf{n}^H(t)\mathbf{n}(t)] = M(M+1)\sigma^4$

2) $E[\mathbf{n}^H(t)\mathbf{n}(t)\mathbf{n}^T(\tau)] = \mathbf{0}$ *and* $E[\mathbf{n}(t)\mathbf{n}^T(\tau)] = \mathbf{0}$ *for all t and* τ (B.9)

For $t \neq \tau$, the result is evident since are independent.

For $t = \tau$,

$$E[\mathbf{n}^H(t)\mathbf{n}(t)\mathbf{n}^T(t)] = E\left\{\left[\sum_{i=1}^{M}\overline{n}_i^2(t)+\tilde{n}_i^2(t)\right]\mathbf{n}^T(t)\right\} = \begin{bmatrix} E\{[\overline{n}_1^3(t)+\tilde{n}_1^3(t)]n_1(t)\} \\ E\{[\overline{n}_2^3(t)+\tilde{n}_2^3(t)]n_2(t)\} \\ \vdots \\ E\{[\overline{n}_M^3(t)+\tilde{n}_M^3(t)]n_M(t)\} \end{bmatrix}^T$$

$$= \begin{bmatrix} E[\overline{n}_1^3(t)+\tilde{n}_1^3(t)] \\ E[\overline{n}_2^3(t)+\tilde{n}_2^3(t)] \\ \vdots \\ E[\overline{n}_M^3(t)+\tilde{n}_M^3(t)] \end{bmatrix}^T = \mathbf{0}$$

$$E[n_i^2(t)] = E[\overline{n}_i^2(t) + 2j\,\tilde{n}_i(t)\overline{n}_i(t) - \tilde{n}_i^2(t)] = E[\overline{n}_i^2(t) - \tilde{n}_i^2(t)] = \sigma^2 - \sigma^2 = 0$$

Note that the third-order moments of Gaussian noise are equal to zero.

3) $\mathrm{Re}(\mathbf{u})\,\mathrm{Re}(\mathbf{v}^T) = \frac{1}{2}[\mathrm{Re}(\mathbf{u}\mathbf{v}^T) + \mathrm{Re}(\mathbf{u}\mathbf{v}^H)]$

$$\begin{aligned} \mathrm{Im}(\mathbf{u})\,\mathrm{Im}(\mathbf{v}^T) &= -\frac{1}{2}[\mathrm{Re}(\mathbf{u}\mathbf{v}^T) - \mathrm{Re}(\mathbf{u}\mathbf{v}^H)] \\ \mathrm{Re}(\mathbf{u})\,\mathrm{Im}(\mathbf{v}^T) &= \frac{1}{2}[\mathrm{Im}(\mathbf{u}\mathbf{v}^T) - \mathrm{Im}(\mathbf{u}\mathbf{v}^H)] \\ \mathrm{Im}(\mathbf{u})\,\mathrm{Re}(\mathbf{v}^T) &= \frac{1}{2}[\mathrm{Im}(\mathbf{u}\mathbf{v}^T) + \mathrm{Im}(\mathbf{u}\mathbf{v}^H)] \end{aligned} \tag{B.10}$$

4) If $\mathbf{H}$ is a nonsingular complex matrix, and denote its inverse by $\mathbf{G} \overset{\Delta}{=} \mathbf{H}^{-1}$, then

$$\begin{bmatrix} \overline{\mathbf{H}} & -\tilde{\mathbf{H}} \\ \tilde{\mathbf{H}} & \overline{\mathbf{H}} \end{bmatrix}^{-1} = \begin{bmatrix} \overline{\mathbf{G}} & -\tilde{\mathbf{G}} \\ \tilde{\mathbf{G}} & \overline{\mathbf{G}} \end{bmatrix} \tag{B.11}$$

Proof: Because $\mathbf{HG} = (\overline{\mathbf{H}} + j\tilde{\mathbf{H}})(\overline{\mathbf{G}} + j\tilde{\mathbf{G}}) = \mathbf{I}$, the followings can be obtained:

$$\begin{aligned} \overline{\mathbf{H}}\,\overline{\mathbf{G}} - \tilde{\mathbf{H}}\,\tilde{\mathbf{G}} &= \mathbf{I} \\ \overline{\mathbf{H}}\,\tilde{\mathbf{G}} + \tilde{\mathbf{H}}\,\overline{\mathbf{G}} &= \mathbf{0} \end{aligned}$$

Thus, the matrix multiplication is as follow:

$$\begin{bmatrix} \overline{\mathbf{H}} & -\tilde{\mathbf{H}} \\ \tilde{\mathbf{H}} & \overline{\mathbf{H}} \end{bmatrix} \begin{bmatrix} \overline{\mathbf{G}} & -\tilde{\mathbf{G}} \\ \tilde{\mathbf{G}} & \overline{\mathbf{G}} \end{bmatrix} = \begin{bmatrix} \overline{\mathbf{H}}\,\overline{\mathbf{G}} - \tilde{\mathbf{H}}\,\tilde{\mathbf{G}} & -(\overline{\mathbf{H}}\,\tilde{\mathbf{G}} + \tilde{\mathbf{H}}\,\overline{\mathbf{G}}) \\ \tilde{\mathbf{H}}\,\overline{\mathbf{G}} + \overline{\mathbf{H}}\,\tilde{\mathbf{G}} & -\tilde{\mathbf{H}}\,\tilde{\mathbf{G}} + \overline{\mathbf{H}}\,\overline{\mathbf{G}} \end{bmatrix} = \begin{bmatrix} \mathbf{I} & \mathbf{0} \\ \mathbf{0} & \mathbf{I} \end{bmatrix}$$

5) If **A** and **D** are nonsingular square matrices, then one has the following expression (Abadir & Magnus 2005):

$$\begin{bmatrix} \mathbf{A} & \mathbf{B} \\ \mathbf{C} & \mathbf{D} \end{bmatrix}^{-1} = \begin{bmatrix} \mathbf{A}^{-1} + \mathbf{A}^{-1}\mathbf{B}\mathbf{E}^{-1}\mathbf{C}\mathbf{A}^{-1} & -\mathbf{A}^{-1}\mathbf{B}\mathbf{E}^{-1} \\ -\mathbf{E}^{-1}\mathbf{C}\mathbf{A}^{-1} & \mathbf{E}^{-1} \end{bmatrix}, \quad here \quad \mathbf{E} = \mathbf{D} - \mathbf{C}\mathbf{A}^{-1}\mathbf{B} \qquad \text{(B.12)}$$

The method to prove equation (B.12) is similar to that for equation (B.11).

To obtain the CRLB covariance matrix:

$$\mathbf{J}^{-1}(\boldsymbol{\theta}) = E\left[\frac{\partial \ln \mathbf{L}}{\partial \boldsymbol{\theta}} \left(\frac{\partial \ln \mathbf{L}}{\partial \boldsymbol{\theta}} \right)^{T} \right]^{-1} \qquad \text{(B.13)}$$

the following notations introduce are introduced:

$$\mathbf{H} = \frac{\sigma^2}{2} \mathbf{A}^{H} \mathbf{A}$$
$$\mathbf{G} = \mathbf{H}^{-1}$$
$$\boldsymbol{\Delta}_k = \frac{2}{\sigma^2} \mathbf{A}^{H} \mathbf{D} \mathbf{S}(k)$$

Based on equations (B.3) – (B.12), the elements in the Fisher information matrix $\mathbf{I}(\boldsymbol{\theta})$ can be derived:

$$
\begin{aligned}
E\left[\left(\frac{\partial L}{\partial \sigma^2}\right)^2\right] &= E\left\{\left[-\frac{MN}{\sigma^2}+\frac{1}{\sigma^4}\sum_{t=1}^{N}\mathbf{n}^H(t)\mathbf{n}(t)\right]^2\right\} \\
&= \frac{M^2N^2}{\sigma^4}-\frac{2MN}{\sigma^6}\sum_{t=1}^{N}E[\mathbf{n}^H(t)\mathbf{n}(t)]+\frac{1}{\sigma^8}\sum_{t=1}^{N}\sum_{\tau=1}^{N}E[\mathbf{n}^H(t)\mathbf{n}(t)\mathbf{n}^H(\tau)\mathbf{n}(\tau)] \\
&= \frac{M^2N^2}{\sigma^4}-\frac{2M^2N^2}{\sigma^4} \\
&\quad +\frac{1}{\sigma^8}\left\{(N^2-N)\underset{t\neq\tau}{E}[\mathbf{n}^H(t)\mathbf{n}(t)\mathbf{n}^H(\tau)\mathbf{n}(\tau)]+NE\{[\mathbf{n}^H(t)\mathbf{n}(t)]^2\}\right\} \\
&= -\frac{M^2N^2}{\sigma^4}+\frac{1}{\sigma^8}[(N^2-N)*M^2\sigma^4+N*M(M+1)\sigma^4] \\
&= \frac{MN}{\sigma^4}
\end{aligned}
\tag{B.14}
$$

$$
\begin{aligned}
E\left[\frac{\partial L}{\partial \bar{\mathbf{s}}(k)}\left(\frac{\partial L}{\partial \bar{\mathbf{s}}(l)}\right)^T\right] &= \frac{4}{\sigma^4}E\{\mathrm{Re}[\mathbf{A}^H\mathbf{n}(k)]\mathrm{Re}[\mathbf{A}^H\mathbf{n}(l)]^T\} \\
&= \frac{2}{\sigma^4}E\left(\mathrm{Re}\{\mathbf{A}^H\mathbf{n}(k)[\mathbf{A}^H\mathbf{n}(l)]^T\}+\mathrm{Re}\{\mathbf{A}^H\mathbf{n}(k)[\mathbf{A}^H\mathbf{n}(l)]^H\}\right) \\
&= \frac{2}{\sigma^4}E\left(\mathrm{Re}\{\mathbf{A}^H\mathbf{n}(k)[\mathbf{A}^H\mathbf{n}(l)]^H\}\right)=\frac{2}{\sigma^4}\mathrm{Re}\{\mathbf{A}^HE[\mathbf{n}(k)\mathbf{n}^H(l)]\mathbf{A}\} \\
&= \frac{2}{\sigma^2}\mathrm{Re}[\mathbf{A}^H\mathbf{A}]\delta_{k,l}=\overline{\mathbf{H}}\delta_{k,l}
\end{aligned}
\tag{B.15}
$$

here $\delta_{k,l}$ is the Kronecker Delta function, which is equal to 1 if $k=l$ or zero if $k\neq l$.

$$
\begin{aligned}
&E\left[\frac{\partial L}{\partial \bar{\mathbf{s}}(k)}\left(\frac{\partial L}{\partial \tilde{\mathbf{s}}(l)}\right)^T\right] = \frac{4}{\sigma^4} E\{\mathrm{Re}[\mathbf{A}^H\mathbf{n}(k)]\,\mathrm{Im}[\mathbf{A}^H\mathbf{n}(t)]^T\} \\
&= \frac{2}{\sigma^4} E\Big(\mathrm{Im}\{\mathbf{A}^H\mathbf{n}(k)[\mathbf{A}^H\mathbf{n}(l)]^T\} - \mathrm{Im}\{\mathbf{A}^H\mathbf{n}(k)[\mathbf{A}^H\mathbf{n}(l)]^H\}\Big) \\
&= -\frac{2}{\sigma^4} E\Big(\mathrm{Im}\{\mathbf{A}^H\mathbf{n}(k)[\mathbf{A}^H\mathbf{n}(l)]^H\}\Big) = -\frac{2}{\sigma^4}\mathrm{Im}\{\mathbf{A}^H E[\mathbf{n}(k)\mathbf{n}^H(l)]\mathbf{A}\} \\
&= -\frac{2}{\sigma^2}\mathrm{Im}[\mathbf{A}^H\mathbf{A}]\delta_{k,l} = -\tilde{\mathbf{H}}\delta_{k,l}
\end{aligned}
\tag{B.16}
$$

$$
\begin{aligned}
&E\left[\frac{\partial L}{\partial \tilde{\mathbf{s}}(k)}\left(\frac{\partial L}{\partial \bar{\mathbf{s}}(l)}\right)^T\right] = E\left[\frac{\partial L}{\partial \bar{\mathbf{s}}(k)}\left(\frac{\partial L}{\partial \tilde{\mathbf{s}}(l)}\right)^T\right]^T \\
&= -\frac{2}{\sigma^2}\mathrm{Im}[\mathbf{A}^H\mathbf{A}]^T\,\delta_{k,l} = -\frac{2}{\sigma^2}\mathrm{Im}[\mathbf{A}^H\mathbf{A}]^T\,\delta_{k,l} \\
&= -\frac{2}{\sigma^2}\mathrm{Im}[\mathbf{A}^T\mathbf{A}^*]\delta_{k,l} = -\frac{2}{\sigma^2}\mathrm{Im}[(\mathbf{A}^H\mathbf{A})^*]\delta_{k,l} \\
&= \frac{2}{\sigma^2}\mathrm{Im}[\mathbf{A}^H\mathbf{A}]\delta_{k,l} = \tilde{\mathbf{H}}\delta_{k,l}
\end{aligned}
\tag{B.17}
$$

$$
\begin{aligned}
&E\left[\frac{\partial L}{\partial \tilde{\mathbf{s}}(k)}\left(\frac{\partial L}{\partial \tilde{\mathbf{s}}(l)}\right)^T\right] = \frac{4}{\sigma^4} E\{\mathrm{Im}[\mathbf{A}^H\mathbf{n}(k)]\,\mathrm{Im}[\mathbf{A}^H\mathbf{n}(t)]^T\} \\
&= -\frac{2}{\sigma^4} E\Big(\mathrm{Re}\{\mathbf{A}^H\mathbf{n}(k)[\mathbf{A}^H\mathbf{n}(l)]^T\} - \mathrm{Re}\{\mathbf{A}^H\mathbf{n}(k)[\mathbf{A}^H\mathbf{n}(l)]^H\}\Big) \\
&= \frac{2}{\sigma^4} E\Big(\mathrm{Re}\{\mathbf{A}^H\mathbf{n}(k)[\mathbf{A}^H\mathbf{n}(l)]^H\}\Big) = \frac{2}{\sigma^4}\mathrm{Re}\{\mathbf{A}^H E[\mathbf{n}(k)\mathbf{n}^H(l)]\mathbf{A}\} \\
&= \frac{2}{\sigma^2}\mathrm{Re}[\mathbf{A}^H\mathbf{A}]\delta_{k,l} = \overline{\mathbf{H}}\delta_{k,l}
\end{aligned}
\tag{B.18}
$$

$$
\begin{aligned}
E\left[\frac{\partial L}{\partial \bar{\mathbf{s}}(k)}\left(\frac{\partial L}{\partial \boldsymbol{\varphi}}\right)^T\right] &= \frac{4}{\sigma^4} E\{\mathrm{Re}[\mathbf{A}^H\mathbf{n}(k)]\sum_{t=1}^{N}\mathrm{Re}\left[\mathbf{S}^H(t)\mathbf{D}^H\mathbf{n}(t)\right]^T\} \\
&= \frac{2}{\sigma^4} E\begin{pmatrix} \mathrm{Re}\{\mathbf{A}^H\mathbf{n}(k)\sum_{t=1}^{N}\left[\mathbf{S}^H(t)\mathbf{D}^H\mathbf{n}(t)\right]^T\} \\ +\mathrm{Re}\{\mathbf{A}^H\mathbf{n}(k)\sum_{t=1}^{N}\left[\mathbf{S}^H(t)\mathbf{D}^H\mathbf{n}(t)\right]^H\} \end{pmatrix} \\
&= \frac{2}{\sigma^4} E\left(\mathrm{Re}\{\sum_{t=1}^{N}\mathbf{A}^H\mathbf{n}(k)\left[\mathbf{S}^H(t)\mathbf{D}^H\mathbf{n}(t)\right]^H\}\right) \\
&= \frac{2}{\sigma^4}\mathrm{Re}\{\sum_{t=1}^{N}\mathbf{A}^H E[\mathbf{n}(k)\mathbf{n}^H(t)]\mathbf{D}\mathbf{S}(t)\} \\
&= \frac{2}{\sigma^2}\mathrm{Re}[\mathbf{A}^H\mathbf{D}\mathbf{S}(k)] = \overline{\boldsymbol{\Delta}}_k
\end{aligned}
\tag{B.19}
$$

$$
E\left[\frac{\partial L}{\partial \boldsymbol{\varphi}}\left(\frac{\partial L}{\partial \bar{\mathbf{s}}(k)}\right)^T\right] = E\left[\frac{\partial L}{\partial \bar{\mathbf{s}}(k)}\left(\frac{\partial L}{\partial \boldsymbol{\varphi}}\right)^T\right]^T = \frac{2}{\sigma^2}\mathrm{Re}[\mathbf{A}^H\mathbf{D}\mathbf{S}(k)]^T = \overline{\boldsymbol{\Delta}}_k^T \tag{B.20}
$$

$$
\begin{aligned}
E\left[\frac{\partial L}{\partial \tilde{\mathbf{s}}(k)}\left(\frac{\partial L}{\partial \boldsymbol{\varphi}}\right)^T\right] &= \frac{4}{\sigma^4} E\{\mathrm{Im}[\mathbf{A}^H\mathbf{n}(k)]\sum_{t=1}^{N}\mathrm{Re}\left[\mathbf{S}^H(t)\mathbf{D}^H\mathbf{n}(t)\right]^T\} \\
&= \frac{2}{\sigma^4} E\begin{pmatrix} \mathrm{Im}\{\mathbf{A}^H\mathbf{n}(k)\sum_{t=1}^{N}\left[\mathbf{S}^H(t)\mathbf{D}^H\mathbf{n}(t)\right]^T\} \\ +\mathrm{Im}\{\mathbf{A}^H\mathbf{n}(k)\sum_{t=1}^{N}\left[\mathbf{S}^H(t)\mathbf{D}^H\mathbf{n}(t)\right]^H\} \end{pmatrix} \\
&= \frac{2}{\sigma^4} E\left(\mathrm{Im}\{\sum_{t=1}^{N}\mathbf{A}^H\mathbf{n}(k)\left[\mathbf{S}^H(t)\mathbf{D}^H\mathbf{n}(t)\right]^H\}\right) \\
&= \frac{2}{\sigma^4}\mathrm{Im}\{\sum_{t=1}^{N}\mathbf{A}^H E[\mathbf{n}(k)\mathbf{n}^H(t)]\mathbf{D}\mathbf{S}(t)\} \\
&= \frac{2}{\sigma^2}\mathrm{Im}[\mathbf{A}^H\mathbf{D}\mathbf{S}(k)] = \tilde{\boldsymbol{\Delta}}_k
\end{aligned}
\tag{B.21}
$$

$$
E\left[\frac{\partial L}{\partial \boldsymbol{\varphi}}\left(\frac{\partial L}{\partial \tilde{\mathbf{s}}(k)}\right)^T\right] = E\left[\frac{\partial L}{\partial \tilde{\mathbf{s}}(k)}\left(\frac{\partial L}{\partial \boldsymbol{\varphi}}\right)^T\right]^T = \frac{2}{\sigma^2}\mathrm{Im}[\mathbf{A}^H\mathbf{D}\mathbf{S}(k)]^T = \tilde{\boldsymbol{\Delta}}_k^T \tag{B.22}
$$

$$
\begin{aligned}
E\left[\frac{\partial L}{\partial \boldsymbol{\varphi}}\left(\frac{\partial L}{\partial \boldsymbol{\varphi}}\right)^T\right] &= \frac{4}{\sigma^4} E\left(\sum_{t=1}^{N} \mathrm{Re}\left[\mathbf{S}^H(t)\mathbf{D}^H\mathbf{n}(t)\right] \sum_{\tau=1}^{N} \mathrm{Re}\left[\mathbf{S}^H(\tau)\mathbf{D}^H\mathbf{n}(\tau)\right]^T\right) \\
&= \frac{4}{\sigma^4} E\left(\sum_{t=1}^{N}\sum_{\tau=1}^{N} \mathrm{Re}\left[\mathbf{S}^H(t)\mathbf{D}^H\mathbf{n}(t)\right]\mathrm{Re}\left[\mathbf{S}^H(\tau)\mathbf{D}^H\mathbf{n}(\tau)\right]^T\right) \\
&= \frac{2}{\sigma^4} E\left(\sum_{t=1}^{N}\sum_{\tau=1}^{N} \mathrm{Re}\left\{\left[\mathbf{S}^H(t)\mathbf{D}^H\mathbf{n}(t)\right]\left[\mathbf{S}^H(\tau)\mathbf{D}^H\mathbf{n}(\tau)\right]^H\right\}\right) \\
&= \frac{2}{\sigma^4} \sum_{t=1}^{N}\sum_{\tau=1}^{N} \mathrm{Re}\{\mathbf{S}^H(t)\mathbf{D}^H E[\mathbf{n}(t)\mathbf{n}(\tau)^H]\,\mathbf{DS}(\tau)\} \\
&= \frac{2}{\sigma^2} \sum_{t=1}^{N} \mathrm{Re}\{\mathbf{S}^H(t)\mathbf{D}^H\mathbf{DS}(t)\} \\
&\overset{\Delta}{=} \boldsymbol{\Gamma}
\end{aligned}
\tag{B.23}
$$

Based on (B.14) – (B.23), the Fisher information matrix can be derived as:

$$
\mathbf{J}(\boldsymbol{\theta}) = E\left[\frac{\partial L}{\partial \boldsymbol{\theta}}\left(\frac{\partial L}{\partial \boldsymbol{\theta}}\right)^T\right] = \left[\begin{array}{c|cccccc|c}
\frac{MN}{\sigma^4} & & & \mathbf{0} & & & & \mathbf{0} \\
\hline
 & \overline{\mathbf{H}} & -\tilde{\mathbf{H}} & & & & & \overline{\boldsymbol{\Delta}}_1 \\
 & \tilde{\mathbf{H}} & \overline{\mathbf{H}} & & \mathbf{0} & & & \tilde{\boldsymbol{\Delta}}_1 \\
\mathbf{0} & & & \ddots & & & & \vdots \\
 & & \mathbf{0} & & \overline{\mathbf{H}} & -\tilde{\mathbf{H}} & & \overline{\boldsymbol{\Delta}}_N \\
 & & & & \tilde{\mathbf{H}} & \overline{\mathbf{H}} & & \tilde{\boldsymbol{\Delta}}_N \\
\hline
\mathbf{0} & \overline{\boldsymbol{\Delta}}_1^T & \tilde{\boldsymbol{\Delta}}_1^T & \cdots & \overline{\boldsymbol{\Delta}}_N^T & \tilde{\boldsymbol{\Delta}}_N^T & & \boldsymbol{\Gamma}
\end{array}\right]
= \begin{bmatrix} \mathbf{Z}_{11} & \mathbf{Z}_{12} \\ \mathbf{Z}_{21} & \boldsymbol{\Gamma} \end{bmatrix}
\tag{B.24}
$$

The Fisher information matrix in (B.24) is partitioned into four blocks by two solid lines. Thus, the CRLB of $\boldsymbol{\varphi}$ can be derived as:

$$\begin{aligned}\mathrm{var}_{CRLB}^{-1}(\hat{\boldsymbol{\varphi}}) &= \boldsymbol{\Gamma} - \mathbf{Z}_{21}\mathbf{Z}_{11}^{-1}\mathbf{Z}_{12} \\ &= \boldsymbol{\Gamma} - [\overline{\boldsymbol{\Delta}}_1^T \;\; \tilde{\boldsymbol{\Delta}}_1^T \;\; \cdots \;\; \overline{\boldsymbol{\Delta}}_N^T \;\; \tilde{\boldsymbol{\Delta}}_N^T] \begin{bmatrix} \overline{\mathbf{G}} & -\tilde{\mathbf{G}} & & \\ \tilde{\mathbf{G}} & \overline{\mathbf{G}} & & \mathbf{0} \\ & & \ddots & \\ & \mathbf{0} & & \overline{\mathbf{G}} \;\; -\tilde{\mathbf{G}} \\ & & & \tilde{\mathbf{G}} \;\; \overline{\mathbf{G}} \end{bmatrix} \begin{bmatrix} \overline{\boldsymbol{\Delta}}_1 \\ \tilde{\boldsymbol{\Delta}}1 \\ \vdots \\ \overline{\boldsymbol{\Delta}}_N \\ \tilde{\boldsymbol{\Delta}}_N \end{bmatrix}\end{aligned} \tag{B.25}$$

where

$$\begin{aligned}[\overline{\boldsymbol{\Delta}}_t^T \;\; \tilde{\boldsymbol{\Delta}}_t^T] \begin{bmatrix} \overline{\mathbf{G}} & -\tilde{\mathbf{G}} \\ \tilde{\mathbf{G}} & \overline{\mathbf{G}} \end{bmatrix} \begin{bmatrix} \overline{\boldsymbol{\Delta}}_t \\ \tilde{\boldsymbol{\Delta}}_t \end{bmatrix} &= [\overline{\boldsymbol{\Delta}}_i^T \;\; \tilde{\boldsymbol{\Delta}}_i^T] \begin{bmatrix} \overline{\mathbf{G}}\,\overline{\boldsymbol{\Delta}}_t - \tilde{\mathbf{G}}\,\tilde{\boldsymbol{\Delta}}_t \\ \tilde{\mathbf{G}}\,\overline{\boldsymbol{\Delta}}_t + \overline{\mathbf{G}}\,\tilde{\boldsymbol{\Delta}}_t \end{bmatrix} = [\overline{\boldsymbol{\Delta}}_i^T \;\; \tilde{\boldsymbol{\Delta}}_i^T] \cdots \begin{bmatrix} \mathrm{Re}(\mathbf{G}\,\boldsymbol{\Delta}_t) \\ \mathrm{Im}(\mathbf{G}\,\boldsymbol{\Delta}_t) \end{bmatrix} \\ &= \mathrm{Re}[\boldsymbol{\Delta}_t^H \mathbf{G}\,\boldsymbol{\Delta}_t]\end{aligned} \tag{B.26}$$

Based on equations (B.25) and (B.26), the following expression is derived:

$$\begin{aligned}\mathrm{var}_{CRLB}^{-1}(\hat{\boldsymbol{\varphi}}) &= \boldsymbol{\Gamma} - \sum_{t=1}^{N} \mathrm{Re}[\boldsymbol{\Delta}_t^H \mathbf{G}\,\boldsymbol{\Delta}_t] \\ &= \frac{2}{\sigma^2} \sum_{t=1}^{N} \mathrm{Re}\{\mathbf{S}^H(t)\mathbf{D}^H\mathbf{D}\mathbf{S}(t) - \mathbf{S}^H(t)\mathbf{D}^H\mathbf{A}(\mathbf{A}^H\mathbf{A})^{-1}\mathbf{A}^H\mathbf{D}\mathbf{S}(t)\} \\ &= \frac{2}{\sigma^2} \sum_{t=1}^{N} \mathrm{Re}\{\mathbf{S}^H(t)\mathbf{D}^H[\mathbf{I} - \mathbf{A}(\mathbf{A}^H\mathbf{A})^{-1}\mathbf{A}^H]\,\mathbf{D}\mathbf{S}(t)\}\end{aligned} \tag{B.27}$$

Thus, $\mathrm{var}_{CRLB}(\hat{\boldsymbol{\varphi}})$ can be expressed as:

$$\mathrm{var}_{CRLB}(\hat{\boldsymbol{\varphi}}) = \frac{\sigma^2}{2} \left[\sum_{t=1}^{N} \mathrm{Re}\{\mathbf{S}^H(t)\mathbf{D}^H[\mathbf{I} - \mathbf{A}(\mathbf{A}^H\mathbf{A})^{-1}\mathbf{A}^H]\,\mathbf{D}\mathbf{S}(t)\} \right]^{-1} \tag{B.28}$$

If the transformation of parameters is as follows:

$$\begin{aligned}\boldsymbol{\alpha} &= \mathbf{g}(\boldsymbol{\theta}) \\ &= \left[\sigma^2, \bar{\mathbf{s}}^T(1), \tilde{\mathbf{s}}^T(1), \cdots, \bar{\mathbf{s}}^T(N), \tilde{\mathbf{s}}^T(N), \boldsymbol{\beta}^T\right]^T \quad (1+2KN+K)\times 1 \quad \textit{vector}\end{aligned}$$

where

$$\boldsymbol{\beta} = [\beta_1, \beta_2, \cdots, \beta_K]^T$$
$$\beta_k = arc\cos(\frac{\lambda}{2\pi d}\varphi_k) \qquad k = 1, 2, \cdots, K$$

Because $\frac{\partial \mathbf{g}(\boldsymbol{\theta})}{\partial \boldsymbol{\theta}}$ is a diagonal matrix, so the CRLB of AOA $\hat{\beta}_k$ can be derived as:

$$\mathrm{var}_{CRLB}(\hat{\beta}_k) = \left(\frac{\partial \beta_k}{\partial \varphi_k}\right)^2 \left\{ \frac{\sigma^2}{2} \left[\sum_{t=1}^{N} \mathrm{Re}\{\mathbf{S}^H(t)\mathbf{D}^H[\mathbf{I} - \mathbf{A}(\mathbf{A}^H\mathbf{A})^{-1}\mathbf{A}^H]\mathbf{D}\mathbf{S}(t)\} \right]^{-1} \right\}_{k\,k}$$
$$= \frac{\sigma^2}{2} \left\{ \left[\sum_{t=1}^{N} \mathrm{Re}\{\mathbf{S}^H(t)\mathbf{D}^H[\mathbf{I} - \mathbf{A}(\mathbf{A}^H\mathbf{A})^{-1}\mathbf{A}^H]\mathbf{D}\mathbf{S}(t)\} \right]^{-1} \right\}_{k\,k} \Big/ \left(2\pi \frac{d}{\lambda} \sin\beta_K\right)^2$$

(B.29)

APPENDIX C: INVESTIGATION OF SIGNAL TO NOISE RATIO AT THE PEAK OF THE CORRELATION FUNCTION

Based on the contents in Section 2.2.2, the IS-95 pilot signal impinging the receiver antenna can be expressed as:

$$s(t) = 2A\left[PN_I(t)\cos(2\pi f_c t + \phi) + PN_Q(t)\sin(2\pi f_c t + \phi)\right] \tag{C.1}$$

Suppose that the signal is corrupted by the band pass "white" Gaussian noise with zero mean, the noise can be expressed as

$$n(t) = 2\left[n_I(t)\cos 2\pi f_c t + n_Q(t)\sin 2\pi f_c t\right] \tag{C.2}$$

where $n_I(t)$ and $n_Q(t)$ are the noises of I and Q components as shown in Figure C.1.

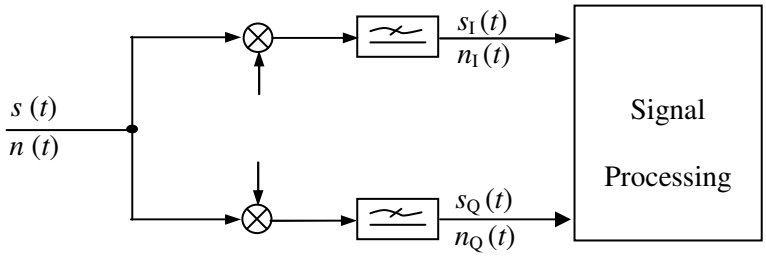

Figure C.1: Demodulation of the CDMA IS-95 Signal

After demodulation, the base band components of $s(t)$ can be obtained as:

$$\begin{aligned} s_I(t) &= A\left[PN_I(t-t_d)\cos(2\pi f_e t + \phi) + PN_Q(t-t_d)\sin(2\pi f_e t + \phi)\right] \\ s_Q(t) &= A\left[-PN_I(t-t_d)\sin(2\pi f_e t + \phi) + PN_Q(t-t_d)\cos(2\pi f_e t + \phi)\right] \end{aligned} \tag{C.3}$$

In order to derive the signal to noise ratio at the peak of the correlation function conveniently, here assume that $f_e = 0$ and $\phi = 0$. Thus the complex base band signal and noise can be expressed as

$$\begin{aligned} \tilde{s}(t) &= A\left[PN_I(t) + j\,PN_Q(t)\right]\ \exp[-j(2\pi f_e t + \phi)] \\ &= A\left[PN_I(t) + j\,PN_Q(t)\right] \\ \tilde{n}(t) &= n_I(t) + j\,n_Q(t) \end{aligned} \tag{C.4}$$

where $n_I(t)$ and $n_Q(t)$ are "white" Gaussian noises with distribution of $\mathcal{N}(0,\ \sigma^2/2)$, which has $E[n_I(t)n_Q(t)] = 0$ and $E[n_I(t_1)n_I(t_2)] = E[n_Q(t_1)n_Q(t_2)] = 0 \quad t_1 \neq t_2$. After the incoming signal passes through a low pass filter with the bandwidth of $1/T_C$ (T_C is the chip period of PN code) and sampled with the rate of $2/T_C$, the noises at the sample points have the following relationship:

$$E[n_I(k_1)n_I(k_2)] = E[n_Q(k_1)n_Q(k_2)] = 0 \quad k_1 \neq k_2 \tag{C.5}$$

If defining *SNR* as the signal to noise ratio before despreading, it can be expressed as:

$$SNR = \frac{E[|\,s(k)\,|^2]}{E[|\,n(k)\,|^2]} = \frac{2A^2}{\sigma^2} \tag{C.6}$$

In the correlation process of IS-95 pilot signal, if the integration time is one PN code period, the correlation function value at the peak can be derived as:

$$\begin{aligned} r_s(0) &= \max[r_s(\tau)] \\ &= \sum_{k=0}^{2K-1} s(k)s_I(k) = \sum_{k=0}^{2K-1} s(k)[PN_I(k) - j\,PN_Q(k)] = 4KA \end{aligned} \tag{C.7}$$

where $s_l(k) = PN_I(k) - j\,PN_Q(k)$ is the local generated signal for correlation process; $K = 2^{15}$.

Meanwhile the noise output at the correlation function peak can be expressed as:

$$r_n(0) = \sum_{k=0}^{2K-1} n(k)s_l(k) \tag{C.8}$$

Based on equation (C.5), the variance of $r_n(0)$ can be derived as:

$$\begin{aligned} E[|\, r_n(0)\,|^2] &= E\left\{\left[\sum_{k=0}^{2K-1} n(k)s_l(k)\right]\left[\sum_{k=0}^{2K-1} n(k)s_l(k)\right]^*\right\} \\ &= E\left[\sum_{k=0}^{2K-1} \left|n(k)s_l(k)\right|^2\right] \\ &= E\left[\sum_{k=0}^{2K-1} \left|n(k)\right|^2 \left|s_l(k)\right|^2\right] \\ &= \sum_{k=0}^{2K-1} E\left[\left|n(k)\right|^2\right]\left|s_l(k)\right|^2 \\ &= 4K\sigma^2 \end{aligned} \tag{C.9}$$

As a result, the signal to noise ratio at the peak of correlation function can be obtained as:

$$SNR_{peak} = \frac{\max[|\, r_s(\tau)\,|^2]}{E[|\, r_n(0)\,|^2]} = \frac{16K^2A^2}{4K\sigma^2} = 4K\,SNR \tag{C.10}$$

For M elements of antenna array processing, the signal to noise ratio at the peak of correlation function can be expressed as:

$$SNR_{\Sigma\ peak} = \frac{\max[|\, r_{\Sigma s}\,(\tau)\,|^2]}{E[|\, r_{\Sigma n}(0)\,|^2]} = 4KM\,SNR \tag{C.11}$$

Furthermore, if the integration time is p periods of PN code, the signal to noise ratio at the peak of correlation function can be derived as:

$$SNR_{\Sigma\ peak} = \frac{\max[|\, r_{\Sigma s}\,(\tau)\,|^2]}{E[|\, r_{\,\Sigma n}(0)\,|^2]} = 4\,pKM\ SNR \tag{C.12}$$

where $K = 2^{15}$; M is the number of antenna elements; p is the integration time; SNR is signal to noise ratio before despreading.

APPENDIX D: INVESTIGATION OF TCXO ALLAN VARIANCE

TCXO stands for Temperature Compensated Crystal Oscillator. Its *frequency stability* is expressed by frequency change within a given time interval τ and usually stated in parts per million (ppm). There are two ways to describe frequency stability: *Short-term stability (Allan variance*) within 1~100 seconds and *long-term stability (aging)* within 1 day ~ 1 year (10 years). Here Short-term stability is investigated.

Allan variance is defined by one half of the time average over the sum of the squares of the differences between successive readings of the frequency deviation sampled over the sampling period. It is normally expressed by:

$$\sigma_y^2 = \frac{1}{2(M-1)} \sum_{i=1}^{M-1} [y(i+1) - y(i)]^2$$

$y(i)$ = $[x(i+1) - x(i)] / t$ is called the fractional frequency value averaged over measurement interval t, which is computed by two adjacent sampled data $x(i)$; M is the number of fractional frequency values. These parameters are described in Figure D.1.

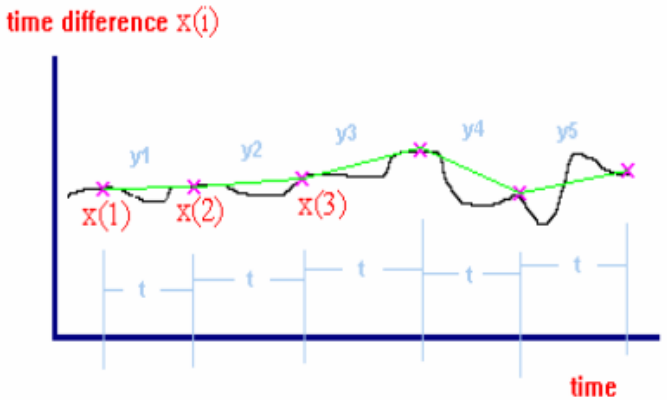

Figure D.1: Allan Variance Description

Here $y_1 = [x(2) - x(1)] / t$ and $x(i)$ is also called clock signal's "phase" because different points show different statuses of the signal. The data rate is $10^7/2^{16}$ = 152 samples/second (the clock is 10 MHz and the counter is 16-bit). So the number of data collected in 1000 seconds is 1000*152 = 152000 samples. The calculation of Allan Deviation at τ = 1 s requires about 100 seconds of data (Fruehauf 1991). In this research, 15 hours of data have been collected. Figure D.2 is the circuit to collect the clock data based on FPGA.

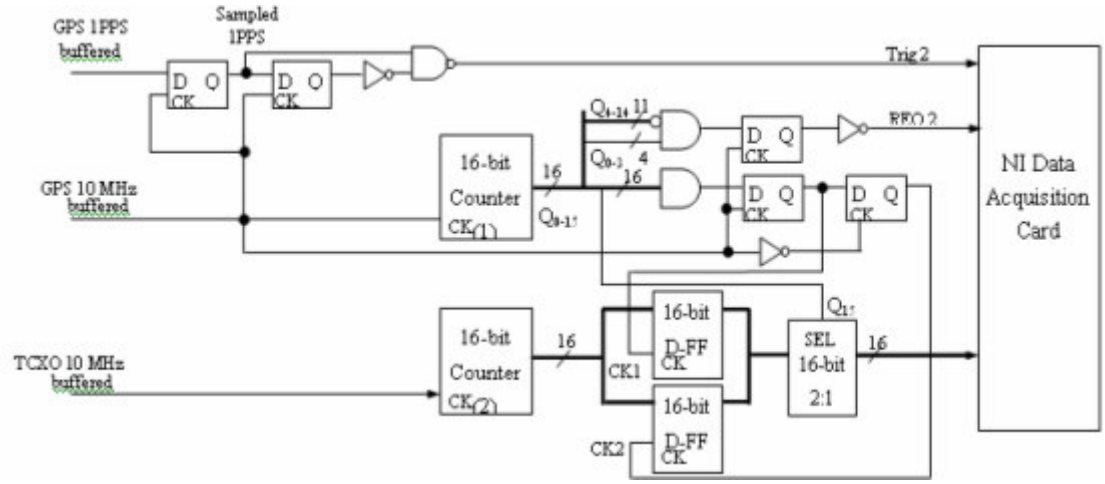

Figure D.2: FPGA-based Circuit for Allan Variance Measurement

Figure D.3 is the result for square root of Allan variance which is called Allan deviation (ADEV). The time interval is from 1 ~ 10000 seconds. The conclusions are as follows:

1. When τ <15 (Rubidium) ~ 50 (TCXO) seconds, the ADEV increases; This trend is different from the theoretical Allan deviation curve. This is due to the

   (a) initial aging process

   (b) system noise

(c) data discontinuity

2. After 15~50 seconds, the ADEV goes down correctly.

3. The sinusoidal noise exists in the plot due to the uncertainty of the measured Allan variance (Hou 2004).

4. The rubidium is Ball Efratom FRK mode. It has more stable curves with respect to the different warm-up time than that of the TCXO.

5. Rubidium is more close to the specifications in (Fruehauf 1991) as Table D.1.

6. Both TCXO data and rubidium data are collected in 15 hours which has a total of 8208000 samples.

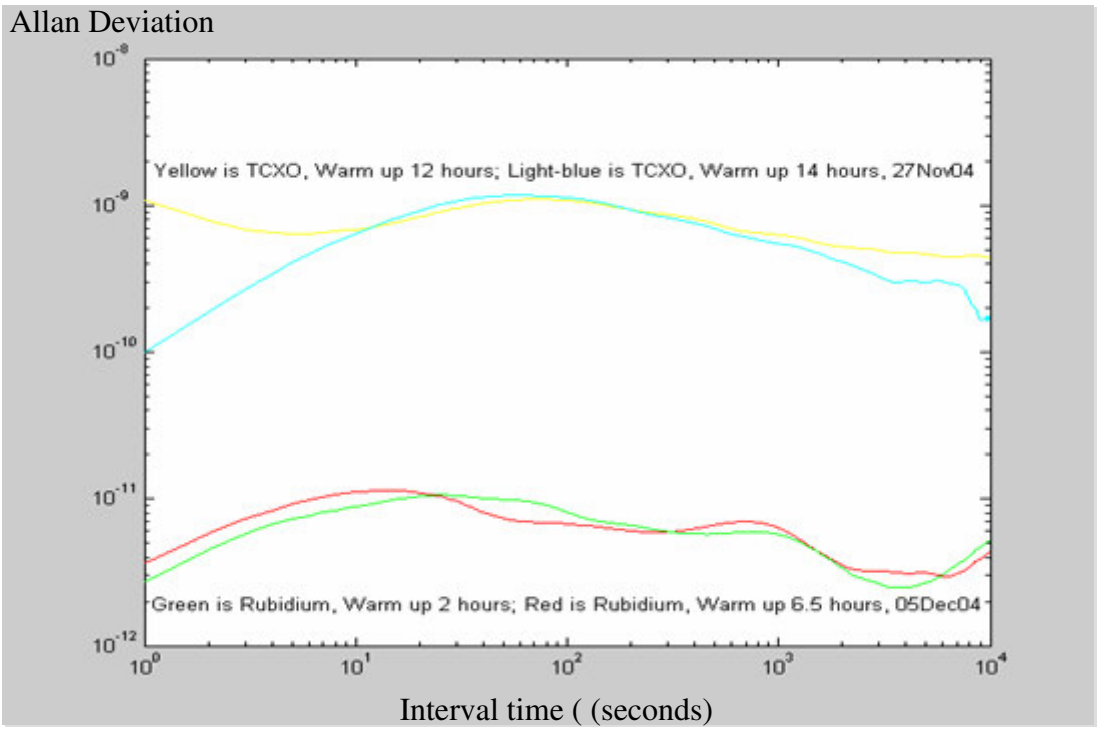

Figure D.3: Measured Allan Deviation for TCXO and Rubidium

Table D.1 Allan Deviation for Rubidium

Time Interval	Specifications	Measured Values
$\tau = 1$ s	3×10^{-11}	3×10^{-12}
$\tau = 10$ s	1×10^{-11}	1×10^{-11}
$\tau = 100$ s	3×10^{-12}	6×10^{-12}
$\tau = 1$ hr	1×10^{-12}	2×10^{-12}

Table D.2 Allan Deviation for TCXO

Time Interval	Specifications	Measured Values
$\tau = 1$ s	1×10^{-11}	1×10^{-10}
$\tau = 10$ s	1×10^{-12}	6×10^{-10}
$\tau = 100$ s	1×10^{-12}	9.5×10^{-10}
$\tau = 1$ hr	3×10^{-11}	2.5×10^{-10}

Even though the measured result for this particular TCXO is not as good as the specifications, it is stable enough for this research. For example, if the TCXO stability is 1×10^{-10} in one second, then the frequency change at RF 1.9 GHz will be 0.19 Hz which is small for this application.

APPENDIX E: DEVELOPMENT OF THE SECOND GENERATION RECEIVER FOR LOCATION SYSTEM

The second generation receiver still receives five channels signals parallel from the RF front end. After down conversion to IF signal, it comes to a digital board as shown in Figure E.1. The digitized signals of five channels are transferred to FPGA serially through the OE (output enable) control signal. The input and output data of FPGA are all differential voltages. Inside the FPGA, the serial input 8-bit I and Q data of five channels are converted to parallel data in order to be sent to AGC unit and frequency de-rotation unit as shown in Figure E.2. The function of frequency de-rotator is to measure the frequency offset or called the Doppler frequency caused by the clock uncertainty and the movement of the receiver and then compensate that frequency offset. This step is newly added with respect to the first generation receiver. The benefit is to make signal acquisition in laptop finished quickly without 2-D search and then the coarse PN code phase can be sent back from laptop to FPGA tracking unit via USB port. So the second generation receiver can work in real time mode. The tracking unit consists of 50 correlators for one signal's tracking and each of them is shown in Figure E.3 (Alfredo et al 2006). The use of accumulator can greatly reduce the amount logic cells required. The control of whether the accumulator should add or subtract is determined by the local PN bit. If the bit is 1, then the accumulator should add; otherwise, it should subtract. The accumulator is initialized with zero and is reset at every one PN code epoch. The 50 correlators outputs of one signal are sent to PC for displaying as shown in Figure E.4, where the correlation functions of five signals from five base stations are given. The peak

of the correlation function determines the time of arrival. In order to track one signal, the local PN code generator's phase is adjusted based on the peak value located in one of 50 correlators outputs.

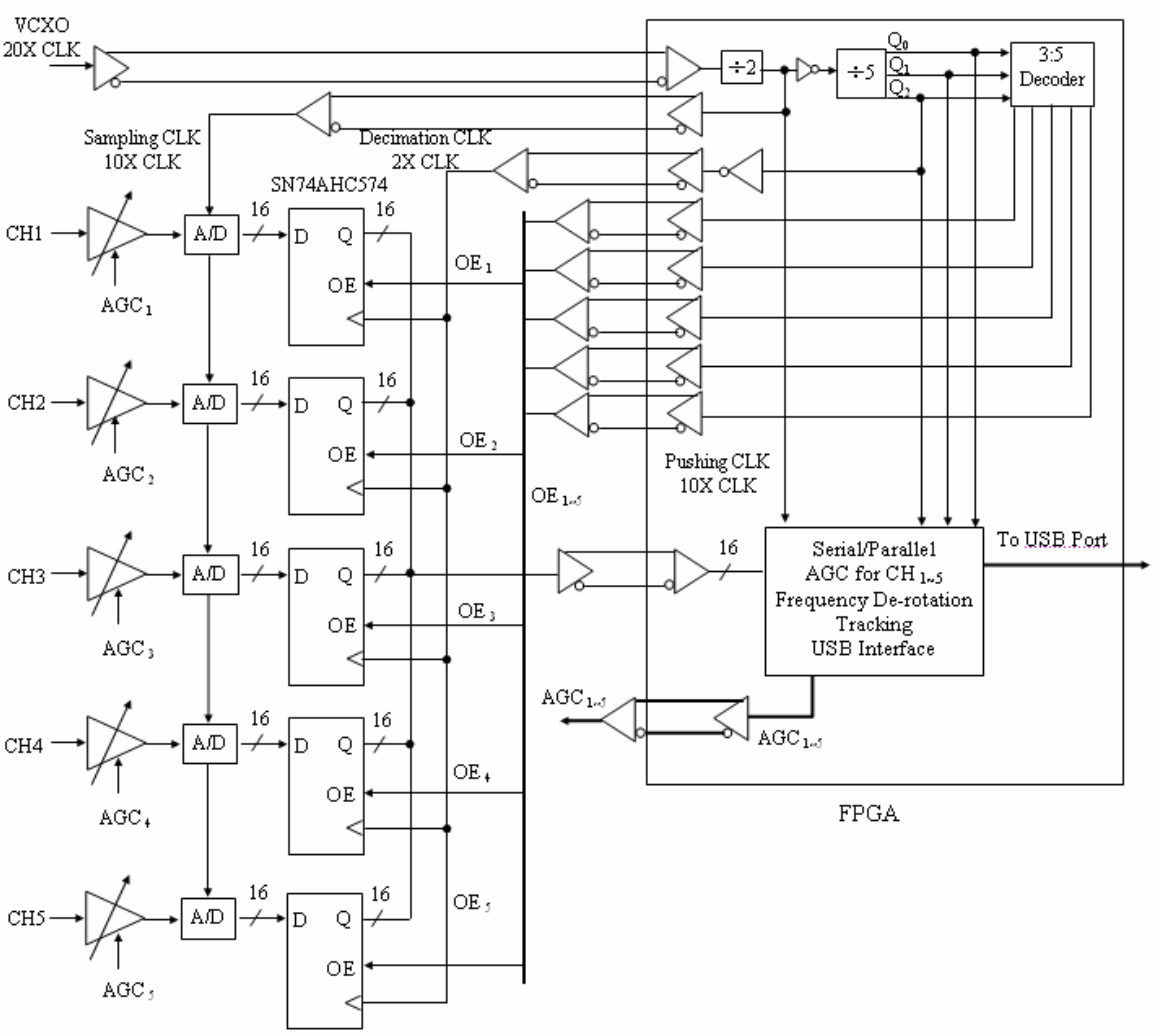

Figure E.1: Digital Circuit Diagram of the Second Receiver

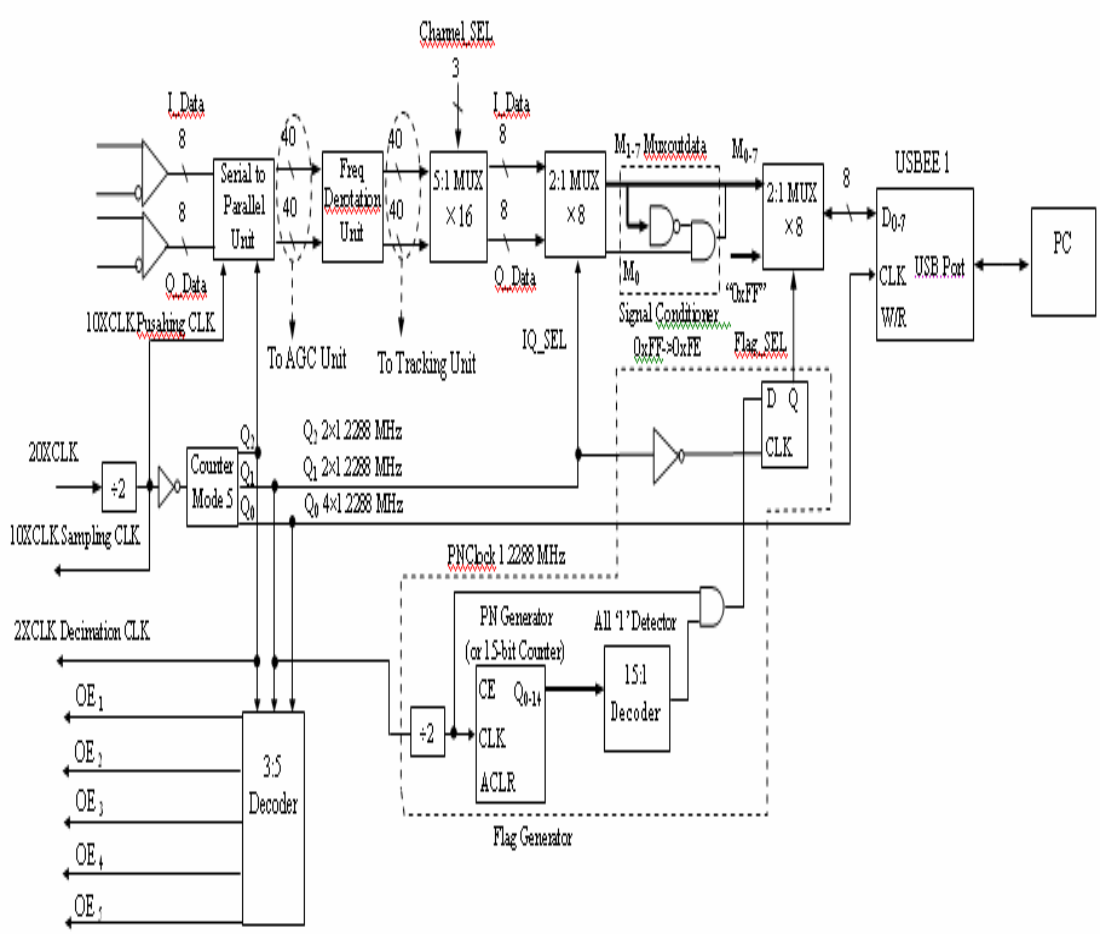

Figure E.2: FPGA Design Diagram in the System

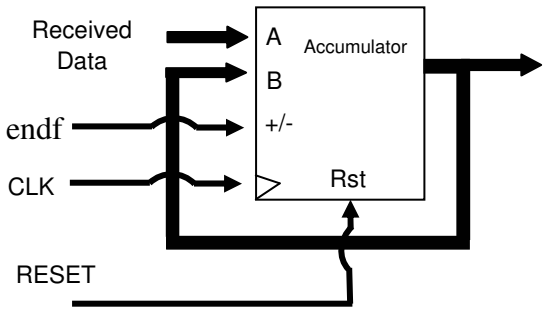

Figure E.3: Accumulator-based Correlator

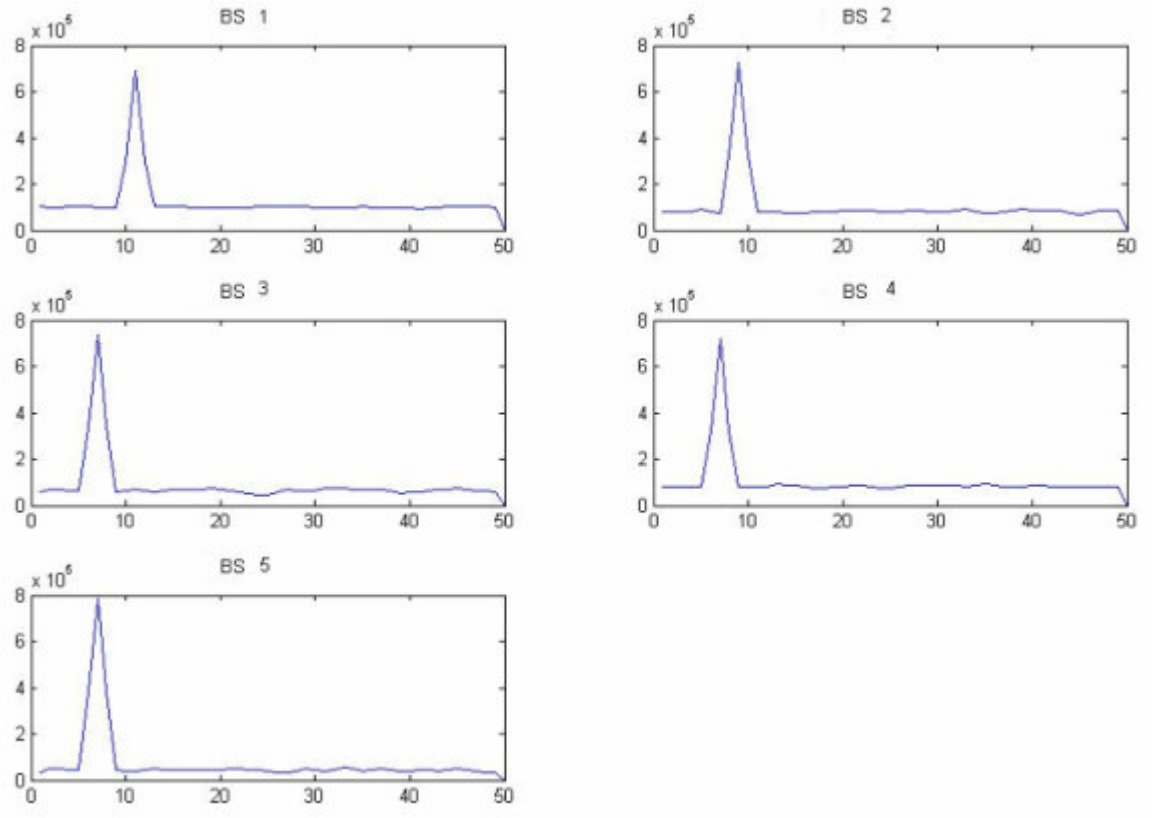

Figure E.4: Correlator Outputs from Five Different Base Stations

APPENDIX F: DERIVATION OF TOA CRLB FOR IS-95 PILOT SIGNAL

Note that the time delay for TOA is within the range of

$$0 \le \tau < T$$

where T is one period of PN sequence.

Let's consider the first term of the denominator of equation (3.63):

$$\begin{aligned}\sum_{t=1}^{N}\left|\frac{\partial PN(t-\tau)}{\partial \tau}\right|^2_{0\le \tau < T/T_S} &= \frac{1}{T_S}\sum_{n=1}^{N}\left|\frac{\partial PN(nT_S-\tau)}{\partial \tau}\right|^2_{0\le \tau < T}\cdot T_S \\ &= \frac{1}{T_S}\sum_{n=1}^{N}\left|\frac{\partial PN(nT_S-\tau)}{\partial (nT_S-\tau)}\right|^2_{0\le \tau < T}\cdot T_S \\ &\approx \frac{1}{T_S}\int_{T_S-\tau}^{NT_S-\tau}\left|\frac{dPN(t)}{dt}\right|^2 dt = \frac{1}{T_S}\int_0^T\left|\frac{dPN(t)}{dt}\right|^2 dt\end{aligned} \tag{F.1}$$

Using Fourier transform properties, one has the following formula:

$$\int_0^T\left|\frac{dPN(t)}{dt}\right|^2 dt = \frac{1}{2\pi}\int_{-\infty}^{+\infty}\left|\omega PN(\omega)\right|^2 d\omega \tag{F.2}$$

where $PN(\omega)$ is the spectrum of $PN(t)$, which can be expressed as:

$$\begin{aligned}&PN(\omega) = T_C\,\mathrm{sinc}(\frac{\omega T_C}{2})\sum_{k=0}^{K-1}[I(k)+jQ(k)]\exp(-j\omega kT_C) \\ &I(k)\ and\ Q(k)\ are\ the\ discrete\ PN\ sequences \\ &K: the\ length\ of\ PN\ sequences\end{aligned} \tag{F.3}$$

Thus

$$\int_0^T \left|\frac{dPN(t)}{dt}\right|^2 dt = \frac{1}{2\pi}\int_{-\infty}^{+\infty} \left|\omega PN(\omega)\right|^2 d\omega$$

$$= \frac{1}{2\pi}\int_{-\infty}^{+\infty} 4\sin^2(\frac{\omega T_C}{2}) \sum_{k=0}^{K-1}\sum_{l=0}^{K-1}[I(k)+jQ(k)][I(l)-jQ(l)]\exp[-j\omega(k-l)T_C]d\omega$$

$$= \frac{2}{\pi}\sum_{k=0}^{K-1}\sum_{l=0}^{K-1}[I(k)+jQ(k)][I(l)-jQ(l)]\int_{-\infty}^{+\infty} \sin^2(\frac{\omega T_C}{2})\exp[-j\omega(k-l)T_C]d\omega$$

$$= \frac{2}{\pi}\sum_{k=0}^{K-1}\sum_{l=0}^{K-1}[I(k)+jQ(k)][I(l)-jQ(l)]\int_{-\infty}^{+\infty} \sin^2(\frac{\omega T_C}{2})\cos[\omega(k-l)T_C]d\omega$$

If the bandwidth of $PN(\omega)$ is $\omega \in [-2\pi/T_C, 2\pi/T_C]$, it yields:

$$\int_0^T \left|\frac{dPN(t)}{dt}\right|^2 dt = \frac{1}{2\pi}\int_{-\infty}^{+\infty} \left|\omega PN(\omega)\right|^2 d\omega$$

$$= \frac{2}{\pi}\sum_{k=0}^{K-1}\sum_{l=0}^{K-1}[I(k)+jQ(k)][I(l)-jQ(l)]\int_{-2\pi/T_C}^{2\pi/T_C} \sin^2(\frac{\omega T_C}{2})\cos[\omega(k-l)T_C]d\omega$$

$$= \frac{2}{\pi T_C}\sum_{k=0}^{K-1}\sum_{l=0}^{K-1}[I(k)+jQ(k)][I(l)-jQ(l)]\int_{-2\pi}^{2\pi} \sin^2(\frac{\omega}{2})\cos[(k-l)\omega]d\omega$$

$$= \frac{1}{\pi T_C}\sum_{k=0}^{K-1}\sum_{l=0}^{K-1}[I(k)+jQ(k)][I(l)-jQ(l)]\int_{-2\pi}^{2\pi} [1-\cos\omega]\cos[(k-l)\omega]d\omega$$

considering that

$$\frac{1}{\pi T_C}\int_{-2\pi}^{2\pi} [1-\cos\omega]\cos[(k-l)\omega]d\omega = \begin{cases} \frac{4}{T_C} & k-l=0 \\ -\frac{2}{T_C} & k-l=\pm 1 \\ 0 & others \end{cases}$$

$$\sum_{k=0}^{K-1}[I(k)+jQ(k)][I(k)-jQ(k)]=2K$$

$$\sum_{k=0}^{K-1}[I(k)+jQ(k)][I(k\pm1)-jQ(k\pm1)]\approx 0$$

Finally one has the following result:

$$\int_0^T \left|\frac{dPN(t)}{dt}\right|^2 dt = 8K/T_C\,. \tag{F.4}$$

Next, let's investigate the second term of the denominator of equation (3.63). Similar to equation (F.1), one has the following expression:

$$\begin{aligned}
\frac{1}{\sqrt{N}}\mathrm{Im}\sum_{t=1}^{N} PN(t-\tau)\frac{\partial PN^*(t-\tau)}{\partial\tau} &\approx \mathrm{Im}\left[\frac{1}{\sqrt{N}T_S}\int_0^T PN(t)\frac{dPN^*(t)}{dt}\,dt\right] \\
&= \frac{1}{\sqrt{N}T_S}\int_0^T \left[\frac{dPN_I(t)}{dt}PN_Q(t)-PN_I(t)\frac{dPN_Q(t)}{dt}\right]dt \\
&= \frac{2}{\sqrt{N}T_S}\int_0^T \frac{dPN_I(t)}{dt}PN_Q(t)\,dt-\frac{1}{\sqrt{N}T_S}PN_I(t)PN_Q(t)\Big|_0^T \\
&= \frac{2}{\sqrt{N}T_S}\int_0^T \frac{dPN_I(t)}{dt}PN_Q(t)\,dt
\end{aligned} \tag{F.5}$$

Intuitively, $\frac{dPN_I(t)}{dt}PN_Q(t)$ can be taken as a random signal, therefore the following result can be obtained:

$$\mathrm{Im}\frac{1}{\sqrt{N}T_S}\int_0^T PN(t)\frac{dPN^*(t)}{dt}dt=\frac{2}{\sqrt{N}T_S}\int_0^T \frac{dPN_I(t)}{dt}PN_Q(t)\,dt\approx 0$$

It can be proven in the frequency domain. The integration in (F.2) can be changed to a convolution format through the following definitions:

- $\tilde{Q}(k)$: the symbol of the reverse PN sequence $Q(k)$
- $PN_{\tilde{Q}}(t)$: the expression of $\tilde{Q}(k)$

That is

$$\begin{aligned} &\tilde{Q}(k) = Q(K-1+k) \;\; (k = 1, 2, \cdots, K-1) \;\; \textit{and} \;\; K = 2^{15} \textit{ is the length of PN sequences}) \\ &PN_{\tilde{Q}}(T-t) = PN_{Q}(t) \qquad 0 \le t \le T \end{aligned} \quad . \tag{F.6}$$

Based on equations (F.5) and (F.6), the following relationship is obtained:

$$\begin{aligned} \int_0^T \frac{dPN_I(t)}{dt} PN_Q(t)\, dt &= \int_0^t \frac{dPN_I(\tau)}{dt} PN_{\tilde{Q}}(t-\tau)\, d\tau \Big|_{t=T} \\ &= \frac{dPN_I(\tau)}{dt} * PN_{\tilde{Q}}(t) \Big|_{t=T} \end{aligned} \tag{F.7}$$

By defining $F[\cdot]$ as Fourier transform, the following Fourier transform properties are used:

$$\begin{aligned} &F\left[\frac{dPN_I(t)}{dt}\right] = j\omega PN_I(\omega) \\ &F[x(t) * y(t)] = X(\omega)Y(\omega) \quad \textit{here} \quad F[x(t)] = X(\omega), \quad F[y(t)] = Y(\omega) \\ &x(t) * y(t)\big|_{t=T} = \frac{1}{2\pi}\int_{-\infty}^{\infty} X(\omega)Y(\omega)\exp(j\omega T)\, d\omega \end{aligned} \tag{F.8}$$

Based on equations (F.3) and (F.8), the convolution value in equation (F.7) is derived as:

$$\int_0^T \frac{dPN_I(t)}{dt} PN_Q(t)\,dt = \int_0^t \frac{dPN_I(\tau)}{dt} PN_{\tilde{Q}}(t-\tau)\,d\tau \Big|_{t=T}$$

$$= \frac{dPN_I(\tau)}{dt} * PN_{\tilde{Q}}(t) \Big|_{t=T}$$

$$= \frac{1}{2\pi} \int_{-2\pi/T_C}^{2\pi/T_C} j\omega PN_I(\omega) PN_{\tilde{Q}}(\omega) \exp(j\omega T)\,d\omega$$

$$= \frac{j}{2\pi} \int_{-2\pi/T_C}^{2\pi/T_C} \omega \operatorname{sinc}(\frac{\omega T_C}{2}) \sum_{k=0}^{K-1} I(k) \exp(-j\omega k T_C) PN_{\tilde{Q}}(\omega) \exp(j\omega T)$$

$$\cdot \operatorname{sinc}(\frac{\omega T_C}{2}) \sum_{l=0}^{K-1} Q(K-1-l) \exp(-j\omega l T_C) \exp(j\omega T)\,d\omega$$

$$= \frac{j}{2\pi} \sum_{k=0}^{K-1} \sum_{l=0}^{K-1} I(k) Q(K-1-l) \int_{-2\pi/T_C}^{2\pi/T_C} \omega \operatorname{sinc}^2(\frac{\omega T_C}{2}) \exp[j\omega(K-k-l)T_C]\,d\omega$$

Considering the even and odd properties of the integrated function, the above integration is expressed as:

$$\int_0^T \frac{dPN_I(t)}{dt} PN_Q(t)\,dt$$

$$= \frac{1}{\pi} \sum_{k=0}^{K-1} \sum_{l=0}^{K-1} I(k) Q(K-1-l) \int_0^{2\pi/T_C} \omega \operatorname{sinc}^2(\frac{\omega T_C}{2}) \sin[\omega(K-k-l)T_C]\,d\omega$$

$$= \frac{2}{\pi T_C} \sum_{k=0}^{K-1} \sum_{l=0}^{K-1} I(k) Q(K-1-l) \int_0^{2\pi/T_C} \operatorname{sinc}(\frac{\omega T_C}{2}) \sin(\frac{\omega T_C}{2}) \sin[\omega(K-k-l)T_C]\,d\omega \tag{F.9}$$

Because $\sin(\frac{\omega T_C}{2}) \sin[\omega(K-k-l)T_C]$ is periodical, the above integration is close to zero. It can be proven as follow.

Defining *a* and *b* as:

$$a = (K-k-l+1/2)T_C \qquad b = (K-k-l-1/2)T_C$$

and substituting $\text{sinc}(\frac{u}{2}T_C) \approx 1-(u\frac{T_C}{2\pi})^2$ into equation (F.9) yields:

$$
\begin{aligned}
&\int_0^{2\pi/T_c} \text{sinc}(\frac{\omega T_C}{2})\sin(\frac{\omega T_C}{2})\sin[\omega(K-k-l)T_C]\,d\omega \\
&\quad = \int_0^{2\pi/T_c}\left[1-(\omega\frac{T_C}{2\pi})^2\right]\sin(\frac{\omega T_C}{2})\sin[\omega(K-k-l)T_C]\,d\omega \\
&\quad = -\int_0^{2\pi/T_c}(\omega\frac{T_C}{2\pi})^2\sin(\frac{\omega T_C}{2})\sin[\omega(K-k-l)T_C]\,d\omega \\
&\quad = \frac{1}{2}\int_0^{2\pi/T_c}(\omega\frac{T_C}{2\pi})^2\{\cos[\omega(K-k-l+1/2)T_C]-\cos[\omega(K-k-l-1/2)T_C]\}d\omega \\
&\quad = \frac{1}{2}\left(\frac{T_C}{2\pi}\right)^2\left(\frac{\omega^2}{a}\sin a\omega+\frac{2\omega}{a^2}\cos a\omega-\frac{2\omega}{a^3}\sin a\omega\right)\Bigg|_0^{2\pi/T_c} \\
&\qquad -\frac{1}{2}\left(\frac{T_C}{2\pi}\right)^2\left(\frac{\omega^2}{b}\sin b\omega+\frac{2\omega}{b^2}\cos b\omega-\frac{2\omega}{b^3}\sin b\omega\right)\Bigg|_0^{2\pi/T_c} \\
&\quad = \frac{1}{2}\left(\frac{T_C}{2\pi}\right)^2\left(\frac{2\omega}{a^2}\cos a\omega-\frac{2\omega}{b^2}\cos b\omega\right)\Bigg|_{\omega=2\pi/T_c} \\
&\quad = \frac{1}{2}\left(\frac{T_C}{2\pi}\right)^2\left(\frac{1}{b^2}-\frac{1}{a^2}\right)=\frac{1}{8\pi^2}\left(\frac{1}{(K-k-l-1/2)^2}-\frac{1}{(K-k-l+1/2)^2}\right)
\end{aligned}
\qquad \text{(F.10)}
$$

When $|K-k-l|>2$, $\left(\frac{1}{(K-k-l-1/2)^2}-\frac{1}{(K-k-l+1/2)^2}\right)\to 0$, the equation (F.5) can be simplified to:

$$
\begin{aligned}
&\frac{2}{\sqrt{N}T_S}\int_0^T \frac{dPN_I(t)}{dt} PN_Q(t)\,dt \\
&= \frac{4}{8\pi^3 T_C \sqrt{N} T_S} \sum_{k=0}^{K-1}\sum_{l=0}^{K-1} I(k)Q(K-1-l)\left(\frac{1}{(K-k-l-1/2)^2} - \frac{1}{(K-k-l+1/2)^2}\right)\Bigg|_{\substack{K-k-l \\ =\pm 1,\pm 2}} \\
&= \frac{1}{2\pi^3 \sqrt{N} T_C T_S} \sum_{k=0}^{K-1} \frac{32}{9} I(k)Q(k) - \frac{32}{9} I(k)Q(k-2) + \frac{64}{225} I(k)Q(k+1) - \frac{64}{225} I(k)Q(k-3) \\
&\approx 0
\end{aligned}
\tag{F.11}
$$

Based on (F.4) and (F.11), the CRLB of TOA for an IS-95 pilot signal is as follows:

$$
\begin{aligned}
\mathrm{var}_{CRLB}(\hat{\tau}) &= \frac{\sigma^2}{\gamma^2} \frac{1}{2M\sum_{t=1}^{N}\left|\frac{\partial PN(t-\tau)}{\partial \tau}\right|^2 - \left\{\mathrm{Im}\left[\frac{1}{\sqrt{N}}\sum_{t=1}^{N} PN(t-\tau)\frac{\partial PN^*(t-\tau)}{\partial \tau}\right]\right\}^2} \\
&= \frac{\sigma^2}{\gamma^2} \frac{1}{2M\sum_{t=1}^{N}\left|\frac{\partial PN(t-\tau)}{\partial \tau}\right|^2} \\
&= \frac{\sigma^2}{\gamma^2} \frac{T_S T_C}{16MK} \quad (T_S = T_C/2) \\
&= \frac{T_C^2}{32MK \cdot SNR}
\end{aligned}
\tag{F.12}
$$

where $SNR = \dfrac{\gamma^2}{\sigma^2}$ is the signal to noise ratio before despreading; $K = 2^{15}$ is the length of IS-95 PN sequences; M is the array elements and T_C is the chip period .